Traffic Flow Modelling to Improve Traffic State Prediction

by

Yuechuan Yin

A thesis submitted in partial fulfillment of the requirements for the degree of

Doctor of Philosophy

In

Transportation Engineering

Department of Civil and Environmental Engineering
University of Alberta

Abstract

In this research, the relationship between microscopic car-following models and macroscopic models has been explored and it was found that, based on the traditional assumption that traffic density equals to the inverse of space headway under steady state homogeneous traffic conditions, most of the existing macroscopic speed-density relations can be derived from microscopic car-following models. The traditional assumption does not hold under non-homogeneous traffic, in which a different headway-density relationship has to be formulated and a class of macroscopic traffic models can be derived from the new formulation.

For model application, first, the compatibility between the macroscopic and microscopic simulation was investigated. The microscopic simulation model, VISSIM, was calibrated and validated on Whitemud Drive, an urban freeway in the city of Edmonton, Alberta. The VISSIM outputs were compared with the predicted traffic speed, density and flow from the second-order macroscopic model, METANET. Three levels of traffic demands and seven different time step lengths in macroscopic simulation were applied to evaluate the compatibility of the two models. It was concluded that, in macroscopic simulation, there exists an optimum time step length. Under moderate to heavy traffic demands, the predicted traffic states from the macroscopic simulation are consistent with the outputs from the microscopic simulation, and under stop-and-go traffic states, a significant difference exists between the two models.

In addition, the impact of merging and weaving from freeway ramps on the performance of macroscopic simulation models was experimentally investigated. Several merging and weaving formulations in speed dynamics were evaluated and their contributions to the predicted traffic speed were quantitatively analyzed. Analysis of variances were carried out on the prediction errors from different models and it was concluded that, for the given formulation, the impact of merging and weaving terms on the prediction accuracy was not statistically significant. Based on these findings, merging and weaving terms can be omitted in macroscopic simulation models. This will improve model computation efficiency and simplify model calibration.

Finally, several improvements on the macroscopic simulation models were proposed, including boundary conditions on density dynamics and various modifications on speed dynamics. The improved models were applied to two freeways and compared with outputs from the original model, using both simulation data as well as field measured data from Whitemud Drive and Berkeley Highway Laboratory system in California. Based on the simulation results, it was concluded that the models with the proposed improvements have obviously better performance than the original model, especially in congested traffic conditions. The improved models can catch most of the significant sudden speed drops resulting from traffic congestion.

Acknowledgement

I would like to express my deepest gratitude to my supervisor, Dr. Zhi-Jun (Tony) Qiu for his full support, expert guidance and inspiration throughout the course of my study and research. I am greatly influenced by his rigorous attitude toward scientific research and always enjoy discussing research questions with him. Without his timely wisdom and counsel, my dissertation would have been an overwhelming pursuit and never-ending journey.

Sincere appreciation goes to the members of my PhD defense committee: Dr. Yasser Mohamed, Dr. Karim El-Basyouny, Dr. Morris Flynn and Dr. Liping Fu for their thoughtful questions, valuable comments and suggestions.

I would like also thank my fellow graduate students and colleagues at the Centre for Smart Transportation in the University of Alberta for their cooperation and generous help with data collection for the research.

Lastly, but definitely not the least, special thanks go to my family for their endless support, sacrifice, encouragement and understanding in the course of all of my studies.

Table of Contents

List of Tables

List of Figures

List of Abbreviations

Acronym	Definition
ANOVA	Analysis of Variance
ATM	Active Traffic Management
ATDM	Active Traffic and Demand Management
BHL	Berkeley Highway Laboratory
CA	Cellular Automata Model
CTM	Cell Transmission Model
CD	Capacity Drop
FD	Fundamental Diagram
GM	General Motor
FOT	Field Operation Test
IDM	Intelligent Drive Model
ITS	Intelligent Transportation Systems
kph	Kilometres per hour
LWR	Lighthill-Whitham-Richards Model
MAE	Mean Absolute Error
MOE	Measure of Effectiveness
MPC	Model Predictive Control
OD	Origin-Destination
OV	Optimum Velocity Model
PRT	Perception-Reaction Time
RG	Route Guidance

Acronym	Definition
RM	Ramp Metering
RMSE	Root Mean Square Error
SGW	Stop-and-go Wave
SL	Speed Limit
SQP	Sequential Quadratic Programming
STD	Standard Deviations
TAC	Transportation Association of Canada
TTD	Total Travel Distance
TTS	Total Time Spent
TTT	Total Travel Time
vphpl	Vehicles per hour per lane
vpkpl	Vehicles per kilometre per lane
VSL	Variable Speed Limit
WMD	Whitemud Drive

List of Notations

Symbol	Definition	Unit
L_i	length of segment *i*	km (kilometre)
λ_i	number of lanes in segment *i*	—
Θ	speed variance	
Θ_0	traffic pressure constant	
P_e	traffic pressure	
$Q_{max,\,i}$	capacity of segment *i*	vphpl
V_{free}	free-flow speed	kph
V_w	shockwave speed	kph
w	congestion wave speed	kph
ρ_c, ρ_{cr}	critical density	vpkpl
ρ_m, ρ_{max}	jam density	vpkpl
α	parameter of the fundamental diagram	—
τ	model parameter of reaction time	hr (hour)
κ	model parameter of density constant	vpkpl
κ_m	model parameter of density constant in merge term	vpkpl
κ_w	model parameter of density constant in weave term	vpkpl
η	model parameter of anticipation factor	km^2/h
η_0	viscosity coefficient	
l	distance headway exponent in car-following model	—
m	speed exponent in car-following model	—
δ_c	factor in convection term	—
δ_d	factor in anticipation term	—
$\rho(i)$	density on segment i	vpkpl
v(i)	speed on segment i	kph

Symbol	Definition	Unit
v_r	speed at on-ramp	kph
q(i)	flow on segment i	vphpl
q_{on}(k)	inflow from on-ramp	
q_{off}(k)	outflow from off-ramp	
$r_i(k)$	measured/predicted on-ramp flow at time index k	vph
$s_i(k)$	measured/predicted off-ramp flow at time index k	vph
$V[\rho(k)]$	equilibrium speed for traffic density ρ at time index k	kph
Ve	equilibrium speed	
k	simulation time index	—
K	total simulation time steps	—
N_p	number of prediction steps	—
T	simulation time step length	hr

Chapter 1 Introduction

1.1 Introduction

Traffic congestion is one of the major problems in modern society. The ever-increasing number of vehicles and travel demands on roadways leads to traffic jams that not only cause tremendous time losses but also compromise road safety and increase air pollution. The areas that most suffer from these problems are large cities and freeways. Recurrent congestion occurs regularly during peak hours at freeway bottlenecks, on-ramp and off-ramps. Non-recurrent congestion often takes place as a result of traffic incidents, road construction, maintenance as well as inclement weather conditions. Congestion causes inefficient operation of freeways and increased user costs. Expanding road infrastructure is one of the solutions, but is often constrained by the available right-of-way and capital investments. A more efficient use of existing road networks is a promising solution that transportation practitioners have been seeking. Active Traffic Management (ATM), such as ramp metering (RM), variable speed limits (VSL) and route guidance (RG), are state-of-the-art methods in Intelligent Transportation Systems (ITS), which aim to improve the efficiency of the existing roadways.

RM is an on-ramp control measure to reduce or eliminate recurrent traffic jams on freeways by restricting the number of vehicles allowed access to the mainline freeway from on-ramps, so as to achieve and maintain capacity flow and avoid congestion on the freeway near the ramps. This is achieved by placing traffic control signals at the freeway on-ramps. The traffic signals regulate the number of vehicles allowed to enter the freeway, depending on the traffic states on the mainline freeway.

As RM will increase the waiting time of vehicles at the on-ramps, a trade-off exists between reducing congestion on the freeway and keeping the queue length at the on-ramp to an acceptable level, because if the queues at the on-ramps are too long, it may block the roadway network connected to the on-ramps. With proper control settings, the total delay for the freeway and the on-ramps can be reduced.

According to its principle, RM can only affect the section immediately downstream of the controlled ramps. It has no control of the behaviour of vehicles already on the freeway and, thus cannot mitigate traffic congestion caused by disturbances on the freeway itself. Traffic breakdowns may happen at weaving or lane-drop sections (Persaud et al. 1998, Chung et al. 2007, Şahin and Altun 2008) or locations with geometric constraints, such as sharp curves and steep upgrades. Other control measures, such as VSL and RG, need to be used to deal with those situations.

Unlike ramp metering, VSL can only control traffic flow on the mainline freeway. It does not have direct control of vehicles entering from on-ramps. The

main purpose of VSL is to increase the traffic flow on the mainline freeway by reducing or eliminating the effects of traffic shock waves, which can lead to congestion. The use of VSL along freeway mainlines is in an effort to control collective driver behaviour, so as to reduce the speed differences between vehicles. This will make traffic flow more stable, smooth and have a higher flow rate. In addition, VSL systems can reduce the risk of collision due to the reduced speed differences and provide warning to drivers about hazardous roadway conditions. It can also postpone or prevent congestion and reduce emissions and fuel consumption. Benefits, such as improved traffic flow rates, lower travel times, smooth speed and density distribution and possibly lower pollution, have been discussed in literatures and in some cases analyzed using mainly macroscopic traffic flow models (Bertini et al. 2006; Hoogen and Smulders 1994, Abdel-Aty et al. 2006a; Abdel-Aty et al. 2006b; Lee et al. 2006; Lee et al. 2004; Lee et al. 2003; Piao and McDonald 2008).

A route guidance system suggests alternate routes for particular destinations; these alternate routes may have better traffic conditions. The systems typically display traffic information on variable message signs (VMSs) that point out the alternative routes or provide information about the delay, queue length or travel time on the alternative routes (Heutinck at el. 2006, Kotsialos at el. 1999). Route guidance attempts to provide the information available to drivers in regards to their route choice decisions. By directing some traffic flows to alternate roadways, the RG

system can reduce the non-recurrent congestion on freeways. RG is helpful mostly in the case of a non-recurrent event that makes the traffic conditions unpredictable (Wang et al. 2006). It can be implemented with the existing infrastructure and only limited investments are required. The network level benefit of the RG system has been studied by many researchers (Koutsopoulos and Lotan 1989, Mahmassani and Jayakrishnan 1991, Al-Deek and Kanafani 1993, Emmerink et al. 1995, and Hall 1996). It has been shown that the total travel time can be reduced by using the RG system compared to the situations without the RG system.

Independent applications of RM, VSL and RG have been in existence for many years. Combined applications are limited due to complexity of control and coordination of all measures. To systematically implement those traffic control systems, complex model predictive control (MPC) has to be applied. MPC (Camacho and Bordons 1995, Maciejowski 2002) of traffic flow is an online control technique used for optimal control of ramp metering, VSL or a combination of several control measures. It uses traffic models to predict the future traffic state evolution for a given traffic demand. This approach utilizes traffic models to design the traffic control measures in such a way that the desired control objectives are achieved (such as to reduce the total travel time, or to maximize the flow number, etc.). MPC is preferable because it operates in a closed loop (Gartner 1984), in which the traffic states and the current demands are regularly fed back to the controller.

To effectively manage and control traffic flow and improve mobility, traffic state variables need to be accurately predicted in real-time. These will rely on appropriate traffic flow models to simulate and forecast traffic flow states. The first attempts to develop a mathematical theory for traffic flow dated back to the 1930s (Greenshields 1935, Adams 1936), but even until today, we do not have a satisfactory and general mathematical theory to describe various real-world traffic flow conditions. This is because traffic phenomena are complex and nonlinear, depending on the interactions of a large number of vehicles. Moreover, vehicles do not interact simply by following the laws of physics but are also influenced by the psychological reactions of human drivers. As a result, we observe chaotic phenomena, such as cluster formation and backward propagating shockwaves of vehicle speed/density (Bose et al. 2000), that are difficult, if possible, to be accurately described with mathematical models. Because of this, in traffic control, simulation models are often applied. Simulation models can be broadly categorized into microscopic models, mesoscopic models and macroscopic models, each of which has its respective focus of applications. Macroscopic simulation models are suitable for real-time traffic control due to the low computational complexity and relative ease of calibration. However, macroscopic models may overlook detailed local variation of traffic state conditions, such as local traffic disturbance, which may lead to traffic breakdown.

Microscopic simulation can describe the detailed operation on merging, diverging and weaving sections. However, due to the high demand of computation, it is difficult to use them for online control of large-scale networks. In many situations, macroscopic and microscopic models can be used on the same project to their respective advantages. For example, prior to the field implementation of a traffic control strategy, the effects of the control strategy are often evaluated using microscopic simulations to check whether the control strategy will have the expected performance. This can be carried out off-line and usually there is not much of a time limitation to calibrate and adjust the microscopic simulation model. Once the microscopic simulation shows that the traffic control strategy is appropriate, it can be implemented in the field using macroscopic models for online traffic state prediction and control. There is an important question that needs to be answered: can the outputs from the microscopic simulation represent the outputs from the macroscopic simulation under varying traffic conditions? There are still many issues on the applications that need to be further studied.

1.2 Statement of Problems

Macroscopic traffic models are often used to predict future traffic states for MPC purposes. In practice, traffic models need to be transformed into discrete form with respect to time and space. Time is discretized into short time slots (time intervals or

time steps) and space (roadway) is discretized into short segments. Traffic states are predicted at each time step and appropriate control values are exercised based on the predicted traffic states in the near future. This requires high accuracy of models to predict traffic states under a wide range of traffic conditions. Several elements affect model performance, but have not been clearly studied. These are discussed in the subsequent sections.

1.2.1 Relationship between Microscopic and Macroscopic Models

One of the fundamental differences between microscopic and macroscopic traffic flow models is the scale of variables. Microscopic models track the behaviour of each individual vehicle in relation to the roadway and other vehicles in the flow. Microscopic characteristics (individual vehicle speed, time or distance headway, acceleration/deceleration, vehicle properties, etc.) pertain to an individual vehicle and may be significantly different than the other vehicles in front or behind it. Macroscopic models describe traffic flow in terms of the macroscopic characteristics, such as flow, speed (time-mean speed or space-mean speed) and density. They are average properties of the traffic flow as a whole for a particular location (at a cross section or on a section of roadway) at a time instant or within a time interval.

Microscopic traffic models and macroscopic traffic models are derived from different perspectives to describe the same physical phenomenon of traffic flow.

There are some studies on the relationship between microscopic and macroscopic models. However, most of them were established based on steady state, homogeneous conditions with the assumption that density equals to the inverse of the space headway (Gazis 1959, May 1990) or researchers derived a macroscopic model from a specific microscopic model without the headway-density relationship, as in the gas-kinetic model (Pregogine and Herman 1971). It will be shown that the assumption that density is the reciprocal of headway is questionable under non-homogeneous traffic conditions and, therefore, it is worthwhile to further explore the relationship when the assumption is changed.

1.2.2 Compatibility between Microscopic and Macroscopic Simulation Models

Both microscopic and macroscopic simulations are widely used in transportation studies. Microscopic simulation can explicitly capture interactions among individual drivers and represent the driver's response to traffic control devices at the individual vehicle level. However, this type of application is usually off-line and lacks predictive control functions. On the other hand, the application of macroscopic simulation models is aimed at large-scale roadway networks (Kotsialos et al. 2002, Carlson et al. 2010) or online (real time) traffic control to reduce congestion and improve mobility (Lu et al. 2010, Hegyi et al. 2005a, 2005b).

Due to traffic operation safety and cost constraints, it is not practical, sometimes even impossible, to carry out experiments of various control measures on freeways.

Traffic simulation is often used for experimental investigation purposes. The effects of a control strategy are often evaluated prior to the field implementation of online traffic control using microscopic simulations to determine whether the control strategy will have the expected performance. In this way, the optimal control policy for various traffic conditions can be determined based on several experimental settings and then used in actual field traffic control.

There are several technical issues that need to be studied before we use the results from microscopic simulation to evaluate online control with macroscopic models. Do both macroscopic and microscopic models provide similar traffic state results under all traffic conditions, including light traffic, moderate traffic and heavily congested traffic? From the previous study carried out by Cremer et al. (1981), we know that simulation time step plays an important role in macroscopic simulation. In previous studies on macroscopic simulation, various time steps were used on different highways (Shladover et al. 2010, Papageorgious et al. 1989, Lamon 2008 and Wu 2002). There has not been a systematic study as to how to set the appropriate time step and whether there is an optimal time step for a particular roadway. If there is an optimal value, does it vary with traffic demand? These issues are addressed in the present thesis.

1.2.3 Impact of Ramp and Weaving on Macroscopic Simulation Models

Freeways have on-ramps and off-ramps. An independent on-ramp may end as a lane drop and form a merge area. If an on-ramp is immediately followed by an off-ramp, a weaving section is formed. Traffic operation near merge areas or on weaving sections is different from that on normal sections. At the individual vehicle level, both merging and weaving involves lane-changing behaviour and drivers need adjust their own speed as well as find and wait for suitable gaps on the target lane and then make the appropriate maneuver. As a result of this process, their speed changes, and so does the distance between vehicles. On the macroscopic level, aside from free flow traffic conditions, a weaving section usually has a lower speed and capacity than sections without merging and weaving. The speed of the traffic flow is affected by vehicles merging, diverging or weaving. Furthermore, the impact of on-ramp flows is important in the formation of traffic jams near the on-ramp area. This congested traffic state indicates the complex phenomena caused by merging vehicles from on-ramps.

Most of the macroscopic modelling efforts on freeway traffic have mainly concentrated on describing uninterrupted traffic flow on freeway sections without ramps. The investigation of interrupted traffic flow due to on-ramps, off-ramps and weaving sections is far from completion. In many studies on freeway macroscopic simulation, the impact of on-ramps, off-ramps and weaving sections had been either

subjectively conjectured (Papageorgious et al. 1989, Ngodgy 2006) or omitted due to the lack of data from ramps (Shladover et al. 2010). How they affect the performance of macroscopic simulation has not yet been systematically studied.

1.2.4 Improvement of Macroscopic Simulation Models

The core of model predictive control (MPC) is the macroscopic traffic models for traffic state prediction. The accuracy of traffic state prediction not only affects the control decisions that will be assigned by the controller, but it will also affect the model calibration and validation process, which is often based on the optimization of traffic flow, in which both the modeled outputs and field measured data are used. Most of the second-order macroscopic models have similar structures to the METANET model (Messmer and Papageorgious 1990), which has been used for many freeway online traffic controls, ramp metering controls and traffic state predictions due to its model structure, discrete form and the fact that it contains both speed and density dynamics. Previous studies (Lu el al. 2011, Lamon 2008) showed that there are some problems regarding speed and density dynamics in macroscopic simulation models. The speed dynamics used in the previous studies do not catch quick and significant changes in congested traffic conditions (Lu et al. 2011). Under stop-and-go traffic states, considerable prediction errors exist between the measured data and the model-predicted traffic states. In addition, boundary constraints were not appropriately considered in some models, which will also affect the prediction

accuracy. From the field studies (Lu et al. 2011), under congested traffic or at locations where the roadway and speed limits change rapidly, the predicted traffic states from the original METANET model did not well-match the measured data. Traffic jams often involve a situation where the traffic state changes rapidly over a short distance. To model this phenomenon, traffic models need to be sensitive enough to catch these details. Therefore, this problem should be investigated to improve model performance under various traffic conditions.

1.3 Research Objectives and Scope

This research is part of a larger research project on the implementation of VSL control on an urban freeway (Whitemud Drive) in the city of Edmonton, Canada. This freeway was also selected as a test bed for Connected Vehicle-related research by the Transportation Association of Canada (TAC). Based on this road, various ITS-related studies and research have been carried out.

The present research intends to provide fundamental support for the macroscopic modelling and real-time control of traffic flow on freeways and solve several technical issues related to the models. The overall objective of the research is to investigate macroscopic traffic modelling to improve traffic state prediction. This can be broken down into several specific sub-objectives:

(a) Explore the relationship between microscopic and macroscopic traffic flow models and their underlying links. This will help us to better understand the difference between the two kinds of traffic models, their intrinsic properties and their application for the purposes of traffic control and cross-validation.

(b) Study the compatibility of microscopic and macroscopic simulation models under various traffic conditions. This can be achieved by comparing the performance of a microscopic simulation model, VISSIM (PTV 2010), and a macroscopic simulation model, METANET (Messmer and Papageorgious 1990), under various traffic conditions, to evaluate how the time-step length and traffic demand impacts the macroscopic simulation performance and to determine the most appropriate time-step length that will be used in VSL control on the studied urban freeway.

(c) Investigate the impact of ramp and weaving sections on macroscopic model performance and provide experimental evidence as to whether explicit merging and weaving terms should be included in the speed dynamics of macroscopic traffic simulation models. If merging and weaving terms have significant impact on the model predicted results, they should be included in the model to improve prediction accuracy. Otherwise, they may be omitted to simplify model calibration and improve computation efficiency.

(d) Modify, improve and extend macroscopic models to improve the accuracy of traffic state prediction so as to provide a realistic representation of traffic dynamics, in particular, for congested traffic flow operations. This can be achieved through investigating different speed dynamics and applying appropriate boundary conditions on density dynamics to improve prediction accuracy of the second-order macroscopic models.

As indicated previously, this research intends to provide fundamental support of macroscopic traffic modelling. The research was focused on non-controlled traffic operations. The scope of this research is restricted to freeways, including on-ramps and off-ramps as well as weaving sections. Arterial roads with signal controls were not included in the study. However, the methodologies and principles used in this study can be extended and applied to other types of roadways. The research was carried out using both simulations and field data obtained from the studied freeways. The main study site is illustrated in Figure 1.1 and the research flow chart is shown in Figure 1.2, respectively.

1.4 Research Contributions

The work presented in this dissertation explored several fundamental aspects of microscopic and macroscopic traffic models and the link between them. Important factors that affect macroscopic traffic simulation, such as time steps, traffic demand,

merging and weaving, were experimentally investigated. These factors are directly related to the application of model predictive control and online traffic state predictions. There are several major contributions of this research to the state-of-the-art knowledge in transportation fields:

(1) Identified the impact of headway-density relationship on the derivation of macroscopic traffic models.

The relationship between various microscopic car-following models and macroscopic speed-density models has been studied for several decades. It was found that almost all existing macroscopic speed-density relationships can be derived from the stimulus-response type of microscopic models based on the equilibrium, homogeneous traffic assumption that traffic density equals to the inverse of space headway. In this research, using the same assumption, a generalized macroscopic speed-density relationship was derived from a generalized microscopic car-following model. The research showed that this assumption does not hold for non-homogeneous traffic, and slightly changing the headway-density relationship will result in different macroscopic models. Using a mathematical definition of density and a new headway-density approximation, a macroscopic model that includes relaxation, convection, anticipation and diffusion (or viscosity) components was derived from a microscopic model corresponding to the delayed response of drivers.

(2) Identified the compatibility between microscopic and macroscopic simulation models and determined the optimum time step for macroscopic simulation.

Two important factors that impact macroscopic simulation, namely time step and traffic demand, have been systematically studied and their effect on the performance of macroscopic simulation models was determined. It was found that in macroscopic simulation models there exists an optimum time-step length at which the macroscopic models have the best prediction accuracy. Under moderate to heavy traffic demands, the predicted traffic states from the macroscopic simulation are consistent with the outputs from the microscopic simulation, and under stop-and-go traffic states, significant differences exist between the two models. This finding can serve as a practical guideline for macroscopic simulation and online traffic control and can improve prediction accuracy by using the optimal time intervals. With this knowledge, any macroscopic online control strategy can be pre-tested and evaluated with microscopic simulation for different scenarios, so that the most effective control strategy can be implemented.

(3) Quantified impact of merging and weaving terms on macroscopic simulation model performance, and concluded that merging and weaving terms do not have significant impact and can be omitted in macroscopic simulations.

The impact of merging and weaving due to ramps on the performance of macroscopic simulation models was experimentally investigated. Several merging

and weaving configurations in speed dynamics were evaluated and their contributions to the predicted traffic speed were calculated. Analysis of variances were carried out on the performance of both the base model (without merging or weaving terms) and the models with explicit merging and weaving terms. It was found that, although merging and weaving impacts prediction accuracy, these impacts are not statistically significant. Based on these findings, merging and weaving terms can be omitted in macroscopic simulation models. This will simplify model calibration, increase computation efficiency and does not significantly impact prediction accuracy.

(4) Quantitatively analyzed each component of density and speed dynamics in macroscopic simulation models.

A program code was developed in the Matlab (2010) environment, which can evaluate each component of the density and speed dynamics of the macroscopic simulation models. The value of each component of the density dynamics and speed dynamics of macroscopic simulation models were quantitatively analyzed for both average values during the full simulation time period and at a specific time step. This allows researchers to quantify the impact of relaxation, convection and anticipation in the speed dynamics and help with the adjustment of models to improve model performance.

(5) Proposed methods to improve macroscopic simulation models to provide better prediction accuracy.

This research proposed several methods to improve the performance of macroscopic simulation models. These include adding boundary conditions to the density dynamics, modifying the convection and anticipation terms of the speed dynamics as well as using various factors in speed dynamics. The modified models were applied to two freeways and compared with the outputs from the original model as well as the field-measured data. According to the modelling results, the models with the proposed improvements have an obviously better performance than the original model, especially for congested traffic conditions. The improved models can catch most of the significant sudden speed drops resulting from traffic congestion.

1.5 Organization of the Dissertation

As shown in Figure 1.2, the focus of this research is the macroscopic traffic simulation modelling. Four major areas of studies related to the research focus were carried out: The relationship between microscopic and macroscopic traffic models (Chapter 3); the compatibility between microscopic and macroscopic traffic simulation (Chapter 4); merging and weaving impacts on macroscopic traffic simulation modelling (Chapter 5) and the improvements of macroscopic traffic simulation models (Chapter 6). These four subtopics, together with a comprehensive

review of traffic flow models (Chapter 2) as well as research conclusions and recommendations (Chapter 7) form the whole dissertation.

A flow chart describing the main components of the thesis is shown in Figure 1.3. There are seven chapters in this dissertation:

Chapter 1 gives an introduction of the relevant research background, statement of problems as well as the objectives and scope of this research. The main contributions of this research are also summarized in this chapter.

Chapter 2 presents a comprehensive literature review on traffic flow models with a special focus on microscopic car-following models as well as first-order and second-order macroscopic models. The traffic models are reviewed with respect to their categories in terms of level of detail, scale of independent variables and nature of independent variables. Various microscopic car-following models are presented. On the macroscopic level, both first-order and second-order models and their respective advantages and disadvantages are discussed. Various modelling approaches for traffic congestion are also discussed in this chapter.

Chapter 3 explores the relationship between microscopic and macroscopic traffic models. The derivations of macroscopic speed-density relations from various car-following models are presented. Detailed discussions on how the assumptions of the headway-density relationship impact the model derivation are provided.

Chapter 4 studies the compatibility between microscopic and macroscopic simulation models. The predicted flow, density and speed from a macroscopic simulation model are compared with those from a microscopic simulation model, using METANET and VISSIM respectively, on a section of urban freeway. Three levels of traffic demands and seven different time-step lengths in macroscopic simulation were applied to evaluate the compatibility of the two models, based on which, the optimal time step in macroscopic simulation is determined.

Chapter 5 experimentally investigates the impact of freeway merging and weaving impacts on the performance of macroscopic simulation models. Several configurations of merging and weaving terms are evaluated and compared with the base model with respect to accumulated prediction errors. Data from both microscopic simulation and field loop detectors are used in the model performance evaluation. Based on these data, all relevant model parameters are estimated using an optimization technique (model calibration). Each macroscopic simulation model is independently calibrated and then used to simulate traffic operations on the studied freeway. Analysis of Variances (ANOVA) are carried out to evaluate the variation of prediction errors of different models, based on which, the statistical significance of merging and weaving impacts on macroscopic model performances are discussed.

Chapter 6 investigates different methods to improve the accuracy of traffic state prediction. Boundary conditions are proposed for density dynamics. Several potential

speed dynamics are proposed and applied in a modified simulation model. Both original and modified models are calibrated and validated with the data from two freeways. The simulation results from both the original model and the improved ones are compared with the measured data.

Chapter 7 summarizes the main conclusions of this research and discusses recommendations for future research works related to macroscopic traffic flow models and simulation.

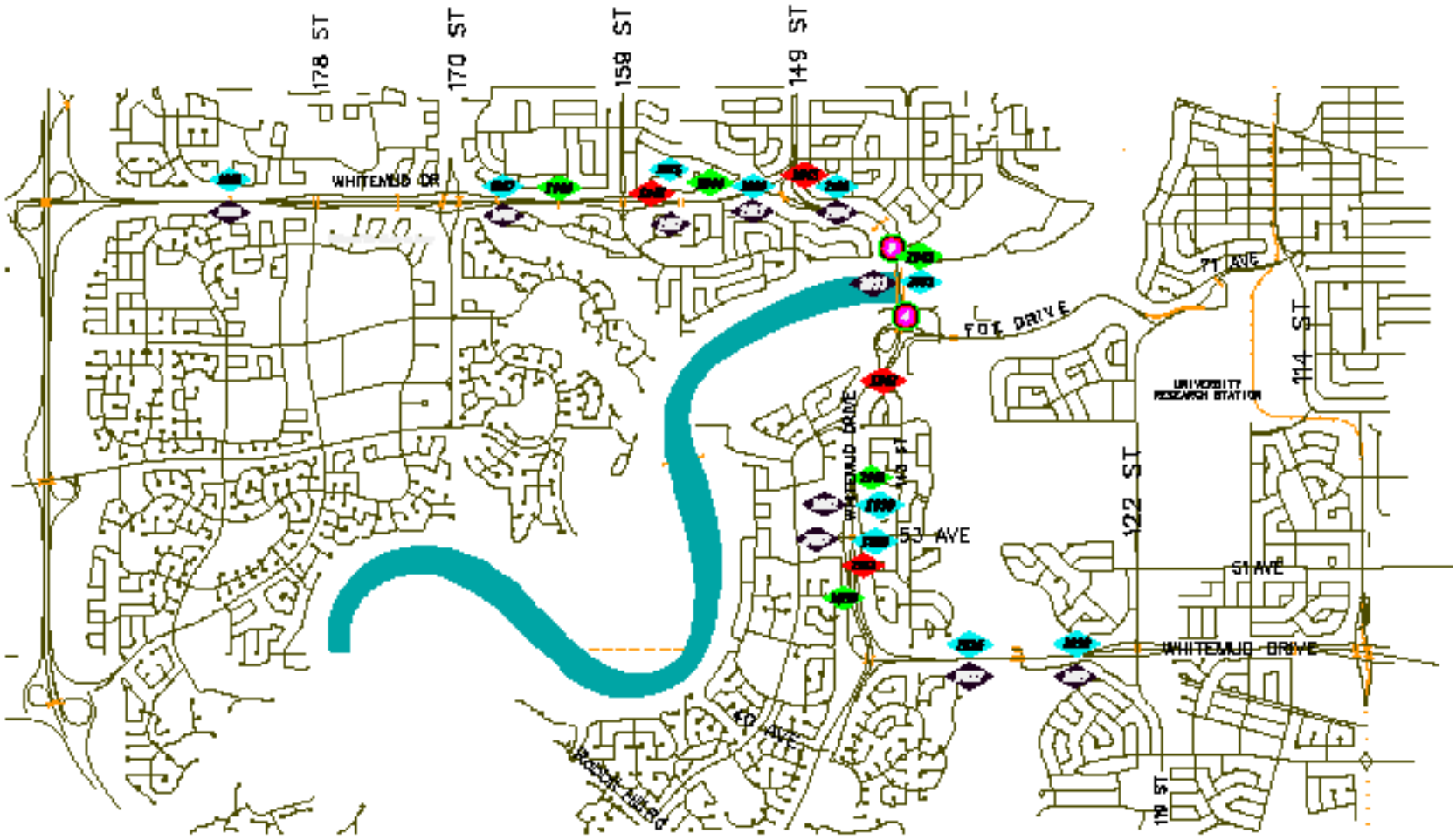

Figure 1.1 The 9-km study site between west of 111 Street and west of 159 Street (Courtesy: city of Edmonton)

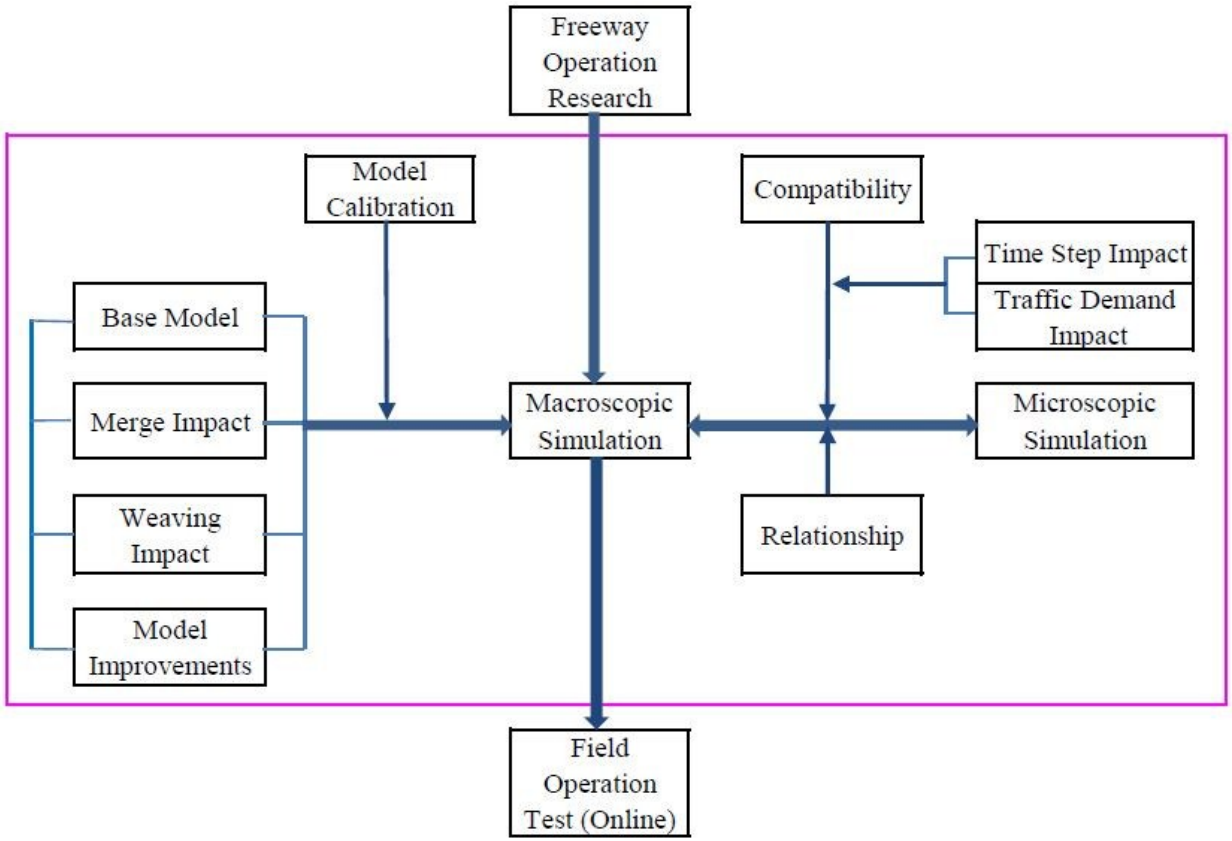

Figure 1.2 Research flow chart

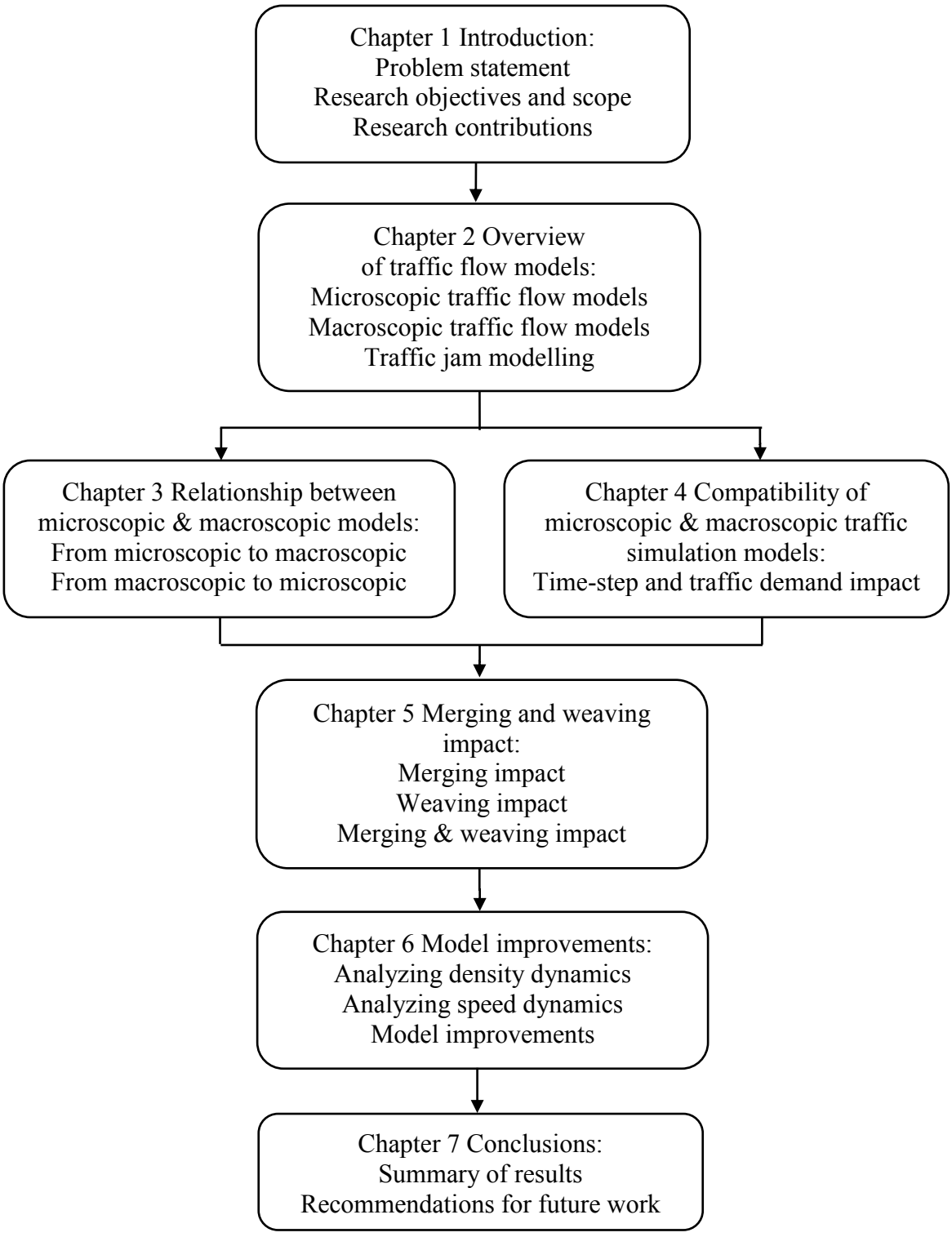

Figure 1.3 Flow chart of the main content of the thesis

Chapter 2 Overview of Traffic Flow Models

Traffic flow models have been studied for over half a century, from simple one-regime linear speed-density relationships to multi-regime, multi-class, nonlinear models. In this chapter, an overview of those models, from their historical evolution to their nature, is provided.

2.1 Historical Review of Traffic Models

Since the mid-1950s, each decade has been dominated by a certain modelling approach (Helbing, 2001). In the fifties, the propagation of shock waves was described by fluid-dynamic models for kinematic waves (Lighthill and Whitham 1955, Richards 1956). In the sixties, the investigations concentrated on microscopic car-following models (Chandler et al. 1958, Gazis et al. 1961). During the seventies, gas-kinetic models (Prigogin and Herman 1971) for the spatio-temporal change of the speed distribution were flourishing. The simulation of macroscopic models (Payne 1979, Cremer and Papageorgiou 1981) began in the late seventies and early eighties. In the nineties, discrete cellular automata models (Nagal 1996, 1998) of vehicle traffic and the cell transmission model (CTM) were developed (Daganzo 1994a, 1994b). Hybrid simulation began sometimes around the end of the last century (Nökel and Schmidt 2002, Bourrel and Lesort 2003, Burghout et al 2005). At present, the research focus is on the systematic investigation of the dynamic solutions of models, and the application of ITS on freeway corridors and networks.

2.2 Category of Traffic Models

Traffic models can be classified based on different perspectives, such as the level of detail represented in the model, the scale of independent variables, the nature of variables used in modelling, etc. These classifications are summarized in Table 2.1. So far, the majority of the applications of traffic models are microscopic and macroscopic, which are discussed in more detail later in this chapter.

2.2.1 Level of Detail

According to the level of detail, traffic models can be classified as sub-microscopic, microscopic, mesoscopic and macroscopic models:

(a) Sub-microscopic models are highly detailed descriptions of vehicle motions and interactions, where even the behaviour of specific vehicle sub-units, such as shift of transmission, is considered in the model (Hoogendorn, 2001].

(b) Microscopic models take each individual vehicle as a unit and its motion and interaction with adjacent vehicles are incorporated in the model. They track the motion of each vehicle and operate based on the properties of each vehicle and on a set of rules. Typical examples of this kind of model are the car-following models for longitudinal movement and the lane-changing models for lateral movement on multi-lane roadways, on-ramps and off-ramps. In the car-following models, each vehicle is considered separately and its behaviour is modeled as it reacts to and anticipates vehicles in front by a dynamic equation.

(c) Mesoscopic models are medium-detailed models where small groups of interacting vehicles are traced, instead of individual vehicle units (Barcelo

2010). Furthermore, behavioural information can be incorporated by means of probabilistic terms.

(d) Macroscopic models are low-detailed representations of traffic states using aggregated variables, such as flow, average speed and density. They describe the collective effect of many vehicles. Individual vehicle motions and interactions are completely neglected. This type of model is often based on hydrodynamic analogies and is also called a continuum model.

2.2.2 Scale of Independent Variables

According to the scale of independent variables, traffic models can be classified as continuous models and discrete models:

(a) The independent variables of continuous models are changing continuously and instantaneously both in time and space; i.e., the domain of the temporal and spatial variables are $t \in [0, \infty)$, and $x \in [0, \infty)$, respectively. These models are often formulated as differential equations in which time and space are treated as continuous variables over the study domain. Most of the car-following models are examples of this approach and so are hydro-dynamic macroscopic models.

(b) Discrete models assume discontinuous changes in both time and space. Accordingly, traffic states are described temporally and spatially at discrete steps along the roadway. For example, the cellular automata model (CA) (Nagel 1996, 1998) uses integer variables to describe the dynamic state of the system, in which the time is discretized into steps and the roadway is divided into short sections (cells) that can be either occupied by a vehicle or empty.

The CTM is another example of a discrete model in a macroscopic scale, in which the roadway is divided into a distance that vehicles travel in one time step in free flow traffic conditions.

2.2.3 Nature of Independent Variables

According to the nature of independent variables, deterministic and stochastic models are distinguished according to the representation of the traffic states. Deterministic models assume exact relationships without randomized model components. Stochastic model descriptions use random variables and a probabilistic approach to describe traffic states.

2.3 Microscopic Traffic Models

Microscopic traffic models describe longitudinal car-following and lateral lane-changing behaviour of individual vehicles. They model the behaviour of individual vehicles in relation to the roadway and other vehicles in the traffic flow. Microscopic models are often used in the form of microscopic simulation, in which vehicles are tracked through the network over small time intervals (usually less than one second). Traffic states can then be aggregated to compare with measured data. Car-following models are a major part of the microscopic model category. They describe the processes by which drivers follow each other in the traffic stream. Car-following models are commonly divided into classes or types depending on the utilized logic. There are three main types of car-following mechanisms: safe distance models, stimulus-response models and psycho-spacing models. An extensive review of car-following models was provided in Brackstone and McDonald (2000) and Rothery (1999).

2.3.1 Safety Distance/Collision Avoidance Model

In safety distance or collision avoidance models, the driver of the following vehicle is assumed to always keep a safe distance from the vehicle in front, so that a collision will never happen. The safe distance can be specified following Newton's equations of motion, and is calculated as the distance that is necessary to avoid a collision if the front vehicle decelerates suddenly.

Pipes (1953) developed a microscopic car-following model by relating the velocity of a vehicle to the minimum headway that the driver usually keeps with the vehicle in front of it for safety purposes. In the model, the minimum safe distance between the leader and the following vehicle was assumed to be a function of the speed of the following vehicle (in miles per hour [mph]) and the length of the vehicle (in feet [ft]) in front, as indicated in Equation (2.1). This equation indicates that the minimum safe distance between two vehicles corresponds to one car length at a minimum, and that it increases by one car length for every 10-mile increment in the speed of the following vehicle.

$$d_m = (\frac{\dot{x}_{n+1}}{1.47 \times 10}) l_n + l_n \tag{2.1}$$

Where, l_n is the length of vehicle in feet (ft), $(x_{n+1})'$ is the speed of the following vehicle (mph). The 1.47 is a conversion factor to convert from mph to ft/s. Pipe's model is a simple linear car-following model.

There is another safe distance model based on the minimum time headway between two vehicles. This model, developed by Forbes et al. (1958), assumed that the minimal time headway was equal to the class-specific reaction time and the time

required for the vehicle to travel a distance equal to its length. This formulation is very similar to Pipe's theory.

A more complicated formulation of the safe distance model was provided by Kometani and Sasaki (1959):

$$\Delta x(t-\tau) = \alpha \cdot v_{n-1}^2(t-\tau) + \beta \cdot v_n^2(t) + \gamma \cdot v_n(t) + b_0 \quad (2.2)$$

Where τ is the reaction time, α, β, γ and b_0 are constants (model parameters) that need to be determined in model calibration. This model is a nonlinear regression model with parameters related to the speed of the pair of vehicles.

2.3.2 Stimulus-Response Model

The majority of car-following models fall in the class of stimulus-response models. The basic formula to describe the stimulus-response behaviour is:

$$\text{Response } (t+\tau) = \text{Sensitivity x Stimulus } (t) \quad (2.3)$$

A stimulus at time *t* together with the driver's sensitivity causes a driver reaction after a reaction time τ. The stimulus is usually represented by the relative velocity (speed difference) of the leading and the following vehicle or the spacing between the two vehicles. The response is represented by the acceleration of the following vehicle.

(a) First GM car-following model

Typical stimulus-response models were studied by a group of researchers at General Motors (GM) (May 1990). The first GM model (Chandler et al. 1958) assumed that the sensitivity term was a constant and the response was in the form of:

$$\ddot{x}_{n+1}(t+\tau) = \alpha \cdot \left[\dot{x}_n(t) - \dot{x}_{n+1}(t)\right] \quad (2.4)$$

Where, α is the sensitivity of the following vehicle that needs to be determined in

experiments or model calibration. This model is a linear model with speed difference as the stimulus. During the model calibration, a wide range of sensitivity values were observed (May 1990).

(b) Second GM car-following model

Realizing that the sensitivity may be different in acceleration and deceleration, the researchers proposed the second GM car-following model using different sensitivity factors for acceleration and deceleration, respectively:

$$\ddot{x}_{n+1}(t+\tau) = \begin{matrix} \alpha_1 \\ or \\ \alpha_2 \end{matrix} \left[\dot{x}_n(t) - \dot{x}_{n+1}(t)\right] \tag{2.5}$$

This is still a linear car-following model with different sensitivity values: α_1 and α_2. The second GM model can be symmetrical or unsymmetrical. A symmetrical model uses the same parameter values in both acceleration and deceleration situations, whereas an unsymmetrical model uses different parameter values in acceleration and deceleration situations. The asymmetric car-following theory was based on an extension of this idea by Herman and Rothery (1965) and Newell (1965).

(c) Third GM car-following model

In the process of improving car-following models, GM researchers developed the third model:

$$\ddot{x}_{n+1}(t+\tau) = \frac{\alpha_0}{[x_n(t) - x_{n+1}(t)]}\left[\dot{x}_n(t) - \dot{x}_{n+1}(t)\right] \tag{2.6}$$

Where, α_0 is a constant. This is a nonlinear car-following model with the sensitivity inversely proportional to the distance between the two vehicles.

(d) Fourth GM car-following model:

The fourth GM car-following model was proposed with the purpose of further improving the sensitivity term by including the speed of the following vehicle in the sensitivity:

$$\ddot{x}_{n+1}(t+\tau) = \frac{\alpha_{l,m} \cdot \dot{x}_{n+1}(t+\tau)}{[x_n(t) - x_{n+1}(t)]^l}\left[\dot{x}_n(t) - \dot{x}_{n+1}(t)\right] \tag{2.7}$$

Again, it is a nonlinear car-following model with more consideration to the sensitivity term.

(e) Generalized GM car-following model

The family of GM's car-following models has evolved with the attempt to improve the description of the sensitivity of the following vehicle. This includes introducing the distance between two vehicles (as in the third model) and the speed of the following vehicle (as in the fourth model) and considering exponents of both speed and distance as in the general form. The general form of stimulus-response model is described below and widely referred to as the Gazis-Herman-Rothery (GHR) model (Gazis et al. 1961).

$$\ddot{x}_{n+1}(t+\tau) = \frac{\alpha_{l,m}[\dot{x}_{n+1}(t+\tau)]^m}{[x_n(t) - x_{n+1}(t)]^l}\left[\dot{x}_n(t) - \dot{x}_{n+1}(t)\right] \tag{2.8}$$

Where, $x_n, \dot{x}_n$ represents position and speed of the leading vehicle, respectively, and $x_{n+1}, \dot{x}_{n+1}, \ddot{x}_{n+1}$ represents position, speed and acceleration of the following vehicle, respectively. *m* is the speed exponent and *l* is the distance headway exponent. By assuming different values of *m* and *l*, several special cases of car-following models can be obtained. In Chapter 3, we will show that, under steady state traffic conditions, the generalized GM car-following model is mathematically related to

several macroscopic speed-density relationships.

The GHR models assume that the follower reacts to small changes in the relative speed. The models also assume that the follower reacts to the actions of the leader, even though the distance to the leader is very large, and that the follower's response disappears as soon as the relative speed is zero. This is obviously different from real-world traffic. These shortcomings can be corrected by either extending the GHR-model with additional regimes, e.g., free driving, emergency deceleration, etc., or by using a psycho-physical model or fuzzy logic-based models.

2.3.3 Intelligent Drive Model

The intelligent drive model (IDM) was developed in the late 1990s (Treiber et al. 1999). It is a microscopic model expressed as a vehicle's acceleration in a nonlinear differential equation:

$$\dot{v} = a \cdot \left[1 - \left(\frac{v}{v_0} \right)^{\delta} - \left(\frac{s^*(v, \Delta v)}{s} \right)^2 \right] \tag{2.9}$$

Where, a is a model parameter that gives the maximum possible acceleration value. δ is a model parameter. v and v_0 are vehicle speed and desired speed, respectively. s and s^* are distance and desired distance to the leading vehicle, respectively. Δv is the speed difference of the pair of vehicles.

The acceleration Equation (2.9) is a superposition of two parts: the acceleration under free flow $a \cdot [s^*(v,\Delta v)/s]^2$ and a deceleration due to braking $a \cdot [1-(v/v^*)^{\delta}]$. The deceleration term depends on the ratio of the desired gap s^* and the actual gap s. The desired gap is given by (Treiber et al.1999):

$$s^*(v, \Delta v) = s_0 + s_1 \cdot \sqrt{\frac{v}{v_0}} + T \cdot v + \frac{v \cdot \Delta v}{2\sqrt{a \cdot b}} \tag{2.10}$$

Where, T is safe time headway, s_0 is the jam distance, s_1 is a distance parameter that can be specified for the model (e.g., s_1=10m). s_1 is also allowed to be set to zero. b is a constant representing a comfortable deceleration value.

The four terms on the right hand side (RHS) of Equation (2.10) are corresponding to the minimum distance, comfortable distance, safe time headway and anticipation, respectively (van der Horst 2011). The desired gap dynamically varies with the speed and the speed difference, representing intelligent driving behaviour.

2.3.4 Optimum Velocity Model

The optimum velocity model (OV) was proposed by Bando and Hasebe (1995) and was based on the idea that each vehicle has its ideal velocity, which depends on the distance from its leading vehicle. The response of the follower is not directly coupled with the speed of the leader, but rather it depends on the deviation with respect to the speed that fits best to the actual following distance. The follower adapts its speed to a certain optimal value (the "optimal velocity"). It was shown that, under certain conditions, small perturbations can be amplified and grow into traffic jams, which can be used to study stop-and-go traffic patterns (Bando and Hasebe 1995). The model is:

$$\ddot{x}_n = a \cdot \left[V(\Delta x_n) - \dot{x}_n \right] \tag{2.11}$$

Where, a is a constant representing driver sensitivity, Δx_n is the space headway between two vehicles and $V(\Delta x_n)$ is the optimal velocity function (desired speed), which is dependent on the headway. In essence, this model still belongs to the

stimulus-response category.

2.3.5 Psycho-Physical/Action Point Models

Another approach to the car-following modelling is based on behavioural thresholds referred to as action points and was first proposed by Michaels (1963). The idea is that it is possible to identify space-time thresholds that trigger different acceleration profile characterizations of a driver. Drivers will react to changes in speed difference or spacing only when these thresholds are reached (Leutzbach, 1988). The evolution of such a concept led to the definition of the psycho-physical models. Psycho-physical models apply to a bi-dimensional space, with axes representing the distance Δx_i and speed difference Δv_i of a vehicle i with respect to the vehicle in front. Such space is divided into several areas, demarcated by the aforementioned action points, corresponding to different driver reactions.

The microscopic simulation package, VISSIM (PTV 2012), uses the psycho-physical driver behaviour model proposed by Wiedemann (1974). This car-following model utilizes a number of boundaries and regimes to describe the longitudinal motion of individual vehicles, as shown in Figure 2.1.

The main concept of this car-following model is that the follower starts to adjust its speed by applying continuous deceleration as it reaches its own perception threshold to a slower lead vehicle. However, the follower cannot exactly determine the speed of the lead vehicle. So, the follower's speed will drop below the lead vehicle's speed until the follower applies slight acceleration after reaching another perception threshold. This will result in an iterative process of acceleration and

deceleration (see the loop in Figure 2.1). There are four different stages of following a lead vehicle (PTV 2012):

(a) Free driving: In this mode, there is no influence of the lead vehicle. The follower travels at its desired speed.

(b) Approaching: In this mode, the follower tries to adapt to the lead vehicle's speed. The follower applies a continuous deceleration so that the speed difference between them is zero when it reaches its desired safety distance.

(c) Following: In this mode, two close vehicles maintain a safe distance, and their relative speed fluctuates around zero. The follower maintains its speed close to the lead vehicle without any conscious acceleration or deceleration.

(d) Braking: In this mode, the relative distance between vehicles falls below a safe distance. This could be a result of a sudden deceleration of the lead vehicle, a third vehicle merges in front of the follower, etc.

2.3.6 Fuzzy Logic-Based Models

Fuzzy-logic-based car-following models (Kikuchi and Chakroborty, 1992) use fuzzy sets as conditions (logic condition sets) that trigger certain driver actions. These sets can then be used in logical rules, such as “the distance is too close,” and “use emergency deceleration,” etc.

In fuzzy-logic models, drivers usually do not know exactly what the relative speed or the spacing is. Instead, they are assumed only to be able to conclude a category of those trigger conditions in the fuzzy sets. The fuzzy sets may overlap one another and in such cases, a probabilistic density function must be used to deduce how the drivers observe the current variables that trigger a certain action. Usually the

logic condition sets are linked to fuzzy output sets via logical operators (such as, "IF," "THEN," "AND," "OR," etc.)

In essence, fuzzy-logic-based models can fall in either the stimulus-response category or the action points class, or even a combination of different models. The advantage of fuzzy-logic-based models is that they can more accurately describe driver behaviour due to the flexibility of option sets. In addition, the assumption that drivers do not know exactly the relative speed or spacing is more realistic to the real-world situation.

2.3.7 Lane-Changing Model

Lane changing refers to the lateral movements of vehicles from one lane to another. It may happen mandatorily at merge and diverge areas, or voluntarily at multi-lane roadways. Near on-ramp or lane-drop areas, merging manoeuvres are one of the direct causes for the overloading of certain lanes and may lead to traffic breakdown (Cassidy and Bertini, 1999). In addition, voluntary lane changing can be the origin of perturbations that may lead to jams in dense and unstable traffic. Although lane-changing models are not as widely studied as car-following models, it is essential to incorporate this mechanism in traffic flow models.

A famous lane-change model is the one by Wiedemann (1974), the principle of which is that drivers try to avoid discomfort in their own lane (for example, the vehicle in front is too slow compared with their desired speed) and seek the speed advantage of other lanes. This desire for lane change leads to a lane change manoeuvre, if the gap in the target lane is sufficient to perform a safe manoeuvre.

Different from car-following, in the lane-changing model, the drivers' behaviour

in the presence of interacting vehicular flows cannot be described as a function of the state of the leading vehicle, but must also take into account the distance and speed of the back and front vehicles on the target lane. Considering lane changing in microscopic models allows for the realization of necessary (mandatory) lane changes at on-ramps or lane closures as well as discretionary lane changes in preparation for passing slower vehicles.

In VISSIM simulation, a rule-based logic was adopted to model the lane-changing behaviour of a driver for lateral movement. VISSIM simulates two types of lane change (PTV 2012):

(a) Necessary lane change that results from route choice,

(b) Free lane change to get more room from the front vehicle and maintain a higher speed.

For both the free and necessary lane changes, when a driver tries to change lanes, the first step that VISSIM checks is the availability of a suitable gap in the target lane.

2.4 Macroscopic Traffic Models

Macroscopic traffic models represent traffic flow in terms of aggregate variables as a function of location (x) and time (t). They describe the dynamics of traffic density $\rho(x, t)$, mean speed $v(x, t)$ and/or flow rate $q(x, t)$.

Two basic equations always hold in all of the macroscopic traffic flow models. One is the conservation equation, which states that the change in number of vehicles on the roadway segment $(x, x + dx)$ during time interval $(t, t+dt)$ is equal to the number of vehicles flowing into that segment minus the number of vehicles flowing out of that segment. That is, vehicles are neither automatically generated nor taken

away on an enclosed section of roadway. This is expressed as a partial differential equation (Gartner el al. 2001):

$$\frac{\partial \rho}{\partial t} + \frac{\partial q}{\partial x} = g(x,t) \tag{2.12}$$

Or as in an integration form:

$$\frac{\partial}{\partial t}\int_{x1}^{x2} \rho(x,t)dx = q(x_1,t) - q(x_2,t) + g(x,t) \tag{2.13}$$

Where, q stands for flow, ρ for density and v for space-mean-speed. g is the generation rate within the road segment (from on-ramps and off-ramps), x and t stands for space and time, respectively.

Another equation is the basic traffic flow equation, namely, flow equals to the density times the space-mean-speed.

$$q = v \cdot \rho \tag{2.14}$$

Equations (2.12) and (2.14) form a system of two independent equations with three unknown variables ρ, v and q. To solve this system, another independent equation is required. The different formulations of the third equation resulted in a series of macroscopic models. In this section, we discuss the two major types of macroscopic traffic models, namely, the first-order traffic models and the second-order traffic models.

First-order traffic models contain a conservation equation: flow equals to the speed multiplied by density and a steady-state speed-density relation. Second-order traffic models have an independent speed dynamics in addition to the first-order models. There are even higher order models than the second-order models, such as conservation of momentum, etc.; however, they are out of the scope of this research

and, therefore, are not discussed here.

2.4.1 First-Order Macroscopic Traffic Models

The most widely used first-order macroscopic traffic model was developed by Lighthill and Whitham (1955), and Richards (1956) independently (LWR model), which is a continuous macroscopic representation of traffic variables. In the LWR model, the speed and/or flow rate are considered as a function of density:

$$v(x,t) = V_e[\rho(x,t)] \tag{2.15}$$

Then,

$$q(x,t) = q_e[\rho(x,t)] = \rho(x,t) \cdot V_e[\rho(x,t)] \tag{2.16}$$

Where, V_e denotes the equilibrium speed. It is a monotonically decreasing function of density. The relationship between density $\rho(x, t)$ and flow $q(x, t)$ is called the fundamental diagram (FD). The flow function is convex with a downward concavity (LeVeque 1992). Since Equation (2.16) does not specify the functional form of the FD, many specific functions have been proposed either from fitting the measured data or from analytical deliberations, or a combination of both.

The solution of the nonlinear Equation (2.12), (2.14) and (2.15) is of the general form as in Equation (2.17) (Gazis 1967), which means that all points are on a straight line with slope v having the same density:

$$\rho(x,t) = F(x - v \cdot t) \tag{2.17}$$

Where, F is an arbitrary function. Equation (2.17) implies that inhomogeneity, such as changes in density of vehicles, propagates along a stream of traffic at a constant speed $V_w = \partial q / \partial \rho$, which is positive or negative with respect to a stationary observer, depending on whether the density is below or above the optimum density

corresponding to maximum q (Figure 2.2). The shockwave speed is expressed in Equation (2.18) and shown in Figure 2.2.

$$V_w = \frac{q_b - q_a}{\rho_b - \rho_a} \tag{2.18}$$

Within the category of first-order traffic models, it is worthwhile to mention the cell transmission model (CTM), which is widely used in macroscopic simulation.

CTM is a first-order discrete macroscopic model developed by Daganzo (1994a, 1994b). In this model, the roadway is discretized into small segments (cells) of uniform length. One cell may have at most one on-ramp and one off-ramp. The length of cells is set equivalent to the distance vehicles travel in one clock tick (time interval or time step) in light traffic (free flow). Under light traffic, all vehicles in a cell can be assumed to advance to the next cell in each time interval. The model functions based on the law of vehicle conservation: the number of vehicles in cell *i* at the next time step *(k+1)* equals to the number of vehicles currently in cell *i*, plus the inflow from the upstream cell *(i-1)* to cell *i* and minus the outflow to the downstream from cell *i* to cell *(i+1)* between the time indexes *k* and *(k+1)*. That is:

$$n_i(k+1) = n_i(k) + y_{i-1}(k) + r_i(k) - y_i(k) - s_i(k) \tag{2.19}$$

Where, *i* is the cell index and *k* is the time index. $n_i(k)$ is the number of vehicles in cell *i* at time index *k*. $y_i(k)$ is the number of vehicles flowing out from cell *i*. $r_i(k)$ is the number of vehicles flowing into cell *i* from the on-ramp. $s_i(k)$ is the number of vehicles flowing out from cell *i* at the off-ramp.

The number of vehicles from one cell advancing to the next cell is controlled by boundary conditions, which guarantee the number of vehicles that can flow to

downstream cells. CTM has three boundary conditions: at the upstream of the first cell, an adequate number of vehicles can flow into the first cell. Downstream of the last cell has sufficient capacity to allow vehicles to move away from the last cell. Between any pair of adjacent cells, the number of vehicles can flow to the next cell subject to the constraint:

$$y_i(k) = \min\{v_f \cdot \rho_c,\ Q_i, w_{i+1} \cdot (\rho_{\max} - \rho_c)\} \tag{2.20}$$

Where, v_f is the free flow speed, ρ_c, ρ_{max} is the critical and jam density, respectively. w_{i+1} is the shockwave speed in the immediate downstream cell.

The average speed is determined by a steady-state speed-density relationship, assuming all traffic speeds abide by this relationship at all traffic states. This is the exact the same assumption as in the LWR model. In fact, it was shown that the CTM model is a discrete approximation to the LWR model (Daganzo 1994). Originally, the FD corresponding to the speed-density relationship in CTM was assumed to be a trapezoidal shape, but it was further adapted to accommodate any continuous, piecewise differentiable FDs, such as a triangular fundamental diagram.

If we divide Equation (2.19) by the length of the cell, we obtain the density of the cells on both sides of the equation. Therefore, CTM is essentially a density dynamics model that evolves with boundary conditions.

CTM is often used for real-time traffic control purposes. For example, it was used for arterial traffic signal control (Lo 2001; Almasri and Friedrich 2005) and for freeways with ramp metering control (Gomes et al. 2008; Zhang and Levinson 2010; Gomes and Horowitz 2006). Very low computational effort is required to predict traffic variables in real-time with the CTM (Gomes et al. 2008).

First-order traffic models, such as LWR, can capture most of the important traffic flow characteristics, such as formation and dissipation of shock waves. However, they have several deficiencies (Gartner et al. 2001). In first-order models, it is assumed that traffic flow will instantly adapt to the flow-density relationship. The shocks in the model have no transition region. In reality, drivers always need some reaction time to adjust to traffic conditions. Another serious shortcoming of the model is its inability to model traffic instability (Zhang 1998). In LWR model, drivers can always manage to change speeds in the right amount of time and with the right magnitude that traffic disturbances can be absorbed completely. In reality, drivers respond to traffic events with a time delay. As a result, some disturbances in traffic may become magnified as they propagate through the traffic stream and cause traffic breakdowns. To address these deficiencies, several methods have been proposed (Zhang 2001). One common approach of improvement is to adopt multi-branches of the FD (may be discontinuous) for different traffic conditions, such as free flow, acceleration flow and deceleration flow. Another key approach is to adopt additional dynamics to form higher-order models, especially second-order models, which are more and more widely used in both theoretical analysis and simulation.

2.4.2 Second-Order Macroscopic Traffic Models

The first-order macroscopic traffic models are characterized by a single dynamical partial differential equation for flow and density. The speed of these models does not possess any independent dynamics, since they solely rely on a static speed-density relationship. Such models can describe traffic breakdowns at bottlenecks due to

insufficient capacity and the propagation of shockwaves due to traffic state changes. From a microscopic point of view, the instantaneous vehicle speed adaptations imply unbounded acceleration, which is unrealistic and masks traffic phenomena that results from driver behaviour, such as delayed response to traffic conditions, because any disturbance can be absorbed by infinite speed adaptation. In reality, finite speed reaction and adaptation are the main factors leading to growing traffic waves, capacity-drop phenomena and to traffic flow instabilities. Consequently, LWR models cannot describe these observations.

Due to the shortcomings of first-order models, many efforts were made to extend the LWR theory to capture instabilities in practical traffic flow. One direction leads to higher order traffic models by coupling the conservation of flow with an independent acceleration equation that provides speed dynamics of traffic flow. Such a speed dynamics describes the local acceleration as a function of speed and/or density as well as other possible exogenous factors.

As early as the mid-1950s, Lighthill and Whitham (1955), in their seminal work on kinematic waves, suggested that higher order terms be added to account for some traffic properties, such as inertia and anticipation, and they proposed a general form of a motion equation:

$$\frac{\partial q}{\partial t} + c\frac{\partial q}{\partial x} + T\frac{\partial^2 q}{\partial t^2} - D\frac{\partial^2 q}{\partial x^2} = 0 \tag{2.21}$$

Where, c is the traffic wave speed, T is the inertia time constant for adjustment of speed, D is the coefficient of diffusion. The authors did not provide an independent speed dynamics for this model.

Payne (1971) recognized that delayed response and anticipation behaviour of drivers are fundamental in macroscopic traffic flow models if one wishes to account for traffic instability. Payne approximated individual driver behaviour:

$$v[(t+\tau), x(x, t+\tau)] = V_e\{\rho[t, x(t)+\Delta x]\} \tag{2.22}$$

This equation expresses that the speed of an individual vehicle after a reaction time τ is equal to the equilibrium speed corresponding to the density some distance Δx downstream. After repeatedly applying linear Taylor approximations to Equation (2.22) and using the density at the midway of two vehicles to represent the space headway, the following dynamic equation for the average speed was obtained (Payne 1971):

$$\frac{\partial v(x,t)}{\partial t} + \underbrace{v(x,t)\frac{\partial v(x,t)}{\partial x}}_{convection} = \underbrace{\frac{V_e[\rho(x,t)] - v(x,t)}{\tau}}_{relaxation} - \underbrace{\frac{c_0^2(x,t)}{\rho(x,t)} \cdot \frac{\partial \rho(x,t)}{\partial x}}_{anticicipation} \tag{2.23}$$

$$c_0^2(x,t) = -\frac{1}{\tau}\frac{dV_e[\rho(x,t)]}{d\rho} \tag{2.24}$$

Where c_o is the anticipation factor. A similar model was also proposed independently by Whitham (1974). Therefore, the above model is also referred to as the PW model.

The left-hand side of Equation (2.23) is the total time derivative of the average speed, that is, the time evolution of the average speed as it would be seen by an observer travelling with equilibrium speed V_e. There are three different terms in the equation:

- Convection: The convection term accounts for the change in average speed at a location due to vehicles leaving or arriving with different speeds. It is the transportation of speed along with the flow.

- Relaxation: The relaxation term describes the adaptation of drivers to the density-dependent equilibrium speed, which corresponds to the homogeneous steady state in the flow. It is assumed that an equilibrium speed $V_e(\rho)$ exists, but the traffic state can deviate from the equilibrium. When other influences (reflected by the convection and anticipation terms) are small, traffic tends to relax to the equilibrium speed.
- Anticipation: The anticipation term accounts for the fact that traffic approaching a spatial change of traffic conditions (reflected by the spatial variation of density) adapts its speed to these conditions.

Based on Equation (2.23), Payne (1979) developed a macroscopic model in discrete form; this model is widely used in freeway simulations. The speed dynamics of the well-known macroscopic simulation model, METANET (Messmer and Papageorgiou 1990) is also based on Equation (2.23). We will discuss the METANET model in Chapter 4 of this dissertation.

Payne's modelling approach solves two drawbacks of the LWR model. Firstly, the relaxation term allows traffic to deviate from the equilibrium speed when the spatial conditions are not homogeneous. When driving into or out of congestion, this mechanism results in average speeds (and also flow rates) that deviate substantially from the equilibrium state. Secondly, the anticipation term reflects the reaction of drivers to the traffic conditions in front of them. As a result, the second-order models avoid the zero reaction time as in LWR model and the acceleration or deceleration of traffic need not be instantaneous. Since drivers tend to react to the spatial variation of density, discontinuous behaviour is avoided.

With explicit speed dynamics, it is possible to adjust the speed for more complex traffic conditions and not be restricted by the FD, which represents the static equilibrium condition. Higher order models built on the behavioural assumptions of car-following models are more suitable for traffic modelling and simulation because first-order models rely only on the FD to describe speed evolution, which does not have the flexibility to adjust to complex traffic conditions, such as stop-and-go traffic, traffic hysteresis, dual capacity phenomenon, etc.

Payne-type models were criticized by Daganzo (1995) mainly for not being anisotropic and because they may predict negative flow and speed under some circumstances. In reaction to this criticism, Aw and Rascle (2000), Zhang (1998, 2002) and Liu et al. (1998) proposed variant models or improvements that avoid the identified flaws. Because of the ability to describe uniform flow and stop-and-go waves without discontinuities (Orosz et al. 2010), the second-order models are widely used in traffic state prediction and macroscopic simulation.

In addition to the PW model, there are other second-order models not subject to all of the criticisms. From different approaches, Prigogine and Herman (1971) as well as Phillips (1979) proposed traffic models in which the continuity equation for the density and the acceleration equation were derived from kinetic principles. Since the density equation is also based on conservation law, it is the same as in the first-order models. The acceleration equation is expressed as (Phillips 1979):

$$\frac{\partial v}{\partial t} + v\frac{\partial v}{\partial x} = \frac{V_e(\rho) - v}{\tau} - \frac{1}{\rho}\frac{\partial P_e}{\partial x} \tag{2.25}$$

Where, P_e is the "traffic pressure." This term was adopted from gas-kinetic

considerations where the pressure term describes a purely kinematic (statistical) effect of speed variance without a single vehicle accelerating or braking. In traffic flow models, the pressure term is also referred to as the anticipation, which reflects the driver's anticipation to downstream traffic conditions and can be expressed as:

$$P_e = \rho \cdot \Theta_e = \upsilon \cdot \Theta_0 (1 - \rho / \rho_{\max}) \geq 0 \tag{2.26}$$

Where, Θ_e is the density dependent speed variance and Θ_0 is a positive constant (model parameter) that needs to be estimated.

Kerner and Konhauser (1993) introduced a viscous term into the acceleration equation for the purpose of smoothing discontinuous traffic, while at the same time considering the speed variance as a positive constant Θ_0. The model read as:

$$\frac{\partial v}{\partial t} + v\frac{\partial v}{\partial x} = \frac{V_e(\rho) - v}{\tau} - \frac{\Theta_0}{\rho} \cdot \frac{\partial \rho}{\partial x} + \frac{\eta_0}{\rho} \cdot \frac{\partial^2 v}{\partial x^2} \tag{2.27}$$

η_0 is the viscosity coefficient. A similar model, but with a density-dependent viscosity coefficient was proposed by Lee el al. (1998), which has similar model properties as Kerner and Konhauser (1993).

The viscosity term is also called diffusion in macroscopic models (i.e., the second-order derivatives with respect to space). The intention of using this term is to smooth sharp transitions and shocks. From a statistical physics perspective, "a diffusion term in the continuity or acceleration equation is a consequence of erratic microscopic motion components (random motion of particles described by their velocity variance which is proportional to the temperature of physical systems)" (Treiber and Kesting 2013).

Aw and Rascle (2000) derived a second-order model to avoid the negative speed

of PW model, as criticized by Daganzo (1995), which also includes a density-dependent traffic pressure coefficient. The model can be written as:

$$\frac{\partial v}{\partial t} + v\frac{\partial v}{\partial x} = \frac{V_e(\rho) - v}{\tau} + \rho \cdot p'(\rho) \cdot \frac{\partial v}{\partial x} \tag{2.28}$$

Where, $p(\rho)$ is the density-dependent traffic pressure coefficient.

Zhang (1998, 1999, 2000, 2001 and 2002) derived several acceleration equations with different properties. The Zhang (2002) model can be written as:

$$\frac{\partial v}{\partial t} + v\frac{\partial v}{\partial x} = \frac{V_e(\rho) - v}{\tau} - \frac{[\rho \cdot V'(\rho)]^2}{\rho} \cdot \rho_x \tag{2.29}$$

Where, $[\rho V'(\rho)]^2$ is the traffic sound speed. In this model, the traffic sound speed will never be faster than the actual traffic speed and, thus, avoids the back traveling problem, as in Payne's model, as criticized by Daganzo (1995).

In another study, Zhang (2003) derived a full viscous model from a car-following model:

$$\frac{\partial v}{\partial t} + [v + 2\beta \cdot c(\rho)]\frac{\partial v}{\partial x} = \frac{V_e(\rho) - v}{\tau} - \frac{c^2(\rho)}{\rho} \cdot \frac{\partial \rho}{\partial x} + \mu(\rho)\frac{\partial^2 v}{\partial x^2} \tag{2.30}$$

Where, β is a parameter. μ is the viscosity coefficient. c is the traffic sound speed. This model not only includes relaxation, convection and anticipation components, but it also has a traffic diffusion term and viscous properties.

All above models share similar properties. They all account for the driver's delayed response (relaxation) and convection. The difference lies in the functional form of anticipation or traffic pressure and the viscous term (higher order derivative of speed or density with respect to space). The models can be generalized as:

$$Vehicle\ \ Acceleration = \mathrm{Re}laxation + Convection + Anticipation(or\ \mathrm{Pr}essure) + Diffusion(or Viscous term) \tag{2.31}$$

An example of this model framework is provided by Treiber and Kesting (2013), as Equation (2.32):

$$\frac{\partial v}{\partial t} + v\frac{\partial v}{\partial x} = \frac{V_e(\rho) - v}{\tau} - \frac{\Theta_0}{\rho}\cdot\frac{\partial \rho}{\partial x} + \frac{\eta_0}{\rho}\cdot\frac{\partial^2 v}{\partial x^2} \tag{2.32}$$

2.5 On-Ramp and Off-Ramp Modelling

Compared to the modelling of traffic flow on road sections, there are much fewer theoretical modelling studies done on freeway ramps. To study the effects of lane-drops and on-ramps on freeway traffic flow, traffic simulation has been carried out by Munjal et al. (1971) as well as Munjal and Pipes (1971). From the law of conservation of vehicles, ramps are modeled by adding a source term into the continuum equations, as in Equation (2.12). The generation term represents the number of vehicles from on-ramps and/or to off-ramps on the mainline roadway. To model speed dynamics, some authors, such as Cremer and Ludwig (1986), Papageorgiou et al. (1989), Michalopoulos et al. (1993), Liu et al. (1996) and Bellemans (2003), introduced a traffic friction term into the speed dynamics of Payne's (1971) model to account for the impact of the merging and/or diverging flow as well as weaving on the speed of the mainline traffic flow. The acceleration equation for the interrupted traffic flow by ramps is described below:

$$\frac{\partial v}{\partial t} + v\frac{\partial v}{\partial x} = \frac{V_e(\rho) - v}{\tau} - C(\rho)\cdot\frac{\partial \rho}{\partial x}_x + F(x,t) \tag{2.33}$$

In above equation, *F(x, t)* is the traffic friction. So far, there is no conclusion as to

what functional form can most accurately represent the ramp impact on the speed dynamics. Different formulations of the traffic friction have resulted in various models (Cremer and Ludwig 1986, Papageorgiou et al. 1989, Michalopoulos et al. 1993, Liu et al. 1996 and Bellemans, 2003).

2.6 Traffic Jam Modelling

In the literature, traffic congestion and breakdown may appear as different names, such as traffic jam, stop-and-go traffic state, stop-and-go wave (SGW), or wide moving jam (Kerner 2009). These terms are often used interchangeably even though differences exists between their definitions. Based on the frequency, traffic congestion can be classified into two types: recurrent or non-recurrent. Recurrent congestion happens regularly during peak hours in specific locations along roadways. Recurrent congestion may be caused by high traffic demand that comes close to or exceeds freeway capacity, or it may be caused by road geometry constraints that reduce freeway operation speed and capacity, such as merge and diverge areas, weaving sections, lane drops, work zones with lower speed limits and change of roadway geometry with steep grade and/or sharp curves with reduced operation speed. Non-recurrent congestion is unpredictable and can be caused by different incidents, such as traffic accidents, disabled vehicles, slow moving trucks, adverse weather conditions and possibly roadway or roadside debris that disrupts smooth traffic flow states.

Traffic breakdown does not occur in free flow conditions. One of the premises for its occurrence is that the traffic density is sufficiently high so that an internal or external disturbance will be amplified and propagate backwards to upstream.

Understanding the mechanism of traffic breakdown, the formation, evolution and propagation processes, can help researchers to develop traffic models for efficient traffic control and application of ITS to mitigate traffic congestion.

2.6.1 Modelling Approaches

There are several different explanations on the generation and evolution of stop-and-go traffic conditions. Treiterer and Taylor (1966) evaluated vehicle trajectories based on aerial photographs and clearly identified the stop-and-go traffic states from the space-time diagram. However, since they did not find a reason for the formation of stop-and-go traffic, they refer to it as a "phantom traffic jam," (Helbing 2001, Flynn et al. 2009) which is formed spontaneously. Other researchers tried to explain the phenomenon using both microscopic and macroscopic approaches. According to Daganzo (2002a) and Ahn et al. (2007), traffic breakdown can be attributable to a lane change on a roadway with high density, and there are physical reasons for the formation of traffic jams. Cassidy et al. (2001) and Daganzo (2002b) suggested that due to a "pumping effect" at on-ramps, small traffic oscillations may grow in amplitude. Polus et al. (2002) and Daganzo et al. (1999) claimed that, under high traffic densities combined with lane/speed changes, traffic breakdown can occur spontaneously. Yeo et al. (2009) used the asymmetric microscopic driving behaviour theory to explain the generation and evolution of the stop-and-go traffic phenomenon. All of these explanations are driving behaviour-related at the microscopic level.

Banks (2002) suggested that traffic breakdown can be explained by either microscopic flow instability or macroscopic flow instability. The former may occur in the car-following process, while the latter occurs if the fluctuation of traffic density is

large enough to cause significant and irreversible decreases in speed. On the macroscopic level, stop-and-go wave is an observable phenomenon that consists of a sequence of traffic jams separated by small groups of free or less congested traffic. SGWs propagate upstream with a speed around 15 to 20 km/h (Orosz et al. 2010). Kerner (2009) established the three-phase traffic theory, namely free flow, synchronized flow and wide moving jams. Traffic breakdown can emerge spontaneously in a synchronized flow phase from growing, narrow moving jams. Various mathematical models were developed to describe the formation and evolution of traffic jams on a macroscopic level (Berthelin et al. 2008, Laval and Leclercq 2010). However, the direct application of complicated mathematical models on freeway traffic control is not straightforward. In a later part of this dissertation, efforts on applying macroscopic simulation to re-produce traffic jams is presented and discussed. The macroscopic simulation model can be used for online ramp metering (RM), variable speed limit (VSL) control and active traffic management (ATM) on freeways.

Although there are several different explanations on stop-and-go traffic states, mathematical modelling is far more complicated than a heuristic explanation. This is due to the fact that on a microscopic level, individual drivers have different driving behaviours with different reaction and action times. On a macroscopic level, the aggregation and averaging of vehicle characteristics may mask some fundamental causes for the traffic jam phenomenon, especially for jams that do not happen at a very high density. A summary of both approaches on traffic modelling are provided in Table 2.2 and discussed in the following sub-sections.

2.6.2 Traditional Car-Following Models

Microscopic traffic models describe longitudinal car-following and lateral lane-changing behaviour of individual vehicles. They model the behaviour of individual vehicles in relation to the roadway and other vehicles in the traffic flow. As the traffic flow increases, the distance between vehicles becomes short and the interaction between a follower and its leader becomes strong. Stop-and-go traffic is an unstable traffic state caused by the strong interaction of a leading vehicle and its followers. Herman et al. (1959) analyzed two types of stability in the car-following mechanism: local stability, which is concerned with the car-following behaviour of two vehicles, and asymptotic stability, which is regarding a line of vehicles consisting of one leading vehicle and an infinite number of following vehicles. The product *(C)* of the reaction time *(Δt)* and sensitivity value *(α)* was used as a parameter corresponding to traffic stability (Herman et al. 1959).

$$C = \alpha \cdot (\Delta t) \tag{2.34}$$

Based on the *C* value, local stability was divided into three regions (Herman et al. 1959): non-oscillatory, damped oscillatory and increased oscillatory. Asymptotic stability was divided into two regions: damped oscillatory and increased oscillatory. Traffic stability in relation to the value of *C* is summarized in Table 2.3.

If the *C* value is high, traffic oscillation will increase and may theoretically lead to rear-end collisions. The following drivers may increase braking to avoid colliding with the vehicle immediately in front of them. This action will amplify the oscillation, which propagates backwards causing stop-and-go waves, or a full stop of vehicles. If the wave meets a region of low traffic density, the oscillation may be absorbed and

the traffic may recover to normal operation conditions, if the density is sufficiently low.

2.6.3 Asymmetric Traffic Theory

The fact that drivers have different behaviours leads to asymmetry in deceleration and acceleration, as proposed by Newell (1965) that in a congested traffic regime, vehicles' deceleration and acceleration will follow different curves. In another study, Yeo and Skabardonis (2009). used two curves, an acceleration curve (A-curve) and a deceleration curve (D-curve), to define different traffic states, namely, free flow, acceleration, stationary, coasting and deceleration, as shown in Figure 2.3 and Figure 2.4. Quasi-stationary and coasting states exist between A and D curves. The difference between quasi-stationary and coasting states is that in the quasi-stationary state, both traffic speed and spacing are close to constant with only minor adjustments, which leads to minor local oscillation. In the coasting state, vehicles have an almost constant speed, but vehicle spacing fluctuates based on the acceleration and deceleration of the consecutive vehicles. For any reason, if the traffic states deviate from the stationary or coasting regions enveloped by D and A curves, the following vehicles will either accelerate or decelerate until they return to the stationary or coasting states.

In car-following, the following drivers may not be able to accurately judge the speed of the leaders. In addition, different drivers have different habits. These lead them to either under-react or overreact to the speed and spacing change of the leaders.

Stop-and-go traffic states often happen in a deceleration state, in which the spacing *(s)* between vehicles are short and the under-reaction or overreaction can

generate a disturbance to traffic flow. There are several consequences of under-reaction and overreaction of a follower: when the leading vehicle (1st vehicle) starts to decelerate, under-reaction of the following vehicle (2nd vehicle) means that the 2nd vehicle does not decelerate enough, resulting in a higher speed than the 1st vehicle and the spacing becomes shorter. The 2nd vehicle needs additional deceleration to resume appropriate spacing. This additional braking usually results in a lower speed than the 1st vehicle and causes a backward propagating shockwave. Similar shockwaves can be generated by the consecutive following vehicles and the effect can be amplified, resulting in stop-and-go traffic conditions. On the other hand, overreaction of the 2nd vehicle means that the 2nd vehicle over decelerates, causing a sharp speed reduction and a backwards propagating shockwave. In congested traffic, the shockwave may trigger stop-and-go traffic conditions. The backward propagating stop-and-go wave may dissipate only if it meets traffic states with large spacing, which can absorb the stop-and-go wave.

Both traditional car-following models and the asymmetry theory can reasonably explain the generation of a traffic breakdown mechanism. However, they do not provide a numerical property of SGW, such as wave speed, length of congestion, etc., as these are macroscopic concept of traffic states.

2.6.4 Traffic Disturbance Model

Nagal et al. (2003) studied traffic jam stability by separating the density into two parts: a constant and some disturbances. This is similar to a stochastic macroscopic model. Nagal's theory is summarized below (Nagel et al 2003). Assuming:

$$\rho(x,t) = \bar{\rho} + \tilde{\rho}(x,t) \tag{2.35}$$

Then, the conservation Equation (2.12) becomes:

$$\partial_t \tilde{\rho}(x,t) + [q'(\bar{\rho}) + \tilde{\rho}(x,t)] \cdot q''(\bar{\rho}) \cdot \partial_x \tilde{\rho}(x,t) = 0 \tag{2.36}$$

After omitting terms with a higher order of , the above equation reduces to:

$$\partial_t \tilde{\rho}(x,t) + q'(\bar{\rho}) \cdot \partial_x \tilde{\rho}(x,t) = 0 \tag{2.37}$$

If we consider the disturbance as a wave,

$$\tilde{\rho}(x,t) = Ae^{i(kx-\omega t)} \tag{2.38}$$

Then, a wave solution can be obtained:

$$\tilde{\rho}(x,t) = Ae^{ik(x-ct)} \tag{2.39}$$

Where, $c = q'(\bar{\rho})$.

Equation (2.39) means that a disturbance in traffic density is superimposed on homogeneous constant density of $\bar{p}$ and travels with the speed of $c = q'(\bar{\rho})$.

If $\bar{\rho}$ is high and the disturbance is large enough, the density wave may grow and cause traffic breakdown or stop-and-go traffic states.

2.6.5 Phase Transition Model

In both the LWR and Payne models, the assumption that the average speed be uniquely determined by traffic density is reasonable in free flow traffic conditions, but it may be inadequate to describe congested flows. In congested traffic, density *(ρ)* no longer uniquely determines the speed *(v),* or equivalently the flow *(q),* of the vehicles. Scattered data points on flow-density plots are very common in congested traffic. Figure 2.5 shows the flow-density plot from a loop detector on I-80 freeway in California, which shows that in a congested traffic regime, there may be several possible ρ values corresponding to a q value. In addition, a capacity drop can also be identified from the plot.

Colombo (2002 a, b) proposed a two-regime model, free flow and congested flow, respectively, to account for the scattering of the density-flow relationship. In the free flow regime, the model was composed of a conservation law with a speed-density relationship exactly the same as in the LWR model. In a congested flow regime, the density ρ and the flow q are treated as two independent variables and the model is composed of a conservation law, which is an equation expressing that the speed is a function of both density and flow, and an evolution equation of flow. Free-to-congested flow phase transitions are defined based on speed, density and flow values. Colombo's phase transition model is expressed as (Colombo 2002a):

For free flow:

$$\begin{cases} \partial_t \rho + \partial_x(\rho v) = 0 \\ v = v(\rho) \end{cases} \tag{2.40}$$

For congested flow:

$$\begin{cases} \partial_t \rho + \partial_x(\rho v) = 0 \\ \partial_t q + \partial_x[(q - q^*)v] = 0 \\ v = v(\rho, q) = \frac{q}{\rho}(1 - \frac{\rho}{\rho_{max}}) \end{cases} \tag{2.41}$$

Where ρ_{max} is jam density. The parameter $q^* > 0$ is introduced to account for the change of flow due to shockwaves. In Colombo's model, both the two-regime phenomenon and the impact of the shockwave on flow are explicitly represented. However, there are no explicit speed dynamics, and driver's delayed response is not included in the model.

2.6.6 Macroscopic Simulation of Traffic Jams

As discussed in previous sections, first-order macroscopic models can describe the formation and dissipation of shock waves. The shockwaves will be formed at each interface of different traffic states and propagate backward or forward depending on

the traffic states at both sides of the interface. For stop-and-go traffic, multiple shockwaves will be formed and interact during the propagation. However, the first-order macroscopic models do not have a closed form of equation to describe the speed change due to the interaction of shockwaves, because the first-order models do not have independent speed dynamics.

In the second-order macroscopic models, independent speed dynamics can adjust the speed depending on the local traffic conditions and, thus can describe stop-and-go traffic. This can be applied in simulation with the second-order macroscopic models as well. In macroscopic simulation, the roadway is divided into discrete segments, and the time is discretized into short time intervals (time step). Each road segment is a homogeneous unit, in which the number of lanes remains unchanged. On- and off-ramps are always located at the beginning and end of the segments, respectively. The concept of road segment index *(i)* and state variables, density *(ρ),* speed *(v)* and flow *(q)*, are illustrated in Figure 2.6. The aggregated traffic flow variables are defined for each segment and updated each time step. Based on spatial and temporal discretization, the traffic state variables (speed, density and flow) are calculated at each time step k for each segment i.

It should be noted that to simulate traffic jams, an independent and appropriate speed dynamics is required to catch the sudden change of traffic states. A distinct advantage of macroscopic simulation over analytical models is its flexibility of model representation. Analytical models use one or several closed form equations to represent traffic state evolution over time and space, but they have difficulty to describe the transition between different traffic states. Simulation models can not only

use the same model representations as in analytical models, but they can also combine other models in simulation. For example, they can add fuzzy logic in the model or use multiple conditions and choices in the model, so that an appropriate set of equations can be chosen to calculate traffic states for a particular traffic condition.

2.7 Summary

This chapter provided an overview on the state-of-the-art of traffic flow models with a special focus on microscopic car-following models and second-order macroscopic models. The traffic models were reviewed with respect to their categories in terms of level of detail, scale of independent variables, nature of independent variables and model representations. Various microscopic car-following model formulations, ideologies and properties were discussed. On the macroscopic level, both first- and second-order models and their respective advantages and disadvantages were presented. Even though higher order macroscopic traffic models have been established from different perspectives, they share many similar properties, such as delayed response of drivers and their anticipation of downstream traffic conditions. While microscopic traffic models track each individual vehicle movement and its relation with other vehicles during all time horizons, macroscopic traffic models consider the average value of the aggregated traffic flow properties and ignore the interaction between individual vehicles. Therefore, microscopic traffic models are ideally suited for off-line simulation to evaluate detailed local traffic operations, while macroscopic traffic models are more suited for large-scale, network-wide operation and online control purposes. These reviews provide comprehensive background information for establishing the relationship between microscopic

car-following models and macroscopic traffic models, which will be presented in Chapter 3, as well as model extension, modification and improvements discussed in the following chapters.

Chapter 2 also discussed various theories and methods on traffic jam (stop-and-go traffic) modelling from both a microscopic and macroscopic approach. These include traditional microscopic car-following models, asymmetric traffic theory, traffic disturbance model, phase transition model as well as first-order and second-order macroscopic models. The mechanisms of stop-and-go waves, causes, generation, propagation, and absorption were discussed. It can be concluded that the stop-and-go traffic state is formed by three conditions: high traffic demand, insufficient road capacity and traffic disturbance. When traffic density is sufficiently high, a small disturbance in the traffic flow can be amplified, causing a stop-and-go wave propagating backwards, and the disturbance can be explained by microscopic car-following and lane-changing behaviour.

Table 2.1 Category of traffic models

Criteria	Model categories
Level of detail	Sub-microscopic, microscopic, mesoscopic and macroscopic models
Scale of independent variables	Discrete, continuous models
Nature of independent variables	Deterministic, stochastic models
Model representation	Analytical, simulation models

Table 2.2 Summary of traffic jam modelling techniques

Traffic Models	Traffic Jam Modelling Principles
Car-following	Local and asymptotic stability
Asymmetric traffic theory	Different behaviour of acceleration, deceleration and speed adjustment
Traffic disturbance	Disturbance causing backward propagating density wave
Phase transition	Two traffic flow regimes
First-order macroscopic	Shockwave
Second-order macroscopic	Speed dynamics considering driver reaction and anticipation, etc.
Macroscopic simulation	May combine different models

Table 2.3 *C* value vs local and asymptotic stability (Herman et al. 1959)

C Value	0 ~ 0.37	0.37 ~ 1.57	1.57 ~ 2.0
Local Stability	Non-Oscillatory	Damped Oscillatory	Increased Oscillatory

C Value	0 ~ 0.50	0.50 ~ 2.0
Asymptotic Stability	Damped Oscillatory	Increased Oscillatory

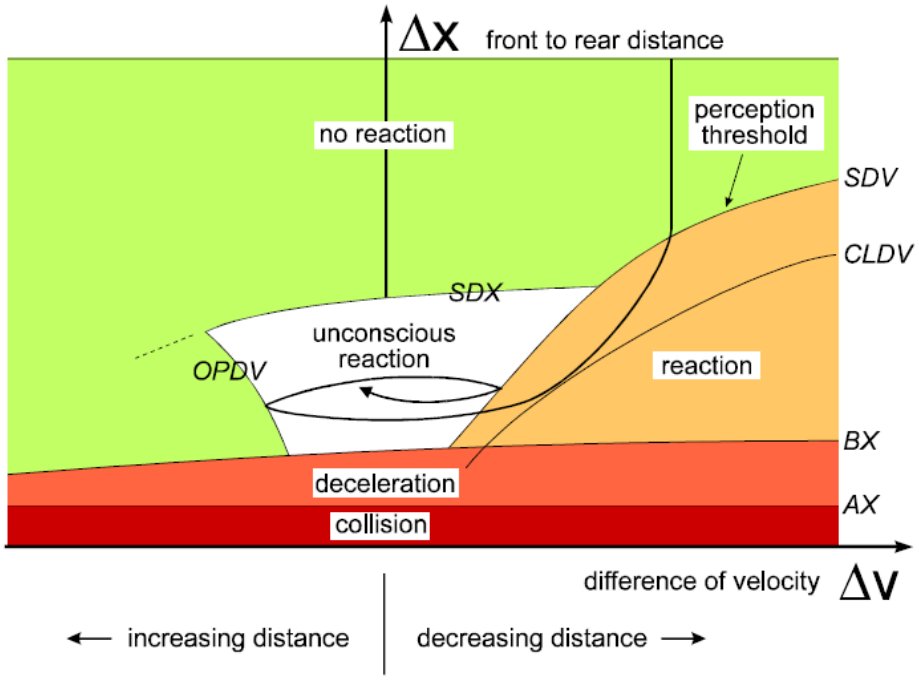

Figure 2.1 Psycho-physical car-following model (Wiedemann 1974 and PTV 2012)

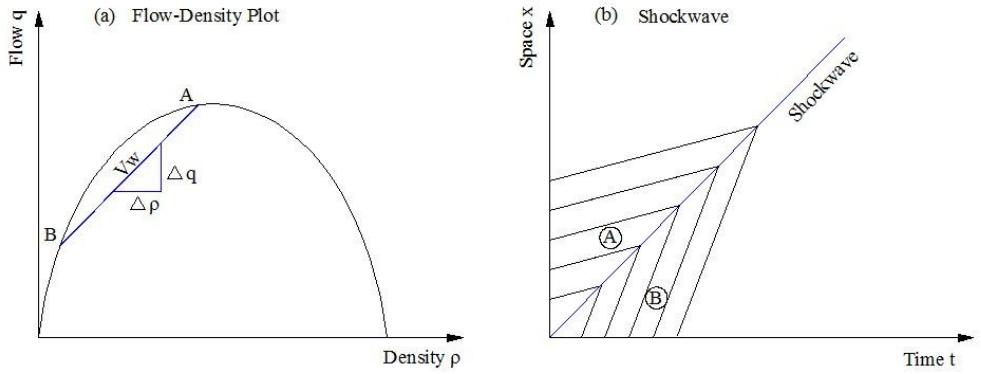

Figure 2.2 Shock wave formations resulting from the solution of the conservation equation

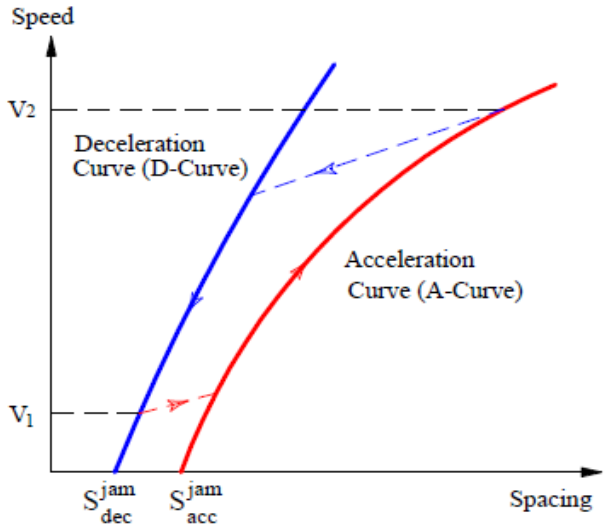

Figure 2.3 Acceleration and deceleration curves (Newell 1965)

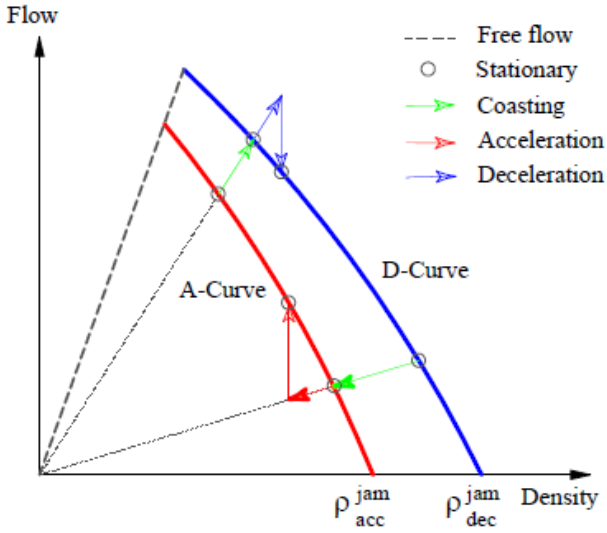

Figure 2.4 Traffic States diagram (Yeo and Skabardonis 2009)

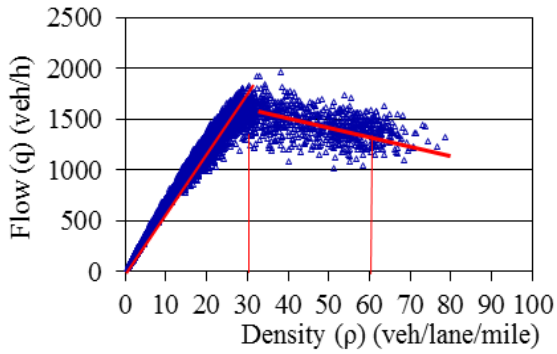

Figure 2.5 Flow-density recorded on I-80 freeway

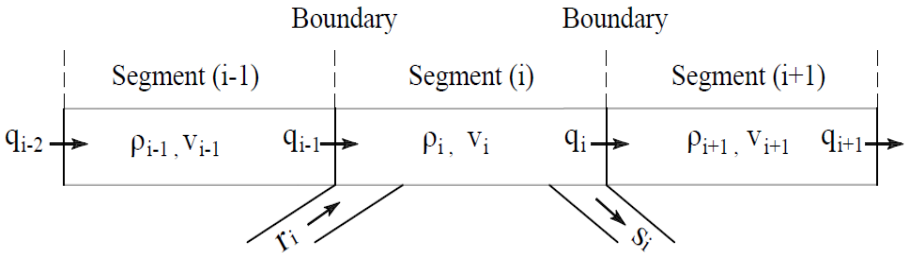

Figure 2.6 Discretization of a roadway section

Chapter 3 Relationship between Microscopic and Macroscopic Traffic Models

3.1 Introduction

Early macroscopic traffic models were developed without any link to microscopic models. Instead, they were formulated either by fitting observed flow-speed data (Greenshields 1935, Adams 1936, Greenberg 1959, Underwood 1961, Gartner et al. 2001) or by analogy to fluid mechanics (Lighthill and Whitham 1955, Richards 1956). Deriving macroscopic traffic models from microscopic traffic models and establishing the links between them has been realized since the late 1950s (Gazis et al.1959, Newell 1961). Gazis et al (1959, 1961) showed that, under steady-state traffic conditions, some car-following models can be related to a particular shape of the equilibrium flow-density relationships. This phenomenon was further studied by many other researchers (May and Keller 1967, May 1990, Ni 2013). Some of the studies considered driver behaviour (Gazis et al 1961, Payne 1971, Zhang 2002, Zhang 2003, Treiber and Helbing 2003), such as delayed response, from which more complex macroscopic models can be developed.

There are also microscopic car-following models derived from macroscopic models (Castillo 1996, Aw et al 2002). Most of these studies were based on a long single-lane section of roadway traffic. As a different approach, there is a branch of traffic flow theory on macroscopic models based on the statistical description of individual vehicle's behaviour, represented by the work of Prigogine and Herman

(1971). More recently, some models have tried to combine several approaches (hybrid models), for instance by embedding a microscopic model into a macroscopic one (Tampère et al 2003).

With further studies, it was found that the relationships between the various model classes are more complex than it appears due to several reasons. First, microscopic traffic flow models are strictly empirical, with a weak connection to experimental reality if traffic conditions are changed. The parameters used in microscopic models vary widely even from very similar test settings. This means that there might be several different microscopic formulations to describe the same traffic flow pattern. Second, actual traffic is non-homogeneous and traffic conditions vary along a section of roadway. It is difficult to use one microscopic differential equation to describe various traffic flow patterns along a section of roadway. Furthermore, most microscopic-macroscopic links are made under the assumption of steady-state traffic conditions and may be no longer valid under dynamic traffic states. Derivations of macroscopic models from microscopic ones, or vice versa, include additional assumptions or simplifications, which generally make the final model quite different from the initial one.

Even with these difficulties, more understanding of the relationship between microscopic and macroscopic models is beneficial in several ways. For one thing, some microscopic models can be used to study the impact of disturbance on traffic stream, traffic instability and the stop-and-go traffic phenomenon (Bando and Hasebe 1995, Berg 2000). On the other hand, many observed traffic patterns can be explained from individual driver behaviour's perspective (Kim 2002).

The objective of this chapter is to further explore the relationship between microscopic car-following models and macroscopic models to provide insight on traffic modelling.

3.2 From Microscopic to Macroscopic Models

Most of the studies on microscopic modelling are focused on car-following models. These studies modeled traffic flows at the individual vehicle level, tracking each driver's interaction with the leader. The models are often formulated as a differential equation for each vehicle's movement with time and location as their variables. Macroscopic models study the aggregated behaviour of many vehicles. They are often formulated as continuum equations with traffic speed, density and flow rate as variables with respect to location and time. As both types of the models describe the motion of vehicles on the roadway and have common variables (even though some of the variables may be on different scales), mathematical relationships may be established through the manipulation of closely related variables.

There are several ways to derive macroscopic models from microscopic ones:

(1) The first approach is by integrating microscopic traffic models (Gazis et al.1959, Shladover et al. 2010).

Most of the microscopic car-following models are in the form of the acceleration of a follower in relation to the leader(s). On a macroscopic level, flow is often characterized by a steady-state, speed-density relationship. This leads to the consideration of integrating a microscopic acceleration equation to obtain a macroscopic speed function. This extends the study range from two (or a couple more vehicles, if considering several vehicles ahead) to a long section of road.

The integration of a set of dynamic equations must follow a set of rules: the boundary conditions of the microscopic models (for example, maximum acceleration and deceleration, absolute minimum headway, etc.) should correspond to the macroscopic model (such as free flow speed, maximum density, etc.), based on which the constants emerging from the integration process can be identified. Opposite to the integrating process, microscopic traffic models can be obtained by taking derivatives of macroscopic traffic models. There is no constant that needs to be specified when taking derivatives. In this way, derivation can be taken on any macroscopic speed-density relationship. From mathematics, we know that taking derivatives is much easier than integration, as by integrating a function, a class of functions with extra constants needs to be identified and many complicated functions cannot be integrated. On the other hand, taking derivatives will result in the disappearance of some constants.

(2) Models can also be derived based on an intuitive understanding of traffic behaviour, such as delayed response of drivers to the traffic conditions ahead. Representative works in this direction are the models by Payne (1971) and Zhang (2003). Through taking the total derivation of speed with respect to time and using Taylor series expansion with respect to time and space, a separate speed dynamics (acceleration equation) can be obtained. Each component of the acceleration can be linked to the physical explanation of driver behaviour, such as relaxation, anticipation and speed convection, between fast and slow drivers. Some of the derived macroscopic models may have viscous components (Zhang

2003) and diffusion terms (Kerner and Konhauser 1993). Due to this independent acceleration equation, traffic speed is allowed to deviate from the equilibrium speed and those models can describe more complex traffic conditions (Zhang 1998).

(3) Models can be derived from a gas-kinetic approach (Prigogine and Herman 1971, Paveri-Fontana, 1975, Helbing, 1996, Wagner el at. 1996). This approach assumes that the individual vehicle is similar to gas particles and, therefore, can be modeled from gas-kinetic principles. Instead of modelling each vehicle with an independent differential equation, kinetic models are based on the construction of a distribution of individual behaviour laws (such as speed distribution function) to obtain the probability of finding a vehicle with a certain velocity in a given position on the road at time *t*. The averages over the distribution function are represented by macroscopic variables (such as speed, density and flow). Therefore, we can obtain macroscopic models from a kinetic equation by means of an average procedure.

In the following sections, we discuss several macroscopic models derived from popular car-following models.

3.2.1 Safe Distance Model

Pipe's (1953) safe distance model, presented in Chapter 2, is probably one of the earliest and simplest car-following models. We can re-write the model as:

$$h = (\frac{\dot{x}_{n+1}}{1.47 \times 10}) \cdot l_n + l_n = l_n \cdot [1 + \alpha \cdot \dot{x}_{n+1}] \tag{3.1}$$

It is a linear car-following model with the speed of the leading vehicle as its argument.

Under steady-state uniform traffic conditions, all vehicles have the same length and properties: $l_n=l$, and individual vehicle speed is the same as traffic flow speed v. Assuming density ρ is the reciprocal of headway, then:

$$\rho = \frac{1}{h} = \frac{1}{l \cdot (1 + \alpha \cdot \dot{x}_{n+1})} \tag{3.2}$$

Solving for the speed, we have the steady-state speed-density relationship corresponding to Pipe's model:

$$v = \frac{1}{\alpha}\left(\frac{\rho_{\max}}{\rho} - 1\right) \tag{3.3}$$

Where $\rho_{max}=1/l$ is the maximum density (bumper to bumper). This model has several properties: $\rho \rightarrow \rho_{max}$, $v \rightarrow 0$ *and* $\rho \rightarrow 0$, $v \rightarrow \infty$. These properties are similar to the properties that the Greenshields (1935) model has. Boundary conditions have to be specified as density $\rho \rightarrow 0$ to make the model meaningful for light traffic.

3.2.2 Intelligent Drive Model (IDM)

The IDM is the interpolation of two opposite driver actions: acceleration and deceleration. Direct integration in the model is difficult because it includes irrational part in the formula. However, the model can be simplified under the assumption of an equilibrium traffic state, at which the IDM can be solved analytically. Under equilibrium, both speed difference and individual vehicle acceleration are zero. All drivers intend to keep a speed-dependent equilibrium space to the front vehicle. This equilibrium space is given by Treiber et al. (1999, 2000):

$$s_e(v) = s^*(v,0)[1 - (\frac{v}{v_0})^{\delta}]^{-\frac{1}{2}} \tag{3.4}$$

For some special cases, $s_0=s_1=0$ and $\delta=1$, the equilibrium speed of traffic flow can be solved from Equation (3.4) (Treiber et al. 1999):

$$v_e(s) = \frac{s^2}{2v_0T^2}\left(-1+\sqrt{1+\frac{4T^2v_0^2}{s^2}}\right) \tag{3.5}$$

Where, T is safe time headway, v_0 is the desired speed, s is the distance between vehicles under equilibrium traffic states.

3.2.3 Generic Car-Following Model

The derivation of macroscopic models from microscopic ones, or vice versa, relies heavily on the speed-density relationships, as shown in the safe distance model. There are also other studies establishing macroscopic traffic models from the specification of microscopic models for individual driving behaviour. Zhang (2003) derived a macroscopic model from a generic microscopic one:

$$v_n(t+\tau) = F_*[x_{n-1}(t)-x_n(t)] + G_*[v_{n-1}(t)-v_n(t)] \tag{3.6}$$

Where, τ is the adaptation time of the following vehicle. F_* is a function of headway, which increases with the distance between the n^{th} vehicle and its leader, the $(n\text{-}1)^{th}$ vehicle. G_* is a function of the speed difference between the two vehicles. It is a monotonically increasing function.

The function F_* is related to the equilibrium speed V_e, which is a function of headway or density with the assumption that density equals to the inverse of the headway. That is:

$$F_* = F_*[x_{n-1}(t)-x_n(t)] = V_e[\rho(t,x(t)+\Delta x] \tag{3.7}$$

The function G_* is assumed to be related to the strength of traffic viscosity. After using Taylor expansion on both sides of Equation (3.6), Zhang (2003) obtained a

macroscopic model:

$$\frac{\partial v}{\partial t}+[v+2\beta\cdot c(\rho)]\frac{\partial v}{\partial x}=\frac{V_e(\rho)-v}{\tau}-\frac{c^2(\rho)}{\rho}\cdot\frac{\partial \rho}{\partial x}+\mu(\rho)\frac{\partial^2 v}{\partial x^2} \tag{3.8}$$

Where, β is a constant parameter, $\mu(\rho)$ is the viscosity coefficient, which depends on traffic density, $c(\rho)$ is the traffic sound speed, which also depends on traffic density. Equation (3.8) is a viscous model, which is the general form of almost all well-known continuum models (Zhang 2003).

3.2.4 Stimulus-Response Models

Stimulus-response models are most widely used in theoretical analysis, among which the GM family models had been studied for more than half a century.

(a) First and second GM car-following models

The first and the second GM model (Chandler et al. 1958) are both linear car-following models and can be expressed as:

$$\ddot{x}_{n+1}(t+\tau)=\binom{\alpha 1 or}{\alpha 2}\cdot\left[\dot{x}_n(t)-\dot{x}_{n+1}(t)\right] \tag{3.9}$$

The only difference between them is that in the second GM model, different sensitivity was used for acceleration and deceleration, respectively.

Integrating both sides, we have:

$$v=\alpha_0\cdot(\frac{1}{\rho})+C \tag{3.10}$$

Using boundary conditions $\rho\rightarrow\rho_{max}$, $v\rightarrow 0$, we get the constant C=-$\alpha_0/\rho_{\max}$.

So, the corresponding macroscopic model is:

$$v=\alpha_0\cdot(\frac{1}{\rho}-\frac{1}{\rho_{\max}})=\frac{\alpha_0}{\rho_{\max}}(\frac{\rho_{\max}}{\rho}-1) \tag{3.11}$$

This model has the same structure as the model derived from Pipe's (1953) safe

distance model. This is understandable as both of them are simple linear car-following models. The model has the property: $\rho \to \rho_{max}$, $v \to 0$ *and* $\rho \to 0$, $v \to \infty$. This means that it does not apply to light traffic, or traffic speed has to be defined for very light traffic conditions.

(b) Third GM car-following model

The third GM model (Gazis et al. 1961) is a nonlinear car-following model:

$$\ddot{x}_{n+1}(t+\tau) = \frac{\alpha_0}{[x_n(t) - x_{n+1}(t)]}\left[\dot{x}_n(t) - \dot{x}_{n+1}(t)\right] \tag{3.12}$$

Integrating both sides with respect to t, we have:

$$\dot{x}_{n+1}(t) = \alpha_0[\ln(x_n - x_{n+1})] + C_1 \tag{3.13}$$

That is:

$$v = \alpha_0 \ln(\frac{1}{\rho}) + C_1 \tag{3.14}$$

With boundary conditions and with mathematical substitution: $\rho \to \rho_{max}$, $v \to 0$ and $\rho \to 0$, $v \to v_f$, we obtain the corresponding macroscopic speed-density equation:

$$v = v_f \ln(\frac{\rho_j}{\rho}) \tag{3.15}$$

This is the Greenberg (1959) model describing the macroscopic relationship between speed and density of the field observed data.

The above equation can also be derived through a different approach. A nonlinear car-following model can be expressed as (Gazis 1959):

$$M\ddot{x}_{n+1}(t) = \lambda_1[\frac{(\dot{x}_n - \dot{x}_{n+1})}{x_n - x_{n+1})}]_{t-\tau} \tag{3.16}$$

Where, M is the mass of the vehicle and λ_1 is a sensitivity coefficient. Integrating both sides with respect to t, we get:

$$M\dot{x}_{n+1}(t) = \lambda_1 \ln[L^{-1}(x_n - x_{n+1})]_{t-\tau} \tag{3.17}$$

Where, L is the length of each vehicle measured from the bumper of the leading vehicle to the bumper of the following vehicle. For a steady state traffic, the time lag τ disappears and individual vehicle speed can be replaced by traffic flow speed, yielding:

$$v = \frac{\lambda_1}{M} \ln[\frac{L^{-1}}{x_n - x_{n+1}}] = v_f \ln(\frac{\rho_{\max}}{\rho}) \tag{3.18}$$

Which is the same as Equation (3.15). In equation (3.18), $v_f=\lambda_1/M$ is the free flow speed, $\rho_{max}=L^{-1}$ is the jam density and $\rho=(x_n-x_{n+1})^{-1}$ is the traffic density.

Conversely, differentiate Equation (3.18) with respect to t with the use of the relationship $\rho=(x_n-x_{n+1})^{-1}$ and the assumption of $\tau=0$ leads immediately to Equation (3.16).

(c) Fourth GM car-following model

The fourth GM car-following model was proposed with the purpose of improving the sensitivity term by including the speed of the following vehicle in the sensitivity. The model reads:

$$\ddot{x}_{n+1}(t+\tau) = \frac{\alpha \cdot \dot{x}_{n+1}(t+\tau)}{[x_n(t) - x_{n+1}(t)]}[\dot{x}_n(t) - \dot{x}_{n+1}(t)] \tag{3.19}$$

Again, it is a nonlinear car-following model.

Following similar integration procedures, we can obtain the corresponding macroscopic speed-density relation as:

$$v = (\frac{C}{\rho})^{\alpha} \tag{3.20}$$

Where, C is an integration constant that cannot be determined from boundary conditions for this specific case.

Most of the macroscopic speed-density relations $v=f(\rho)$ are based on field data observations, such as Greenshields (1935) and Greenberg (1959). It is noted that none of the models fit from field data correspond to the fourth GM model.

(d) Fifth GM car-following model

The fifth GM model is a generalized car-following model. It is regarded as the general form of a stimulus-response model, described as (Gazis et al. 1961):

$$\ddot{x}_{n+1}(t+\tau)=\frac{\alpha_{l,m}[\dot{x}_{n+1}(t+\tau)]^{m}}{[x_n(t)-x_{n+1}(t)]^{l}}\left[\dot{x}_n(t)-\dot{x}_{n+1}(t)\right] \tag{3.21}$$

Where, $x_n, \dot{x}_n$ represents position and speed of the leading vehicle, respectively $x_{n+1}, \dot{x}_{n+1}, \ddot{x}_{n+1}$ represents position, speed and acceleration of the following vehicle, respectively. m is the speed exponent and l is the distance headway exponent. By assuming different values of m and l, several special cases of stimulus-response car-following models can be obtained, as shown in Table 3.1 (May 1990, Brackstone and McDonald 1999, Ni 2013).

The generalized speed-density equation proposed by May (1990) does not include the case (either m or l=1), and the range of l, and m is l>1 and 0≤m<1. We shall discuss these cases to complete the mathematical derivations.

Case 1, m=1, l≠1:

Under this case, the corresponding car-following model is:

$$\ddot{x}_{n+1}(t+\tau)=\frac{\alpha_{l,1}[\dot{x}_{n+1}(t+\tau)]}{[x_n(t)-x_{n+1}(t)]^{l}}\left[\dot{x}_n(t)-\dot{x}_{n+1}(t)\right] \tag{3.22}$$

Under steady-state and uniform traffic flow conditions, the model can be simplified: the time lag τ can be dropped, the individual vehicle speed can be replaced by traffic flow speed *v* and the relationship that headway equals to the inverse of density applies.

Integrating both sides with respect to *t*, and with a boundary condition that when $\rho=0$, $v=v_f$, the integration constant can be determined. We can obtain the speed-density equation:

$$v = e^{\left(\frac{\alpha}{1-l}\cdot\rho^{l-1}\right)} - e^{\left(\frac{\alpha}{1-l}\cdot\rho_m^{l-1}\right)} \tag{3.23}$$

With similar procedures and assumptions, we can obtain the speed-density equation for the case $m\neq1$, $l=1$, and $m=1$, $l=1$ respectively.

Case 2, $m\neq1$, $l=1$:

The speed-density equation is:

$$v^{1-m} = \alpha(m-1)\ln(\frac{\rho}{\rho_m}) \tag{3.24}$$

Case 3, $m=1$, $l=1$:

The speed-density equation is:

$$v = (\frac{C}{\rho})^{\alpha} \tag{3.25}$$

This is exactly the same speed-density function obtained from the fourth GM car-following model. The constant *C* cannot be determined from boundary conditions for this specific case.

To the best of the author's knowledge, no speed-density functions have been tested by field observed data for the three cases discussed above.

With the special cases of m and l values discussed, we can now derive the general macroscopic speed-density equation from the generalized GM car-following model (Equation 3.21).

For the case $l \neq 1$, $m \neq 1$, let

$$\alpha_{l,m} = \frac{l-1}{1-m} \cdot \frac{v_f^{1-m}}{\rho_m^{l-1}} \tag{3.26}$$

The generalized GM car-following model becomes:

$$\ddot{x}_{n+1}(t+\tau) = \frac{l-1}{1-m} \cdot \frac{v_f^{1-m}}{\rho_m^{l-1}} \cdot \frac{[\dot{x}_{n+1}(t+\tau)]^m}{[x_n(t) - x_{n+1}(t)]^l} [\dot{x}_n(t) - \dot{x}_{n+1}(t)] \tag{3.27}$$

Under steady-state uniform flow, the time lag τ can be dropped, the individual vehicle speed can be replaced by traffic flow speed v, and the relationship that headway equals to the inverse of density applies.

Integrating the car-following equation with respect to time t, we get:

$$v^{1-m} + C_1 = -\frac{v_f^{1-m}}{\rho_m^{l-1}} \cdot \rho^{l-1} + C_2 \tag{3.28}$$

C_1 and C_2 are integration constants. Applying the boundary conditions, $\rho=0$, $v \rightarrow v_f$ and $\rho=\rho_m$, $v \rightarrow 0$, we get

$$v^{1-m} = v_f^{1-m} \left[1 - \left(\frac{\rho}{\rho_m} \right)^{l-1} \right] \tag{3.29}$$

This is the general macroscopic speed-density equation proposed by May (1990). From the derivation, we also get the sensitivity equation in the generalized GM car-following model presented in Equation (3.26).

In fact, there is an alternative way to derive the generalized macroscopic speed-density function from Equation (3.21), as discussed by Bryne (1980).

Under steady-state traffic conditions, Equation (3.21) can be re-arranged as:

$$\frac{dv}{v^m} = \frac{\alpha ds}{s^l} \tag{3.30}$$

Where s is the spacing from bumper to bumper: $s=x_n(t)-x_{n+1}(t)$.

The solution to Equation (3.30) is given by Gazis et al. (1961) in a general form:

$$F_m(v) = a \cdot G_l(\rho) + b \tag{3.31}$$

Where a and b are constants, while m and l are model parameters.

Equation (3.31) is a macroscopic model describing the relationship between v and ρ. Left hand side (LHS) F_m is a function of speed with speed exponent m, while right hand side (RHS) G_l is a function of density, with parameters a and b as well as distance exponent l. Many well-known macroscopic speed density relations fall into this formula, as listed in Table 3.2.

As can be seen from Table 3.2, free flow speed, optimum (or critical) density and maximum density are common parameters used in the speed functions. The traffic flow speed is modeled as a monotonous decreasing function of traffic density.

3.2.5 Discussion on the Relationship between Microscopic and Macroscopic Models

Most of the above-discussed microscopic-macroscopic relationships and derivations are based on the assumption that density equals to the inverse of headway: $\rho=1/h$. However, this relationship between the headway and density is debatable from a microscopic perspective, especially for non-homogeneous traffic. In strict mathematical terms, this relationship may be subject to more detailed scrutiny. An example was provided by Berg et al. (2000) under the situation that vehicles are

placed at non-equal distances. For example, suppose a set of identical cars are positioned along a section of road at x=1,2,4,8, . . ., 2^{n-1}. The n^{th} car is placed at the position y. Then, the headway of the car placed at position x is $h=x$. Now we calculate the total number of vehicles on the section *[1~y]*.

First, we consider the discrete case, for n cars, the total distance headway is:

$$\sum headway = 1 + 2 + 4 + \cdots + 2^{n-1} = 2^n - 1 \tag{3.32}$$

Which equals to the interval length *(y-1),* i.e.:

$$2^{n-1} - 1 = y - 1 \tag{3.33}$$

Solving the equation, we get the number of cars placed in the interval *[1,y]:*

$$n = \log_2 y \tag{3.34}$$

However, using the relationship that density equals to the inverse of headway, we extend the density to a continuous domain. The number of vehicles *(m)* placed in the interval *[1~y]* is:

$$m = \int_1^y \frac{1}{x} dx = \log_e y \tag{3.35}$$

Obviously, $n>m$.

It also shows that as $y \to \infty$, $m \to n$. This means that, for a very long section of road and homogeneous vehicles, the approximation of density by reversing the distance headway is appropriate.

In fact, for an arbitrary length of road, density can be defined as:

$$\int_{x_i}^{x_{i+1}} \rho(x) dx = 1 \tag{3.36}$$

The headway is $h=x_{i+1}-x_i$, and the mathematical relationship between distance headway and density is (Berg et al 2000):

$$\int_{x_i}^{x+h(x,t)} \rho(x',t) dx' = \int_0^{h(x,t)} \rho(x+y,t) dy = 1 \tag{3.37}$$

Berg et al (2000) expanded the second integral in powers of *y* and integrated it to obtain the asymptotic series:

$$h\rho + \frac{1}{2!}h^2\rho_x + \frac{1}{3!}h^3\rho_{xx} + \cdots\cdots = 1 \tag{3.38}$$

Solving for headway *h*, we have:

$$h \approx \frac{1}{\rho} - \frac{\rho_x}{2\rho^3} - \frac{\rho_{xx}}{6\rho^4} + \frac{\rho_x^2}{2\rho^5} + \cdots\cdots \tag{3.39}$$

Berg et al (2000) assumed that on the RHS of each term is of a smaller order of magnitude than the one preceding it, which is equivalent to the assumption that changes in traffic density occur over the distance of several vehicle lengths.

The first term on the RHS of Equation (3.39) represents the often-used relationship between headway and density. The second term is similar to the anticipation terms in Payne's (1971) model as it contains the change of density along the roadway. It is also similar to the pressure term in the gas-kinetic model. The third term is the diffusion term, which is the second-order derivative of density with respect to space.

We can use this approximation in a car-following model similar to the optimum velocity model:

$$\ddot{x}_n = \frac{1}{\tau} \cdot \left[V(h\ ) - \dot{x}_n \right] \tag{3.40}$$

Where, τ is the reaction time, *h* is the space headway and *V(h)* is the headway-dependent desired speed.

Use three terms of the RHS of Equation (3.39), the desired speed can be expressed as:

$$V(h) = V(\frac{1}{\rho} - \frac{\rho_x}{2\rho^3} - \frac{\rho_{xx}}{6\rho^4}) \tag{3.41}$$

Using Taylor expansion to the RHS and taking $[-\rho_x/(2\rho^3)-\rho_{xx}/(6\rho^4)]$ as a small headway increment, we have:

$$V(h) = V(\frac{1}{\rho}) + V'(\frac{1}{\rho})(-\frac{\rho_x}{2\rho^3} - \frac{\rho_{xx}}{6\rho^4}) \tag{3.42}$$

Let us set:

$$V(\frac{1}{\rho}) = V_e(\rho) \tag{3.43}$$

Then,

$$V'(\frac{1}{\rho}) = -\rho^2 \cdot V_e'(\rho) \tag{3.44}$$

Taking full derivatives of the LHS of Equation (3.40) and combining it with Equation (3.42), (3.43) and (3.44), we obtain the acceleration equation in the second-order model:

$$v_t + \underbrace{v \cdot v_x}_{convection} = \underbrace{\frac{[V_e(\rho) - v]}{\tau}}_{relaxation} + \underbrace{\frac{V_e'(\rho)}{2 \cdot \tau \cdot \rho} \cdot \rho_x}_{anticicipation} + \underbrace{\frac{V'_e(\rho)}{6 \cdot \tau \cdot \rho^2} \cdot \rho_{xx}}_{diffusion} \tag{3.45}$$

This is a second-order macroscopic model that is very similar to Kerner and Konhauser model (1993). The RHS of this model can be interpreted as relaxation, anticipation and diffusion or viscosity term.

If we use two terms of the RHS of Equation (3.39), and the same procedures presented above, we can directly obtain Payne's model (1971), as shown in Equation (3.46). It was also found that Payne's assumption that headway equals to the

reciprocal of the density at a location midway between two vehicles is equivalent to using the two terms of the RHS of Equation (3.39).

$$v_t + \underbrace{v \cdot v_x}_{convection} = \underbrace{\frac{[V_e(\rho) - v]}{\tau}}_{relaxation} + \underbrace{\frac{V_e'(\rho)}{2 \cdot \tau \cdot \rho} \cdot \rho_x}_{anticicipation} \tag{3.46}$$

If we directly use the relationship that headway equals to the inverse of the density in Equation (3.40), we can obtain the acceleration equation:

$$v_t + \underbrace{v \cdot v_x}_{convection} = \underbrace{\frac{[V_e(\rho) - v]}{\tau}}_{relaxation} \tag{3.47}$$

This model contains only relaxation and convection components. This means, slightly changing the headway-density relationship will result in different macroscopic models.

Let us turn to Payne's model (1971) as it is closely related to the macroscopic simulation models used in this research. Payne derived four acceleration equations from two different car-following models: a linear car-following model and a delayed response car-following model.

(1) The first way Payne derived an acceleration equation was from a linear car-following model with the minimum distance *d*:

$$\dot{x}_{n+1}(t+T) = \lambda\left[x_n(t) - x_{n+1}(t) - d\right] \tag{3.48}$$

After the reaction time *T*, the vehicle is at the location *[x+T·v(x,t)]* with the speed:

$$\dot{x}_{n+1}(t+T) \to v\left[x + T \cdot v(x,t),\ t+T\right] \tag{3.49}$$

Through Taylor's expansion on the LHS in *T*, we have:

$$\dot{x}_{n+1}(t+T) \to \left[v(x,t) + T\frac{dv}{dt}(x,t) + O(T^2) \right] \tag{3.50}$$

Omitting the higher order value $O(T^2)$ and using the full derivative, we get:

$$\frac{dv}{dt} = v_t + vv_x \tag{3.51}$$

Combing Equations (3.48) and (3.51) and using the relationship that density equals to the inverse of headway, we get the acceleration equation corresponding to the linear car-following model (3.48):

$$\frac{dv}{dt} = -\frac{1}{T}(v - \frac{\lambda}{\rho} + \lambda \cdot d) \tag{3.52}$$

This model includes $\boldsymbol{\lambda}$ and d and it is not often used in the application.

(2) The second acceleration equation Payne derived was from a linear car-following model without the minimum distance d:

$$\dot{x}_{n+1}(t+T) = \lambda[x_n(t) - x_{n+1}(t)] \tag{3.53}$$

Instead of using the relationship that density equals to the inverse of headway, Payne used the inverse of the density at a location midway between two vehicles to approximate the headway, i.e.:

$$x_n(t) - x_{n+1}(t) \to 1/\rho[x + 1/2\rho(x,t), t] \tag{3.54}$$

Following the same procedures as above, we get:

$$v + T \cdot \frac{dv}{dt} = \lambda(\frac{1}{\rho} - \frac{\lambda}{2\rho^3}\rho_x) \tag{3.55}$$

Which can be expressed as:

$$\frac{dv}{dt} = -\frac{1}{T}(v - \frac{\lambda}{\rho} + \frac{\lambda}{2\rho^3}\rho_x) \tag{3.56}$$

Alternatively, if we use a different headway-density relationship, taking the first two

terms from the RHS of Equation (3.39):

$$x_n(t) - x_{n+1}(t) \to \frac{1}{\rho} - \frac{\rho_x}{2\rho^3} \tag{3.57}$$

Putting Equation (3.57) into (3.53), we get exactly the same model as (3.55).

If we use,

$$x_n(t) - x_{n+1}(t) \to \frac{1}{\rho} \tag{3.58}$$

The resulting model will be:

$$\frac{dv}{dt} = -\frac{1}{T}(v - \frac{\lambda}{\rho}) \tag{3.59}$$

If we use the first three terms of the headway-density relationship in Equation (3.39), then the acceleration equation is:

$$v + T \cdot \frac{dv}{dt} = \lambda(\frac{1}{\rho} - \frac{\lambda}{2\rho^3}\rho_x - \frac{\rho_{xx}}{2\rho^4}) \tag{3.60}$$

This model contains the traffic diffusion term. This means that, using different headway-density relationships will generate different acceleration equations. The more components used from a headway-density approximation, the more terms will be in the acceleration equation.

(3) The third way Payne (1971) derived the acceleration equation is from a car-following model expressed as:

$$\frac{dv}{dt} = -\frac{1}{T}[v - v_e(\rho)] \tag{3.61}$$

Payne also used the inverse of density at the location midway between the two vehicles to approximate vehicle spacing $[x_n(t)-x_{n+1}(t)]$ as in Equation (3.54). Following a similar expansion, we have:

$$\frac{dv}{dt} = -\frac{1}{T}[v - v_e(\rho) - \frac{u_e'(\rho)}{2\rho}\rho_x] \tag{3.62}$$

Combined with the full derivative of speed *[(dv/dt)=v_t+$v \cdot v_x$]*, we get:

$$v_t = \frac{1}{T}[v_e(\rho) - v] - vv_x + \frac{1}{T} \cdot \frac{u_e'(\rho)}{2\rho}\rho_x \tag{3.63}$$

This is the widely used form of the second-order model with relaxation, convection and anticipation terms. Note that the structure of Equation (3.63) is the same as Equation (3.46).

(4) The fourth way Payne derived acceleration was from a more general form of the car-following model to derive a speed dynamics:

$$\frac{dv}{dt} = -\frac{1}{T}[v - v_e(\rho) + g(\rho, \rho_x)] \tag{3.64}$$

Using the full derivatives of speed for the LHS, the speed dynamics becomes:

$$v_t + vv_x = -\frac{1}{T}[v - v_e(\rho) + g(\rho, \rho_x)] \tag{3.65}$$

Applying finite difference method to both sides, we get:

$$v_j^{n+1} = v_j^n + \frac{\Delta t}{T}[v_e(\rho_j^n) - v_j^n] + \frac{\Delta t}{\Delta x}v_j^n \cdot [v_{j-1}^n - v_j^n] - \frac{1}{T}g(\rho_j^n, \frac{(\rho_{j+1}^n - \rho_j^n)}{\Delta x}) \tag{3.66}$$

Note that in this fourth way, Payne did not provide a specific function form for the density gradient term.

A direct application of the relationship between microscopic and macroscopic models is a derivation of the second-order macroscopic model in discrete form from a linear car-following model. The speed dynamics is (Payne 1971, 1979):

$$v_i(k+1) = v_i(k) + \frac{T}{\tau}\{V[\rho_i(k)] - v_i(k)\} + \frac{T}{L_i} \cdot v_i(k) \cdot [v_{i-1}(k) - v_i(k)] - \frac{\eta \cdot T}{\tau \cdot L_i} \frac{\rho_{i+1}(k) - \rho_i(k)}{\rho_i(k)} \tag{3.67}$$

This speed dynamics is used in many freeway simulation and online traffic controls (Messmer and Papageorgious 1990, Kotsialos et al. 2002, Hegyi et al. 2005a,b, Carlson et al. 2010). *)*. It is noted that Equation (3.67) was derived with forward finite difference method for density derivative, backward finite difference method for speed derivative, assuming density and speed were continuous functions. The function form may change if other finite difference methods are used.

3.3 From Gas-Kinetic Theory

Kinetic models are based on the construction of a distribution of individual behaviour laws, such as a speed or density distribution function (*f*) to obtain the probability of finding a vehicle with a certain velocity (*u*) in a given position *(x)* on the road at time (*t*). The averages over the distribution function are represented by macroscopic variables (such as speed, density, and flow). Therefore, we can obtain macroscopic models from a kinetic equation by means of an average procedure.

The number of vehicles in the system is obtained by integrating the distribution function (*f)* over a section of road:

$$N(t) = \iint f(x,t,u)du\,dx \tag{3.68}$$

The relation between the microscopic measure of the distribution function (*f*) and macroscopic measure of traffic density (ρ) is established through the integration of the distribution function:

$$\rho(x,t) = \int f(x,t,u)du \tag{3.69}$$

The flow and speed are obtained by

$$q(x,t) = \int v \cdot f(x,t,u)du \tag{3.70}$$

$$u(x,t) = \frac{q(x,t)}{\rho(x,t)} \tag{3.71}$$

where v is the average speed.

Due to the paired interaction of vehicles, the evolution of the distribution function with respect to time and space abides by the balance principle (Piccoli and Tosin 2011). That is

$$\frac{\partial f}{\partial t} + v\frac{\partial f}{\partial x} = J[f] \tag{3.72}$$

where $J[f]$ is an operator acting on the distribution function f, describing the interactions and their effects on the states of the vehicles. Different specification of $J[f]$ will result in different models.

Integrating Equation (3.72), and then combining with Equation (3.69), (3.70), and (3.71), we can obtain the macroscopic mode expressed as the following (Piccoli and Tosin 2011):

$$\frac{\partial \rho}{\partial t} + \frac{\partial}{\partial x}(\rho u) = 0 \tag{3.73}$$

3.4 From Macroscopic to Microscopic Models

As previously discussed, if we take derivatives of a macroscopic speed-density relationship, we can get an average acceleration of an individual vehicle. Macroscopic traffic models describe the collective behaviour of drivers, the speed of which is often expressed as a function of traffic density. Microscopic models

describe individual vehicle movement, which is often expressed as differential equations. Take the Drake (1967) model as an example, the macroscopic speed-density model is:

$$v = v_f \cdot e^{-\frac{1}{2}(\frac{\rho}{\rho_0})^2} \tag{3.74}$$

Where, ρ_0 is the optimum density. Equation (3.74) is equivalent to:

$$\ln v = \ln v_f - \frac{\rho^2}{2\rho_0^2} \tag{3.75}$$

For steady-state traffic, each vehicle has the same properties. Taking derivatives on both sides and using the relationship $h=1/\rho$, we have

$$\ddot{x}_{n+1}(t) = \frac{\dot{x}_{n+1}(t)}{\rho_0^2} \frac{[\dot{x}_n(t) - \dot{x}_{n+1}(t)]}{[x_n(t) - x_{n+1}(t)]^3} \tag{3.76}$$

Which is a nonlinear car-following model that is very similar to the GM family of car-following models.

Following similar procedures and assumptions, we can derive the generalized GM car-following model from May's (1990) generalized speed-density relationship:

$$v^{1-m} = v_f^{1-m}\left[1 - \left(\frac{\rho}{\rho_m}\right)^{l-1}\right] \Rightarrow \tag{3.77}$$

$$\ddot{x}_{n+1}(t+\tau) = \frac{l-1}{1-m} \cdot \frac{v_f^{1-m}}{\rho_m^{l-1}} \cdot \frac{[\dot{x}_{n+1}(t+\tau)]^m}{[x_n(t) - x_{n+1}(t)]^l}\left[\dot{x}_n(t) - \dot{x}_{n+1}(t)\right]$$

Where, $l \neq 1$ and $m \neq 1$, as discussed previously.

3.5 Summary and Conclusions

This chapter explored the relationship between microscopic and macroscopic traffic flow models. Almost all of the existing well-known macroscopic speed-density

relationships can be derived from microscopic car-following models. This is achieved by integrating microscopic car-following models and applying proper assumptions on traffic conditions and headway-density approximations as well as boundary conditions. On the other hand, taking derivatives of macroscopic speed-density relationships will result in microscopic traffic models (acceleration equations) and the process is easier than integration.

Most of the microscopic-macroscopic derivation was based on the assumptions of steady-state and homogeneous traffic conditions and that headway equals to the inverse of the density. Therefore, these models apply only for steady state traffic conditions. Under these assumptions, a generalized macroscopic speed-density relationship was derived from the generalized stimulus-response microscopic car-following model, which includes a speed exponent parameter m and distance headway exponent parameter l. With different combination of m and l values, almost all of the well-known macroscopic speed-density models can be derived from this generalized car-following model.

It was found that the relationship between headway and density has important implications on model derivation. The traditional headway-density assumption does not hold for non-homogeneous traffic and the research showed that slightly changing the headway-density relationship will result in different macroscopic models. Using a mathematical definition of density and a new headway-density approximation, a macroscopic model that includes relaxation, convection, anticipation and diffusion (or viscosity) components was derived from a microscopic model corresponding to the delayed response of drivers.

Table 3.1 Car-following models and macroscopic models in *m* and *l* matrix

m	*l*	Microscopic Models	Macroscopic Models
0	0	GM 1, GM 2,	Pipe (1953), Forbes and Simpson (1968)
0	1	GM3	Greenberg (1959)
0	2	—	Greenshields (1935)
1	1	GM 4	—
1	0	—	—
1	2	—	Underwood (1961)
1	3	—	Drake (1967)
m	*l*	GM5	Generalized v-ρ equation (May 1990)

Table 3.2 Speed-density relationships in general form

Model	F(v)	G(p)	a	b
Greenshields (1935): $v=v_f-v_f(\rho/\rho_m)$	v	(ρ/ρ_m)	$-v_f$	v_f
Greenberg (1959): $v=v_f\cdot\ln(\rho_m/\rho)$	v	$\ln(\rho_m/\rho)$	v_f	0
Underwood (1961): $v=v_f\cdot e^{(-\rho/\rho_0)}$	v	$e^{(-\rho/\rho_0)}$	v_f	0
Drake (1967): $v=v_f\cdot e^{-½\cdot(\rho/\rho_0)^2}$	v	$e^{-½\cdot(\rho/\rho_0)^2}$	v_f	0
Drew (1965): $v=v_f-v_f(\rho/\rho_m)^{(n+½)}$	v	$(\rho/\rho_m)^{(n+½)}$	$-v_f$	v_f
Pipes-Munjal (1967, 1971): $v=v_f-v_f(\rho/\rho_m)^n$	v	$(\rho/\rho_m)^n$	$-v_f$	v_f
General Model (May 1990): $v^{(1-m)}=v_f^{(1-m)}[1-(\rho/\rho_m)^{(l-1)}]$	$v^{(1-m)}$	$-(\rho/\rho_m)^{(l-1)}$	$v_f^{(1-m)}$	$v_f^{(1-m)}$

ρ, ρ_0, ρ_m are traffic density, optimum density and maximum density, respectively, v_f is the free flow speed.

Chapter 4 Compatibility Analysis of Macroscopic and Microscopic Traffic Simulation Modelling[1]

4.1 Introduction

Microscopic traffic models were established in the 1950s and represented by car-following models (Brackstone el at. 1999, Olstam el at. 2004). Over the past several decades, many studies have been carried out on the related theories and their applications. Due to model mechanisms, microscopic simulation models are often used in evaluating detailed local operations, such as congested intersections (Messer 1998), freeway bottlenecks (Halkias et al. 2007), weaving sections (Stewart et al. 1996), merging and lane changing (Hidas 2002), transportation corridor operations (Gomes et al. 2004), etc. They can also be used to analyze control scenarios, such as ramp control (Hasan et al. 2002, Beegala et al. 2005) and intelligent transportation strategies (Chu et al. 2004). Hasan et al. (2002) evaluated four kinds of control measures: access control, route guidance, lane management and integrated control, with a microscopic traffic flow simulator (MITSIM Lab) and demonstrated the capability of microscopic simulation to explicitly capture interactions among individual drivers and represent the driver's response to control devices at the

[1] A version of this chapter has been published. Yin, D. and Qiu, Z.T. (2013). Compatibility analysis of macroscopic and microscopic traffic simulation modeling. *Canadian Journal of Civil Engineering*. 40(7), pp.613-622.

individual level. However, this type of application is mainly off-line and lacks the predictive control functions. Instead, microscopic simulation is an effective tool to evaluate the performance of control measures before their implementation.

On the other hand, the application of macroscopic simulation models is aimed at large-scale roadway networks (Kotsialos et al. 2002, Carlson et al. 2010) or online (real-time) traffic control to reduce congestion and improve mobility (Lu et al. 2010, Hegyi et al. 2005a, Hegyi et al. 2005b). In Hegyi et al.'s (2005b) study, the authors used a macroscopic traffic flow model, METANET, as the state prediction model for optimal coordination of variable speed limits and ramp metering in a freeway network and found that the coordinated control can result in a higher outflow and a significantly lower total travel time in the road network.

The formulation of macroscopic simulation models varies depending on whether merging, weaving or other factors are considered in the model (Shladover et al. 2010). Papageorgious et al. (1989) modeled an arterial street in Paris. The effects of several components of the speed dynamics equation were studied and it was concluded that dropping the merge term had no evident impact on model accuracy (on the studied roadway), but will evidently increase simulation speed.

There are only limited studies on the comparison of macroscopic and microscopic model performances. Cluitmans et al. (2006) compared a macroscopic model and a microscopic simulation model on a freeway in the Netherlands and concluded that both models used in their study were not able to simulate well when traffic demand was very high. Lamon (2008) used METANET and PARAMICS simulation on a freeway for a short peak period. Both good agreements and wide

discrepancies were observed between the outputs from the two models. Wu (2002) applied a macroscopic model, NETCELL, and a microscopic simulation model, VISSIM, for a congested freeway and found that NETCELL can reproduce the congested traffic condition much better than VISSIM, while the latter can represent the real-world traffic conditions better in free-flow. Ishak et al. (2006) evaluated the performance of a macroscopic model, CTM, and a microscopic simulation model, CORSIM, on a congested freeway and showed that performances of both simulation models are comparable in terms of link density and total network travel time.

The studies by Shladover et al. (2010), Papageorgious et al. (1989), Lamon (2008) and Wu (2002) used only one time step length in each macroscopic simulation, and it varied from 2.5 seconds (s) in Papageorgious et al. (1989) to 60s in Shladover et al. (2010). In those studies, whether the time step length impacted the model performance was not evaluated. Cremer et al. (1981) studied the time step length effects on the differences (total errors) of the macroscopic simulation and found that the optimal value is related to the segment length. However, whether the optimal time step length varies with traffic demand was not studied.

Previous studies showed mixed results as to whether microscopic and macroscopic simulations have similar performances. There is no systematic study on the combined effects of traffic demand and time step length used in macroscopic simulation on the model performance. For a particular application of active traffic management (ATM), a systematic comparative study on microscopic and macroscopic models under varied traffic demand is required to calibrate and adjust the macroscopic models that will be used for online traffic control purposes.

The objectives of this study are to compare the performance of a microscopic simulation model, VISSIM (PTV 2010), and a macroscopic simulation model, METANET (Messmer and Papageorgious 1990), under various traffic conditions, to evaluate how the time step length (time interval) impacts the macroscopic simulation performance and to determine the most appropriate time step length that will be used in VSL and RM control on the studied urban freeway. This chapter is organized into sections: after this introduction, the methodology and simulation models used in this study are presented. An experimental design is discussed, according to which data is compared and analyzed. Conclusions are presented after detailed discussions.

4.2 Methodology

In this portion of the study, the compatibility between a macroscopic and a microscopic simulation model was analyzed on a section of urban freeway with relatively low speed limits and a lane drop in a construction zone. The microscopic simulation model, VISSIM, was calibrated and validated using field measured traffic volume and speed data. A macroscopic simulation model, METANET, was modified and used for the same section of freeway. The study considered two critical factors, traffic demand and time step length, and their effect on macroscopic simulation and on the compatibility of the macroscopic and microscopic simulation models. The macroscopic simulation model was run with different traffic demands and time step lengths and compared with the outputs from the microscopic simulation with the same initial traffic states. The prediction errors from the macroscopic model were used as measures of effectiveness (MOE) and were evaluated with respect to time

step length and traffic demand. The conclusions were obtained from the comparative analysis. Figure 4.1 shows the flowchart of this study.

4.2.1 Studied Freeway Corridor

The site selected for the study was a section of the westbound direction of Whitemud Drive, which is an urban freeway in the city of Edmonton, Alberta, Canada. It runs from east of 122 Street to west of 159 Street. This 8.5 km long freeway section has five on-ramps and six off-ramps. At the time this study was carried out, there was a construction zone in the middle of this freeway section with a posted speed limit of 50 km/h. The remaining sections have a posted speed limit of 80 km/h. The number of through lanes varies from two lanes in the construction zone to four lanes near the end of the freeway section and three lanes for the majority of the freeway. Figure 4.2 shows the characteristics of the studied freeway corridor. This freeway experiences recurrent heavy congestion during the morning and afternoon commute peak hours due to the construction zone and several bottlenecks. Coordinated RM and VSL controls are under study and will be implemented in the near future to address increased traffic demand, which is expected after completion of the construction. At the time of the study, loop detectors were installed at seven cross-sections of the mainline freeway and video cameras were installed at the ramps.

4.2.2 Microscopic Simulation Model

Microscopic simulation models simulate the movement of individual vehicles based on car-following and lane-changing theories. They describe the behaviour of individual vehicles in relation to the roadway and other vehicles in the flow. Vehicles are tracked through the network over small time intervals (usually less than one

second) and then vehicle performances are aggregated to assess the traffic performance on the roadway. A microscopic simulation package, VISSIM, was used in this study. VISSIM uses a link-and-connector approach to represent roadway sections and merge/diverge points. Links are used to build the roadway sections. A number of attributes can be assigned to links, including number of lanes, lane widths, road gradient, lane restrictions as well as car-following and lane-changing behaviours. Connectors are used to connect links to build road networks. All of the turning movements at intersections and roadway merging/diverging points need to be joined by connectors. Roadway characteristics were represented in detail, including turning radius, the exact location of on-ramps and off-ramps, auxiliary lane and tapers length, configuration of weaving sections and exact location of traffic control measures.

In the VISSIM model, vehicles were loaded into the roadway according to a predefined distribution based on total traffic demand. The traffic data was obtained from two sources: dual loop detector-measured data on each lane of the mainline at seven cross-sections (in Segment 4, 7, 9, 10, 12, 14 and 20 of Figure 4.2) and video traffic data at on- and off-ramps. The origin-destination (OD) matrix was estimated using TFlowFuzzy procedure in VISUM (PTV 2010). The Whitemud Drive corridor connectivity matrix was considered as a seed matrix and the OD was estimated to match the field traffic counts. This estimated OD from VISUM was then converted to a routing matrix to establish the vehicle routing input in VISSIM. During simulation, virtual detectors were placed on each lane at the middle of each segment as well as at the on- and off-ramps to measure flow and speed. The VISSIM outputs (flow and

speed) were aggregated according to the required time intervals and used as initial inputs for the macroscopic simulation model.

4.2.3 Macroscopic Simulation Model

Macroscopic simulation models are based on the deterministic relationships of the flow, speed and density of the traffic stream along a section of roadway. They describe the traffic flow on an aggregated basis rather than by tracking individual vehicles. Therefore, macroscopic simulation is much faster than microscopic simulation. However, they do not have the ability to analyze detailed local characteristics, such as merging points, in as much detail as the microscopic models.

A macroscopic simulation model, METANET, was used in this study. A detailed description of METANET is well documented in literature (Kotsialos et al. 2002, Carlson et al. 2010, Messmer and Papageorgious 1990) and is not repeated here. Modifications were made to account for local conditions.

In macroscopic simulation, the roadway was subdivided into a number of segments and the time was discretized into short time intervals (denoted by T). The aggregated traffic state variables were defined for each segment and updated each time step. The freeway for this study was divided into 20 segments based on the distances and number of lanes between on-ramps and off-ramps (Figure 4.2b). The segment length varied from 285m to 500m. The construction zone was from segment 8 to segment 15. Each segment was a homogeneous unit, in which the number of lanes must remain unchanged. Usually short acceleration/deceleration lanes, merging/diverging tapers at lane adding/dropping or at ramps cannot be modeled as a lane, because the short length does not satisfy minimum segment length

requirements. Geometric details of the roadway, such as curvature, grade and lane width cannot be represented directly in the model. On- and off-ramps were always located at the beginning and end of the segments, respectively, and traffic control measures were located at the beginning of segments.

Based on spatial and temporal discretization, traffic state variables were calculated for each segment *i* at each time step *k* by the following equations (Carlson et al. 2010):

$$\rho_i(k+1) = \rho_i(k) + \frac{T}{L_i}[\rho_{i-1}(k) \cdot v_{i-1}(k) - \rho_i(k) \cdot v_i(k) + r_i(k) - s_i(k)] \tag{4.1}$$

$$v_i(k+1) = v_i(k) + \frac{T}{\tau}[V(\rho_i(k)) - v_i(k)] + \frac{T}{L_i} \cdot v_i(k) \cdot [v_{i-1}(k) - v_i(k)] - \frac{\eta \cdot T}{\tau \cdot L_i} \frac{\rho_{i+1}(k) - \rho_i(k)}{\rho_i(k) + \kappa} \tag{4.2}$$

$$V_i(k) = v_f \cdot \exp\left[-\frac{1}{\alpha} \left(\frac{\rho_i(k)}{\rho_{cr}} \right)^{\alpha} \right] \tag{4.3}$$

The symbols and notations used in the model are listed below:

k - simulation time step index, which indicates the time instant $t=kT$, $k = 0, 1, 2\ldots, K$.

K - the total simulation time steps.

T - simulation time step length;

L_i - length of segment *i*;

$\rho_i(k)$ - density (veh/km/lane) in segment *i*;

$v_i(k)$ - speed (km/h) in segment *i*;

$v_{i-1}(k)$ - speed (km/h) in segment *i*-1;

$r_i(k)$ - on-ramp flow in segment *i* at time index *k*;

$s_i(k)$ - off-ramp flow in segment *i* at time index *k*;

$V_i(k)$ - desired speed in segment *i* vehicles trying to reach;

ρ_{cr} - critical density (the traffic density at which the traffic flow reaches the capacity);

α - a model parameter for the fundamental diagram;

v_f - free-flow speed (km/h).

τ, η, κ are model parameters that need to be identified in model calibration process. τ is the time delay for the driver's response to the perception of traffic states. η is a sensitivity factor and κ is a density constant. For each designed T value (a pre-determined constant), all segments will use the same set of model parameters, which are obtained in the model calibration process. Different T values will have different sets of parameters and result in different macroscopic models.

Equation (4.1) is based on the conservations of vehicles that results directly from the definition of the traffic variables. Equation (4.3) is an empirical equation describing the static speed-density relationship corresponding to the FD. Equation (4.2) is the speed dynamics, which is derived from a car-following mechanism (Payne 1971). The meaning of each term has been explained in Kotsialos et al. (2002), Carlson et al. (2010) and Cremer et al. (1981).

In some research (Papageorgious et al. 1989, Papageorgious et al. 1990, Sanwal et al. 1996 and Bellemans 2003), the speed dynamics Equation (4.2) was extended by including additional terms to directly account for the impacts from on-ramps, lane drops or the blocking of lanes due to incidents. These terms may appear in different forms. For example, a merge term can be expressed in the following form:

$$\Delta v_{merge,i}(k) = -(\frac{\delta_m \cdot T}{n_i \cdot L_i}) \frac{q_{on}(k) \cdot [v_i(k) - v_r(k)]}{\rho_i(k) + \kappa_m} \tag{4.4}$$

Where, δ_m is a tuning parameter for the merging term and κ_m is a model constant. $v_i(k)$ and $v_r(k)$ are vehicle speeds on segment i and an on-ramp, respectively. n_i is the number of merging lanes and q_{on} is the flow from an on-ramp. A similar structure to Equation (4.4) can also be included in Equation (4.2) to represent lane-drop effects.

However, the disadvantage of including more terms is that they will bring more model parameters and add complexity in model calibration, as model parameters may have interactive effects. On the other hand, not including merge and lane-drop terms does not necessarily mean that those impacts have not been considered in the model. In fact, they are reflected indirectly. For on-ramps or lane drops, the merging of additional traffic volume may increase the density of the corresponding freeway sections. Density, in its turn, influences mean speed through the speed-density relationship. In addition, entering vehicles from on-ramps usually have a lower speed than vehicles on the through lanes and this low speed is included in the model calculation.

The merge and lane-drop terms are not included in this study for two reasons: First, field observations of peak hour traffic operations under existing road configuration indicated that vehicles from on-ramps often wait at the painted tip of the on-ramps when traffic density on the main road was high. This is similar to a yield sign control at the on-ramps, rather than a real merge. Second, while most of the studies on macroscopic simulation excluded the on-ramp or lane-drop terms (Cremer 1981, Calson et al. 2010, Kotsialos et al. 2002), some research that did include on-ramp or lane-drop terms (Papageorgious et al. 1989, Papageorgious, 1990) reported that including the on-ramp term in the model "did not lead to any visible amelioration" and "the importance of lane drop coefficient is moderate." Nevertheless, the possible merging and weaving impacts are investigated in a later part of this dissertation.

Different from regular freeways, the studied urban freeway has several speed limit signs with a relatively low value. The free-flow speed on this freeway is different from a conventional freeway concept. By definition, the free-flow speed is the mean speed when the drivers are not restricted by any other vehicles on the freeway. Based on field observations, the freeway flow speed is approximately 1.1 times of the posted speed limits when the posted speed value is less than 90 km/h. Therefore, the desired speed Equation (4.3) is replaced by Equation (4.5) in simulation. The flow in segment *i* was calculated by Equation (4.6).

$$V_i(k) = \min\{V_{control,i}(k), 1.1 \times V_{control,i} \cdot \exp\left[-\frac{1}{\alpha}\left(\frac{\rho_i(k)}{\rho_{cr}}\right)^{\alpha}\right]\} \tag{4.5}$$

$$q_i(k) = \rho_i(k) \cdot v_i(k) \tag{4.6}$$

Where, $V_{control,i}$ is the posted speed limit in segment *i*, $q_i(k)$ is the predicted flow (veh/hr/lane) in segment *i* during time step *k*.

4.2.4 Initial States and Boundary Conditions

In a comparative analysis of different models, the initial traffic state at each segment should be set the same so that traffic dynamics can be compared over the temporal and spatial evolvement. At the beginning of the macroscopic simulation, the initial traffic state in each segment (density and space mean speed) is the same as in the VISSIM simulation. This was achieved by aggregating the VISSIM outputs (flow, speed and calculated density) in the corresponding time intervals used in macroscopic simulation.

In microscopic simulation, boundary conditions are the traffic demands at the upstream and on-ramps. They are given as direct input data. The speed is not required, since it will be calculated based on the car-following mechanism imbedded

in the model. Macroscopic simulation models need more boundary conditions than are required for microscopic simulation models. To run the METANET model, traffic states (flow and speed) upstream of the first modeled segment and downstream of the last modeled segment of the main roadway as well as all on-ramps are required. There are three ways to obtain the speed information as inputs to the METANET model. The first method is based on the available or assumed FD. Vehicle speeds were obtained by knowing flow states of the traffic demand. The second method is using continuously measured, real-time field data. Using a third approach in this study, the traffic demand and speed were obtained from VISSIM by aggregating VISSIM data according to the adopted time intervals to guarantee the same boundary conditions as in VISSIM.

4.3 Model Calibration and Performance Measures

Two separate sets of data were prepared for VISSIM calibration and validation, respectively: dual loop detector data on the mainline at seven cross-sections and video traffic data at on- and off-ramps for two hours (4:00 p.m. – 6:00 p.m.). The calibration of VISSIM was carried out in a preceding study (Wang et al. 2012), which includes two stages: qualitative and quantitative calibration. In the first stage, VISSIM was run starting with model default parameters and driver behaviour was observed at on-ramps, merge sections and bottlenecks. Vehicle characteristics and performance data, including vehicle length, maximum speed and maximum acceleration/deceleration rates, were adjusted to match local traffic conditions. The driver behaviour parameter sets were adjusted to change the aggressiveness of drivers at merge locations. The safety distance reduction factor was changed from the default value of 0.6 to 0.1, 0.2,

and 0.05. Headway time (CC1 parameter) was set to 1.20, 1.30 and 1.40 for the weaving section, lane drop and construction zone, respectively. Visibility parameters (emergency stop and lane change) were also adjusted at each link connector. These parameters were adjusted with a trial and error method and numerous iterations until the simulation reasonably represents the observed field traffic operation, especially at merge points and bottlenecks.

In the second stage, quantitative calibration was carried out by comparing the modeled results (capacity, volume and travel time) with field-measured data. The parameters were adjusted iteratively until the modeled results fell within the acceptable range of pre-determined criteria for five simulation runs, with each run at two hours with a different seed value: simulated capacity was within 10% of the field measurements using the macroscopic FD method. For more than 85% of the cases, the simulated link volumes were within 5% when measured volumes were <500 vphpl; within 10% when measured volumes were between 500~1500 vphpl; and within 15% when measured volumes were >1500 vphpl. The summation of the simulated link volumes was kept within 5% of total measured volume. Simulated average travel time was within 10% for the measured mainline segments. For validation, the same criteria as in calibration were used and another five simulation runs were performed to compare the modeled results.

Since the purpose of this study was to analyze the compatibility of the microscopic and macroscopic approach, the METANET model was calibrated to VISSIM output data, rather than the field-measured data based on two considerations. First, the VISSIM model was calibrated and validated with the field data and, thus

the output from VISSIM can be taken as the ground truth in the comparative analysis. Second, there are 20 segments in the METANET model, but loop detectors were only installed at seven cross-sections. It is more appropriate to calibrate the METANET model with VISSIM outputs recorded at each segment.

In calibrating the METANET model, the nonlinear optimization method was used to estimate the model parameters. The objective function was the function that calculates the total relative difference (total error) between the outputs from VISSIM and METANET simulation for all segments and in all time steps. In particular, the total error in this study is defined as the sum of squares of relative errors, which is calculated by Equation (4.7):

$$E = \sum_{k=1}^{N_{steps}} \sum_{i \in I_{all}} \left\{ \left[\frac{\hat{q}_i(k) - \tilde{q}_i(k)}{(\hat{q}_i(k) + \tilde{q}_i(k))/2} \right]^2 + \left[\frac{\hat{v}_i(k) - \tilde{v}_i(k)}{(\hat{v}_i(k) + \tilde{v}_i(k))/2} \right]^2 \right\} \quad (4.7)$$

Where, N_{steps} is the total number of simulation time steps, I_{all} is the total number of the segments of the freeway, $\hat{q}_i(k), \hat{v}_i(k)$ are flow and speed from VISSIM in segment i at time step k, respectively, and $\tilde{q}_i(k), \tilde{v}_i(k)$ are flow and speed from METANET in segment i at time step k, respectively.

The model parameters (τ, η, κ, α, ρ_{cr} and ρ_{max}) can be identified by minimizing the total error. The MATLAB Optimization Toolbox (The MathWorks 2010) was used to solve this nonlinear optimization problem. For each T value, a set of model parameters were obtained to constitute one macroscopic model. A different T value will have a different set of model parameters. For example, corresponding to the time interval T=20s, the set of model parameters for this freeway was τ=0.03hr, η = 50 km^2/h, κ= 47 veh/km/lane, α=2.32, ρ_{cr} = 48 veh/km/lane and ρ_{max} = 110 veh/km/lane.

It should be noted that there will be a minor change in the model parameter values if the upper and/or lower bounds are changed in the optimization processes.

Different from the application of traffic control with VSL or RM, in which the total travel time (TTT) and total travel distance (TTD) are often used as the measure of effectiveness (MOE) to evaluate the performance with/without control models, this study evaluated the prediction accuracy between the macroscopic model and microscopic simulation. Therefore, the prediction error (difference, *D*) was used as the performance measure, which is, at each time step and in each segment, defined below:

$$D = \frac{\left| METANET\ Output - VISSIM\ Output \right|}{(METANET\ Output + VISSIM\ Output)/2} \tag{4.8}$$

4.4 Experimental Design

To evaluate the compatibility of microscopic and macroscopic simulation models, a range of traffic demand should be tested to compare model performance under varied traffic conditions. In addition, the simulation time interval in the macroscopic model should also be evaluated because it is a fundamental constituent in macroscopic simulation.

Segment length plays an important role in macroscopic simulation and it is determined by the physical configuration of the freeway, such as distance between on-ramps and off-ramps. In an urban environment, the distance is usually short and there is not much flexibility to adjust the segment length. The basic assumption of the model configuration is that within each segment, speed and density are homogeneous and vehicles in the upstream segment can only move within the

current or to the immediate downstream segment in one time step. Due to physical constraints of the urban roadway, the impact of segment length on the model performance was not evaluated in this study.

Traffic demand should cover the practical range of operations in typical traffic flow control applications. In very light traffic demands, traffic management and control measures are not required. In this study, three traffic demand levels were used to run the microscopic and macroscopic simulations: moderate demand (approximately 933 to 1167 veh/h/lane at the mainline origin), heavy demand (1167 to 1433 veh/h/lane) and excessive demand (1333 to 1667 veh/h/lane). Moderate and heavy traffic demand levels were determined based on field-measured traffic data, with heavy traffic demand corresponding to the actual peak hour (around 4:30 p.m. to 5:30 p.m.) and the moderate demand level corresponding to the half hour prior to and half hour after the actual peak hour. Excessive traffic demand level on the mainline was determined by artificially increasing the mainline volume from the heavy traffic demand to create a long-lasting traffic jam in the construction zone. For the excessive traffic demand level, demand at on-ramps and the proportion of vehicles that exit from off-ramps were kept the same as in the heavy traffic demand level. Within each traffic demand level, flow varied between low and high values during the simulation time period.

The time interval in macroscopic simulation should be neither too short nor too long. If it is too short, sometimes the detector-counted vehicle numbers in VISSIM simulation (or measured by field loop detectors) in one time step could be zero in a segment. This will be exaggerated when converting the vehicle counts in one time

step to the hourly flow rates and, thus generate zero hourly flow rates. On the other hand, if the time interval is too long, the constitutive condition of macroscopic model $L \geq T \bullet V_f$ may be violated, causing the model to be unstable with inaccurate and sometimes erroneous outputs. Also, it is possible that some vehicles may completely skip one segment because in one time step they may have travelled a distance larger than the length of the immediate downstream segment. This "jumping" will result in incorrect predictions. Based on the above considerations, time intervals of 5s, 10s, 15s, 20s, 25s, 30s and 33/35/40s were used in this study. Some erroneous outputs were observed during the macroscopic simulation when time interval was longer than 33s.

4.5 Data Analysis and Discussion

For each traffic demand level, VISSIM was run for a little over 1.5 hours. Excluding warm-up time, a maximum of one hour and 20 minutes of usable data was obtained for the study. The output from VISSIM was aggregated to different data sets depending on the design time step length to run the METANET model.

In the following data analysis, the outputs from VISSIM were taken as the ground truth and the outputs from the METANET model were compared with the outputs from the VISSIM model, based on which, the time step and traffic demand effects are evaluated.

4.5.1 Time Step Length Effects on Simulation Performance

The total errors for a fixed 120 steps of simulation (K=120, when T is 40s, one hour 20 minutes of data can be aggregated to 120 time steps), as previously defined and calculated by Equation (4.7), between the outputs from the VISSIM and METANET

models for different time interval *T* in macroscopic simulation are depicted in Figure 4.3a. The total errors go down quickly as *T* increases from 5s to 10s, remain at a relatively low value as *T* varies from 15s to 25s, and go up after *T* is longer than 30s. Figure 4.3b shows the average error per time step from one-hour simulation (a different data set from Figure 4.3a). As can be seen, the average error in one time step is lowest when *T* is between 15s and 30s. For a given roadway configuration, there exists optimum time intervals in macroscopic simulation. In this study, the optimal time interval was centered around 20s.

Figure 4.3a and 4.3b also confirm that both a too short and a too long time interval may lead to a large prediction error, as explained in the Experimental Design section.

4.5.2 Traffic Demand Effects on Simulation Performance

The traffic demand effects on simulation performance are shown in Figure 4.3 as well. When in moderate to heavy traffic demands, as defined in the Experimental Design section, both the total and average errors were similar for an appropriate time interval *T*. When demand was excessively high, errors were much higher than that in the moderate and heavy traffic demand. This indicates that at the moderate and heavy traffic demand level and with a reasonable time interval, there is no dramatic change in the model prediction performance. However, as the traffic demand is extremely high (stop-and-go traffic state), large differences exist between the outputs from the two models.

Figure 4.3 also shows that, at a particular traffic demand, errors remain relatively low when the time interval varies from 15s to 25s. Thus, it is recommended to use a T value between 15s and 25s for VSL control on this freeway.

As the optimum time interval is centred around 20s, the following comparisons between the outputs from the two models are based on a fixed T of 20s with heavy traffic demand, corresponding to the peak hour of 180 time steps in macroscopic simulation.

4.5.3 Comparison of VISSIM and METANET Outputs in Different Segments

The flow, speed and density outputs from both the VISSIM and METANET models for all segments at particular time instants (time index k=40 and 120, respectively) are illustrated in Figure 4.4. Except a few segments (8, 9, 16, as discussed below in this section and the section that follows), the outputs from METANET and VISSIM have the same trends along the modeled roadway. The outputs from METANET are spatially consistent with the outputs from VISSIM.

The flow data (Figure 4.4a and 4.4b) from the VISSIM model remarkably fluctuates from segment to segment. This is partially due to the inflow and outflow from on- and off-ramps, and partially due to the stochastic nature of microscopic simulation, in which traffic demands are generated following predetermined distribution and change with time quickly. In METANET, the flow has less fluctuation than that in VISSIM.

In segments 8 and 9, a considerable difference in speed and density exist at time index k=120 (Figure 4.4c and 4.4d), because of the construction zone lane drop at segment 8 and an on-ramp at segment 9. During peak traffic demand periods (after

120 time steps), the real-world traffic flow is chaotic at this location and a stop-and-go traffic state exists on the freeway. VISSIM represented this traffic state clearly, while METANET did not. In Figure 4.4c, VISSIM indicated a speed of 25 km/h at segment 9, which is much lower than the posted speed limit of 50 km/h. This low speed was caused by the extremely high density due to the lane drop at segment 8 and the on-ramp at segment 9. While METANET captured this increased density and reduced speed, it had a "smooth effect," changing gradually from one segment to the next.

4.5.4 Comparison of VISSIM and METANET Outputs during All Simulation Time

The density, speed and flow outputs from both the VISSIM and METANET models for the selected segments during one-hour simulation time (180 time steps with 20s time interval) are illustrated in Figure 4.5, Figure 4.6 and Figure 4.7, respectively.

Generally, the density, speed and flow from both models are temporally consistent. The outputs from VISSIM fluctuate frequently with the time index, while the outputs from METANET are smooth with approximately the average value of VISSIM in most of the segments. The fluctuation of VISSIM outputs is due to the stochastic nature of microscopic simulation model, in which vehicles randomly enter the roadway and individual vehicle's speed changes in reaction to the leading vehicles. In METANET simulation, however, the outputs are the average values of a segment at each time step. These values change gradually from one time step to the next.

Figure 4.5 shows the comparison of density from the VISSIM and METANET models in the selected segments (segment 5, 9, 12, 16). The simulated densities from both models match in most of the segments (20 segments in total; most of the well-matched segments were not selected for the figures). An obvious difference exists near segment 9. In segment 9, starting from time step 120, traffic density increases suddenly due to increased traffic inflow from on-ramp #2 (ramp inflows are not shown in the figures), causing a decrease in speed on the freeway, while the total flow on the freeway does not increase significantly. VISSIM depicts this traffic state change clearly, but METANET does not show the dramatic increase in density. In segment 16, the construction zone ends and the number of through lanes increased to three. The posted speed limit increases from 50 km/h to 80 km/h at the beginning of segment 16. In VISSIM simulation, vehicles accelerate in response to this condition immediately, forming a sudden decrease in traffic density due to an instant increase in speed. In METANET simulation, however, this sudden increase in speed is not well caught.

Figure 4.6 shows the comparison of speed from the VISSIM and METANET models in the same selected segments as in density comparison. The predicted speeds from both models match in most of the segments. However, considerable differences exist in segment 9 and 16. In segment 9, after time step 120, traffic density on the freeway increased suddenly due to inflow from the on-ramp, causing a decrease in speed and stop-and-go conditions on the freeway. This is represented clearly in VISSIM, but not so prominently in METANET. In segment 16, the roadway is in a free-flow condition after the construction zone. Vehicles in the

VISSIM simulation adjusted to the new speed limit and free-flow condition immediately from segment 16 to the downstream. In the METANET simulation, the predicted speed increased gradually from segment 16 to downstream. The speed dynamics in the METANET model did not react quickly to the sudden change of traffic conditions.

Figure 4.7 shows the comparison of flow from the VISSIM and METANET simulations in the same selected segments. The simulated flow from both models match very well in all segments. According to the model mechanism, the output flow from VISSIM was counted during the simulation, while in METANET, the flow was calculated from the predicted speed and density. Even though differences between the predicted speed and density existed in some segments, the product of speed and density from METANET model well-matched the counted flow from the VISSIM model.

The average prediction errors, in percentage, as calculated with Equation (4.8), for each segment during all simulation time steps, are shown in Table 4.1. As shown in the table, compared with VISSIM outputs, on average, 10-20% of the prediction error can be expected from METANET on this freeway. It should be noted that the errors in Table 4.1 are all in absolute percentages for every time step. In field control, a model may over-predict traffic states in a previous time step and under-predict in the next time step. After the offset of the positive and negative errors, the average prediction error was much lower (less than 5% in this study) than the values in Table 4.1. A control strategy was given based on the average prediction of several time steps.

4.6 Summary and Conclusions

This section compared the performance of a macroscopic simulation model, METANET, with a microscopic simulation model, VISSIM, under different traffic levels and simulation time steps. Based on the performance of the two models and the comparison analysis presented above, the following main conclusions were found:

- The prediction of traffic states from METANET model is generally consistent with that from VISSIM simulation. The simulated speed, density and flow from VISSIM model fluctuate with time frequently, while those from the METANET model are approximately the average value of that from VISSIM.
- In macroscopic simulation model, there exist optimum time step lengths corresponding to a particular roadway configuration and free-flow speed. The optimum time step lengths do not change significantly with traffic demand. For the studied freeway, the recommended time step length for VSL control is approximately 20s.
- When traffic demand is at moderate to heavy level, the predicted traffic states from the macroscopic simulation are consistent with those from the microscopic simulation. Under excessive traffic demand (stop-and-go traffic conditions), significant differences exist between the simulated speed and density from the two models evaluated. There are some limitations for macroscopic model used in this study to accurately predict traffic states under stop-and-go traffic conditions.

- In VISSIM simulation, the change of speed limits can be captured immediately at the location of the speed limit. In METANET model, the model could not catch the sudden and significant change of traffic speed.

Table 4.1 Average prediction errors in each segment (in absolute value)

Segment No.	1	2	3	4	5	6	7	8	9	10	Average of All Segments
Density (%)	18	16	17	16	17	25	30	28	31	24	
Speed (%)	5	3	2	2	4	13	20	25	33	20	
Flow (%)	12	15	15	15	15	22	21	27	20	12	
Segment No.	11	12	13	14	15	16	17	18	19	20	
Density (%)	21	22	11	14	26	29	24	26	23	24	22
Speed (%)	20	22	9	15	23	23	25	16	10	9	15
Flow (%)	10	9	9	9	18	20	28	21	20	23	17

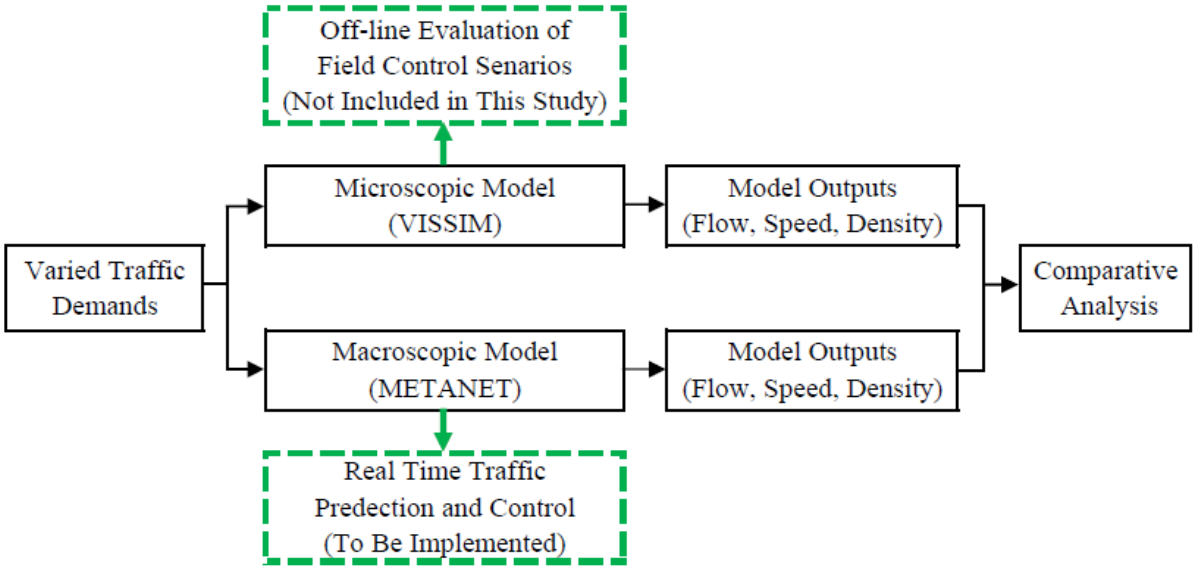

Figure 4.1 Comparative study flowchart

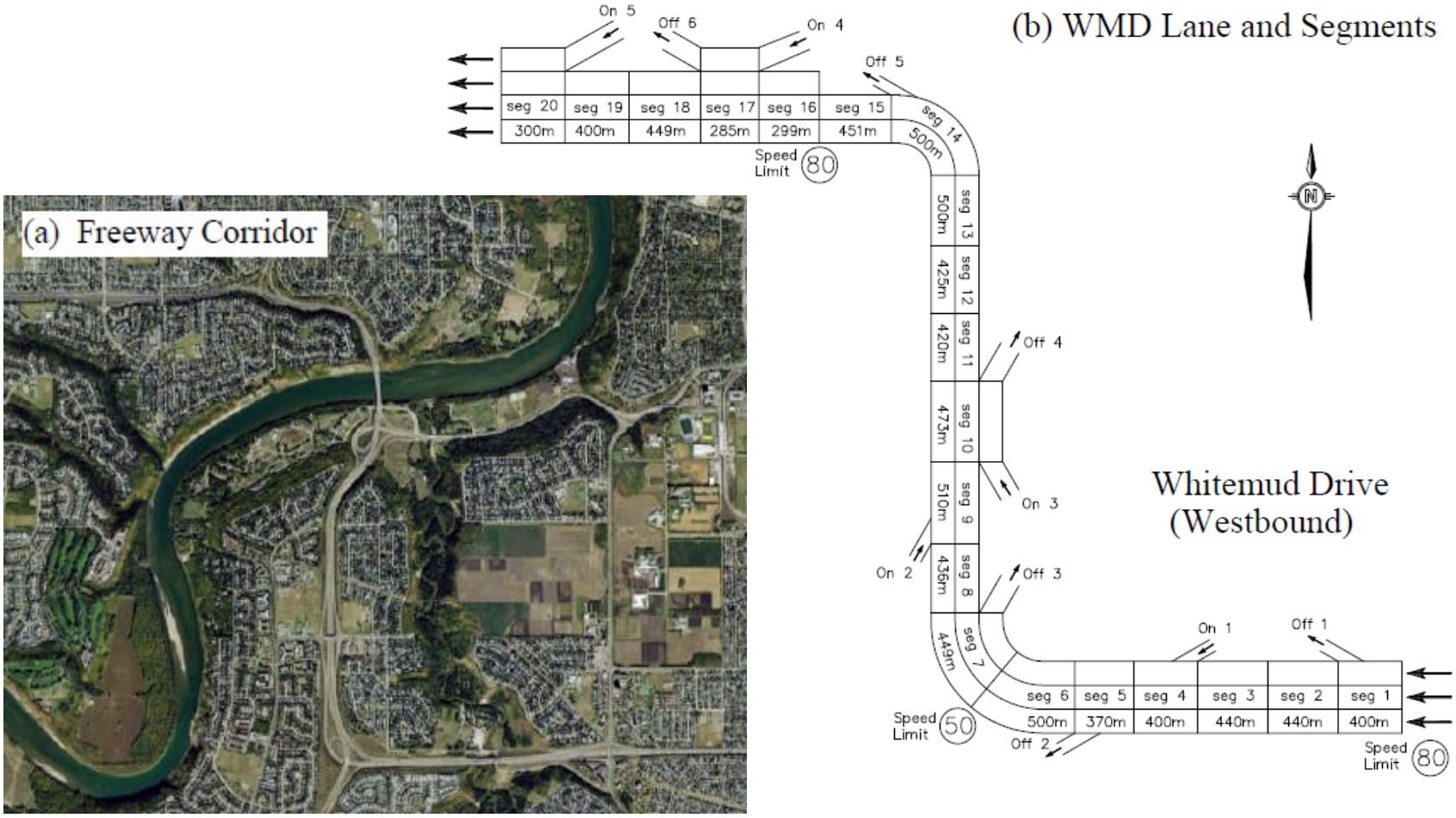

Figure 4.2 Studied freeway corridor

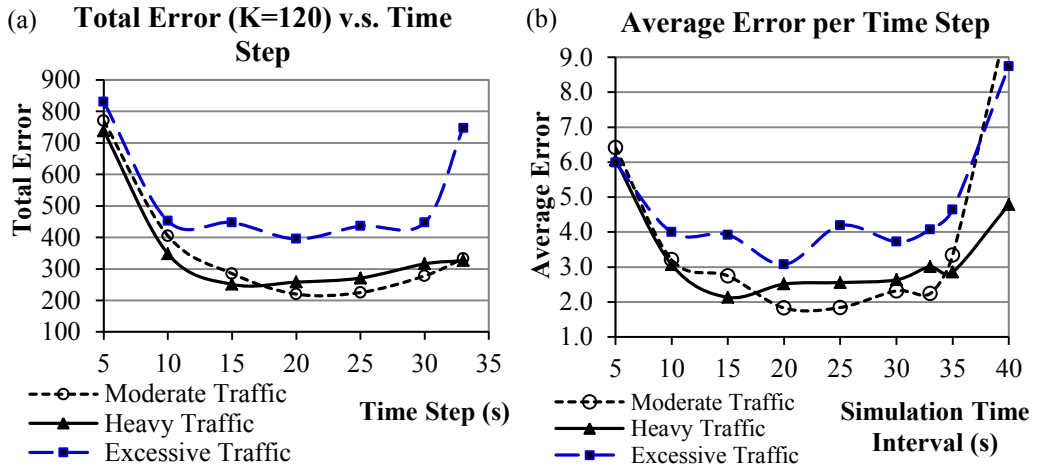

Figure 4.3 Errors with respect to simulation time interval and traffic demand

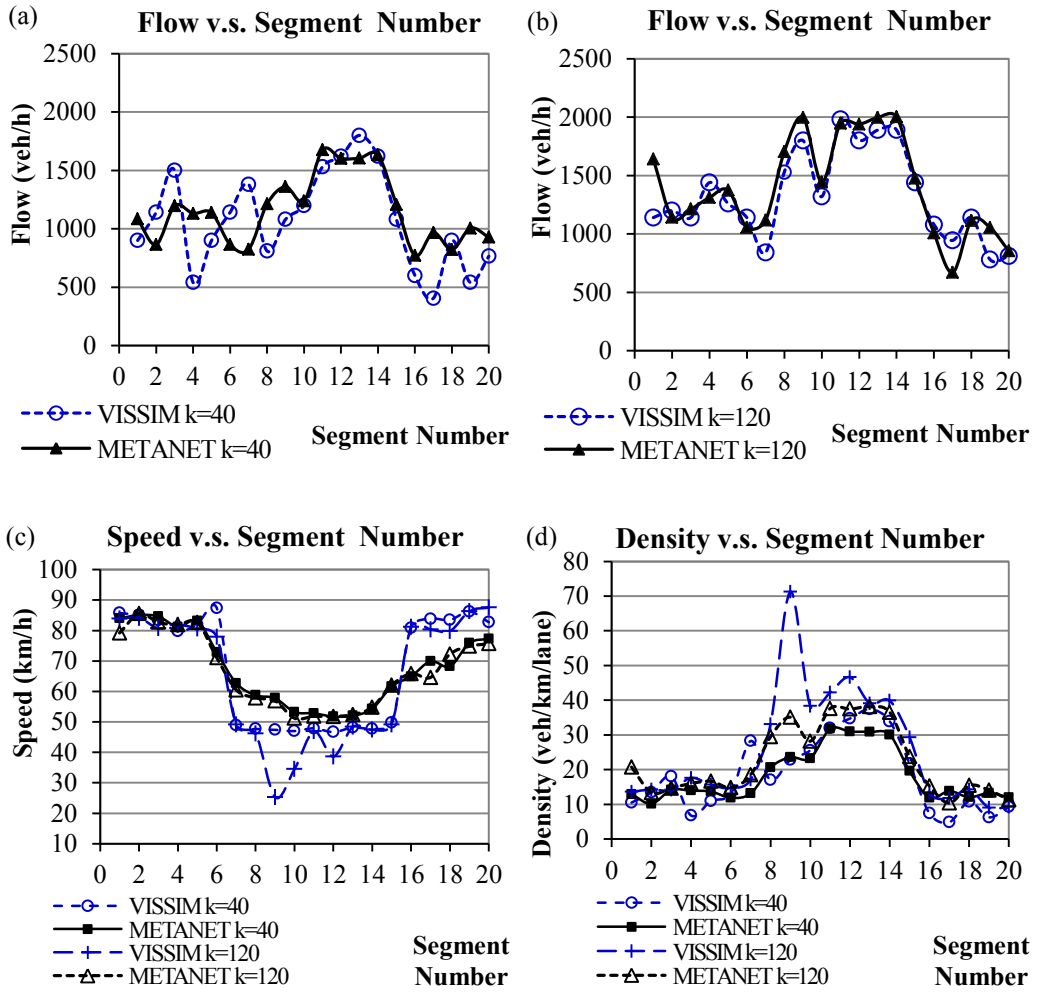

Figure 4.4 Predicted flows, density and speed along freeway

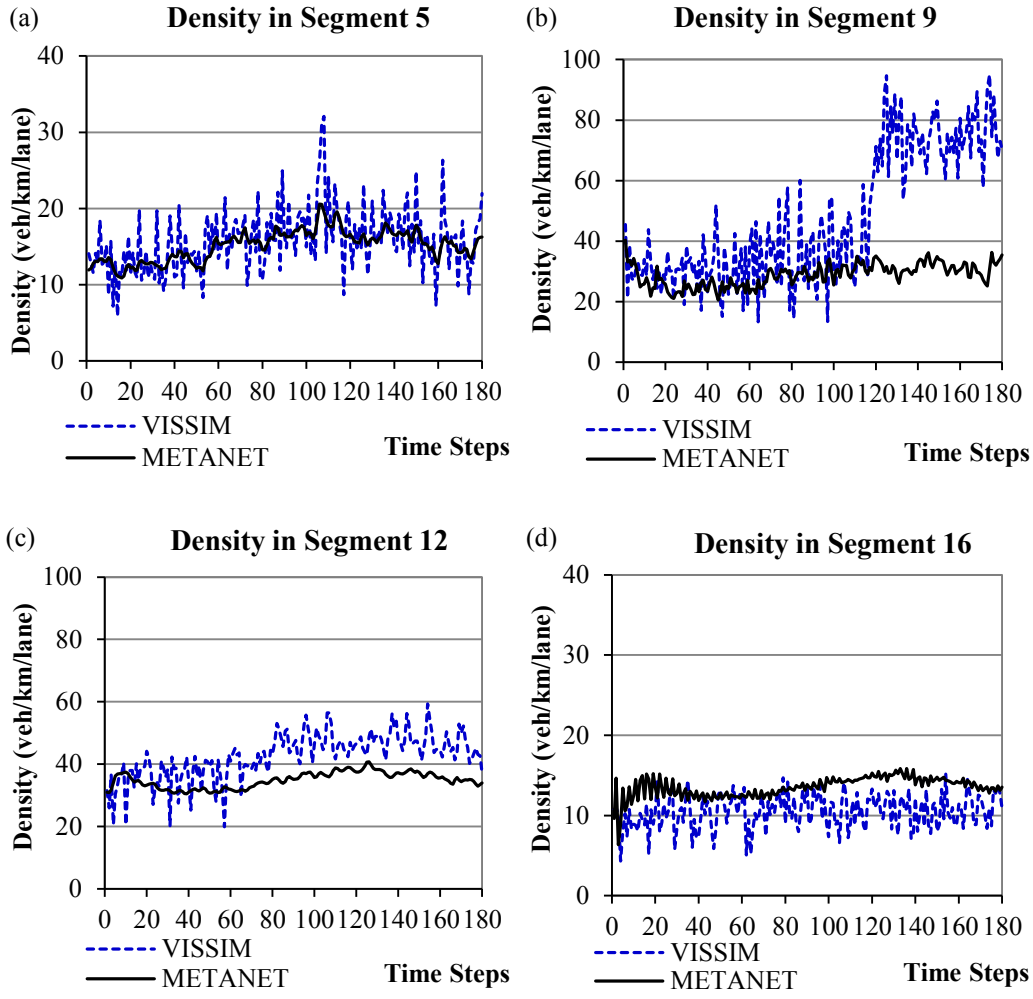

Figure 4.5 Comparison of density from VISSIM and METANET models

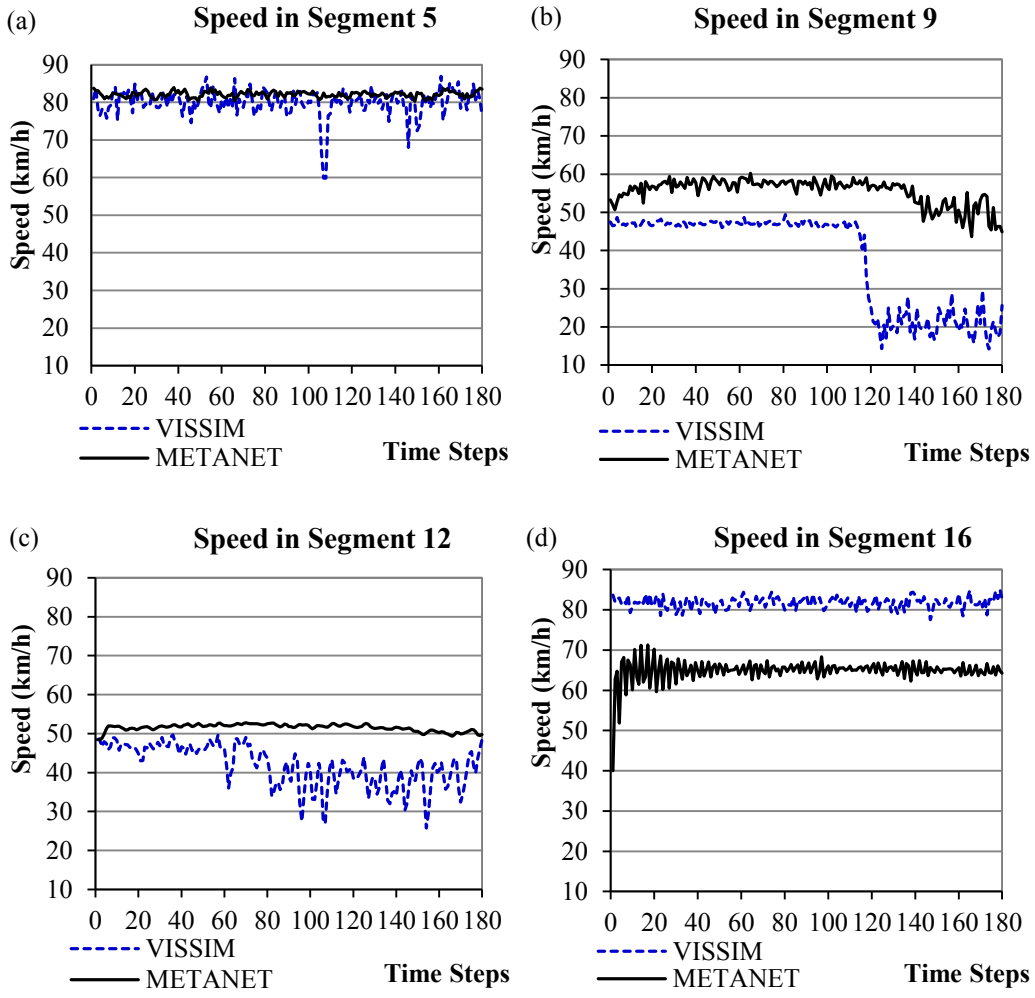

Figure 4.6 Comparison of speed from VISSIM and METANET models

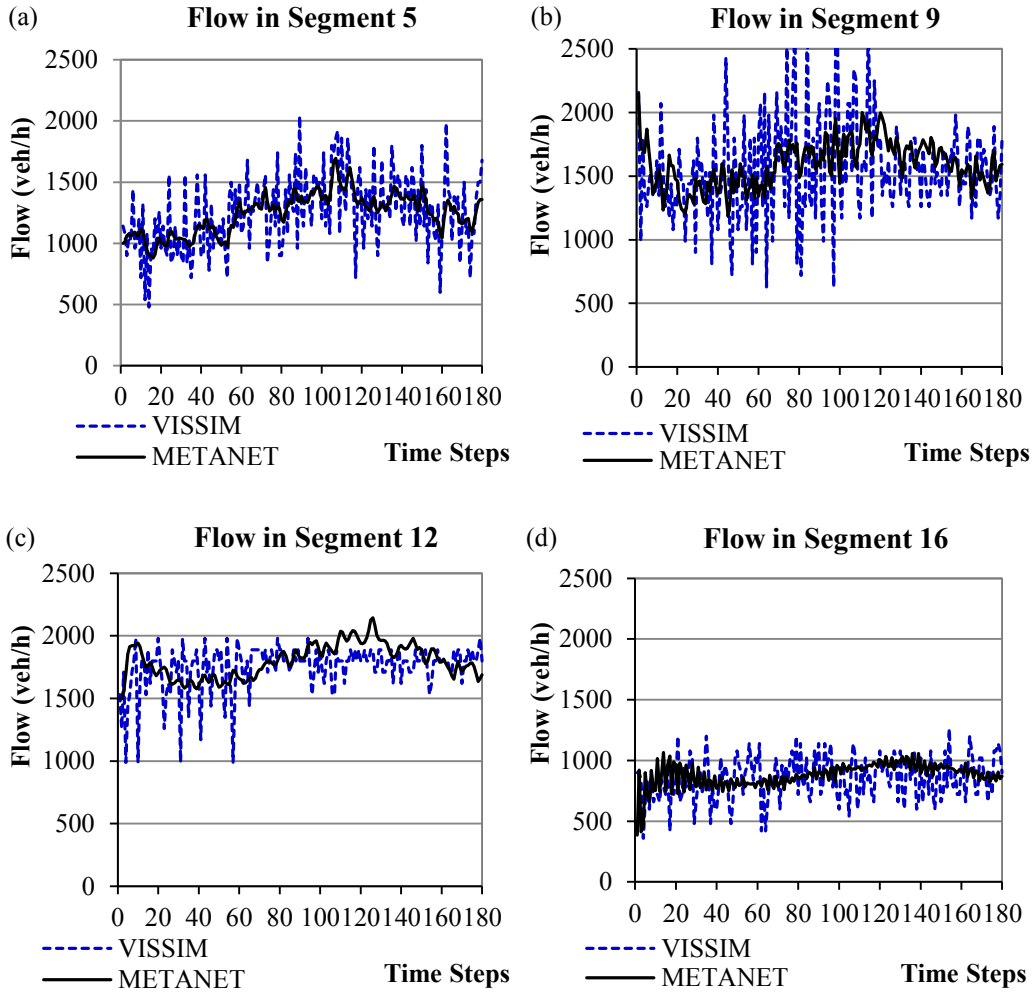

Figure 4.7 Comparison of flow from VISSIM and METANET models

Chapter 5 Experimental Investigation of Merging and Weaving Impacts on Macroscopic Traffic Simulation Models

5.1 Introduction

Many intelligent transportation system (ITS) applications, such as ramp metering (RM), variable speed limits (VSL) and active traffic management (ATM) share a common feature: they all rely on traffic models to predict future traffic states (speed, density and flow) on the roadways, so that appropriate control measures can be adopted for the corresponding traffic conditions to reduce congestion or improve traffic efficiency. These model based traffic controls are referred to as model predictive control (MPC). Macroscopic traffic models are often served for this purpose.

In terms of model components, macroscopic traffic models can be classified into first-order, second-order and third or higher-order models. Due to the mathematical complexity and no proven advantages in application, higher-order models are not used in actually traffic control as often as first-order and second-order models.

First-order traffic models are essentially a conservation law coupled with the assumption that there exists an equilibrium speed-density relationship within the

density domain, or equivalently, a flow-density relationship (fundamental diagram, FD). No explicit speed dynamics is required as it is assumed that the speed does not deviate from the speed-density relationship. First-order traffic models can explain major important qualitative features of traffic flow, such as the dissipation of traffic jams at bottlenecks, propagation of disturbance in traffic stream (Zhang 1998). However, it does not allow for a dynamic generation of traffic instabilities. It is impossible to describe correctly the traffic flow under non-equilibrium states, such as phantom traffic jams, stop-and-go waves or forward propagation of disturbance in heavy traffic.

In the second-order traffic models, an explicit speed dynamics is included in addition to the first-order model equations. This allows for speed deviation from the equilibrium speed-density relationship. The speed dynamics describes the evolution of speed in relation to not only traffic density, but also driver's delayed response to the traffic conditions, such as traffic density at the downstream and traffic flow speed. The well-known speed dynamics developed by Payne (1971) can be expressed as an additive function of relaxation, convection and anticipation components. Some other speed dynamics also include diffusion (or viscosity) part depending on how the speed dynamics is derived. Even though the equilibrium speed (or desired speed) is still present in the speed dynamics, the actual traffic speed can deviate from it. This is more flexible to describe traffic speed evolution than the first-order models.

As we know, the speed dynamics are often derived for uninterrupted traffic on a section of roadway without ramps. It is a function of traffic states (speed, density, etc.) without any ingredient of the impact from ramps. In reality, on-ramps and off-ramps can form merge, diverge and weavings depending on roadway configurations. Both merging and weaving may impact the speed on the main road as can be observed in the field or in microscopic simulation. Other than flow and density change, the impact due to the inflow and outflow from ramps on the speed dynamics were not clearly expressed in mathematical models. This limitation was intended to be overcome in macroscopic simulation by adding additional terms in speed dynamics to account for those impacts. However, the disadvantage of including more terms is that they will bring more model parameters and add complexity in model calibration, as model parameters may have interactive effects. In addition, it is still not clear whether the added terms can significantly improve the performance of the macroscopic simulation models, because macroscopic models aggregate traffic behaviour and may overlook local variations. The local disturbances due to the merge, diverge or weaving may or may not be accurately accounted for by the model. For example, Papageorgious et al. (1989) modeled an arterial street in Paris. Effects of several components of the speed dynamics equation was studied and concluded that dropping the merge term will have no evident impact on model accuracy on the studied roadway but will evidently increase simulation speed. This is

only one case and may not be taken as a general conclusion as there is very limited study on this subject. It is necessary to evaluate the impact of merging and weaving terms on the model performance under different flow conditions.

The objective of this study is to systematically investigate the merging and weaving impacts on the speed dynamics of macroscopic simulation models and provide experimental evidence as to whether explicit merging and weaving terms should be include in the speed dynamics of macroscopic simulation models to predict traffic states more accurately. The importance of this study is that if the merging and weaving impact on speed dynamics is significant, it should be included in the model to improve prediction accuracy. Otherwise, they can be omitted to simplify model calibration and improve computation efficiency in macroscopic simulation and traffic control.

5.2 Methodology

The general methodology of this study consists of the following key tasks:

- Selection of study site;
- Development of macroscopic simulation models;
- Experimental design;
- Collection of data;
- Model calibration and
- Data analysis.

These key tasks are described in the following sections.

5.3 Studied Freeway Corridor

The site selected for the study is a section of the westbound direction of Whitemud Drive (WMD), which is an urban freeway in the city of Edmonton, Alberta, Canada, from the west of 111th Street to west of 159th Street (shown in Figure 1.1). This 8.6-km long freeway section has five on-ramps and six off-ramps, which form five merges, six diverges and four weaving sections.

Some road improvements were constructed on this freeway during the years between 2010 and 2013, including the extension of acceleration lanes and added lanes on the bridge crossing North Saskatchewan River. The number of through lanes varies from 3 lanes to 4 lanes in different segments. This test section has a posted speed limit of 80 km/h and an average annual daily traffic (AADT) of about 100,000 vehicles both directions in total. Nine loop detector stations were installed on the mainline, each consisting of dual-loop detector groups on each travel lane. Each of the on-ramps and off-ramps are equipped with loop detectors as well, in addition to those mainline detectors. Furthermore, there are seven traffic cameras along the mainline, which were used for observing vehicle maneuvers resulting from driver behaviour, including lane-changing aggressiveness in different freeway segments, time of congestion formation and congestion duration. Due to the existence of several bottlenecks, this section of roadway experiences recurrent heavy congestions from 7:00 to 9:00 of morning peak hours and 4:00 to 6:00 of afternoon

peak hours, respectively. To reduce traffic congestion, coordinated ramp metering and variable speed limits have been under study and will be implemented in the future to address increased traffic demand.

In macroscopic simulation, the roadway is subdivided into a number of segments and the time is discretized into short time intervals (denoted by T). The aggregated traffic state variables (speed, density and flow) are defined for each segment and updated for each time step. The freeway for this study was divided into segments based on the distances and number of lanes between on-ramps and off-ramps. The discretization of the roadway and the location of ramps are shown in Figure 5.1. It should be noted that the discretization of the roadway for the studies described in this chapter is different from that in Chapter 4, in which some parts of the roadway were under construction (extended some acceleration lanes, added a lane on the bridge crossing the North Saskatchewan River, etc.) and the posted speed limits were different as well due to construction zones. The construction was completed in late 2013 and the study in this chapter is based on the roadway configuration after the construction.

As shown in Figure 5.1, the corridor is discretized into thirteen segments with the lengths vary from 279m to 1140m. Each segment is a homogeneous unit in which the number of lanes remains unchanged. Usually short acceleration/deceleration lanes, merging/diverging tapers at lane adding/dropping or at ramps cannot be

modeled as a lane because the short length which does not satisfy minimum segment length requirements. Geometric details of the roadway, such as curvature, grade and lane width cannot be represented directly in the model. On-ramps and off-ramps are always located at the beginning and end of the segments respectively and traffic control measures are located at the beginning of segments. Five on-ramps are located at segment 3, 6, 7, 9 and 11, and six off-ramps are located at segment 3, 4, 5, 7, 9 and 11, respectively. Four weaving sections are formed on segment 3, 7, 9 and 11.

5.4 Macroscopic Simulation Models

As discussed in Chapter 2, the formulation of macroscopic simulation models varies depending on whether merging, weaving or other components, such as diffusion, are considered in the model. This study starts from a basic second-order macroscopic simulation model developed by Payne (1971, 1979). The impact of merge and/or weaving due to on-ramps and off-ramps were represented by adding corresponding terms to the speed dynamics, which forms different models. The models are then evaluated based on their performances on traffic state predictions.

5.4.1 Base Model

The base model used in this study is very similar to that used in Chapter 4. It consists of four equations: a density dynamics, a speed dynamics, an equilibrium

speed-density relationship and a basic equation that flow equals to the multiplication of speed and density. The model equations are as follows (Carlson et al. 2010):

$$\rho_i(k+1) = \rho_i(k) + \frac{T}{L_i}[\rho_{i-1}(k) \cdot v_{i-1}(k) - \rho_i(k) \cdot v_i(k) + r_i(k) - s_i(k)] \tag{5.1}$$

$$v_i(k+1) = v_i(k) + \frac{T}{\tau}[V(\rho_i(k)) - v_i(k)] + \frac{T}{L_i} \cdot v_i(k) \cdot [v_{i-1}(k) - v_i(k)] - \frac{\eta \cdot T}{\tau \cdot L_i} \frac{\rho_{i+1}(k) - \rho_i(k)}{\rho_i(k) + \kappa}$$

$$V_i(k) = v_f \cdot \exp\left[-\frac{1}{\alpha}\left(\frac{\rho_i(k)}{\rho_{cr}} \right)^{\alpha} \right] \tag{5.2}$$

$$q_i(k) = \rho_i(k) \cdot v_i(k) \tag{5.3}$$

$$\tag{5.4}$$

The symbols and notations used in this model are the same as in Chapter 4 and are not repeated here.

5.4.2 Modelling Impact of On-Ramps

Ramps are essential components of freeway systems and they may impact freeway operation depending on their geometric configuration and also on the traffic volume on both the through lanes and ramps. There are three possible configurations of ramps: isolated on-ramps, isolated off-ramps and an on-ramp immediately followed by an off-ramp. While the impacts of ramp inflow/outflow on the density of road segments can be calculated based on the conservation law, the impacts on speed depends on the traffic conditions of the road segment and the configuration of ramps. This requires a more detailed discussion.

An isolated off-ramp usually has very limited impact on the speed of the through movement, because at freeway off-ramps most exiting vehicles start to decelerate in

deceleration lanes. As long as there is no backup queue of vehicles from the downstream of the off-ramps, the exiting vehicles have a negligible impact on the through movement on the mainline. Therefore, an isolated off-ramp does not need additional consideration on the speed dynamics of the simulation model for the mainline freeway.

Different from isolated off-ramps, isolated on-ramps impact the traffic operations on the mainline due to the inflow from the ramps. An isolated on-ramp is shown in Figure 5.2.

On-ramp vehicles influence the traffic model in two ways. First, the merging of additional traffic volume from on-ramps will increase the density of the corresponding freeway sections. Density, in its turn, influences the mean speed by means of the speed-density relationship. Second, entering vehicles usually have lower speeds than the vehicles on the through lanes. When on-ramp vehicles merge into the through lane, vehicles on the through lane may have to reduce the speed or change to the adjacent lane, which may also affect the speed on the adjacent lane. This seems particularly important in cases of a high entering rate from on-ramps.

As described in Chapter 2, the impact of the merging and/or diverging flow on the speed of the mainline traffic flow can be modeled by adding a traffic friction term into the speed dynamics of Payne's (1971) model. This principle is carried over to macroscopic simulation models. The speed dynamics Equation (5.2) was extended

by including additional terms to directly account for the impacts from on-ramps, or a sudden blocking of lanes due to incidents (Papageorgious et al. 1989, Papageorgious et al. 1990, Sanwal et al. 1996 and Bellemans 2003), because the often-observed slow-down of traffic in the vicinity of an on-ramp cannot be explained by the increased traffic density in the segment fed by the on-ramp alone. A merge term in the speed dynamics accounts for the additional decrease of average speed due to the disturbances caused by the merging traffic from on-ramps and lane-changing vehicles on the mainline. The merging term can be expressed in the following form (Papageorgious et al. 1990, Sanwal el at. 1996, Belleman 2003):

$$\Delta v_{merge,i}(k) = -\left(\frac{\delta_m \cdot T}{n_i \cdot L_i}\right) \frac{q_{on}(k) \cdot v_i(k)}{\rho_i(k) + \kappa_m} \tag{5.5}$$

Where, δ_m is a tuning parameter for the merging term. n_i is the number of through lanes at the merge section and κ_m is a density constant to avoid abnormal model performance, such as zero at the denominator. $q_{on}(k)$ is the inflow from an on-ramp at time step k. $v_i(k)$ is the speed on the mainline freeway.

According to Equation (5.5), the decrease in average speed in the segment i due to the merging traffic is proportional to the inflow $q_{on}(k)$ from the on-ramp. Since the merging of on-ramp traffic becomes more difficult as the speed on the freeway increases, the impact of the merging vehicles (which usually have a slower speed) on the average speed in the freeway segment becomes larger as the speed of the through

movement increases. The merging term in Equation (5.5) is also inversely proportional to the traffic density $\rho_i(k)$ in the segment i. The higher the density on the through lanes, the lower the speed they have and the smaller the impact due to on-ramp merging.

There can be other forms of merge terms based on the factors that impact the traffic speed of the through lanes. For example, to incorporate the speed of the on-ramps, a merge term can be formulated as Equation (5.6) as well:

$$\Delta v_{merge,\,i}(k) = -\left(\frac{\delta_m \cdot T}{n_i \cdot L_i}\right)\frac{q_{on}(k)\cdot[v_i(k) - v_r(k)]}{\rho_i(k) + \kappa_m} \tag{5.6}$$

Where, $v_i(k)$ and $v_r(k)$ are vehicle speeds on segment i and an on-ramp, respectively. The other symbols are the same as in Equation (5.5). Equation (5.6) shows that the higher the speed differences between the mainline and the on-ramp, the larger the impact on the speed of the mainline.

For the purpose of consistency, Equation (5.5) was used in this study, so that the study conclusions can be compared with other studies using the same equation, such as the studies by Papageorgious et al. (1990), Sanwal el at. (1996) and Belleman (2003).

It should be noted that a lane drop will also cause a merge on the through lane. However, it is different from an on-ramp in two ways. First, the speed on the lane that will be terminated is similar to other through lanes at that section, while the

speed of vehicles coming from on-ramps is usually much lower and, thus will have a larger impact on the speed of the through lanes. Second, depending on driver population and traffic demand, vehicles on the dropping lane can merge into the adjacent through lane far before the termination point, while vehicles from on-ramps have no such choice. As a result, on-ramps may have a much larger impact on the speed dynamics and, thus an additional term is required in speed dynamics, while no additional term is necessary for the merging due to a lane drop.

5.4.3 Modelling Impact of Weaving

Weaving is defined as the crossing of several traffic streams moving on the freeway in the same direction (TRB, 2010). A weaving section is composed of an on-ramp immediately followed by an off-ramp, as shown in Figure 5.3.

Entering and exiting vehicles may cause weaving, which will influence mainline vehicle operation. For an entering vehicle, there are two constraints on its speed: the existing decelerating vehicle in front of the entering vehicle and a vehicle on the adjacent through lane parallel to or at the rear back of the entering vehicle. The entering vehicle needs to adjust its speed and look for a gap to merge into the through lane. For an exit vehicle, it needs also to adjust its speed to change into the weaving lane. Due to the complexity of traffic interactions in a weaving area, the traffic operation is deteriorated. As a result, the freeway capacity and speed at the weaving sections are often reduced significantly.

The exchanges of vehicles within freeway weaving sections due to on-ramps and off-ramps are often modeled based on microscopic driving principles. That is, drivers who enter or exit the freeway will change lanes when they find adequate gaps in the target lane. In macroscopic modelling, however, merging and diverging driver behaviour are not considered at the individual vehicle level. Instead, the additional impact on the through lane speed due to weaving operation can be modeled by adding a weaving term to the speed dynamics as in Equation (5.7) to account for the aggregated impact:

$$\Delta v_{weaving,i}(k) = -(\frac{\delta_w \cdot T}{n_i \cdot L_i}) \frac{q_{on}(k) \cdot v_i(k)}{\rho_i(k) + \kappa_w} \tag{5.7}$$

Where, δ_w is a tuning parameter. $q_{on}(k)$ is the inflow from an on-ramp at the time step k. n_i is the number of through lanes at the weaving section and κ_w is a density constant to avoid abnormal model performance. The other symbols are the same as in Equation (5.5).

The impact of weaving on the average speed of the through lane is proportional to the entering traffic volume, as well as the speed on through lanes. It is inversely proportional to the density on the through lane.

Equation (5.7) is very similar to the weaving term proposed by Belleman (2003), in which the critical density ρ_{cr} was used in the denominator, instead of the density on the segment. Belleman's (2003) weaving term can be re-written as:

$$\Delta v_{weaving,i}(k) = -(\frac{\delta_w \cdot T}{n_i \cdot L_i}) \frac{q_{on}(k) \cdot v_i(k)}{\rho_{cr}} \quad (5.8)$$

Neither Equation (5.7) nor Equation (5.8) includes the volume of exiting traffic. In fact, weaving includes both entering and exiting traffic, and the higher the entering and exiting volume, the larger impact on the speed. Therefore, another form of weaving term can be formulated as:

$$\Delta v_{weaving,i}(k) = -(\frac{\delta_w \cdot T}{n_i \cdot L_i}) \frac{[q_{on}(k) + q_{off}(k)] \cdot v_i(k)}{\rho_{cr}} \quad (5.9)$$

Where, $q_{off}(k)$ is the exit flow to an off-ramp at the time step k. Both Equations (5.8) and (5.9) were used in the study, which are listed in the experimental design section of this chapter.

5.5 Experimental design

A true experimental design is a study of a process or system in which certain input variables are manipulated, their effects on the output response is determined and the values of those input variables are randomly assigned to the experimental units. However, sometimes it is not practical to assign some variables to the experimental units at random; rather, it may be possible to assign groups of units to various levels of independent variables at random. This is called a quasi-experiment (Hicks et al. 1999) and this method was used in this study.

5.5.1 Factors in Experimental Design

Two factors that impact the performance of traffic models are investigated in this study: traffic demand and different configuration of merging and weaving terms in macroscopic simulation models. To systematically evaluate the merging and weaving impact on model performance, a range of traffic demands were tested to compare model performance under various traffic conditions. In addition, different combinations of merging and weaving terms were compared in the model to identify which term in speed dynamics significantly impacted model performance.

Traffic demand should cover the practical range of operations in typical traffic flow control applications. In very light traffic demands, traffic management and control measures are not required. In the study, three traffic demand levels were used to run microscopic and macroscopic simulation: moderate demand (approximately 950 to 1200 veh/h/lane at the mainline origin), heavy demand (1200 to 1500 veh/h/lane) and excessive demand (1300 to 1650 veh/h/lane). Moderate and heavy traffic demand levels were determined based on field-measured traffic, with heavy traffic demand corresponding to the actual peak hours (around 4:30 p.m. to 5:30 p.m.) and moderate demand levels correspond to the half hour prior to and half hour after the actual peak hours. Excessive traffic demand levels on the mainline were determined by artificially increasing the mainline volume from the heavy traffic demand by approximately 5% to create a long-lasting traffic jam. The intention of

this increase was to test model performance under increased traffic demand in the future once VSL is implemented on the freeway. For excessive traffic, traffic demand at on-ramps and the proportion of vehicles that exit from off-ramps were maintained the same as in the heavy traffic demand level. Within each traffic demand level, traffic flow varied between low and high values during the simulation time period.

The time interval in macroscopic simulation was 20s based on the studies presented in Chapter 4 as to what simulation time interval is most appropriate in the model.

Traffic models including merge and weave components have been discussed in previous sections. There are six different models investigated in this experimental design. They differ only in their speed dynamics.

- Model A: base model with neither merging nor weaving terms, Equation (5.2);
- Model B: base model plus a merging term, Equation (5.2) + Equation (5.5);
- Model C: base model plus a weaving term, Equation (5.2) + Equation (5.8);
- Model D: base model plus a merging term and a weaving term, Equation (5.2) + Equation (5.5) + Equation (5.8);
- Model E: base model plus a different weaving term, Equation (5.2) + Equation (5.9);
- Model F: base model plus a merging term and a different weaving term, Equation (5.2) + Equation (5.5) + Equation (5.9).

5.5.2 Choice of Experimental Design

The three basic principles of experimental design are replication, randomization and blocking. By replication, we can obtain an estimate of the experimental error, which is a basic unit of measurement of determining whether the observed differences in the data are really statistically different. Randomization is the corner-stone underlying the use of the statistical methods in the experimental design (Montgomery 1997). Statistical methods require that the observations (or errors) be independently distributed random variables. Randomization usually makes this assumption valid. Blocking is a technique used to increase the precision of an experiment. A block is a portion of the experiment material that should be more homogeneous than the entire set of material. Blocking involves making comparisons among the conditions of interest in the experiment within each block (Montgomery 1997). Blocking design can remove some confounding effects from the error variation. However, there is a restriction in the blocking design. That is, the randomization is only within each block.

Choice of design involves the consideration of sample size, the selection of a suitable run order for the experiment trials and the determination of whether blocking or other restrictions should be involved. In this experimental study, a

completely randomized design was adopted. There is no restriction on the run order. Therefore, blocking was not adopted in this experiment.

5.5.3 Sample Size

Selection of an appropriate sample size is one of the most important aspects of any experimental design. The sample size and the probability of a type II error (β, that is, failed to reject a null hypothesis when it is false) are closely related. The β error is a function of sample size. Generally, for a given null hypothesis and a determined difference to be tested, the β error decreases as the sample size increases. This can be depicted by an operating characteristic curve, as shown in many literatures on statistics (Montgomery 1997, Hicks and Turner 1999).

As the sample size gets larger, the probability of a type II error gets smaller for a given difference to be tested with a pre-determined type I error (α, reject a null hypothesis when it is true).

The total number of combinations is determined by the number of factors to be investigated and their levels. In determining the sample size, we need to decide the replication for each level of factor combination. Replication is the observation of two or more samples under identical experimental conditions. In this study, it is the number of simulation runs. It enables us to estimate error effects and obtain a more precise estimate of treatment effects. Replication has two very important properties. First, replication allows us to calculate an estimate of the experimental error, which

is necessary to determine if differences in the data are statistically different. Second, when the sample mean is used to estimate the effect of a factor in the experiment, replication provides better accuracy in estimating this effect. Theoretically, the more replication, the more accurate the test will be. However, we should also consider the nature of the problem as well as the time, cost and available resources. If the sample size is too small, we cannot get enough data to effectively judge whether the results are reliable or are precise enough to draw valid conclusions. If the sample size is larger than necessary, the experiment will waste a lot of resources or take too much time.

For microscopic simulation, usually the required number of runs (with different seed number) can be determined by statistical method depending on the desired confidence level, standard deviation of the statistic and error tolerance of the sample mean. The required number of runs is calculated by Equation (5.10):

$$n = \left(\frac{Z \cdot \sigma}{R} \right)^2 \tag{5.10}$$

Where n is the required simulation runs; Z is the coefficient corresponding to the confidence level. For 95% confidence level, Z is 1.96; σ is the standard deviation of the mean for selected MOE; R is the tolerance for the sample mean, which is the 95% confidence interval of the mean in this study.

Since the purpose of multi-simulation run of the microscopic model in this study is not to obtain an average output of traffic states from the microscopic simulation model, but to generate different data sets as input for macroscopic simulation, the number of simulation runs can also be determined based on the nature of the problem and past experience on microscopic traffic simulation (Tian et al 2002, Yin and Qiu 2011), as well as the observed variability of the model outputs during trial simulation runs. For this study, seven replications in each level of factor combination were determined and the total number of samples was 126 (3×6×7=126).

5.5.4 Experimental Design Matrix

For each combination of traffic demand and speed dynamics (macroscopic model), seven different data sets were replicated for evaluation. Table 5.1 summarizes the combinations of the different model components and traffic demand levels.

The experimental design matrix in Table 5.1 shows a factorial design with two factors: traffic demand (with three levels) and macroscopic models (with six levels). This design allows us to analyze different treatment effects for each of the factors as well as the combined effects. However, our focus is on the comparison of different macroscopic models at the same traffic level.

5.5.5 Model Performance Measures

Since the purpose of this study was to evaluate the impact of different merging and weaving terms on model prediction performance, it is natural to select the model

prediction error as the performance measure, or measure of effectiveness (MOE). The total prediction error (total error, E) is defined as the sum of squares of the relative differences between the model predicted traffic states and the ground truth traffic states. In the experimental analysis, the VISSIM outputs are taken as ground truth data. In the comparison with field measured traffic states, the field measured data are taken as ground truth.

The total error between the outputs from VISSIM (or field data) and from macroscopic simulation models for all segments and in all time steps are calculated from the equation:

$$E = \sum_{k=1}^{N_{steps}} \sum_{i \in I_{all}} \left\{ \left[\frac{\hat{q}_i(k) - \tilde{q}_i(k)}{\hat{q}_i(k)} \right]^2 + \left[\frac{\hat{v}_i(k) - \tilde{v}_i(k)}{\hat{v}_i(k)} \right]^2 \right\} \tag{5.11}$$

Where, N_{steps} is the total number of simulation time steps, I_{all} is the total number of the segments of the freeway, $\hat{q}_i(k), \hat{v}_i(k)$ are flow and speed from VISSIM (or field-measured data) in segment *i* at time step *k,* respectively and $\tilde{q}_i(k), \tilde{v}_i(k)$ are flow and speed from the macroscopic models in segment *i* at time step *k,* respectively.

It should be noted that there are other forms of objective functions that can be used as MOE. For example, root mean relative square error (RMRSE) is also an often-used objective function in comparison of simulation data and measured data. RMRSE is expressed as:

$$RMRSE = \sqrt{\frac{1}{I_{all}} \sum_{I_{all}} \sum_{k=1}^{N_{step}} \left\{ \frac{Simulated\ (v,\rho,q)_{i,k} - Measured\ (v,\rho,q)_{i,k}}{Measured\ (v,\rho,q)_{i,k}} \right\}^2} \quad (5.12)$$

Equation (5.12) has different scales from Equation (5.11) due to the square root and the division of the number of total segments. In this study, Equation (5.11) is used as MOE for prediction errors.

5.6 Data Sources

There were two kinds of data for this study: data from microscopic simulation and field-measured data. As discussed in the experimental design, several replications were required for each combination of traffic demand levels and speed dynamics (macroscopic models). Data from the output of the microscopic simulation model, VISSIM (PTV 2012) were used for this purpose. For the comparison of model-predicted traffic states (speed, density and flow), both VISSIM data and field-measured data were used in the analysis.

5.6.1 Microscopic Simulation

The VISSIM model for WMD was re-constructed based on the completed construction improvements on the freeway. Virtual detectors were coded in the VISSIM model on each lane of each segment, as well as on each on-ramp and off-ramp to measure flow and speed during simulation. This data was used to calibrate and validate the re-constructed VISSIM model against the field data from

loop detectors, following the same procedures described in Chapter 4. After the calibration and validation, VISSIM model was used to generate microscopic simulation data based on the experimental design. Three traffic demand levels were input to the VISSIM model.

Due to the stochastic nature of simulation, the output varies in different runs, because many parameters used in each simulation run will be generated according to specified distributions. The number of simulation runs can be determined based on either statistical principles or past experience, considering the variability of output data and precision requirements. In this study, ten runs with randomly selected seed numbers were performed for each traffic demand level. Two sets of simulation data were used to calibrate and validate different macroscopic simulation models (one set of data was used as a spare set in case any abnormal data was generated), and the remaining seven sets of data were used as ground truth for macroscopic simulation runs in the experimental data analysis (replica).

5.6.2 Field Measured Traffic Data

After the roadway improvement construction, field loop detectors were checked and used to record field traffic data (flow, occupant time, etc.). The dual loop detector data was integrated into 20s intervals. The loop detector data recorded during afternoon peak hours (4:00 – 6:00) on October 17th and 31th of 2013 was used to compare with the model-predicted traffic states. For the loop detector data, there

were some intervals at some locations at which the field data was not recorded by some loop detectors, resulting in abnormal records, such as zero occupancy or zero flow during peak hours, while the previous time interval and next time interval recorded normal data. Abnormal and missing data was treated either by averaging the previous time interval and next time interval on the same segment, or by averaging the immediate upstream and downstream segment data at the same time interval.

5.7 Calibration of Macroscopic Models

As previously discussed, the purpose of this study is to analyze the merging and weaving impact on the performance of macroscopic simulation models. Each macroscopic model (Models A to F) was calibrated with the ground truth data, either from VISSIM outputs in experimental analysis, or from the field-measured data in the comparison of the model-predicted traffic states.

Two data sets from VISSIM simulation at each traffic demand level were randomly selected. These total six data sets were taken as the ground truth for calibrating each of the six macroscopic models; therefore, six groups of model parameters were obtained for each model. Then, for each model, these six groups of parameters were averaged, adjusted and determined to get one set of parameters for each macroscopic model. These final parameters for each model were different from

the parameters obtained for each individual model calibration. In this way, the data sets used in calibration can still be used for model runs (but not used for experimental analysis) to see how the total errors change with different parameters.

In the comparison of model-predicted traffic states with field-measured data, two separate field data sets were prepared: one for calibration and the other for comparison.

In model calibration, the nonlinear optimization method was used to estimate model parameters. The objective function was the function that calculates the total relative difference (total error) between the outputs from macroscopic simulation and the ground truth data for all segments and in all time steps, as shown in Equation (5.11).

The model parameters ($\alpha, \tau, \eta, \kappa, \rho_{cr}, \rho_{max}, \delta_{merge}, \delta_{weave}$ *and* κ_m) can be identified by minimizing the total error. The MATLAB Optimization Toolbox (The MathWorks 2010) was used to solve this nonlinear optimization problem. Each of the macroscopic models (Models A to F) had a separate set of model parameters. For example, the set of model parameters used for the model with both merging and weaving terms was α=1.6, τ=0.01hr, η=8.4 km2/h, κ= 10.0 veh/km/lane, ρ_{cr}= 50 veh/km/lane, ρ_{max} =100 veh/km/lane, δ_{merge}= 0.15, δ_{weave}= 0.20 and κ_m= 11.2 veh/km/lane. The model parameters for Model A to F, calibrated from the simulation

data sets, field measured data sets and used in model runs are listed in Table 5.2 and Table 5.3, respectively.

5.8 Data Analysis

5.8.1 Comparison of Total Errors of Different Models

The total errors, as previously defined and calculated by Equation (5.11), between the outputs from VISSIM and macroscopic simulation models for a two-hour (360 time steps) simulation of three levels of traffic demand for different models, namely Model A (base model), Model B (merge model), Model C (weave model with Equation [5.8]), and Model D (merge and weave model with Equation [5.5] and [5.8]), are shown in Figures 5.4a, b, c and d, respectively, for 10 simulation data sets at each traffic demand level. The plotted curves have very similar fluctuations at each traffic demand level. Within each model, total errors vary with different data sets. In general, the total error was higher with higher traffic demands. But this does not hold for all the cases. For example, for data sets 3 and 5, the total errors for moderate traffic demand were higher than that of heavy traffic demand. For data sets 1 and 10, the total errors for excessive traffic demand were lower than that of heavy traffic demand.

Figures 5.5a, b and c show the comparison of the total errors from the six different models (Model A, B, C, D, E and F) for each traffic demand level and the

10 data sets, respectively. As can be seen, for a particular data set at a certain traffic demand, the total errors were very close from the six different models. At a moderate traffic demand, all six lines almost overlap. At a heavy traffic demand, all six lines almost overlap, except for data sets 8 and 9, where the total error of Model F is a little lower than the other five models. The difference in the total errors among the six models is larger for excessive traffic demands, as shown in Figure 5.5c.

Figure 5.5d shows the average total errors of the 10 data sets from the six models at each traffic demand level. The average total errors from each of the six models were very similar at the same traffic demand level. It can be clearly observed that the total error was larger at a higher traffic demand level than that at a lower traffic demand level.

5.8.2 Comparison of Predicted Traffic States from Different Models

The density, speed and flow outputs from both VISSIM and the six different macroscopic simulation models (Models A to F) for the selected segments during two-hour simulation (360 time steps with 20s time interval) for data set 5 at a heavy traffic demand level are illustrated in Figure 5.6, Figure 5.7 and Figure 5.8, respectively. From the three figures, it can be clearly observed that the predicted density, speed and flow from different models was temporally consistent. The outputs from VISSIM fluctuated frequently with the time index, while the outputs from macroscopic simulation models were smooth with approximately the average

value of VISSIM at most of the time steps. The fluctuation of VISSIM outputs was due to the stochastic nature of the microscopic simulation model in which vehicles randomly enter the roadway and individual vehicle speed changes in reaction to the leading vehicles. In macroscopic simulation, however, the outputs are the average values of a segment at each time step. These values change gradually from one time step to the next.

Figure 5.6 shows the comparison of density from VISSIM and the six macroscopic simulation models in the selected segments (segments 3, 4, 6 and 11, in which segments 3 and 11 are weaving sections, segment 6 has an on-ramp and segment 4 has an off-ramp). The simulated densities from both VISSIM and the macroscopic models match in most of the time steps. Obvious differences between VISSIM and all of the macroscopic models exist in segment 6 at some time steps. In segment 6, starting from time step 70, traffic density increased suddenly due to increased traffic inflow from on-ramp #2 (ramp inflows are not shown in the figures), causing a large decrease in speed on the freeway, while the total flow on the freeway did not increase significantly. VISSIM depicted this traffic state change clearly, but none of the six macroscopic models showed the drastic increase in density. As far as the six macroscopic models are concerned, all of the models predicted very similar density. The plotted lines in Figure 5.6 almost overlap at almost all of the time steps,

except in segment 11 from time step 40 to 100, at which some minor differences exist among some of the macroscopic models.

Figure 5.7 shows the comparison of speed from VISSIM and six macroscopic simulation models in the same selected segments as in the density comparison, shown in Figure 5.6. When the road was not congested (showing a high speed in VISSIM data), the predicted speeds from VISSIM and macroscopic models matched in most of the segments. However, there are obvious differences in the predicted speed from the macroscopic models compared to the speed in VISSIM when the road was very congested. For example, considerable differences exist in segment 6 after time step 70, when traffic density on the freeway increased suddenly due to inflow from the on-ramp, causing a large decrease of speed and stop-and-go conditions on the freeway. This is represented clearly in VISSIM, but not so prominently in all of the macroscopic simulation models. The speed dynamics in all of the macroscopic models did not react quickly to the sudden change of traffic conditions. However, when the macroscopic models were compared, all of them predicted similar speeds at all time steps. If we take a close look at the predicted speed from the six macroscopic models, we can observe that the value of the predicted speed, from high to low order is Model A, E, C, B, F, D. Model E and C include the weaving term only, while Model B, F and D have the merging term. This means that, for the given formulation of merging and weaving terms compared in this study, the merging term has a larger

impact on the predicted speed than the weaving term. This observation is consistent in all segments. The formulation of the weaving term does not have a critical impact on the speed prediction, because the tuning parameter in the weaving term can provide the adjustment for different formulations. In addition, the speed predicted from models with both merging and weaving terms (Models D and F) was lower than that from models that have only a merging or weaving term (Models C and E). Figure 5.7 also shows that adding merging and/or weaving terms will decrease the predicted speed compared to the base model (Model A). However, this may or may not improve the model prediction accuracy depending on whether the ground truth speed was higher or lower than the predicted speed.

Figure 5.8 shows the comparison of flow from VISSIM and the six macroscopic simulation models in the same selected segments as shown in Figure 5.6 and 5.7. The simulated flow from both VISSIM and the six macroscopic models match very well in segments 4, 6 and 11 during almost all simulation time, but some differences exist in segment 3. According to the model mechanism, the output flow from VISSIM was counted during the simulation, while in macroscopic simulation the flow was calculated from the predicted speed and density. Even though differences between the predicted speed and density exist in segments 4, 6 and 11 at some time steps, the product of speed and density from all six macroscopic simulation models well-matches the counted flow from VISSIM model in those segments. The

difference in segment 3 is due to the merge traffic from the on-ramp, causing stop-and-go conditions on the freeway, as shown in the VISSIM speed data. All of the macroscopic models over-predicted the speed, resulting in higher flow than the flow recorded in VISSIM. Once again, all six macroscopic models predicted similar traffic flows in all segments during all time steps.

5.8.3 Comparison of Predicted Traffic States with Field-measured Data

Figures 5.9 to 5.11 show the comparison of the predicted density, speed and flow from the six macroscopic simulation models with the field-measured data. In Figure 5.9, even though some differences exist between the predicted density and the measured density (calculated from occupancy) at some time steps, especially when the measure density was above 40 veh/km/lane, the predicted density from the six models is very similar. As shown in Figure 5.10, all six macroscopic simulation models over-predicted traffic speed in segment 3, while under-predicted speed in segment 6. However, the six macroscopic simulation models match very well in all segments and all time steps. Figure 5.11 also shows that the six simulation models predicted very similar flow in all segments.

5.8.4 Analysis of Variance

The total error from the six macroscopic models can be assessed by an Analysis of Variance (ANOVA), in which the total error from each model is taken as a group. The total error variability from a certain model is defined as within group variability.

The difference of total error between different models is defined as between group variability and can be assessed by ANOVA. Since the within group variability is taken as a basis for comparison in ANOVA, it should be constructed as small as possible to maximize the effectiveness of ANOVA. Therefore, only the total errors at the same traffic demand level were used in this study, because, as it is shown in Figure 5.5d, the total errors at different traffic demand levels are obviously different. The results from one-way ANOVA of total errors from the six macroscopic models (Model A to F) for moderate, heavy and excessive traffic demand is given in Table 5.4, 5.5 and 5.6, respectively. The *p*-value of 1.000 in the three tables indicate that there is no significant difference (at a 95% confidence level) in the total error from the six macroscopic simulation models at each traffic demand level. A two-way ANOVA for the pooled data is given in Table 5.7. Similar to the one-way ANOVA, the *p*-value of 1.000 for the models indicates that there is no significant difference in the total error from the six macroscopic simulation models. The *p*-value of 0.000 for the traffic indicates that the total prediction errors from the six macroscopic simulation models are significantly different at the different traffic demand levels.

ANOVA is based on the assumption of equal variance and independence between each group and each individual value. It is necessary to test whether this basic assumption is reasonable based on the data. A plot of residuals versus normal probability can serve this purpose and is given in Figure 5.12. From the figure, it can

be seen that the normality plot is approximately a straight line, indicating that there is no serious violation of the normality assumption. Thus, the results from ANOVA can be justified.

5.8.5 Value of Merge and/or Weave Terms

As presented in the previous section, ANOVA showed that the impact of merging and/or weaving terms on overall model performance is not statistically significant. Now, we analyze the value of the merging and weaving term and compare the predicted speed from models with and without the merging and weaving terms. Use Model D (with both merging and weaving terms) and field-measured data as an example. The average values of the predicted speed from models with and without merging and weaving terms in a two-hour simulation are given in Table 5.8.

Table 5.8 shows the average values of the merging and weaving terms as well as the sum of merging and weaving terms on the corresponding segments during the two-hour simulation, using the field-measured data. On average, the value of the merging term varied from -4.09 km/h to -0.19 km/h on different segments, which represents -5.03% to -0.22% of the predicted speed. The value of the weaving term varied from -0.66 km/h to -0.3 km/h on different segments, representing -0.82% to -0.36% of the predicted speed. The value of the sum of the merging and weaving terms varied from -4.75 km/h to -0.49 km/h, which is equivalent to -5.85% to -0.58% of the predicted speed. During the two-hour simulation, the largest absolute value of

the merge term was 16.16 km/h, which represents 19.9% of the predicted speed. The largest absolute value of the weave term was 0.92 km/h, which is much smaller than that of the merge term. This seems counterintuitive, but understandable from the formulation of the merge and weave terms. In the macroscopic simulation model, merging traffic will cause an increase of density on the segment, while in weaving there are both inflow and outflow, which may or may not increase the density depending on the net inflow of traffic, and the net increase of density in the weaving segment is much smaller than the net increase of density in the merging segment.

Table 5.9 shows the values of the merging and weaving term as well as the sum of merging and weaving terms on the corresponding segments at time step 50 (k=50). The value of the merging term varied from -7.76 km/h to 0 km/h on different segments, which represents -10.0% to 0.0% of the predicted speed at time step 50 on different segments. The value of the weaving term varied from -0.61 km/h to -0.31 km/h, representing -0.79% to -0.36% of the predicted speed at time step 50 on different segments. The value of the sum of the merge and weave terms varied from -8.37 km/h to -0.31 km/h, which is equivalent to -10.8% to -0.36% of the predicted speed at time step 50 on different segments.

It should be noted that the final predicted speed does not necessarily decrease by the value of the merging and/or weaving terms. There are other terms in speed dynamics (relaxation, convection and anticipation) and model parameters, all of

which impact the final predicted speed. The parameters for the model with or without those terms are different because they are different models. As shown in Table 5.9, there is not much difference between the predicted speed between the model without the merging and/or weaving terms and the model with those terms. It should also be noted that due to the structure of a convection term, adding merge and/or weave terms in speed dynamics will not only affect the predicted speed of the segment having merging and/or weaving terms, it will also affect the prediction on the downstream segments.

5.9 Discussions

The fact that merging and weaving affect traffic speed on the through movement is often observed in the field. All of the macroscopic models used in this study can catch the speed drop that is due to the on-ramps to some degree; but not as prominently as VISSIM does. However, when the macroscopic models are compared, merging and/or weaving terms in the speed dynamics do not make a significant difference. Including merging and/or weaving terms neither obviously improves nor deteriorates the performance of the macroscopic simulation models. This seems counterintuitive; however, if we exam the macroscopic models closely, it is understandable.

In fact, macroscopic simulation models take the whole segment of roadway as a unit (including several through lanes and possibly an on-ramp and an off-ramp) and aggregate the traffic states for that segment. The speed and density difference between the merge/weave lane and other through lanes is averaged across the whole segment. Therefore, the speed and density difference is scaled down from the actual difference between the merge/weave lane and the adjacent through lane. In addition, the speed dynamics of macroscopic simulation models has several components (relaxation, convection, anticipation and possibly merging and/or weaving terms). The value of different components may offset one another, making the combined effect similar to the models without merging and/or weaving terms. Furthermore, in model calibration, a group of model parameters were obtained for each model through the minimization of the objective function. These parameters also affect the final model outputs.

It should be noted that not including merging and/or weaving lane-drop terms does not necessarily mean that those impacts have not been considered in the model. In fact, they are reflected indirectly. For on-ramps/lane drops, the merging of additional traffic volume may increase the density of the corresponding freeway segments. Density, in its turn, influences the desired speed by means of the speed-density relationship, which is part of the macroscopic models. In addition, entering vehicles from on-ramps usually have a lower speed than vehicles on the

through lanes, and this low speed is included in the calculation of the average speed for a segment.

5.10 Summary and Conclusions

This chapter systematically investigated the impact of merging and weaving terms in speed dynamics on the performance of macroscopic simulation models. Several merging and weaving formulas were evaluated and compared with the base model (without merging and/or weaving terms) with respect to the predicted speed, density and flow. Data from both microscopic simulation and field loop detectors were used in the model performance evaluation. Based on these data, all relevant model parameters were estimated in model calibration, using an optimization technique. Each macroscopic simulation model was independently calibrated and then used to simulate traffic operations on the studied freeway. The values of the merging and/or weaving terms was calculated and compared with the total predicted speed from the model.

ANOVA was performed to evaluate the variation of prediction errors of different models. Based on which, the statistical significance of merging and weaving impacts on the performance of macroscopic models was evaluated. There conclusions can be summarized as follows:

- The predicted traffic states from the models without merging and/or weaving terms is very similar to the models with merging and/or weaving terms. Merge and weave terms have no significant impact on the performance of macroscopic simulation models.
- Based on the formulation of the merge and/or weave terms that appeared in the literature and were evaluated in this research, the value of the merge or weave term varied from -6% to 0% of the predicted speed, with the average being approximately -2%.
- Adding merging and/or weaving terms does not necessarily mean better accuracy in traffic prediction with macroscopic simulation models. There is no obvious improvement of traffic state prediction. However, the models with merging and/or weaving terms are not inferior to the original model either.
- Macroscopic simulation model performance is sensitive to traffic demand. The higher the traffic demand, the higher the prediction errors.
- Based on this study, merging and/or weaving terms can be omitted in macroscopic simulation. This can reduce model parameters that need to be calibrated in the multi-parameter optimization process.

Table 5.1 Experimental design matrix

Models / Traffic Demand	Speed Dynamics			
	Base Model	Merge Only	Weave Only	Merge & Weave
	Model A	Model B	Model C	Model D
			Model E	Model F
Excessive	7 Replica	7 Replica	7 Replica	7 Replica
Heavy	7 Replica	7 Replica	7 Replica	7 Replica
Moderate	7 Replica	7 Replica	7 Replica	7 Replica

Table 5.2 Model parameters calibrated from simulation data

Parameters	α	τ	η	κ	ρ_{cr}	ρ_{max}	δ_{merge}	δ_{weave}	κ_m
Model A	1.6	0.020	7.0	9.0	45.0	100.0	—	—	—
Model B	1.7	0.014	6.1	10.0	46.1	100.0	0.05	—	8.3
Model C	1.7	0.010	6.2	10.0	50.0	100.0	—	0.04	—
Model D	1.6	0.010	9.9	9.1	50.0	100.0	0.35	0.10	7.1
Model E	1.5	0.012	9.9	4.8	49.0	100.0	—	0.10	—
Model F	1.6	0.010	8.4	10.0	50.0	100.0	0.15	0.20	11.2

Table 5.3 Model parameters calibrated from field measured data

Parameters	α	τ	η	κ	ρ_{cr}	ρ_{max}	δ_{merge}	δ_{weave}	κ_m
Model A	2.2	0.020	3.8	6.8	49.2	100.0	—	—	—
Model B	3.0	0.010	3.8	10.0	38.5	100.0	0.01	—	7.4
Model C	3.0	0.020	2.0	10.0	50.0	100.0	—	0.01	—
Model D	3.0	0.020	2.0	10.0	50.0	100.0	0.14	0.10	6.5
Model E	2.3	0.020	2.0	3.1	50.0	100.0	—	0.10	—
Model F	3.0	0.020	2.0	10.0	50.0	100.0	0.09	0.01	7.5

Table 5.4 One-way ANOVA at moderate traffic versus model

Source	DF	SS	MS	F	P
Model	5	12	2	0.000	1.000
Error	36	132291	3675		
Total	41	132302			
S = 60.62 R-Sq = 0.01% R-Sq(adj) = 0.00%					

Table 5.5 One-way ANOVA at heavy traffic versus model

Source	DF	SS	MS	F	P
Model	5	59	12	0.000	1.000
Error	36	554817	15412		
Total	41	554876			
S = 124.1 R-Sq = 0.01% R-Sq(adj) = 0.00%					

Table 5.6 One-way ANOVA at excessive traffic versus Model

Source	DF	SS	MS	F	P
Model	5	583	117	0.020	1.000
Error	36	225918	6276		
Total	41	226501			
S = 79.22 R-Sq = 0.26% R-Sq(adj) = 0.00%					

Table 5.7 Two-way ANOVA of traffic demand and model

Source	DF	SS	MS	F	P
Models	5	128	26	0.000	1.000
Traffic	2	575953	287977	34.060	0.000
Interaction	10	526	53	0.010	1.000
Error	108	913026	8454		
Total	125	1489633			
S = 91.95 R-Sq = 38.71% R-Sq(adj) = 29.06%					

Note: DF is the degree of freedom; SS is the sum of square errors; MS is the mean square errors; F and P are statistical values.

Table 5.8 Average value of merging and weaving terms

Component	Index	Formula	Segment	1	2	3	4	5	6	7	8	9	10	11	12	13
v(k+1)noM&W	(1)		Ave	70.76	74.65	77.67	79.55	82.14	82.25	81.50	81.81	82.05	82.62	80.08	81.58	84.61
v(k+1) M&W	(2)		Ave	70.76	75.17	77.26	80.07	82.29	81.65	81.67	83.22	83.78	84.94	81.28	83.13	84.61
Merge	(3)		Ave			-0.79			-2.13	-1.19		-0.19		-4.09		
	(4)	(3) /(2)	%			-1.03			-2.61	-1.46		-0.22		-5.03		
	(5)		Min			-4.21			-9.48	-5.62		-1.44		-16.16		
	(6)		Max			0.00			0.00	0.00		0.00		0.00		
Weave	(7)		Ave			-0.41				-0.42		-0.30		-0.66		
	(8)	(7) /(2)	%			-0.52				-0.51		-0.36		-0.82		
	(9)		Min			-0.54				-0.60		-0.40		-0.92		
	(10)		Max			-0.23				-0.21		-0.19		-0.29		
Merge and Weave	(11)		Ave			-1.20				-1.61		-0.49		-4.75		
	(12)	(11) /(2)	%			-1.55				-1.97		-0.58		-5.85		
	(13)		Min			-4.63				-6.01		-1.74		-16.70		
	(14)		Max			-0.26				-0.21		-0.19		-0.52		

Notes: v(k+1)noM&W: predicted speed at time step (k+1) without merge and/or weave term, km/h
v(k+1) M&W: predicted speed at time step (k+1) with merge and weave term, km/h
Ave: Average value during 360 time steps, km/h
%: Average percentage of the average value to v(k+1) during 360 time steps
Min: Minimum value during 360 time steps, km/h
Max: Maximum value during 360 time steps, km/h

Table 5.9 Value of merging and weaving terms at a time step (k=50)

Component	Index	Formula	Segment	1	2	3	4	5	6	7	8	9	10	11	12	13
v(k+1)noM&W	(1)			73.50	79.25	80.58	80.83	82.78	82.55	81.50	81.50	82.06	82.99	80.90	82.11	80.33
v(k+1) M&W	(2)		Value	73.50	79.90	81.53	82.59	83.63	82.75	82.58	83.42	84.33	85.04	77.51	85.37	80.33
Merge	(3)		Value			-1.01			-2.02	-1.45		0.00		-7.76		
	(4)	(3) /(2)	%			-1.24			-2.44	-1.75		0.00		-10.01		
Weave	(5)		Value			-0.42				-0.40		-0.31		-0.61		
	(6)	(5) /(2)	%			-0.51				-0.49		-0.36		-0.79		
Merge and Weave	(7)		Value			-1.43				-1.85		-0.31		-8.37		
	(8)	(7) /(2)	%			-1.76				-2.24		-0.36		-10.80		

Notes: v(k+1)noM&W: predicted speed at time step (k+1) without merge and/or weave term, km/h
v(k+1)M&W: predicted speed at time step (k+1) with merge and weave term, km/h
Value: value of the term at the time step (k=50), km/h
%: percentage of the term value to v(k+1) at the time step (k=50)

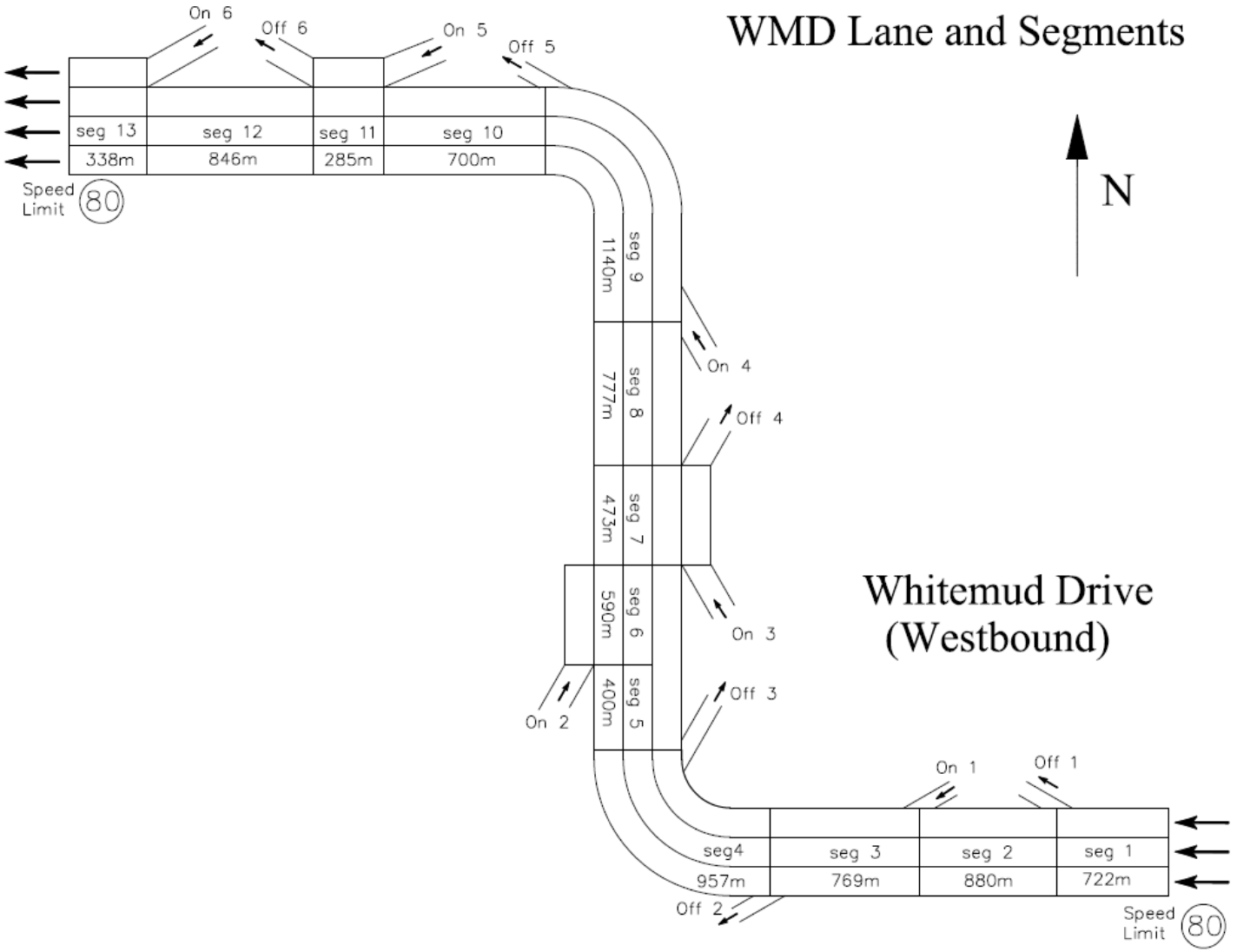

Figure 5.1 The studied freeway corridor WMD. The corridor is discretized into 13 links. (Note: not to scale)

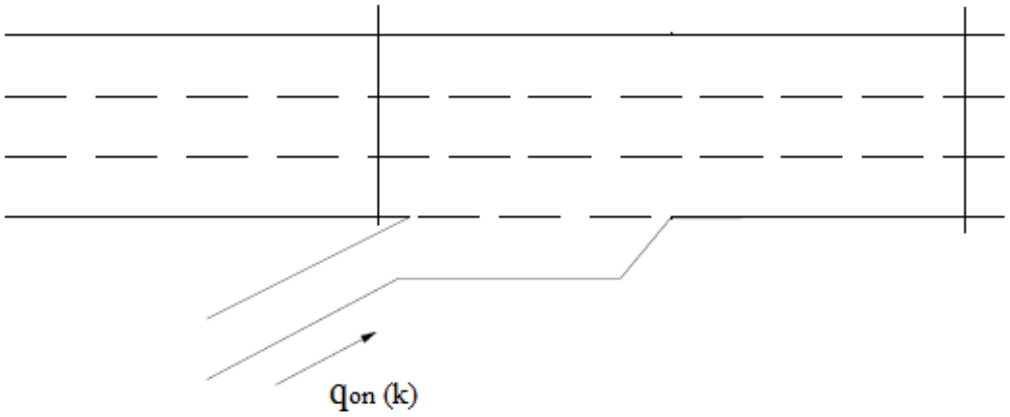

Figure 5.2 An isolated on-ramp

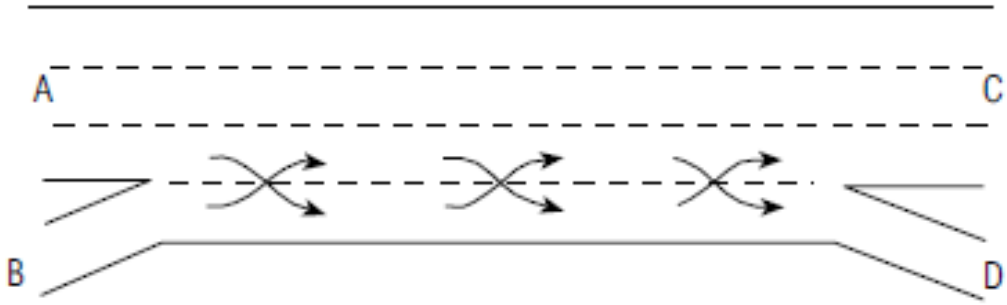

Figure 5.3 Weaving section due to ramps

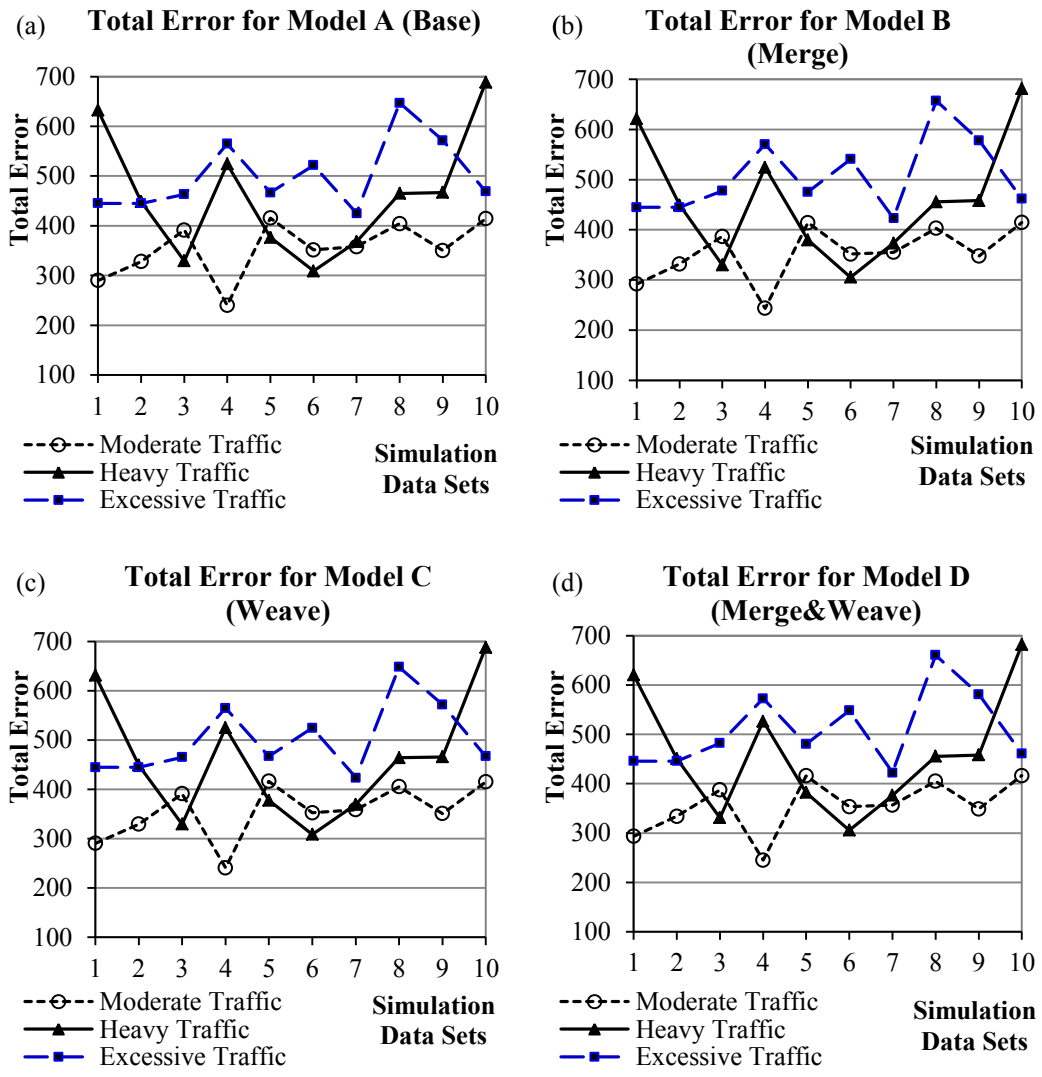

Figure 5.4 Total errors with respect to traffic demands

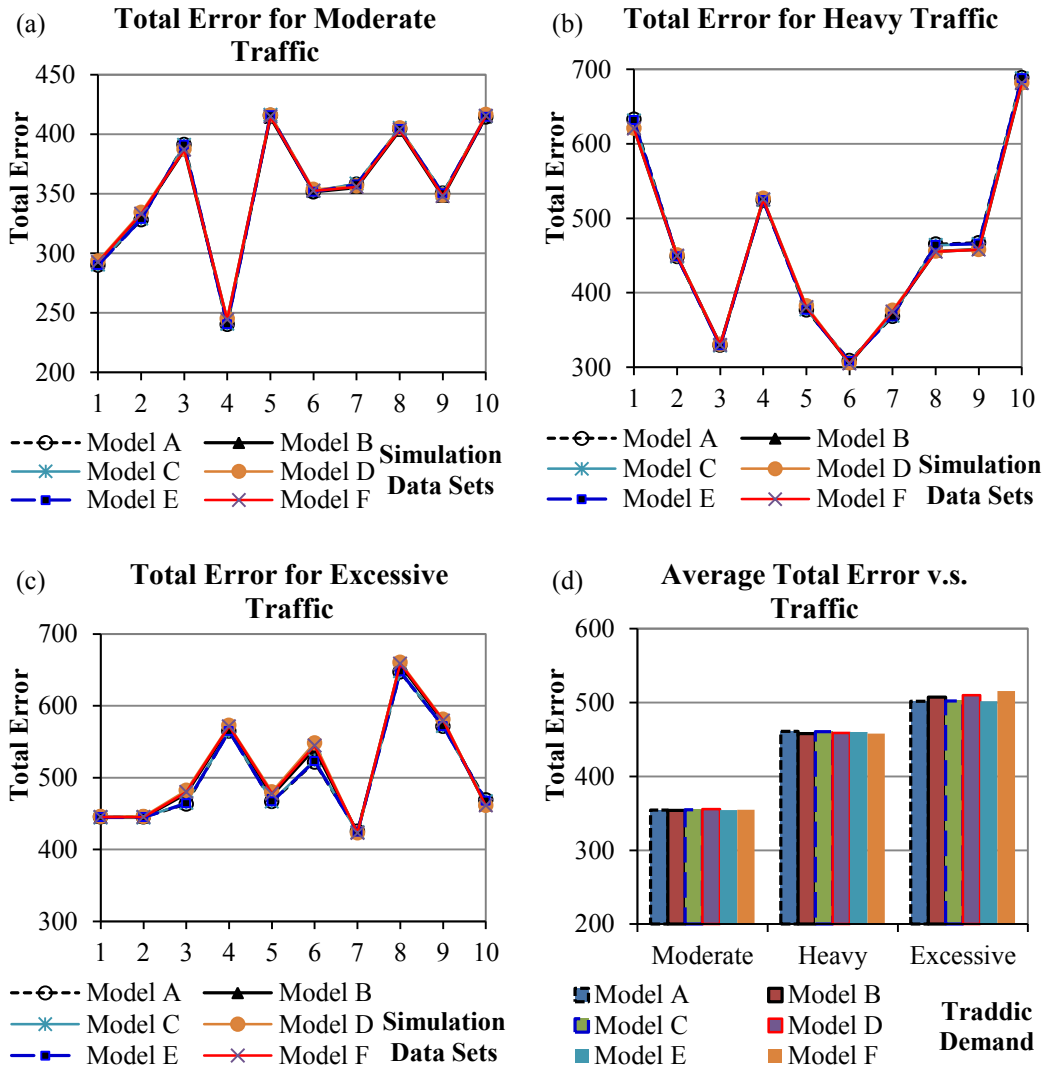

Figure 5.5 Total errors with respect to models

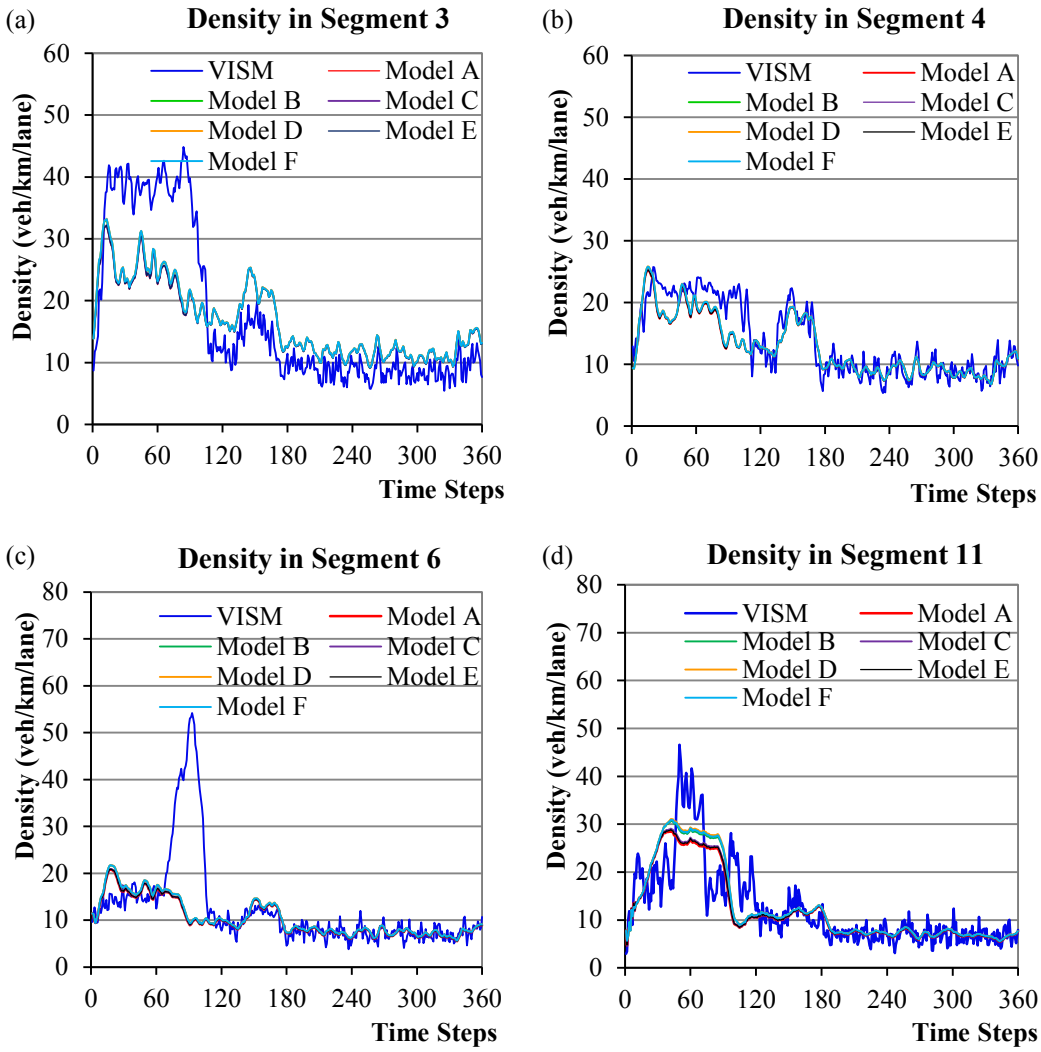

Figure 5.6 Comparison of density from different models with simulation data

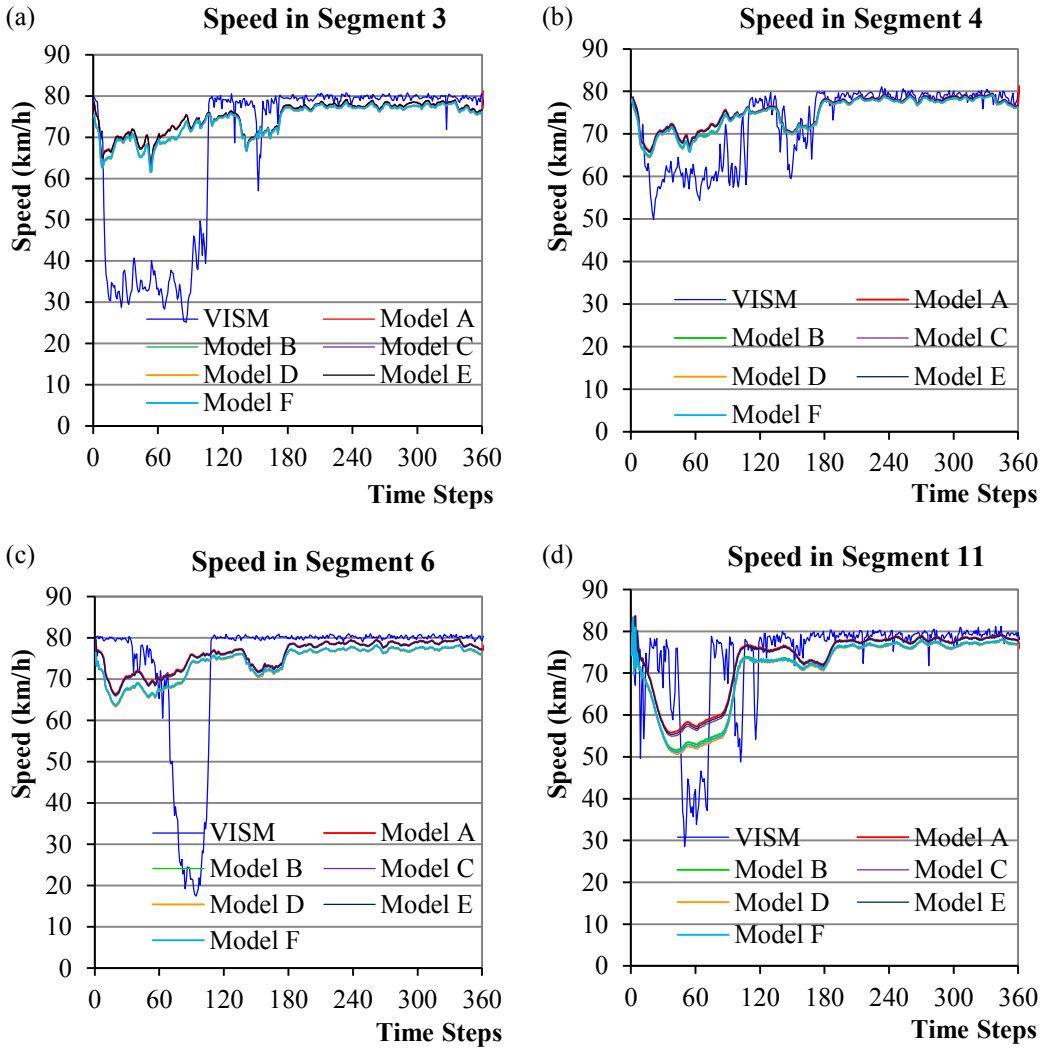

Figure 5.7 Comparison of speed from different models with simulation data

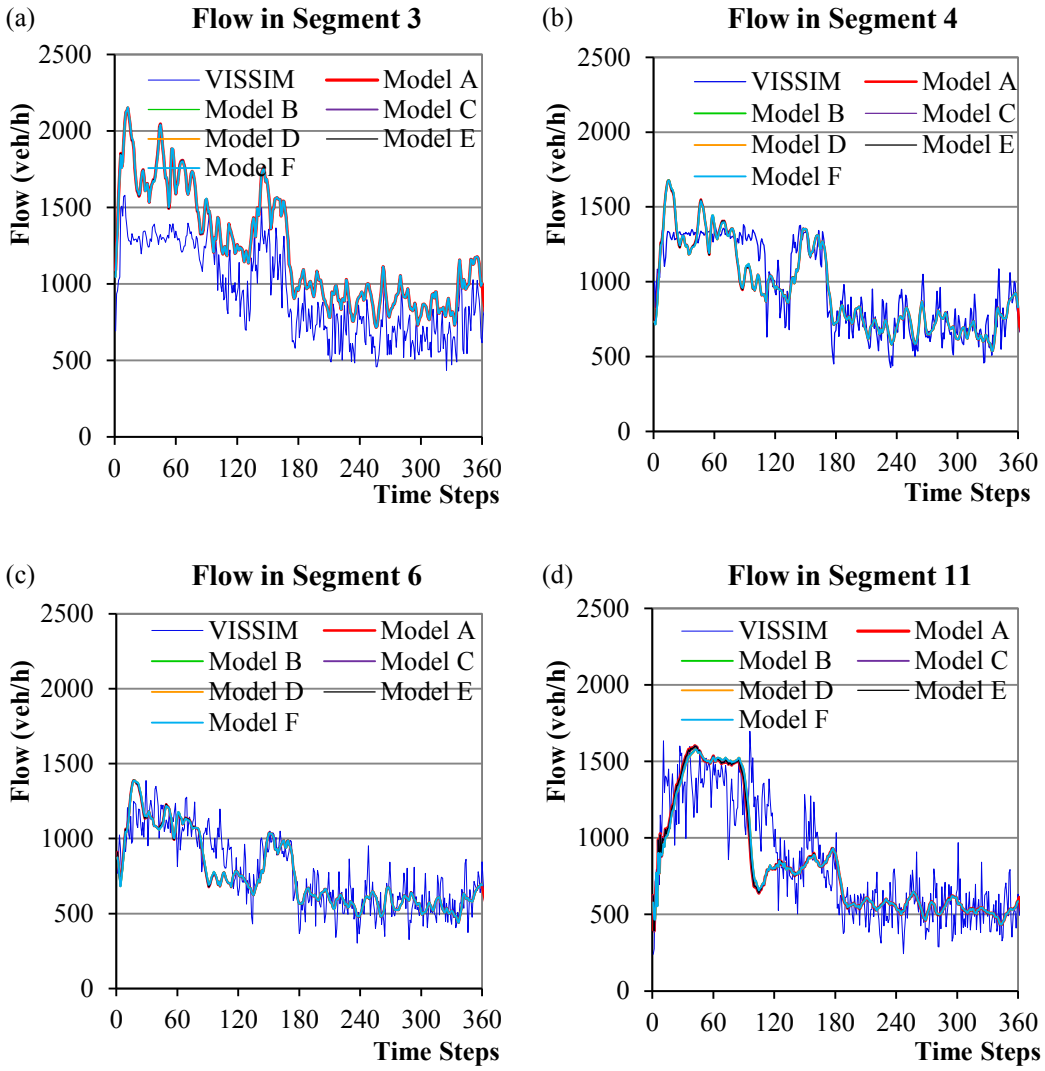

Figure 5.8 Comparison of flow from different models with simulation data

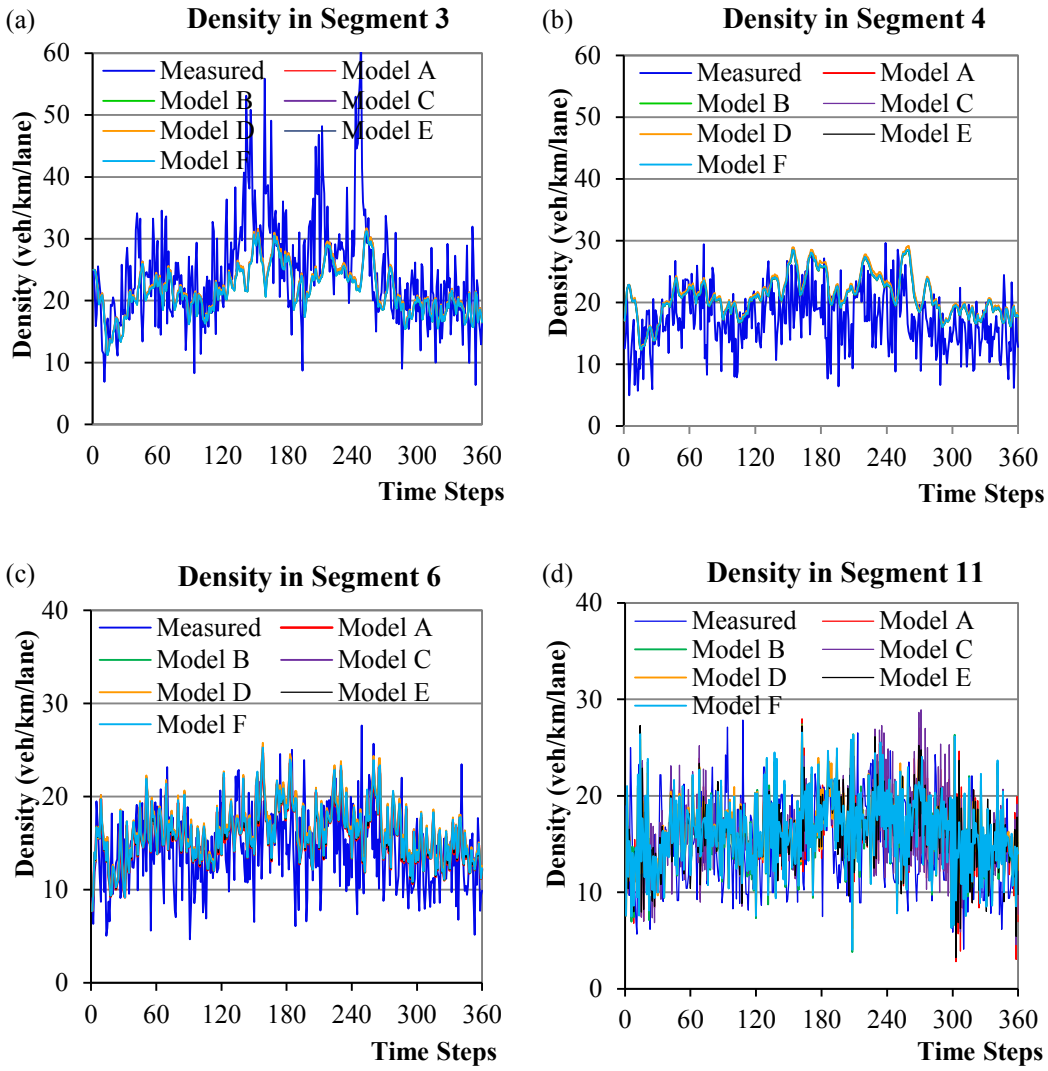

Figure 5.9 Comparison of density from different models with field data

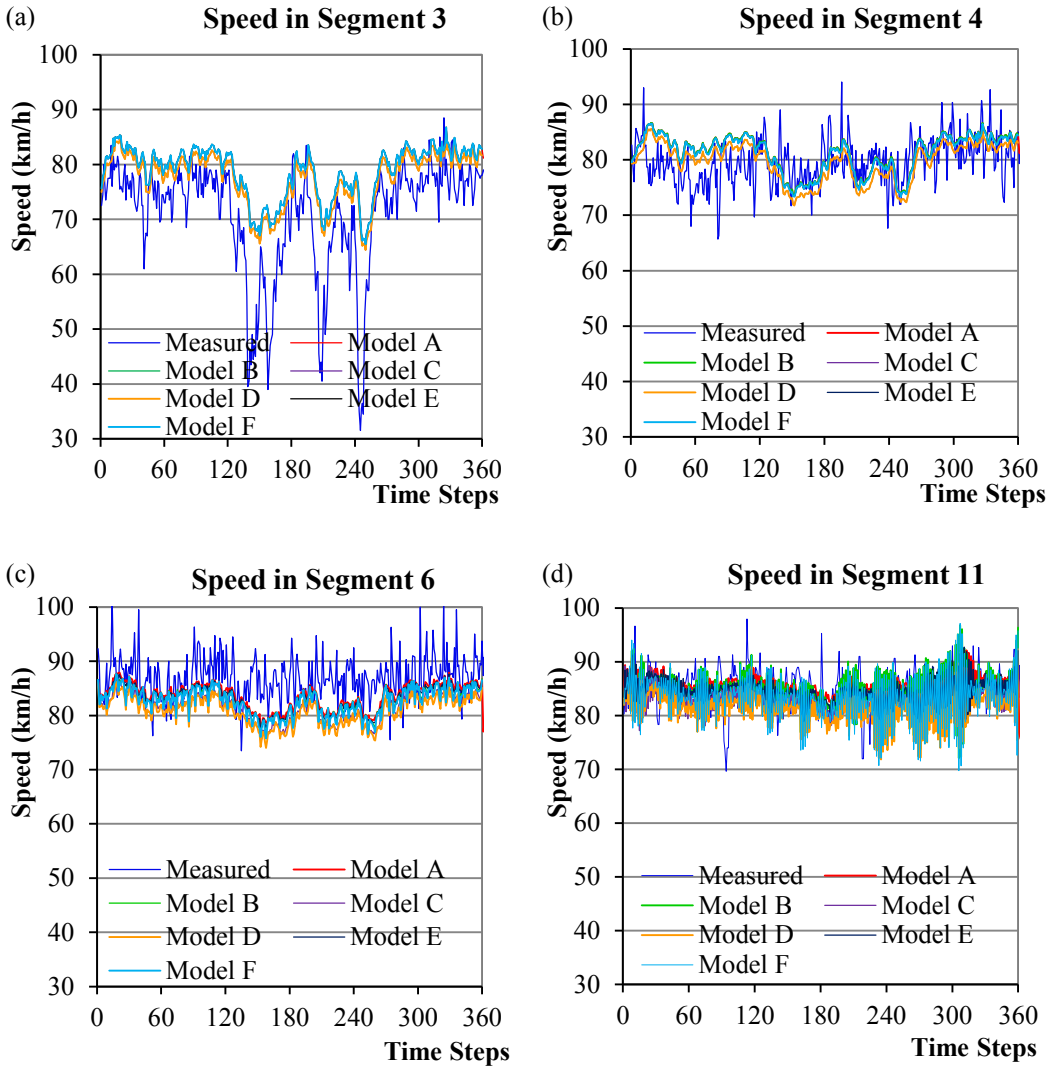

Figure 5.10 Comparison of speed from different models with field data

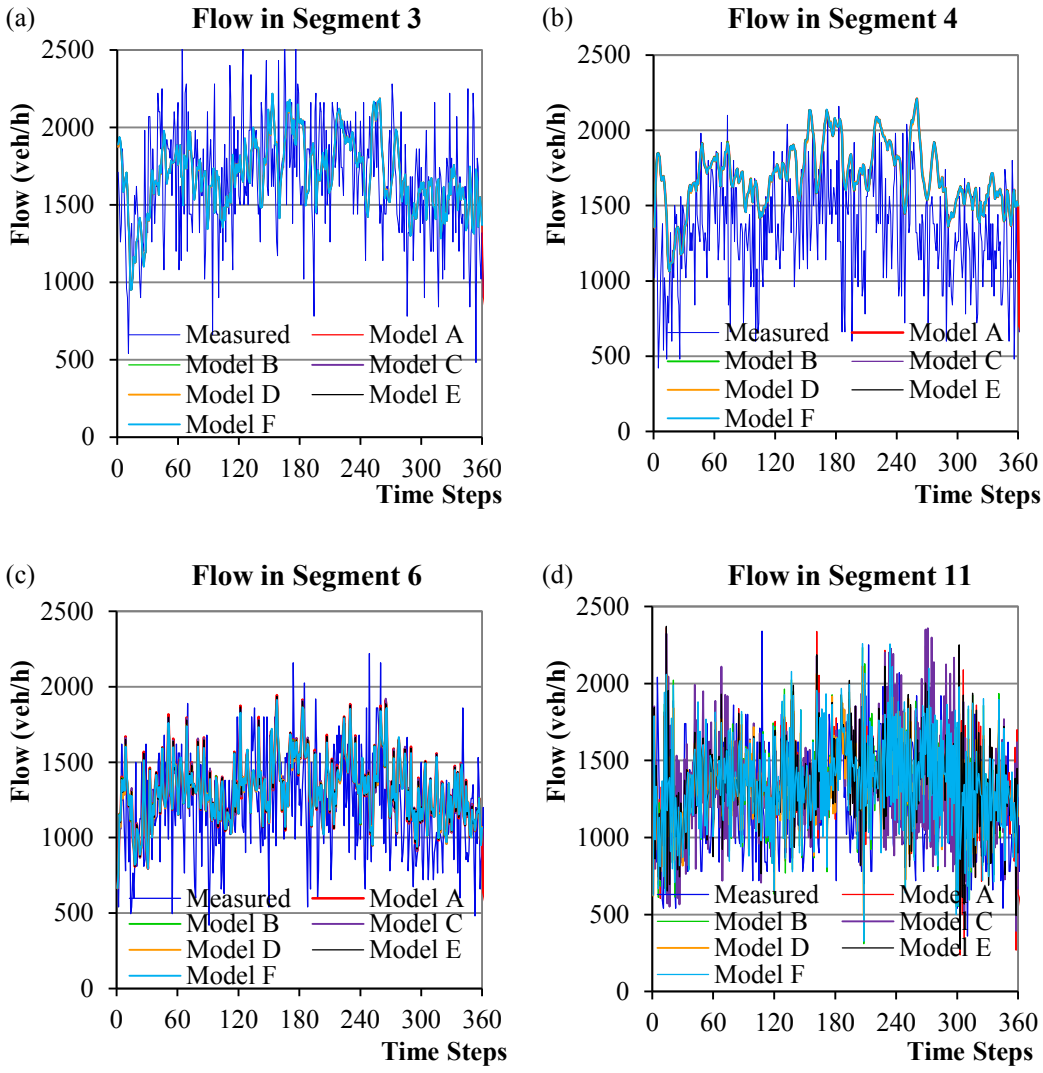

Figure 5.11Comparison of flow from different models with field data

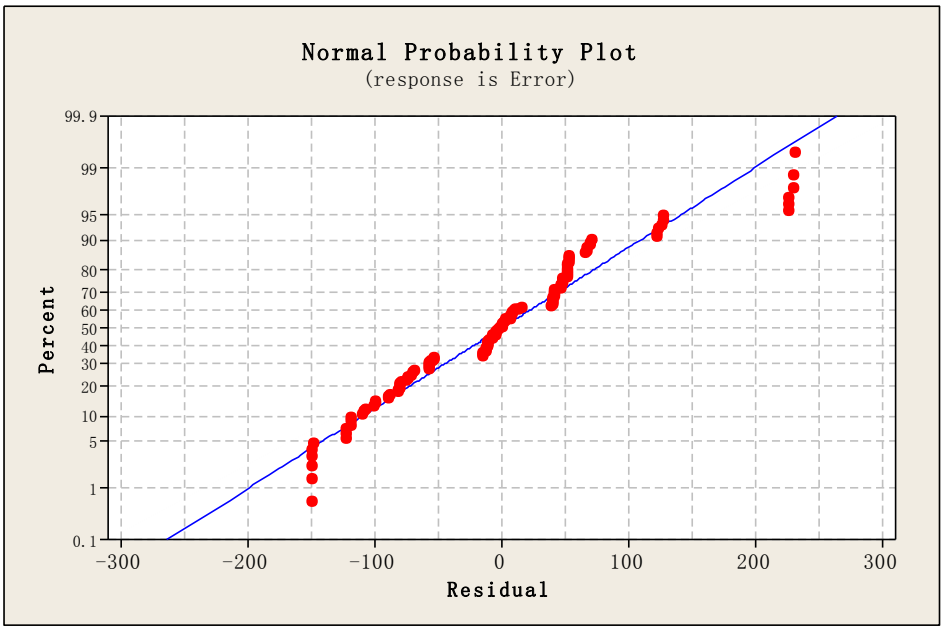

Figure 5.12 Residuals versus normal probability plot

Chapter 6 Improvement of Macroscopic Traffic Simulation Models

6.1 Introduction

Macroscopic traffic simulation models play a crucial role in model predictive control (MPC), such as coordinated ramp metering (RM) and variable speed limit (VSL), of traffic operations. In most of the online traffic control applications, discrete forms of macroscopic simulation models are often used for computer control purposes. Roadways are discretized into segments and time is discretized into time steps. Traffic states (flow, speed and density) are updated for each segment at each time step.

Traffic simulation models based on first-order macroscopic traffic models, such as the cell transition model (CTM), are essentially a density dynamics that evolves with boundary conditions at the cell ends, coupled with a static, equilibrium speed-density relationship. The density is calculated for each cell based on the conservation of vehicles within each cell. The speed is solely dependent on the speed-density relationship and it is assumed that drivers can instantaneously adjust their speed based on the traffic density. Therefore, it lacks the flexibility of catching some traffic phenomena caused by driver behaviour, such as delayed response to the traffic conditions.

Second-order macroscopic traffic models have an explicit, independent speed dynamics, which can be discomposed into several components to incorporate

driver's reaction and delayed response in the speed dynamics, such as relaxation, convection and anticipation. The speed is not only dependent on traffic density, it can also be adjusted based on anticipated traffic conditions.

Payne (1971, 1979) derived a speed dynamics equation from a microscopic car-following mechanism in discrete form. Each part of the speed dynamics is linked with physical explanations, namely, relaxation, convection and anticipation to describe how the desired speed, the speed on the upstream segment and the density on the downstream segment impact the speed on the current segment in a time step. Payne's (1979) speed dynamics has been used in many macroscopic simulation models (Cremer et al. 1981, Messmer and Papageorgiou 1990, Kotsialos et al. 2002, Lamon 2008) with mixed results regarding traffic state prediction accuracy. Cremer et al. (1981) pointed out that adding a factor of the ratio between the density on the upstream and the current segment to the convection term of the speed dynamics equation may avoid difficulties in modelling congested traffic conditions. No details about this approach were provided in Cremer et al.'s study.

The formulation of speed dynamics also varies depending on whether merging, weaving or other factors are considered in the model (Shladover et al. 2010). Papageorgious et al. (1989) modeled an arterial street in Paris and concluded that dropping the merge term will have no evident impact on model accuracy on the studied roadway, but will evidently increase the simulation speed. The investigation presented in Chapter 5 of this dissertation confirmed that adding merge and/or weave terms in the speed dynamics has no significant impact on model prediction accuracy.

Speed dynamics was also modified to avoid the requirement of the fundamental

diagram (FD), because the assumption and calibration of the FD often leads to large errors (Lu et al. 2010). The intended control speed was used to replace the equilibrium speed in the original model. The modified model was applied in combining VSL with RM for freeway traffic control, and a noticeable improvement of traffic flow was achieved.

In Hegyi's studies (2005a, 2005b), the METANET model (Messmer and Papageorgiou 1990) was extended to model dynamic speed limits and main stream metering as opposed to on-ramp control. Speed limits were incorporated in the model and act as a potential upper boundary of the desired speed. The original speed dynamics equation was not modified. The speed dynamics of the METANET model was further studied by Lu et al. (2011) as well as Yin and Qiu (2012), in which several forms of convection terms, considering the convection effect from the further upstream segment, were used to replace the convection term in the original model. Better prediction results were obtained by the modified speed dynamics compared to the original METANET model. The studies also showed that a quicker response to traffic dynamics is required to model congested traffic.

Most of the previous studies on speed dynamics mainly focused on the speed limits, FD and speed convection from upstream. The impact of the speed on the downstream segment was not considered in the model. In addition, the value of the density gradient term in the original Payne's (1979) model was not further studied, which may have considerable impacts on speed predictions. The objective of this study is to investigate different ways to improve the prediction accuracy of the macroscopic simulation models. The remaining part of this chapter is organized as

follows: the two studied corridors and data sources are described after this introduction. Then, the value of each component of the density and speed dynamics are analyzed followed by discussions on various model improvement considerations. The prediction results from both the original and improved macroscopic simulation models are compared with field-measured data as well as with the results of the microscopic simulation, based on which, conclusions from this study are presented.

6.2 Studied Freeway Corridors and Data Sources

Two freeway corridors were selected for this study. The first one is the westbound direction of an urban freeway, Whitemud Drive (WMD), in the city of Edmonton, which is the same location as presented in Chapter 5 and shown in Figure 1.1 and Figure 5.1, respectively. The second corridor for this study was the Berkeley Highway Laboratory (BHL) system, which is a test site that covers 4.3 km of I-80 eastbound/northbound freeway immediately east of the San Francisco-Oakland Bay Bridge in California, USA (Figure 6.1).

There are two kinds of data for WMD: data from the output of microscopic simulation model, VISSIM (PTV 2012), and data from the field loop detectors. Road construction was carried out on WMD during the years 2010 to 2013. The VISSIM model for WMD was re-constructed based on the completed construction improvements. Virtual detectors were coded in VISSIM on each lane of each segment, as well as on each on-ramp and off-ramp to measure flow and speed during simulation. This data was used to calibrate and validate the re-constructed VISSIM model, following the same procedures described in Chapter 4. After the calibration

and validation, the model was used to generate microscopic simulation data for various studies and analyses.

After construction completion, field loop detectors were checked and additional ones installed at the added lanes and used to record field traffic data (flow, occupant time, etc.). This dual loop detector data was integrated into 20s intervals. The loop detector data, recorded during afternoon peak hours on October 17 and 31 of 2013, was used to compare with the model-predicted traffic states. Some data processing and treatments were made at some locations at which the field data was not recorded by some loop detectors, resulting in abnormal records, such as zero occupancy or zero flow during peak hours, while the previous time interval and next time interval recorded normal data. Abnormal and missing data was treated either by averaging the previous time interval and the next time interval on the same segment or by averaging the immediate upstream and downstream segment data at the same time interval.

On the second freeway corridor (BHL), there are five through lanes in each direction and on- and off-ramps at the interchanges. Recurrent traffic congestion occurs during peak hours due to high traffic demand. On each lane of the BHL, detectors are installed at eight cross-sections. Each detector station is a dual loop with 1s update rate and 60 Hz loop on/off information on individual vehicle actuations. Data was processed by cleaning, imputation and correction, and then averaged across all lanes and aggregated into 20s and 60s traffic state variables in space mean speed, density and flow (Lu et al. 2010). This data was then used for model calibration. On- and off-ramp flows were ignored since the measurements

were not available (Lu et al. 2010). The reason for selecting this site was that the field data was available and various macroscopic simulation studies were carried out on this freeway. The data covered 10 hours of traffic operation with various traffic conditions: from free flow to heavy congestion, at which the average traffic speed drops down to approximately 20 km/h. This stop-and-go traffic can be used to test the effect of the model improvements in this study.

6.3 Debriefing of the Macroscopic Simulation Model

To improve macroscopic models, it is essential to understand how different components of the density and speed dynamics affect the predicted traffic states. This debriefing is discussed in this section before the model improvements are discussed.

6.3.1 Original Macroscopic Simulation Model

The original macroscopic simulation model used in this study is the same as the base model described in Chapter 5. It has a density dynamics, a speed dynamics, an equilibrium speed-density relationship and a basic equation that flow equals to the multiplication of speed and density. The model equations are as follows (Carlson et al. 2010):

$$\rho_i(k+1) = \rho_i(k) + \frac{T}{L_i}[\rho_{i-1}(k) \cdot v_{i-1}(k) - \rho_i(k) \cdot v_i(k) + r_i(k) - s_i(k)] \tag{6.1}$$

$$v_i(k+1) - v_i(k) = \frac{T}{\tau}[V(\rho_i(k)) - v_i(k)] + \frac{T}{L_i} \cdot v_i(k) \cdot [v_{i-1}(k) - v_i(k)] - \frac{\eta \cdot T}{\tau \cdot L_i} \frac{\rho_{i+1}(k) - \rho_i(k)}{\rho_i(k) + \kappa} \tag{6.2}$$

$$V(k) = v_f \cdot \exp\left[-\frac{1}{\alpha}\left(\frac{\rho_i(k)}{\rho_{cr}} \right)^{\alpha} \right] \tag{6.3}$$

$$q_i(k) = \rho_i(k) \cdot v_i(k) \tag{6.4}$$

Symbols and notations used in the model are the same as in Chapter 5 and will not be repeated here.

The first term on the right-hand-side (RHS) of Equation (6.2) is generally interpreted as a relaxation term (the average speed in a segment tends to evolve towards the density-dependent equilibrium speed). Relaxation is proportional to the difference between the actual average speed and the equilibrium speed (desired average speed) in segment i. By observing the density, drivers tend to accelerate or decelerate towards the desired speed. The larger the difference between the actual speed and the desired speed, the greater speed adaptation. The impact of the relaxation is also dependent on the drivers' reaction time, which is expressed as τ in the formulation. The shorter the reaction time, the faster the drivers will respond to the speed difference and the greater impact of the relaxation on the speed dynamics.

The second term on the RHS of Equation (6.2) is a convection term, which represents the fact that traffic flow from the upstream segment to the current segment will cause speed changes in the current segment due to the speed difference. Vehicles flowing from an upstream segment to a downstream segment do not instantaneously change the speed. It has a convection effect similar to water flow in a channel, where high speed merges into slow speed over some distance. Convection is proportional to the speed difference between the two segments (i-1) and i. The higher the speed difference, the longer time the vehicles in segment (i-1) will need to accelerate or decelerate while entering segment i, and the greater the impact on the speed adjustment in segment i. Convection is also proportional to the average speed in segment i. The higher the speed, the longer time the vehicles will need to adapt

their speed, and the greater the impacts on the speed adjustment in segment i. The impact of convection is inversely proportional to the length of segment i. The longer the segment, the more vehicles can drive at their desired speeds and, thus the lower the impacts on the average speed in segment i.

Anticipation (also called density gradient) accounts for the fact that drivers are looking ahead and respond to the traffic density downstream accordingly. Anticipation is affected by the relative difference of the density in the downstream segment (i+1) and the current segment (i). If drivers observe higher traffic density ahead, they tend to slow down. Otherwise, if the traffic density ahead is lower than the density on the current segment, drivers will accelerate. Anticipation is proportional to the coefficient η, which has the meaning of traffic pressure, resulting from speed variance. The higher the speed variance, the greater the impact of the density differences on the speed adjustment in segment i. In addition, anticipation is inversely proportional to the length of segment i, because drivers can only start to adjust their speed towards the equilibrium speed of the downstream segment near the end of the current segment. The longer the current segment, the longer the vehicles travel on the current segment without the influence of the density on the downstream segment.

There may be other terms in the speed dynamics, such as a diffusion term and/or a ramp term, depending how the speed dynamics is derived. As indicated in Chapter 5, merging and weaving terms are not statistically significant in terms of their contribution to the overall model performance; therefore, they can be omitted to simplify the model and increase computational efficiency.

6.3.2 Speed-Density Relationships

The equilibrium speed-density relationship plays an important role in the speed dynamics of macroscopic simulation models. It is the major part of the relaxation term, providing the target equilibrium speed (desired speed) based on traffic density. The generalized speed-density relationship (May 1990) was used in many macroscopic models (Papageorgious 1990, Kotsialos et al. 2002, Hegyi 2005a,b). The original formula can be written as:

$$v = v_f \left[1 - \left(\frac{\rho}{\rho_{jam}} \right)^{l-1} \right]^{\frac{1}{1-m}} \tag{6.5}$$

As Equation (6.5) contains parameters l and m, which are difficult to calibrate, a more widely used form was proposed by Papageorgious (1990). Assuming $\alpha=l-1$, we have:

$$\rho_{jam} = \rho_c (\alpha \cdot \frac{1}{1-m})^{\frac{1}{\alpha}} \tag{6.6}$$

As $m \to 1$ and using the special limit:

$$\lim_{x \to \infty} (x - \frac{1}{x})^x = \frac{1}{e} \tag{6.7}$$

We obtain:

$$v = v_f \cdot \exp\left[-\frac{1}{\alpha} \left(\frac{\rho}{\rho_c} \right)^{\alpha} \right] \tag{6.8}$$

Equation (6.8) is a widely used speed-density relationship in many simulation models. The model depends on three parameters, free flow speed v_f, critical density ρ_c and parameter α. They all impact the shape of the FD. By definition, free flow speed is the speed drivers would like to select when there are no other vehicles that affect their speed choice. It is related to road type and is subject to the posted speed

limits. Critical density is also called optimum density, at which a roadway has the maximum flow rate. It is related to road properties and speed limit. α is a parameter that affects the shape of the speed-density curve. Understanding how the three parameters affect the shape of the speed-density curve can help determine the range of parameters in model calibration.

Figure 6.2a and 6.2b show the plot of speed *(v)* versus density with the free flow speed of 90km/h for the critical density of 30 veh/km/lane and 50 veh/km/lane and with a different α values, respectively. It shows that with an increase of the α value, the speed drops slowly at both very small and very large density (ρ), but drops quickly near the critical density (ρ_c) area. At a small α value, speed drops quickly at small density, but slower near critical density than larger α values. The plot also shows that when $\rho<\rho_c$, speed drops slowly with the increasing of density. The larger the ρ_c value, the larger the range of density in which traffic can maintain relatively high speed. For a small ρ_c value, the speed is more sensitive to density, but not sensitive to the α value. For a large ρ_c value, the speed is sensitive to both density and α value.

6.3.3 Analysis of Density Dynamics

In all of the macroscopic models, the density dynamics is based on conservation of vehicles. In discrete simulation, the density on a segment is updated every time step. The density of next time step $\rho_i(k+1)$ is composed of the sum of two parts: the first part is the density on the segment in the current time step $\rho_i(k)$, and the second part is the density change caused by the inflow and outflow of vehicles in the segment during one time step. Table 6.1 shows the average values, minimum value and

maximum value of the two parts of the density dynamics calculated from a density dynamics in each segment during a two-hour simulation (360 time steps with each time step of 20s). The input data (extracted from the VISSIM simulation and taken as the ground truth in this research) is one of the VISSIM outputs under heavy traffic demands, as defined in Chapter 5.

As can be seen from Table 6.1, on average, the first part of the density dynamics is always positive and it consists of over 99.8% of the total predicted density. Part two consists of less than 0.2% of the total density. The average value of the second part is very small due to the fact that the value can be either positive or negative. They are partially offset for the whole simulation time steps. Table 6.1 also shows the minimum and maximum value of the part two during 360 time steps. The value ranges from -3.86 veh/km/ln to 4.16 veh/km/ln on different segments.

Table 6.2 illustrates the predicted density at time step 50 (k=50). The proportion of the first part varies from 96.49% to 102.49% of the total density across all 13 segments. The proportion of the second part varies from -2.49% to 3.51% of the total density across all 13 segments. From the study it was also found that even through the absolute value of the second part of the density dynamics is small, it is still very important to the final predicted density, as the value accumulates with the simulation time.

Figure 6.3 shows the plot of density in selected segments (segment 2, 4, 6 and 11) at each time step for 2 hours simulation. In the figure, VSIM is the density measured in VISSIM simulation, which is taken as ground truth. ρ_{tot} is the predicted density from macroscopic simulation. $\rho(k)$, and ρ_2 are two parts in the density dynamics. As

can be seen from the figure, the first part of the density dynamics $\rho_i(k)$ is very close to the total predicted density $\rho_i(k+1)$, during each time step. The second part of density dynamics ρ_2 fluctuate around zero during the two-hour simulation, no matter the total density in a segment is high or low. Figure 6.3 also shows that there is some difference between the predicted density and the density measured from VISSIM when the density on a road segment is very high (such as in segment 6), or when the density fluctuate quickly (such as in segment 11), even though the density dynamics is strictly based on the conversation of vehicles (as opposed to the speed dynamics which includes assumptions and empirical conjectures in model derivation).

6.3.4 Analysis Speed Dynamics

The speed dynamics used in macroscopic simulation models has several components. The speed of the next time step $v_i(k+1)$ is the sum of four parts: the speed on the segment in current time step $v_i(k)$, relaxation, convection and anticipation (density gradient). In order to diagnose the possible reasons leading to the discrepancy between the model predicted traffic states and measured data, we need to analyze the values of each component in the speed dynamics.

Table 6.3 shows the average values of each component of the speed dynamics on each segment during the 2 hours simulation, using the same data set as in the analysis of density dynamics discussed in the previous section. On average, the first part of speed dynamics $v_i(k)$ consists of over 99% of the predicted speed $v(k+1)$. The value of other three components, namely relaxation, convection and anticipation, can be positive or negative depending on the relative speed and the desired speed (determined strictly by the speed-density relationship), relative speed between the

current segment and the immediate upstream segment as well as the relative density between the current segment and the immediate downstream segment. The proportion of the relaxation value varies from -0.27% to 1.25% of the predicted speed during all time steps and across all segments. The proportion of the convection value varies from -1.54% to 2.28% of the predicted speed during all time steps and the proportion of the anticipation value varies from -3.57% to 1.75% of the predicted speed during all time steps and across all segments. As expected, the values of relaxation, convection and anticipation can offset during each time step. The average combined value of these three terms varies from -0.04 km/h to 0.008 km/h, or -0.069% to 0.01% of the predicted speed.

Table 6.4 gives the values of each component of the speed dynamics in each segment at the time step 50 (k=50). The proportion of the relaxation value varies from -1.64% to 4.94% of the predicted speed at this time step and across all segments. The proportion of the convection value varies from -2.79% to 5.10% of the predicted speed at this time step and the proportion of the anticipation value varies from -11.50% to 3.17% of the predicted speed at this time step and across all segments. The average combined value of these three terms varies from -1.29 km/h to 1.12 km/h, or -1.99% to 1.65% of the predicted speed. This is smaller than the impact of each individual part of the speed dynamics and it is understandable because the values of relaxation, convection and anticipation can offset during each time step.

Figure 6.4 plots each component of the speed dynamics, the predicted speed as well as the measured in VISSIM at the selected segments (segment 2, 4, 6 and 11) at

each time step for 2 hours simulation. Similar to the density analysis, the first part of the speed dynamics is very close to the predicted speed in each segment at each time step. All other three parts of the speed dynamics can be positive or negative.

Figure 6.5 is an enlarged plot of each component of the speed dynamics, the predicted speed as well as the measured speed from VISSIM simulation in segment 7 at each time step for 2-hour simulation. As can be seen, for the most of the time, the values of relaxation and convection have the same sign (positive or negative), and the anticipation has opposite sign to the relaxation term. The largest relaxation, convection and anticipation values (absolute value) happened near time step 120 (they are not at the same time step) when the speed on the segment changes rapidly.

6.4 Model Improvement Considerations

6.4.1 Improvement of Density Dynamics

As indicated in Figure 6.3, even though the density dynamics is strictly based on the vehicle conservation law, there is some discrepancy between the model predicted density and the measured density. This may be due to the macroscopic aggregation and assumptions used in macroscopic simulation models.

In the density dynamics of the original macroscopic model Equation (6.1), the implicit assumption is that the outflow of vehicles $[\rho_i(k) \bullet v_i(k)]$ from the current segment i, can always flow into the downstream segment in the current time step. That means, there is always enough room in the downstream segment to accept the flow from the upstream segment. In real-life traffic, this condition may not hold if the downstream is over congested, such as stop-and-go traffic conditions, in which the traffic speed will decrease suddenly and only part of the flow on the current

segment can proceed into the downstream segment. Similarly, it is possible that not all the outflow from the immediate upstream segment can flow into the current segment due to congestion of the current segment. In addition, the traffic demand from an on-ramp located at the beginning of a segment may be as high as over 1500 veh/h in one lane at some time steps. This amount of traffic will cause local congestion on the through lane adjacent to the on-ramp and merge area. If the segment is congested, only part of the vehicles from the on-ramp can actually flow into the segment. However, if the ramp inflow amount is averaged to several through lanes of the merge area, the impact might look not as prominent as it actually is. This will mask the local congestion near the merge area. To represent these constraints on the flow from upstream segment or on-ramps, boundary conditions should be applied to the density dynamics. Therefore, the density dynamics should be modified as follows to consider those constraints:

$$\rho_i(k+1) = \rho_i(k) + \frac{T}{L_i \cdot \lambda_i}[\lambda_{i-1} \cdot q_{i-1}(k) - \lambda_i \cdot q_i(k)] \tag{6.9}$$

In which:

$$q_{i-1}(k) = \min\{[\rho_{i-1}(k) \cdot v_{i-1}(k) + r_i(k) - s_i(k)], Q_i, \frac{[\rho_i(k) \cdot v_i(k) - \rho_{i-1}(k) \cdot v_{i-1}(k)]}{[\rho_i(k) - \rho_{i-1}(k)]}[\rho_m - \rho_i(k)]\} \tag{6.10}$$

$$q_i(k) = \min\{[\rho_i(k) \cdot v_i(k) + r_{i+1}(k) - s_{i+1}(k)], Q_{i+1}, \frac{[\rho_{i+1}(k) \cdot v_{i+1}(k) - \rho_i(k) \cdot v_i(k)]}{[\rho_{i+1}(k) - \rho_i(k)]}[\rho_m - \rho_{i+1}(k)]\} \tag{6.11}$$

Where $q_{i-1}(k)$, $q_i(k)$ are the outflow of the segment *(i-1)* and *i* at time step *k*, respectively. Q_i and Q_{i+1} are lane capacity of the segment *(i-1)* and *i*, respectively. $r_i(k)$ is the on-ramp flow in segment *i* at time index *k*; $s_i(k)$ is the off-ramp flow in

segment i at time index k; $\rho_i(k)$ is the density (veh/km/lane) in segment i; $v_i(k)$ is the speed (km/h) in segment i and ρ_{max} is the maximum density.

Equation (6.9) is still strictly based on the law of vehicle conservations and holds for all traffic conditions.

6.4.2 Improvement of Speed Dynamics

Compared to density dynamics, which is based on conservation of vehicles and has only two terms with only one parameter (maximum density ρ_{max}), the speed dynamics in macroscopic simulation models is much more complicated. Not only has it more terms, but also the different components have interaction effect. In addition, it has several parameters that need to be calibrated (at least τ, η and κ). Furthermore, the equilibrium speed-density relationship is an empirical equation and has two parameters (α and the critical density ρ_{cr}) that need to be calibrated. The equilibrium speed-density equation might not be accurate under congested traffic conditions.

The study in Chapter 5 showed that adding merging and/or weaving terms to the speed dynamics does not have significant impact on the model prediction accuracy. Other approaches have to be investigated to improve model performance, especially under congested traffic conditions. As indicated in the study by Lu et al. (2011) and can be observed from the speed plots over time evolution in many other studies (Cremer et al. 1981, Papageorgious et al. 1989, Kotsialos et al. 2002, Lamon 2008), the speed dynamics used in macroscopic simulation models, such as (original METANET model) does not catch the significant changes in traffic dynamics

properly. Modification and improvements on the speed dynamics are desirable in order for the model to predict traffic states more accurately.

6.4.2.1 Improvement of convection term

Several methods to improve the convection term of the speed dynamics had been studied by Lu et al. (2011) as well as Yin and Qiu (2012), in which several forms of convection terms, considering the convection effect from the further upstream segment, were used to replace the convection term in the original speed dynamics. Better prediction results were obtained by the modified speed dynamics compared to the original METANET model. For example, if we use the geometric average speed of the current and upstream segment to replace the upstream speed, the convection term becomes (Lu et al. 2011):

$$\Delta v_c = \frac{T}{L_i} \cdot v_i(k) \cdot [\sqrt{v_{i-1}(k) \cdot v_i(k)} - v_i(k)] \tag{6.12}$$

From field observations, the speed on the current segment is not only related to the speed on the upstream segment, which inflow to the current segment, but also to the speed on the downstream segment. If vehicles near the end of the current segment observe the higher speed at the downstream segment, they will accelerate to catch up to the higher speed vehicles downstream, vice versa. This is similar to the "car-following" mechanism but in macroscopic perspective, taking a road segment as one unit. Drivers on the current segment cannot perceive the density on the downstream segment directly. However, they can perceive the speed directly ahead and react to the distance gap resulted from the speed difference. If we consider the impact of the speeds at upstream, current and downstream segment in the convection term, geometric average (or weighted average) of the speed on the three segments

can be used to replace the upstream speed in the convection term. As a result, alternative convection terms can be formed as:

$$\Delta v_c = \frac{T}{L_i} \cdot v_i(k) \cdot [\sqrt[3]{v_{i-1}(k) \cdot v_i(k) \cdot v_{i+1}(k)} - v_i(k)] \tag{6.13}$$

Of the three additional terms in the speed dynamics, both relaxation and anticipation terms have model parameters that have physical explanation and can be identified in model calibration. These model parameters allow the model to adjust the predicted traffic states to match the field measured data as much as possible. It is considered to add a factor to the convection term to account for the fact that convection may only occurs at the segment ends, instead of the full segment. With a factor δ_c, the convection term can be expressed as:

$$\Delta v_c = \delta_c \cdot \frac{T}{L_i} \cdot v_i(k) \cdot [v_{i-1}(k) - v_i(k)] \tag{6.14}$$

6.4.2.2 Improvement of anticipation term

The anticipation term in the original macroscopic model proposed by Payne (1971) does not have a specific function form for macroscopic simulation. It only states that the anticipation is a function of density gradient. In Payne's (1979) simulation model, he used the density $[\rho_i(k)]$ of the current segment in the denominator. Based on the equation, the smaller the density on the current segment, the larger the absolute value of the anticipation term. This is not reasonable if the densities on both current and downstream segment are low, because the anticipation takes effect only when the density exceeds certain threshold, for example, larger than the critical density. To address this deficiency, a density parameter κ is added to the denominator as in some simulation models (Messmer and Papageorgious 1990, Carlson et al 2010). Another way is to use the critical density in the denominator, as in Equation (6.15).

$$\Delta v_a = \frac{\eta \cdot T}{\tau \cdot L_i} \frac{\rho_{i+1}(k) - \rho_i(k)}{\rho_{cr}} \tag{6.15}$$

By analyzing the values of the anticipation term in the original speed dynamics equation, it was found that for a fixed set of model parameters, the value of the density gradient term sometimes was very small, even though the downstream density is obviously larger than that of the current segment. This means, the speed dynamics did not appropriately catch the impact from the density difference between the current and downstream segments. For example, assuming at a given time step the speed on the upstream and current segment are the same as the desired speed with constant density (in this case the values of the relaxation and convection terms are zero), then the speed on the current segment for the next time step becomes a linear function of the density on the downstream segment at the current time step, based on the speed dynamics. This may underestimate the impact of the downstream density on the speed of the current segment because the speed-density relationship is usually not linear, as shown in Figure 6.2. To address this problem, a dynamic factor (F) is added to the anticipation term showing as:

$$\Delta v_a = F \times \frac{\eta \cdot T}{\tau \cdot L_i} \frac{\rho_{i+1}(k) - \rho_i(k)}{\rho_i(k) + \kappa} \tag{6.16}$$

F can be in different forms, such as:

$$F = \rho_{i+1}(k) / \rho_{cr} \tag{6.17}$$

Equation (6.17) means that the larger the density of the downstream segment, the larger impact on the speed of the current segment. If the density on the downstream segment is well below the critical density, the value of the anticipation term should be very small. There can be other forms of the factor, such as a factor considering the

speed and density on the current and downstream segment at the same time step. The intension of using a factor is to scale up or down the impact of anticipation term on the speed dynamics, so that it has a quicker response to the downstream traffic density.

Based on above discussions, the macroscopic simulation model can be composed of a density dynamics with boundary conditions as in Equation (6.9) to (6.11), a speed dynamics with different combination of improvement considerations, and a basic equation that flow equals to the multiplication of speed and density. The simulation results from the combination of different modifications will be discussed after model calibration.

6.5 Objection Function and Model Calibration

6.5.1 Objection Function

Before a traffic model can be used to predict the evolution of the traffic states, it needs to be calibrated and validated. The purpose of model calibration is to find the value of the model parameters so that the model predicted traffic states can be reasonably close to actual traffic states in the prediction horizon. Optimization method is often used in model calibration, in which an objective function is constituted to calculate the difference between the ground truth data and the model predicted data. There can be a single objective function or multiple objective functions in optimization process. The calibration is an optimization procedure that minimizes the value of the objective function(s).

The formulation of objective functions depends on the purpose of calibration. For example, in traffic control the main purpose is to improve network performance.

The most frequently used objective function is to minimize the total time that all vehicles spend (TTS), or total travel time (TTT) in the network (Ghods et al. 2010, Hadiuzzaman et al. 2013), because it is directly related to the average travel time for all vehicles and minimizing the total travel time is equivalent to the most efficient system. For the case of model improvement as in this study, the purpose is to evaluate the prediction accuracy between the original and the improved (modified) macroscopic simulation models. Relative prediction error can be used as performance measure for model calibration and evaluation. The main objective is to minimize the difference between the model predicted traffic states (speed, density and flow) and the measured traffic states (ground truth data). The objective function can be formulated as the sum of a combination of different relative error terms. For example, the total error of the sum of the flow and speed errors is:

$$E = \sum_{k=1}^{N_{steps}} \sum_{i \in I_{all}} \left\{ \left[\frac{\hat{q}_i(k) - \widetilde{q}_i(k)}{\hat{q}_i(k)} \right]^2 + \left[\frac{\hat{v}_i(k) - \widetilde{v}_i(k)}{\hat{v}_i(k)} \right]^2 \right\} \tag{6.18}$$

Where N_{steps} is the total number of simulation time steps, I_{all} is the total number of the segments of the freeway, $\hat{q}_i(k), \hat{v}_i(k)$ are flow and speed from VISSIM (or field measured data) in segment *i* at time step *k* respectively and $\widetilde{q}_i(k), \widetilde{v}_i(k)$ are flow and speed from macroscopic models in segment *i* at time step *k* respectively. There can be other form of the objective function, such as the sum of flow and density, the sum of speed and density or the sum of flow, speed and density. They have similar functions, but with a little different emphasis on the predicted traffic states.

In some other studies (Kotsialos et al 2002, Lu et al 2011, Samwal et al 1996) the objective function is formulated as the sum of direct difference between the

model predicted traffic states and the measured traffic states. In those cases, some weights have to be assigned to different components, so that the values of each error term are on the same order of magnitude. The weighting factor is not necessary if the relative differences are used in the objective function.

6.5.2 Model Calibration

Three groups of data were prepared for model calibration and comparison of the original macroscopic simulation model with the improved ones, namely, data from VISSIM simulate on Whitemud Drive (WMD), field measured data from WMD and field measured data from Berkeley Highway Laboratory (BHL). For each group of data, two separate data sets were prepared: one for the calibration of different models and the other for model results comparison.

In model calibration, nonlinear optimization method was used to estimate model parameters. The objective function is the function that calculates the total relative difference (total error) between the ground truth data (measured on WMD, BHL and VISSIM) and macroscopic simulation for all segments and in all time steps, as expressed in Equation (6.18).

The model parameters can be identified by minimizing the total error. This is a nonlinear optimization problem and can be solved by many mathematical tools. MATLAB Optimization Toolbox (The MathWorks 2010) was used in this study. Different models were obtained from the calibration using different data sets. This means, the model from the measured data sets is different from the model calibrated from simulation data. Model parameters for BHL are also different from that on WMD due to different nature of roadways. For example, one set of model parameters

calibrated from field measured data on WMD is α=2.6, ρ_{cr} = 27.0 veh/km/lane, τ=0.006hr, η = 10.5 km^2/h, κ= 29.6 veh/km/lane, and ρ_{max} = 90.0 veh/km/lane. The model parameters calibrated from one set of the simulation data on WMD, one set of the field measured data on WMD and one set of the field measured data on BHL are summarized in Table 6.5, 6.6 and 6.7, respectively. These tables show examples as to how the model parameters vary with different data sets.

6.6 Simulation Results

Based on the model improvement considerations discussed previously, various modifications on the density and speed dynamics were incorporated into the model. Each of the modified models was calibrated with various data sets from both VISSIM simulation data and field measured data. After numerous model runs on different combination of improvement options with different data sets, the results can be summarized as follows:

(1) Adding boundary conditions in the density dynamics, as Equation (6.9) to (6.11) can improve model performance in very congested traffic states, especially when both the density on the mainline freeway and traffic demand at on-ramps are high. Adding boundary conditions can restrict excessive inflow from on-ramps (vehicles actually proceed slowly on the ramps waiting for gaps to flow into the freeway) and prevent the situation that total traffic flow on a segment is higher than the road capacity.

(2) Using the geometric mean speed of the current and upstream segment to replace the upstream speed in the convection term of the speed dynamics, as in Equation (6.12), can obviously improve the model performance. Using the

geometric mean speed of the current segment, upstream and downstream segment to replace the upstream speed in the convection term has similar effect to that of using geometric mean speed of the current and upstream segment. The predicted traffic states can better match the measured traffic states under most of the cases.

(3) Adding a factor to the convection term (δ_c, which is a model parameter with the range between 0 and 1, and can be identified in model calibration) also has obvious improvement on the overall prediction accuracy. The effect is comparable to that of using the geometric mean speed of the current and upstream segment to replace the upstream speed in the convection term.

(4) Using a dynamic factor (ρ_{i+1}/ρ_{cr}) in anticipation term has a mixed effect on the model performance. It has some improvement on certain data sets (traffic conditions), but not on other data sets. This means that the effect of using the dynamic factor in anticipation term cannot be determined. This is because the anticipation term has three parameters already (τ, η, κ). More factors will bring complicated interaction effect during model calibration and as a result, the model does not necessarily have better performance.

(5) Other dynamic factors, such as $[v_i(k)/v_i(k-1)]$, $[(\rho_{i+1}(k)/\rho_i(k)]$ (including a small constant in denominator to prevent dividing by zero) has also been used, but found that the model was unstable.

(6) Using critical density (ρ_{cr}) to replace the denominator in anticipation term has similar effect to that of adding a dynamic factor (ρ_{i+1}/ρ_{cr}) in anticipation term.

(7) Using the geometric mean speed of the current and upstream segment to

replace the upstream speed in the convection term, and simultaneously adding a dynamic factor (ρ_{i+1}/ρ_{cr}) in anticipation term does not necessarily have better model performance than the original model.

(8) Using the geometric mean speed of the current and upstream segment to replace the upstream speed in the convection term and simultaneously adding a constant factor (δ_d, which is a model parameter) in anticipation term has slightly better performance than the original model.

(9) Adding a factor (δ_c) in convection term and simultaneously adding a dynamic factor (ρ_{i+1}/ρ_{cr}) in anticipation term has similar improvement to that using the geometric mean speed of the current and upstream segment to replace the upstream speed in the convection term.

Three data sets were selected to test the model improvement options, namely VISSIM simulation data with heavy traffic demand on WMD for 2 hours, field measured data during 2-hour afternoon peak hours on WMD and field measured data on BHL freeway for 10 hours. There are four macroscopic simulation models tested on each of the data sets and compared with the ground truth data, namely:

- Model 1: Base (original) model without any improvements;
- Model 2: Using the geometric mean speed of the current, upstream and downstream segments to replace the upstream speed in the convection term;
- Model 3: Adding a constant factor (δ_c) to the convection term;
- Model 4: Adding a constant factor (δ_c) to the convection term and simultaneously adding a dynamic factor (ρ_{i+1}/ρ_{cr}) in anticipation term.

Boundary conditions in the density dynamics were included in all of the improved

models (Model 2, 3 and 4).

Figure 6.6, 6.7 and 6.8 show the predicted traffic speed, density and flow on WMD, respectively, on the selected segments for all the four models and compared with the measured data from VISSIM simulation (taken as ground truth in these figures). It can be observed that each of the improved models has better performance than the original model in most of the cases.

In Figure 6.6c and 6.6d on segment 6 and 7, when the traffic speed in VISSIM simulation is very low (20 to 30 km/h), all the improved models can catch this congested traffic states, but the original model failed to catch this significant speed drop. On segment 3 (Figure 6.6a), the prediction error from all four models is obvious compared with the ground truth data (from VISSIM). This section is a two-sided weaving (TRB 2010) and many vehicles flow into the freeway from the on-ramp located on the right side of segment 3 and flow out the freeway on the left side of the same segment. They cross weave three through lanes on this section. When traffic demand is high, this cross weaving causes significant decrease of speed on this segment. In VISSIM simulation, drivers cautiously select appropriate speed in this section and resulted significant speed drop. However, in macroscopic simulation, no special consideration was given to this special type of cross weaving. As a result, all the four models did not catch the large speed drop. It can also be observed that the improved models have slightly better performance than the original model on this segment as well.

For density prediction as shown in Figure 6.7, the original model did not catch the very congested traffic states on segment 6 and 7 (Figure 6.7c, 6.7d). The three

improved models caught this high density reasonably well. On all other segments, all four models have comparable performance with the improved models slightly better than the original model in most of the cases.

In terms of predicted flow as shown in Figure 6.8, all the four models have very similar performances. Noticeable difference exists between the model predicted flow and measured flow from VISSIM on segment 3, on which all the four macroscopic models predicted much higher speed and a little lower density than the measured data from VISSIM. As a result, the predicted flows from all the four macroscopic simulation models are higher than measured flows from VISSIM.

Figure 6.9, 6.10 and 6.11 show the predicted traffic speed, density and flow on the selected segments from all the four macroscopic simulation models and compared with the field measured data on WMD freeway. For speed prediction shown in Figure 6.9, each of the improved models has better performance than the original model on most of the segments except on segment 3, on which the original model performs slightly better. In terms of density as in Figure 6.10, it can be observed that all the three improved models perform better than the original model. It is difficult to differentiate the performance of the three improved models. For flow prediction, all the four models matched the measured data reasonably well, except in segment 4, on which all four models over predicted flow.

The predicted traffic speed, density and flow from the four models as well as the measured data on BHL freeway are provided in Figure 6.12, 6.13 and 6.14, respectively. In Figure 6.12, overall the predicted traffic speed from the four models matches the measured speed reasonably well, with the three improved models

performing better than the original model on all segments under both free flow and congested traffic states.

For density prediction as shown in Figure 6.13, each of the improved models has better performance than the original model on all segments. It is observed from Figure 6.13 that in congested traffic (from approximately 600 to 900 time steps), some differences exist between the predicted density from all of the four models and the measured density. Also shown in the figures, the three improved model have very similar performances. It is difficult to differentiate from the figures as to which improved model is the best.

For flow prediction, even though some minor difference exists between the predicted flow from the four models and the measured data on segment 3, 4 and 5, all the four macroscopic simulation models have very similar performance and the predicted flows are reasonably close to the measured data.

The average prediction errors from the four models as well as the prediction improvements of Model 2, 3 and 4 compared to Model 1 were calculated and summarized in Table 6.8. The prediction error (difference, D) is defined as in Equation (6.19)

$$D = \frac{\left|\text{Predicted Data} - \text{Measured Data}\right|}{\text{Measured Data}} \times 100\% \tag{6.19}$$

As indicated in Table 6.8, the improved models (Model 2, 3 and 4) have better prediction performance in most of the cases, except the density predicted by Model 4 on WMD and the flow predicted by Model 4 on BHL in which the prediction errors from Model 4 are higher than that from the original model (Model 1). Among the

three improved models, Model 2 has the best prediction performance. It can achieve over 10% improvement on speed prediction, over 5% improvement on density prediction, as well as improved flow prediction on both freeways.

6.7 Summary and Conclusions

In this chapter, the value of each component of the density dynamics and speed dynamics of macroscopic simulation models were quantitatively analyzed for both average values during the full simulation time period and at a specific time step. Various options to improve model prediction accuracy had been discussed. For density dynamics, boundary conditions on each segment were incorporated into the models. For speed dynamics, several improvements on the speed dynamics of the original macroscopic simulation model were proposed and implemented in the macroscopic simulation models. These include: (a) considering the convection effect at both upstream and downstream of the current segment; (b) adding a constant factor to the convection term; (c) adding a dynamic factor to the anticipation term and (d) various combinations of different factors and formulations. The modified simulation models were applied to two freeways and compared with outputs from the original model, using both VISSIM simulation data and field measured data, respectively. Based on the modelling results, it shows that the models with the suggested improvements have obviously better prediction accuracy than the original model, especially for the congested traffic conditions. The improved models can catch most of the significant sudden speed drop resulted from traffic congestions. Based on the study, it can be concluded that:

- In macroscopic simulation, the predicted density on a segment at a time step is mainly composed of the density on the segment in previous time step (on average over 99% of the total predicted density). The impact of inflow and outflow on the density dynamics of a segment in one time step is very small. Their values vary from -2.5% to 3.5% of the predicted density;
- The predicted speed on a segment at a time step is dictated by the speed on the segment in previous time step (on average over 99% of the total predicted speed). The value of relaxation, convection and anticipation terms are small (on average less than ±4% of the total predicted density) and they can partially offset each other. Their combined contribution to the speed dynamics (on average less than ±0.1% of the total predicted density) is smaller than the value of each individual term;
- Boundary conditions should be incorporated in the density dynamics of the macroscopic simulation models to represent the constraints in actual traffic flow on road segments as well as at on-ramps;
- Using the geometric mean speed of the current and upstream segment, or using the geometric mean speed of the current segment, upstream and downstream segment to replace the upstream speed in the convection term can obviously improve the model performance. It can help the model to catch the significant speed drop under congested traffic conditions;
- Adding a factor to the convection term can also improve the overall prediction accuracy. The effect is comparable to that of using the geometric mean speed of the current and upstream segment to replace the upstream

speed in the convection term;

- Adding a factor to the convection term and simultaneously adding a dynamic factor to the anticipation term has similar improvement to that using the geometric mean speed of the current and upstream segment to replace the upstream speed in the convection term.
- By using the geometric mean speed of the current segment, upstream and downstream segment to replace the upstream speed in the convection term, it can achieve over 10% improvements on speed prediction, over 5% improvements on density prediction, as well as obvious improvements on flow prediction.

Table 6.1 Debrief of average density components for 2-hour simulation

Component	Index	Formula	Segment	1	2	3	4	5	6	7	8	9	10	11	12	13
ρ(k+1)	(1)		Ave	15.488	14.613	16.104	12.296	11.558	13.685	18.191	21.321	19.799	13.786	11.929	13.914	11.432
	(2)		Min	6.300	6.695	8.230	5.966	5.301	5.459	7.081	9.071	9.991	4.877	5.809	0.618	0.900
	(3)		Max	33.300	26.192	27.972	20.165	28.140	46.379	56.562	54.920	39.703	25.548	21.919	24.941	21.600
ρ(k)	(4)		Ave	15.488	14.608	16.106	12.300	11.566	13.683	18.203	21.318	19.789	13.769	11.910	13.890	11.432
	(5)	(4) /(1)	ρ(k)/ρ(k+1)	1.000	1.000	1.000	1.000	1.001	1.000	1.001	1.000	0.999	0.999	0.998	0.998	1.000
	(6)		Min	6.300	6.695	8.230	5.966	5.301	5.459	7.081	9.071	9.200	4.300	1.700	0.618	0.900
	(7)		Max	33.300	26.192	27.972	20.165	28.140	46.379	56.562	54.920	39.703	25.548	21.919	24.941	21.600
ρ(in-out)	(8)		Ave	0.000	0.004	-0.002	-0.005	-0.008	0.002	-0.012	0.003	0.010	0.016	0.019	0.024	0.000
	(9)	(8) /(1)	%	0.000	0.028	-0.010	-0.037	-0.067	0.014	-0.064	0.014	0.051	0.120	0.155	0.172	0.000
	(10)		Min	0.000	-3.856	-2.551	-1.702	-3.001	-3.322	-3.413	-2.338	-1.123	-0.933	-0.901	-1.882	0.000
	(11)		Max	0.000	3.089	2.390	1.650	2.108	4.163	3.350	3.261	2.375	2.205	4.109	3.428	0.000

Notes: ρ(k+1): predicted density at time step (k+1), veh/km/lane

ρ(k): density at time step k, veh/km/lane. It is part 1 of the predicted density

ρ(in-out): density change due to inflow and outflow in a segment, veh/km/lane. It is part 2 of the predicted density

Ave: Average value during 360 time steps, veh/km/lane

%: Average percentage of the average value to ρ(k+1) during 360 time steps

Min: Minimum value during 360 time steps, veh/km/lane

Max: Maximum value during 360 time steps, veh/km/lane

Table 6.2 Debrief of density components at k=50

Component	Index	Formula	Segment	1	2	3	4	5	6	7	8	9	10	11	12	13
ρ(k+1)	(1)		Value	18.500	22.910	26.241	18.298	17.029	24.401	37.213	40.738	36.124	24.288	20.833	23.375	17.900
ρ(k)	(2)		Value	18.500	22.362	25.321	18.316	17.452	24.688	36.459	39.856	35.878	24.414	21.124	23.408	17.900
	(3)	(2) /(1)	%	100.00	97.61	96.49	100.10	102.49	101.18	97.97	97.84	99.32	100.52	101.40	100.14	100.00
ρ(in-out)	(4)		Value	0.000	0.548	0.920	-0.018	-0.424	-0.287	0.754	0.882	0.246	-0.126	-0.291	-0.033	0.000
	(5)	(4) /(1)	%	0.000	2.390	3.507	-0.100	-2.487	-1.175	2.027	2.164	0.680	-0.519	-1.396	-0.142	0.000

Notes: ρ(k+1): predicted density at time step (k+1), veh/km/lane

ρ(k): density at time step k, veh/km/lane. It is part 1 of the predicted density

ρ(in-out): density change due to inflow and outflow in a segment, veh/km/lane. It is part 2 of the predicted density

Value: value of the term at time step (k=50), veh/km/lane

%: percentage of the term value to ρ(k+1) at time step (k=50)

Table 6.3 Debrief of speed components for 2-hour simulation

Component	Index	Formula	Segment	1	2	3	4	5	6	7	8	9	10	11	12	13
v(k+1)	(1)		Ave	77.121	75.510	76.829	77.917	74.934	67.078	63.171	65.379	71.718	75.016	72.522	75.960	79.826
v(k)	(2)		Ave	77.121	75.516	76.824	77.909	74.934	67.099	63.214	65.408	71.726	75.013	72.529	75.974	79.826
	(3)	(2) /(1)	v(k)/v(k+1)	1.000	1.000	1.000	1.000	1.000	1.000	1.001	1.000	1.000	1.000	1.000	1.000	1.000
Relaxation	(4)		Ave	0.000	0.133	-0.160	0.002	0.331	0.841	0.680	0.131	-0.195	0.167	0.574	0.071	0.000
	(5)	(4) /(1)	%	0.00	0.18	-0.21	0.00	0.44	1.25	1.08	0.20	-0.27	0.22	0.79	0.09	0.00
	(6)		Min	0.000	-0.687	-1.382	-0.772	-0.655	-0.186	-1.469	-1.928	-1.705	-0.759	-0.647	-1.009	0.000
	(7)		Max	0.000	0.875	0.588	1.514	3.670	4.041	3.242	1.675	0.799	1.525	1.601	0.748	0.000
Convection	(8)		Ave	0.000	0.372	-1.182	-0.260	0.777	1.532	1.346	-0.371	-1.052	-0.995	0.911	-1.235	0.000
	(9)	(8) /(1)	%	0.000	0.493	-1.538	-0.333	1.036	2.284	2.131	-0.568	-1.467	-1.326	1.256	-1.626	0.000
	(10)		Min	0.000	-3.630	-2.634	-1.272	-1.565	-1.770	-2.150	-1.906	-2.104	-2.670	-2.530	-3.299	0.000
	(11)		Max	0.000	2.054	0.267	1.613	5.639	5.165	4.838	0.933	-0.104	0.820	2.201	2.466	0.000
Anticipation	(12)		Ave	0.000	-0.511	1.346	0.266	-1.107	-2.394	-2.069	0.211	1.239	0.831	-1.491	1.150	0.000
	(13)	(12) /(1)	%	0.000	-0.676	1.752	0.341	-1.477	-3.569	-3.275	0.323	1.728	1.107	-2.056	1.514	0.000
	(14)		Min	0.000	-3.079	0.006	-2.834	-10.774	-6.893	-6.233	-0.996	0.478	-0.743	-3.077	-2.744	0.000
	(15)		Max	0.000	1.271	2.833	1.204	2.556	0.070	2.037	2.522	2.200	1.691	4.890	5.001	0.000
Σ(Rel, Cov, Ant)	(16)		Value	0.000	-0.006	0.005	0.008	0.001	-0.021	-0.043	-0.030	-0.008	0.002	-0.007	-0.014	0.000
	(17)	(16) /(1)	%	0.000	-0.008	0.006	0.010	0.001	-0.031	-0.069	-0.045	-0.011	0.003	-0.010	-0.018	0.000

Notes: v(k+1): predicted speed at time step (k+1), km/h, v(k): speed at time step k, km/h

Ave: Average value during 360 time steps, km/h

%: Average percentage of the average value to v(k+1) during 360 time steps

Min: Minimum value during 360 time steps, km/h , Max: Maximum value during 360 time steps, km/h

Σ(Rel, Cov, Ant): Sum of relaxation, convection and anticipation.

Table 6.4 Debrief of speed components at k=50

Component	Index	Formula	Segment	1	2	3	4	5	6	7	8	9	10	11	12	13
v(k+1)	(1)		Value	77.500	70.996	67.744	70.551	64.629	46.971	41.843	45.974	58.096	64.479	65.517	71.076	79.700
v(k)	(2)		Value	77.500	70.046	66.625	70.654	65.915	47.658	42.313	46.309	58.290	64.638	65.741	71.392	79.700
	(3)	(2) /(1)	v(k)/v(k+1)	1.000	0.987	0.983	1.001	1.020	1.015	1.011	1.007	1.003	1.002	1.003	1.004	1.000
Relaxation	(4)		Value	0.000	0.140	0.119	0.494	1.092	2.319	0.697	-0.512	-0.950	0.471	0.763	-0.143	0.000
	(5)	(4) /(1)	%	0.000	0.197	0.175	0.700	1.689	4.936	1.666	-1.113	-1.635	0.730	1.164	-0.201	0.000
Convection	(6)		Value	0.000	1.665	-1.059	-0.839	1.795	2.394	0.230	-0.599	-1.087	-1.796	0.359	-1.939	0.000
	(7)	(6) /(1)	%	0.000	2.345	-1.563	-1.189	2.778	5.097	0.549	-1.304	-1.871	-2.785	0.548	-2.728	0.000
Anticipation	(8)		Value	0.000	-0.854	2.060	0.242	-4.173	-5.399	-1.397	0.776	1.843	1.166	-1.346	1.764	0.000
	(9)	(8) /(1)	%	0.000	-1.204	3.041	0.343	-6.456	-11.495	-3.340	1.688	3.172	1.809	-2.055	2.482	0.000
Σ(Rel, Cov, Ant)	(10)		Value	0.000	0.950	1.119	-0.103	-1.285	-0.687	-0.471	-0.335	-0.194	-0.159	-0.225	-0.317	0.000
	(11)	(10) /(1)	%	0.000	1.339	1.652	-0.146	-1.989	-1.462	-1.125	-0.729	-0.334	-0.246	-0.343	-0.446	0.000

Notes: v(k+1): predicted speed at time step (k+1), km/h

v(k): speed at time step k, km/h

Value: value of the term at the time step (k=50), km/h

%: percentage of the term value to v(k+1) at the time step (k=50)

Σ(Rel, Cov, Ant): Sum of relaxation, convection and anticipation.

Table 6.5 Model parameters calibrated from simulation data on WMD

Parameters	α	τ	η	κ	ρ_{cr}	ρ_{max}	δ_c
Model 1	1.4	0.020	50.0	49.6	50.0	130.0	—
Model 2	3.6	0.020	37.8	20.0	29.1	98.5	—
Model 3	2.6	0.020	48.9	20.0	31.8	81.1	0.56
Model 4	1.8	0.019	44.4	31.0	37.3	88.2	0.07

Table 6.6 Model parameters calibrated from field measured data on WMD

Parameters	α	τ	η	κ	ρ_{cr}	ρ_{max}	δ_c
Model 1	2.6	0.006	10.5	29.6	27.0	90.0	—
Model 2	1.6	0.019	4.1	20.0	48.4	90.5	—
Model 3	2.9	0.0053	5.6	31.3	26.4	90.0	0.67
Model 4	3.2	0.005	9.3	29.9	26.0	90.0	0.32

Table 6.7 Model parameters calibrated from field measured data on BHL

Parameters	α	τ	η	κ	ρ_{cr}	ρ_{max}	δ_c
Model 1	1.0	0.030	14.6	37.6	29.3	120.0	—
Model 2	1.3	0.020	29.9	10.3	26.2	109.9	—
Model 3	1.0	0.030	29.6	23.5	28.8	120.0	1.00
Model 4	1.0	0.030	9.0	22.5	30.3	120.0	1.00

Table 6.8 Average prediction errors (in absolute value) and improvements

Data	Models	Speed	Speed Improve	Density	Density Improve	Flow	Flow Improve
WMD	Model 1	12.7%	—	23.2%	—	17.8%	—
	Model 2	9.8%	22.8%	21.4%	7.8%	16.9%	5.1%
	Model 3	11.2%	11.8%	22.6%	2.6%	16.8%	5.6%
	Model 4	11.2%	11.8%	24.4%	-5.2%	16.9%	5.1%
BHL	Model 1	14.5%	—	19.8%	—	9.3%	—
	Model 2	12.8%	11.7%	18.4%	7.1%	9.3%	0.0%
	Model 3	13.4%	7.6%	19.6%	1.0%	9.2%	1.1%
	Model 4	11.1%	23.4%	17.1%	13.6%	9.8%	-5.4%

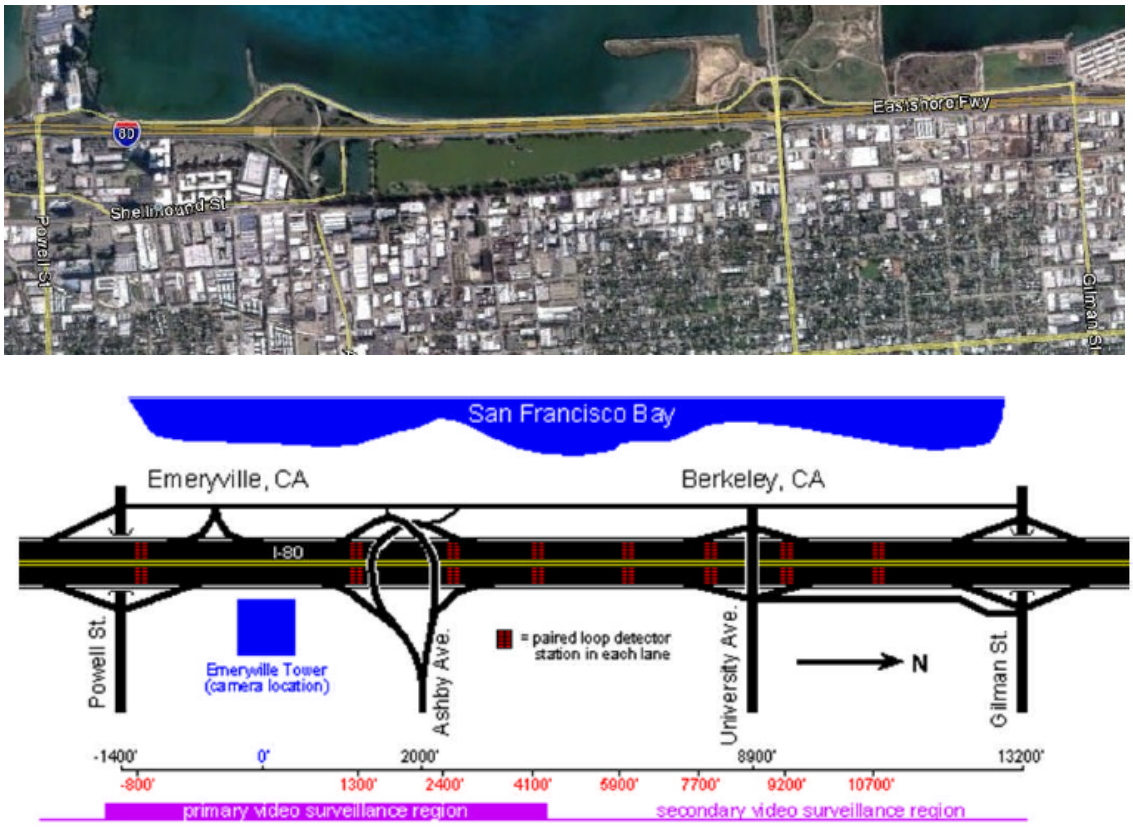

Figure 6.1 Studied freeway corridors in California (Lu et al. 2010, Google Earth)

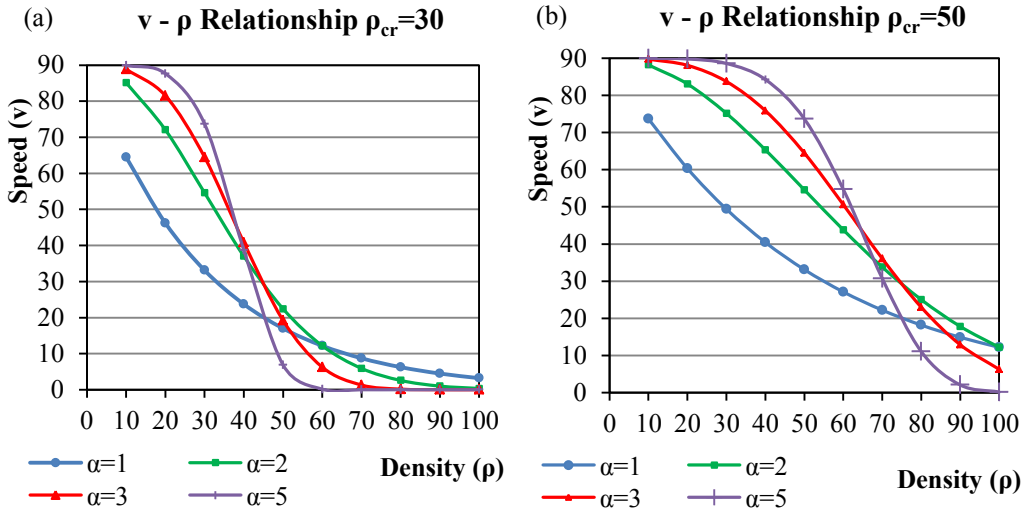

Figure 6.2 Speed-density relationship with respect to ρ_{cr} and α

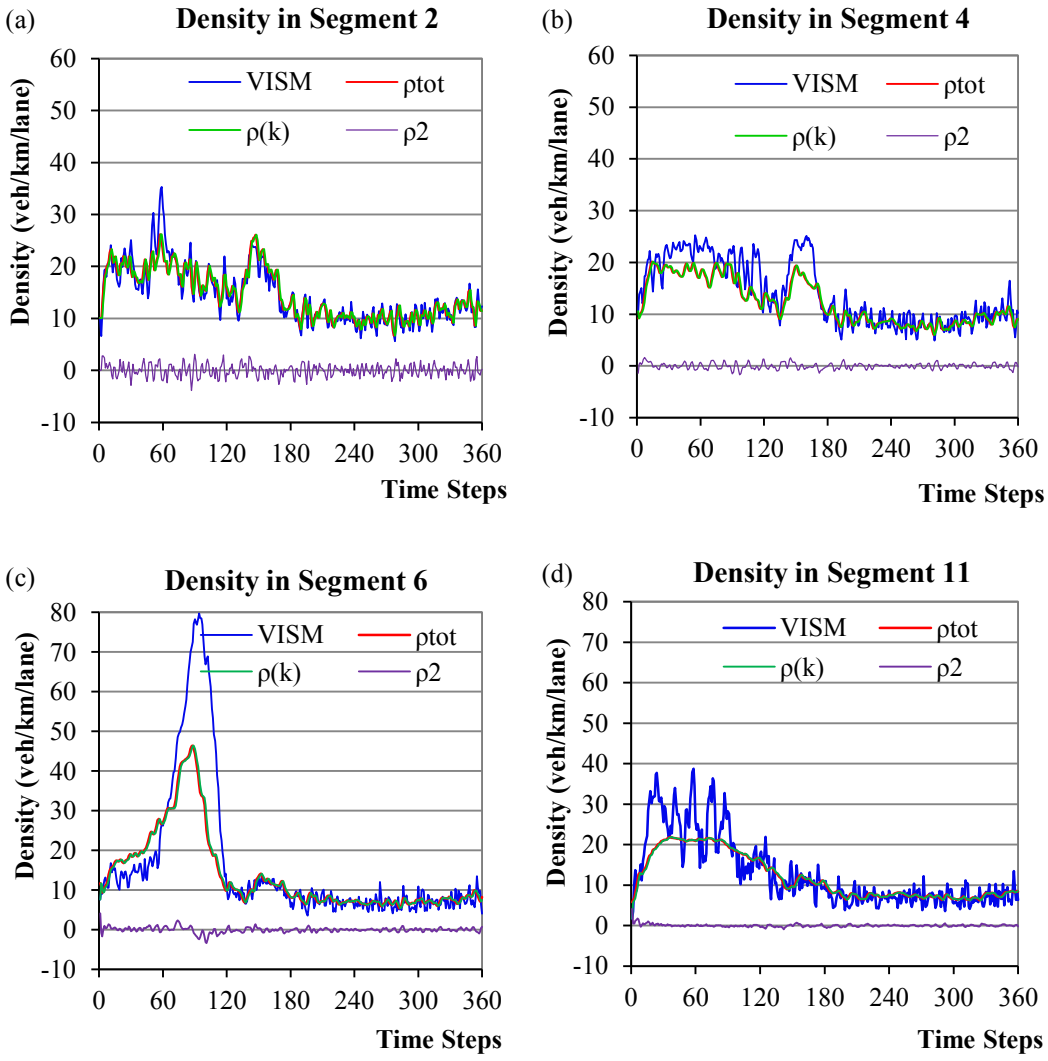

Figure 6.3 Debrief density dynamics on selected segments

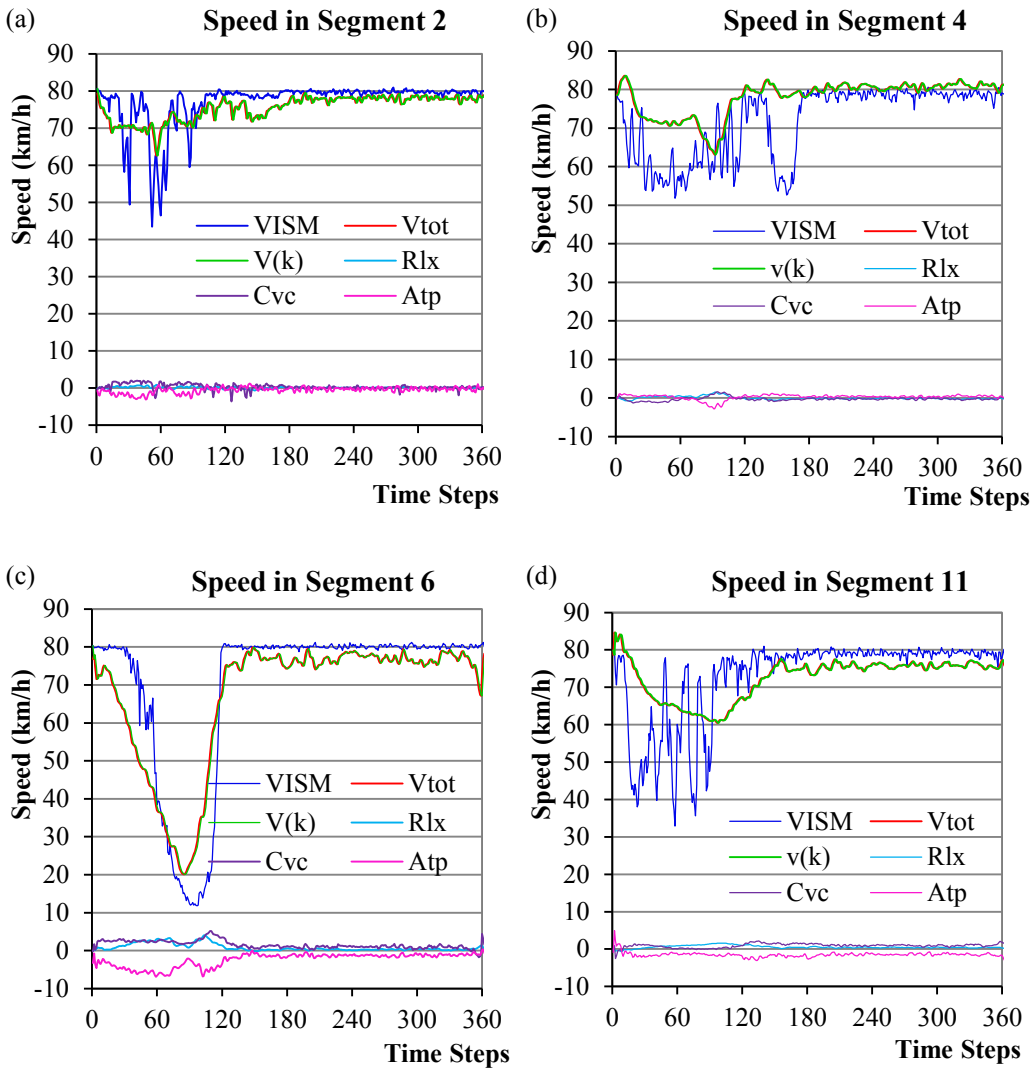

Figure 6.4 Debrief speed dynamics on selected segments

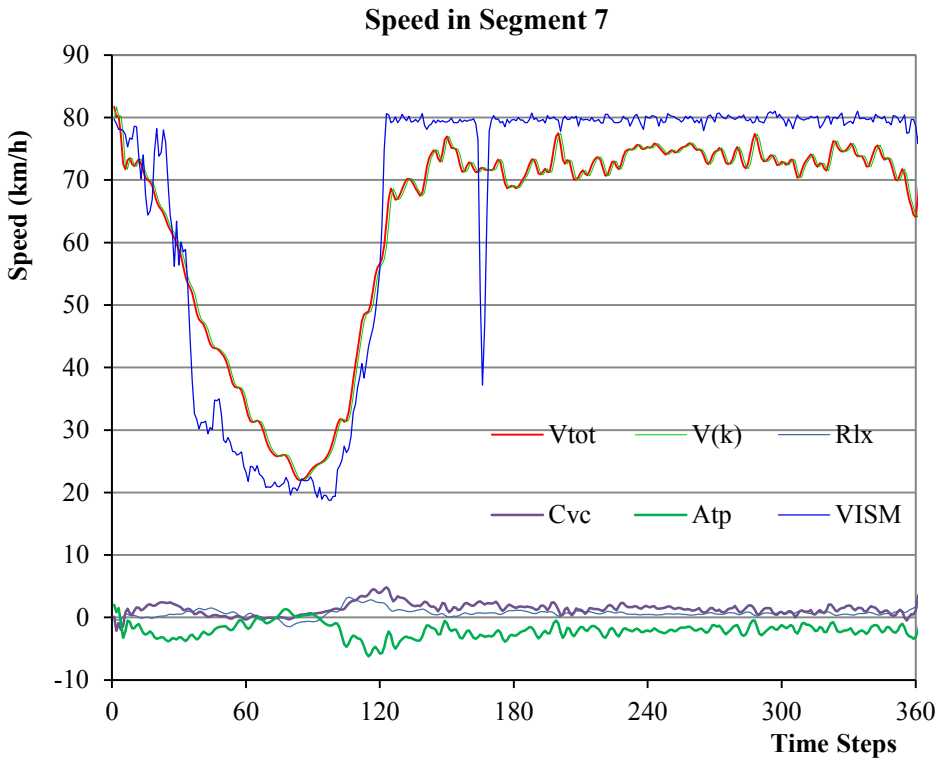

Figure 6.5 Debrief speed dynamics on segment 7

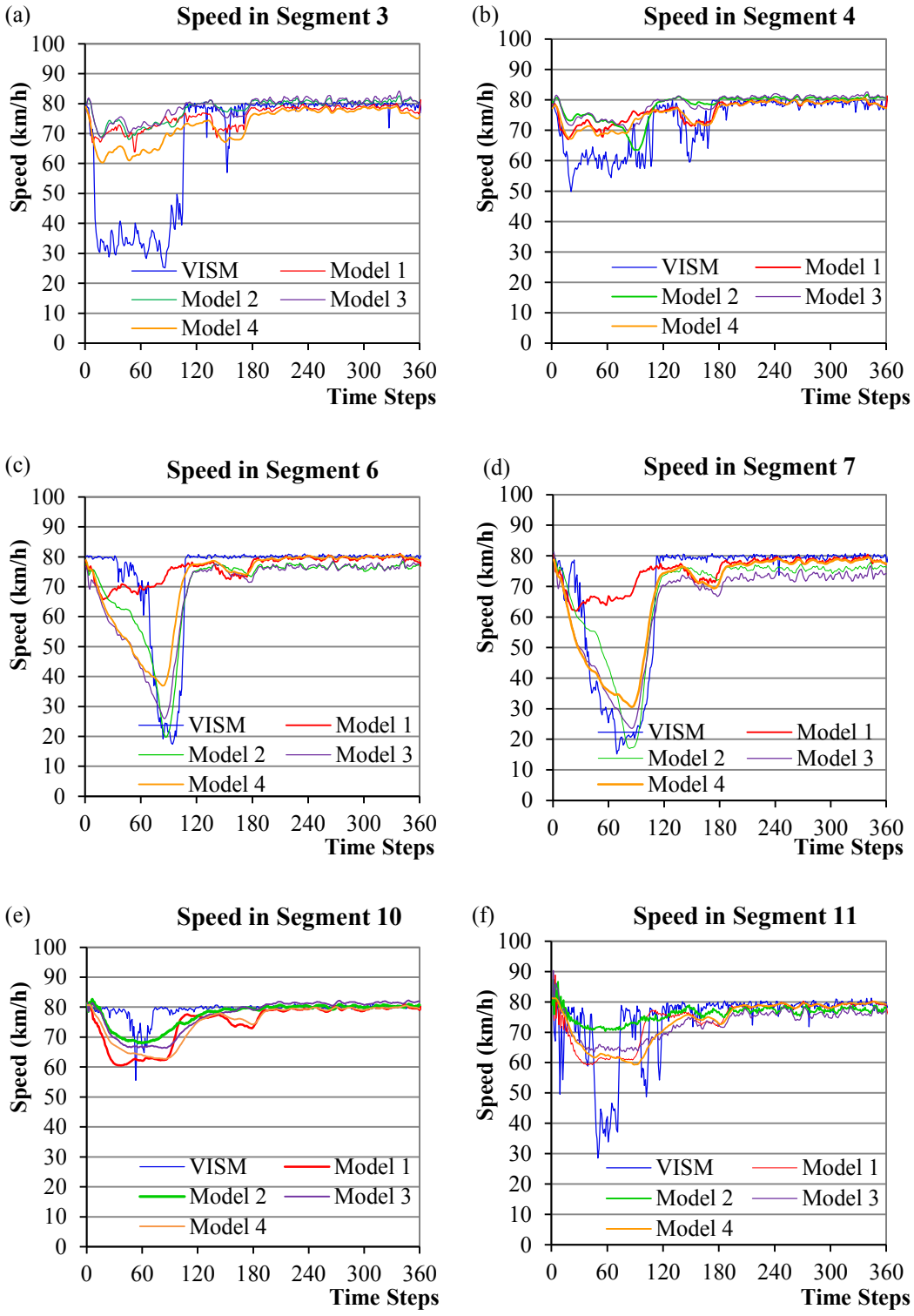

Figure 6.6 Model predicted and VISSIM simulated speed on WMD

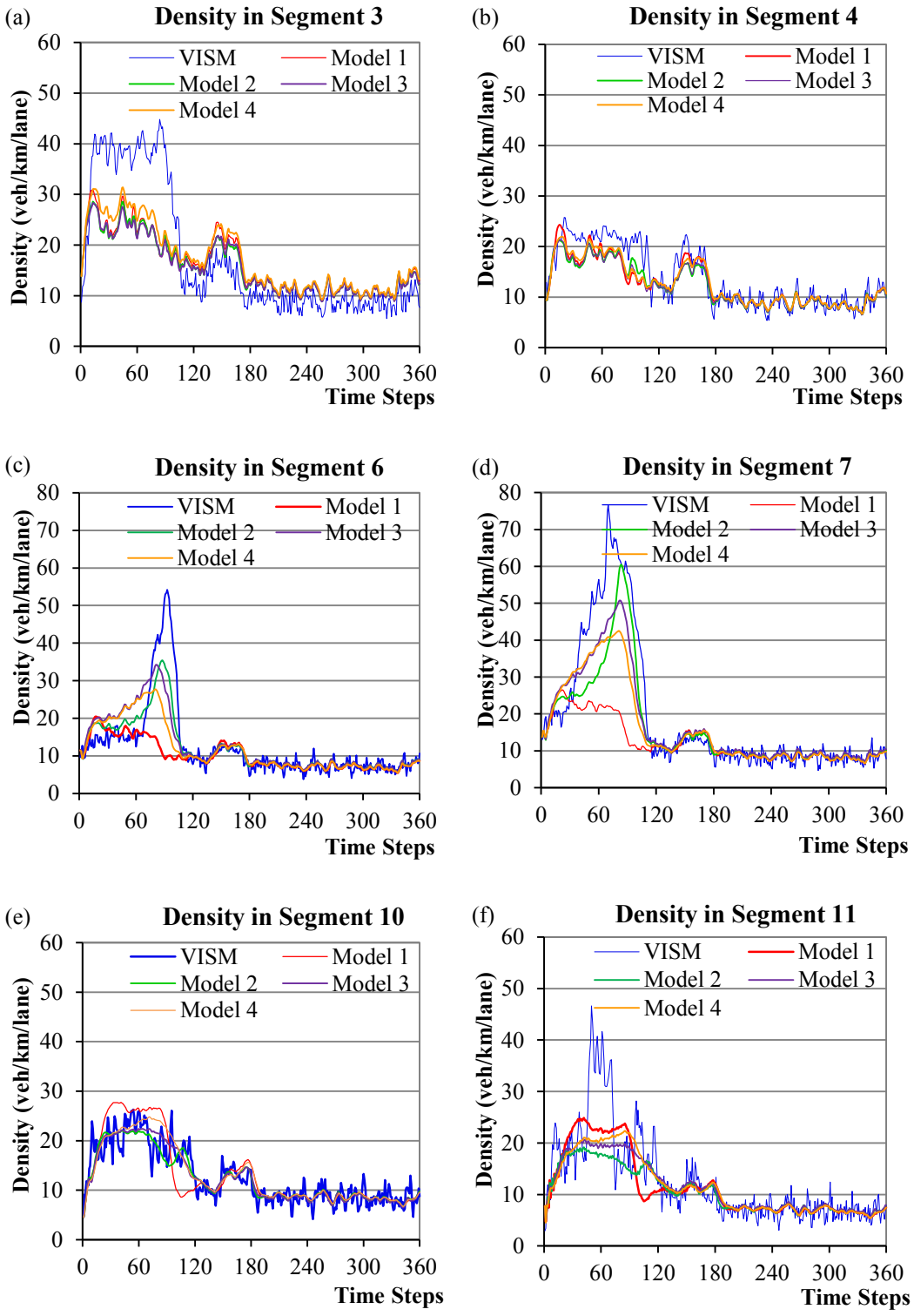

Figure 6.7 Model predicted and VISSIM simulated density on WMD

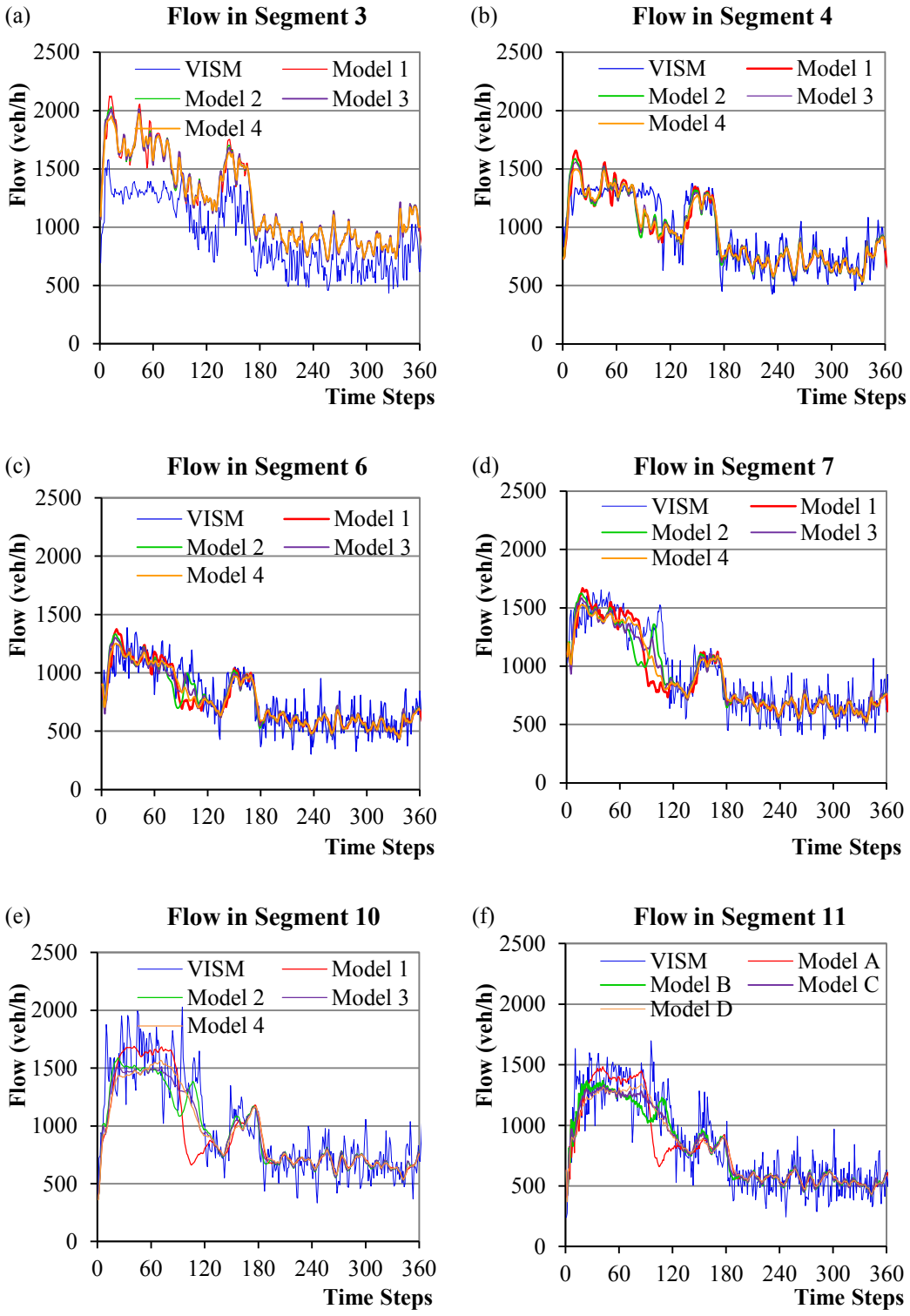

Figure 6.8 Model predicted and VISSIM simulated flow on WMD

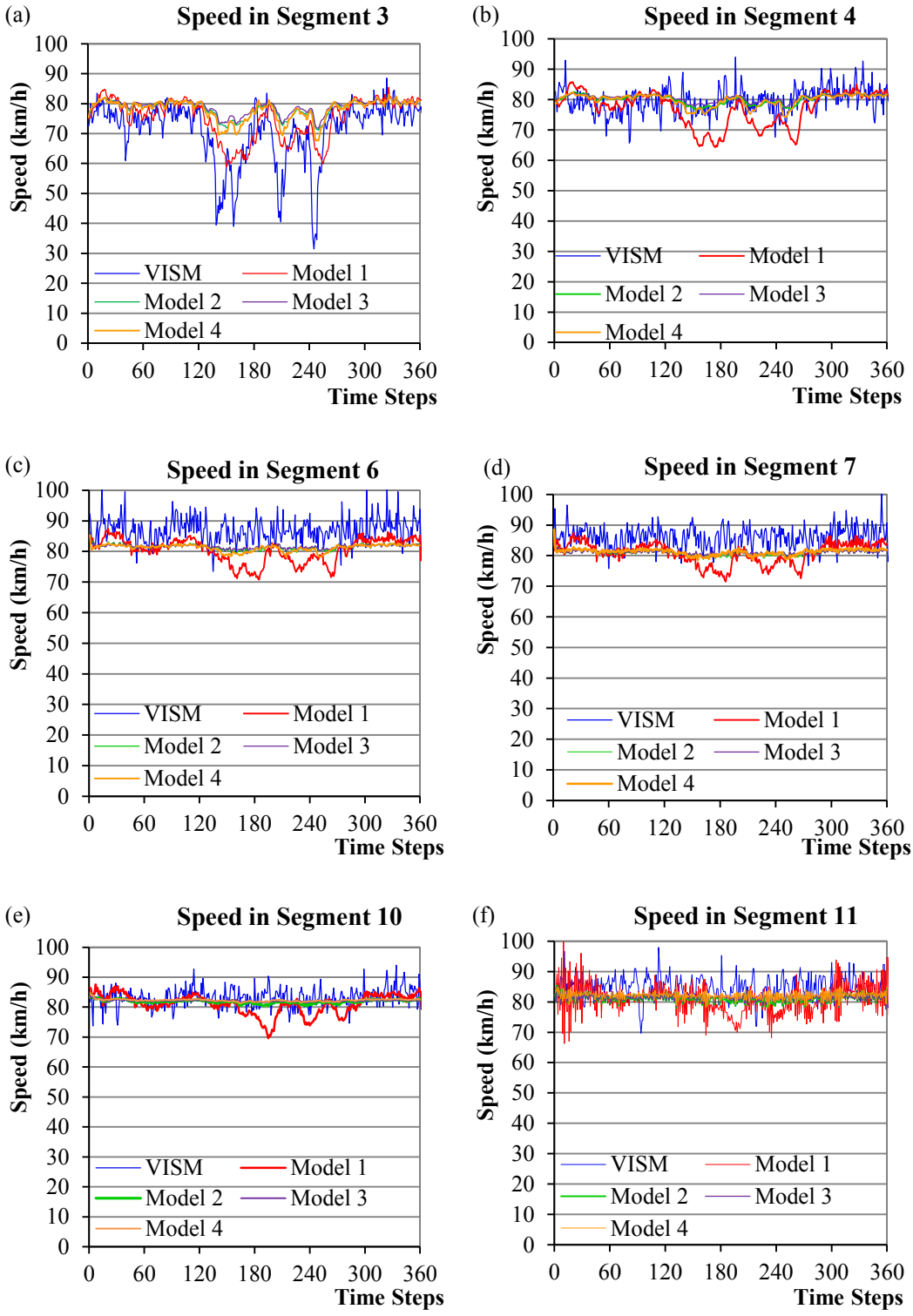

Figure 6.9 Model predicted and measure speed on WMD

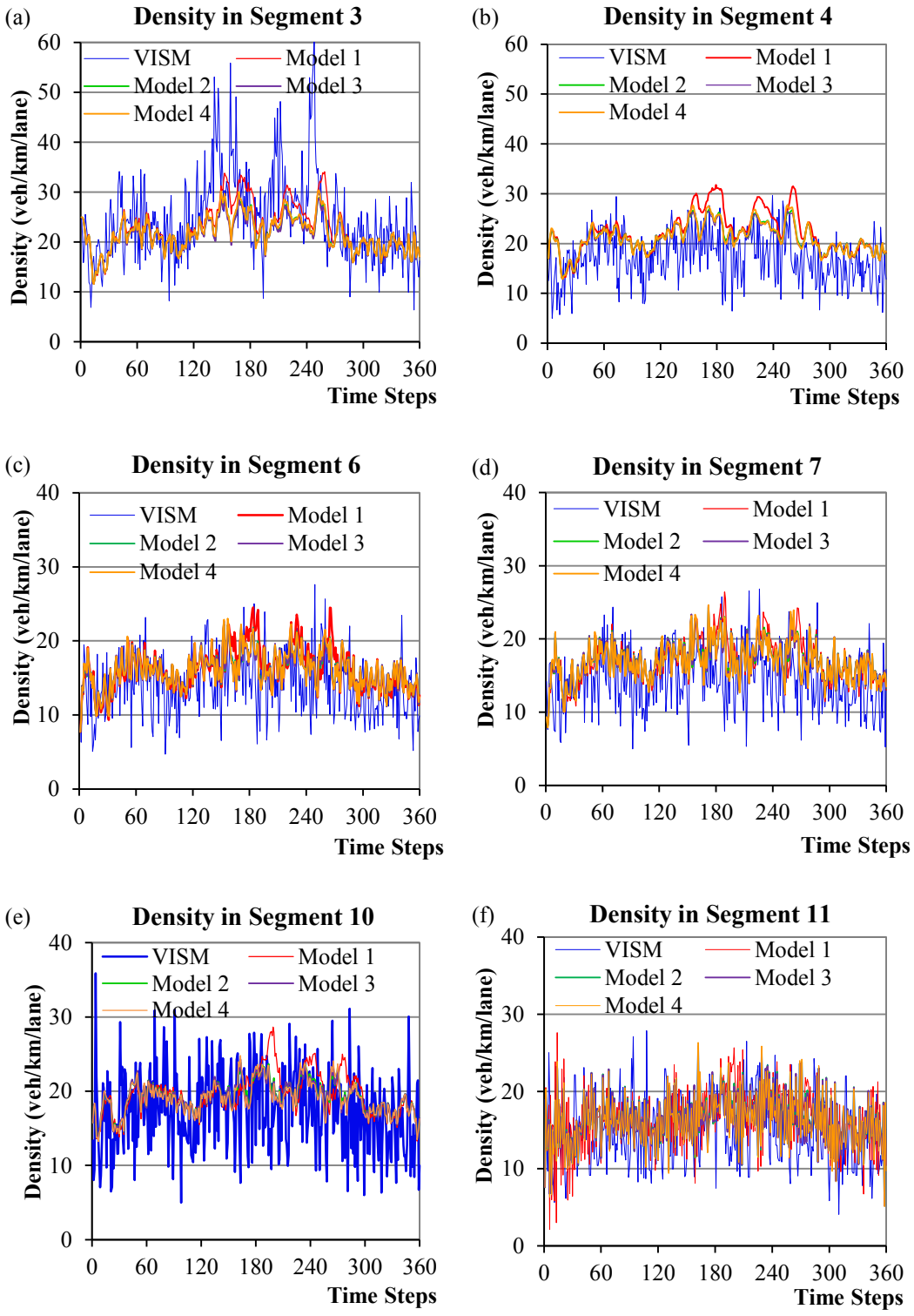

Figure 6.10 Model predicted measured density on WMD

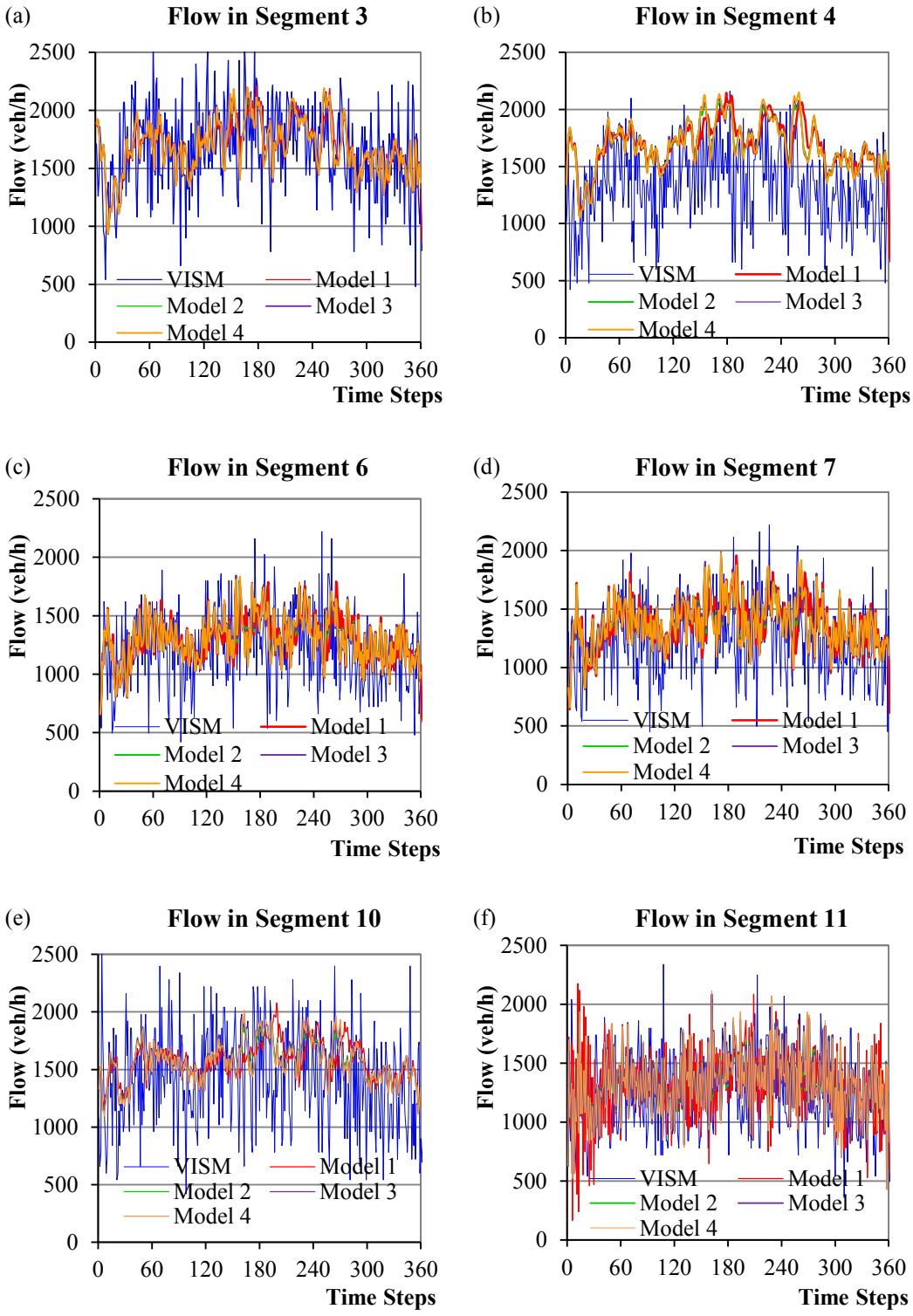

Figure 6.11 Model predicted and measured flow on WMD

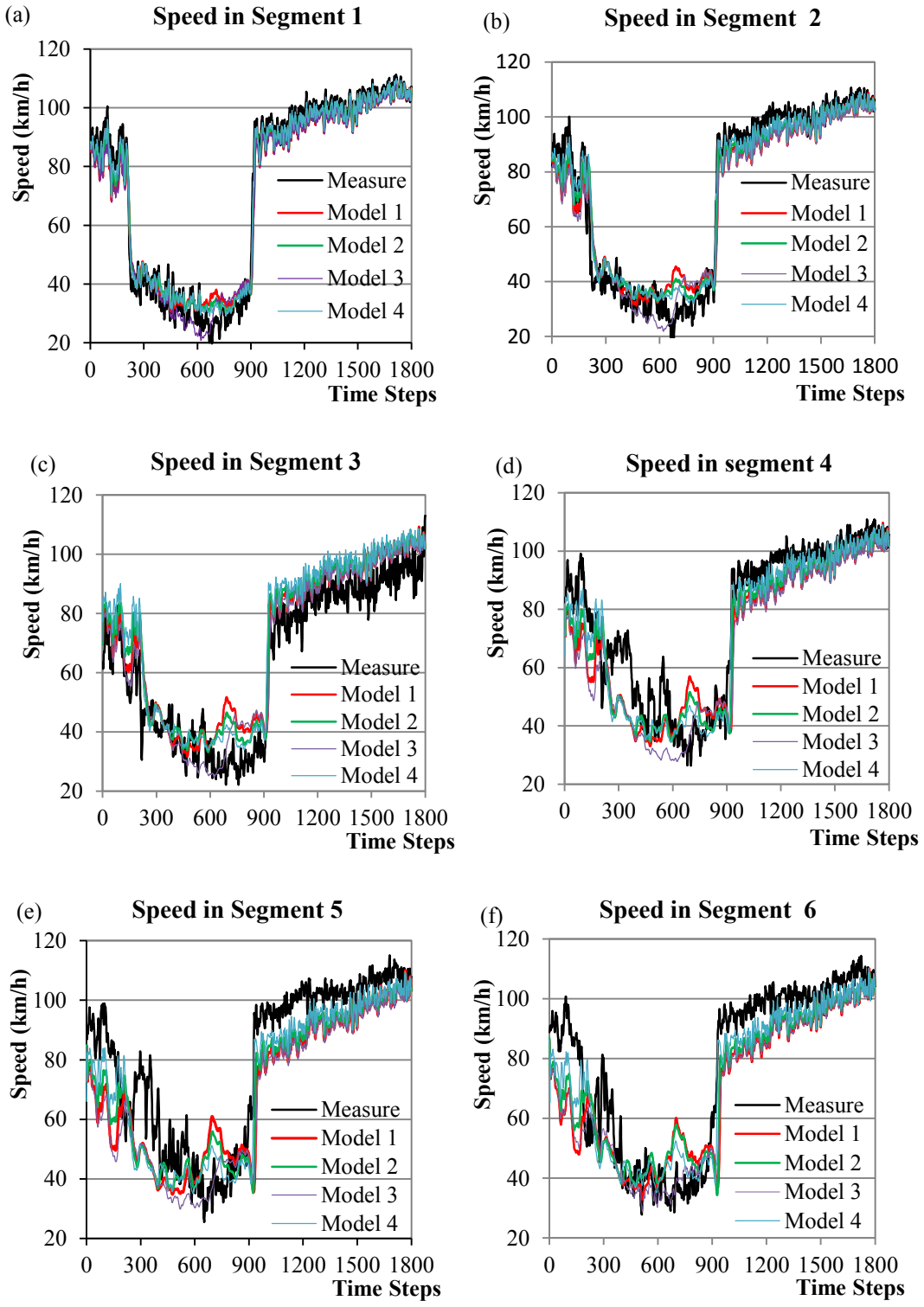

Figure 6.12 Model predicted and measure speed on BHL

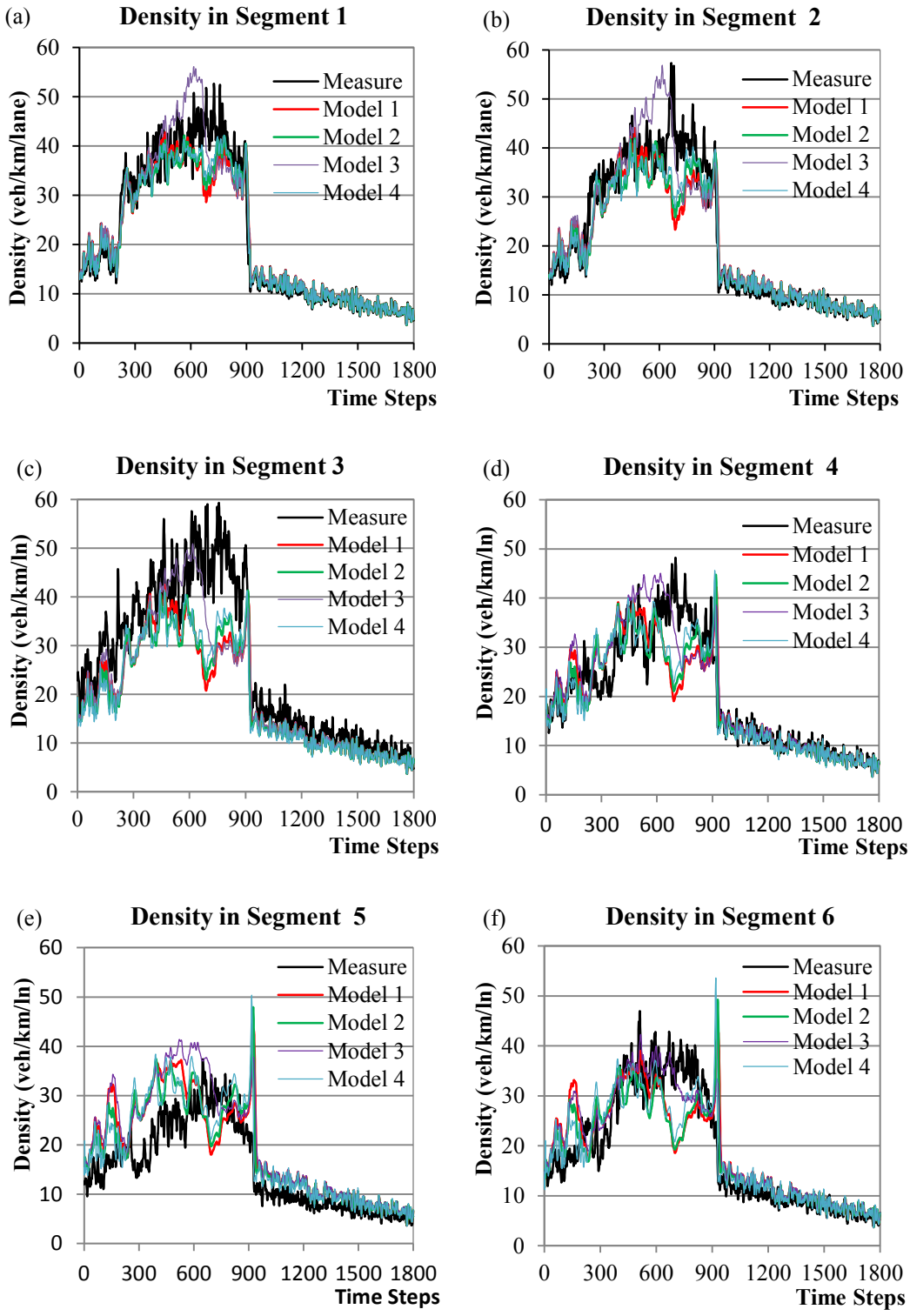

Figure 6.13 Model predicted and measured density on BHL

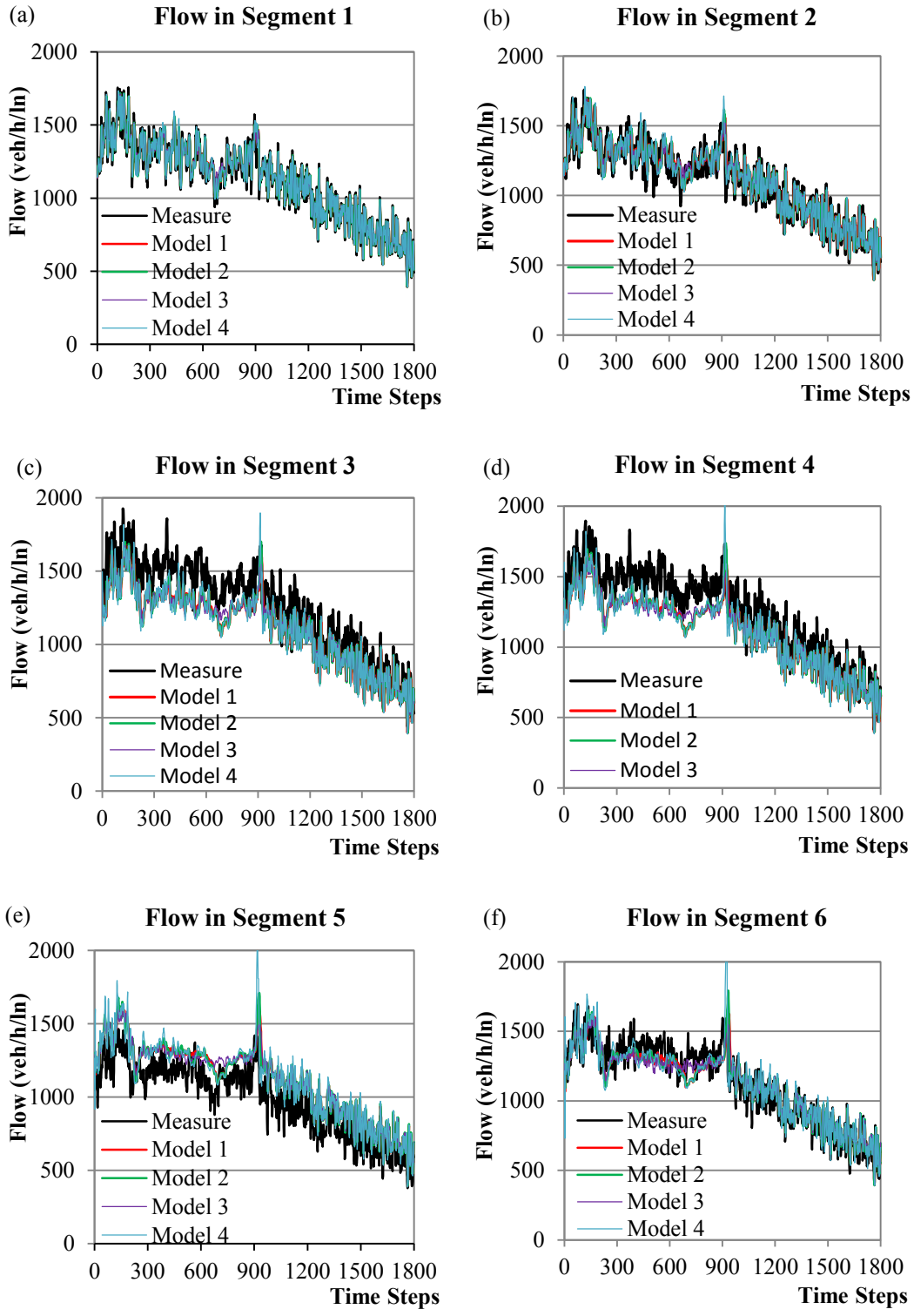

Figure 6.14 Model predicted and measured flow on BHL

Chapter 7 Conclusions and Recommendations

7.1 Conclusions

This research investigated several important issues in freeway traffic flow modelling and simulation. They include the relationship between microscopic car-following models and macroscopic speed-density models, the compatibility of microscopic and macroscopic traffic simulation on freeways, the impact of merging, weaving terms on the macroscopic simulation modelling. The research has also proposed several methods to improve macroscopic simulation models for the prediction of the traffic states, especially under congested traffic conditions. Main conclusions from this research for the chapters are summarized below.

Chapter 2 provided an overview on the state-of-the-art of traffic flow models with a special focus on microscopic car-following models and second-order macroscopic models. The traffic models were reviewed with respect to their categories in terms of level of detail, scale of independent variables, nature of independent variables and model representations. Various microscopic car-following model formulations, ideologies and properties were discussed. On the macroscopic level, both first- and second-order models and their respective advantages and disadvantages were presented. Even though higher-order macroscopic traffic models have been established from different perspectives, they share many similar properties, such as delayed response of drivers and their anticipation of downstream traffic conditions. While microscopic traffic models track each individual vehicle

movement and its relations with other vehicles during all time horizons, macroscopic traffic models consider the average value of the aggregated traffic flow properties and ignore the interaction between individual vehicles. Therefore, microscopic traffic models are ideally suited for off-line simulation to evaluate detailed local traffic operations, while macroscopic traffic models are more suited for large-scale, network-wide operation and online control purposes. These reviews provide comprehensive background information for establishing the relationship between microscopic car-following models and macroscopic traffic models.

Chapter 2 also discussed various theories and methods on traffic jam (stop-and-go traffic) modelling from both microscopic and macroscopic approaches. These include traditional microscopic car-following models, asymmetric traffic theory, traffic disturbance model, phase transition model as well as first-order and second-order macroscopic models. The mechanisms of stop-and-go waves, causes, generation, propagation, and absorption were discussed. It can be concluded that the stop-and-go traffic state is formed due to three conditions: high traffic demand, insufficient road capacity and traffic disturbance. When traffic density is sufficiently high, a small disturbance in the traffic flow can be amplified, causing a stop-and-go wave propagating backwards and the disturbance can be explained by microscopic car-following and lane-changing behaviour.

Chapter 3 explored the relationship between microscopic and macroscopic traffic flow models. Almost all of the existing well-known macroscopic speed-density relationships can be derived from microscopic car-following models. This is achieved by integrating microscopic car-following models and applying

proper assumptions on traffic conditions and headway-density approximations as well as boundary conditions. On the other hand, taking derivatives of macroscopic speed-density relationships will result in microscopic traffic models (acceleration equations) and the process is easier than integration.

Most of the microscopic-macroscopic derivation was based on the assumptions of steady-state and homogeneous traffic conditions and that headway equals to the inverse of the density. Therefore, these models apply only for steady-state traffic conditions. Under these assumptions, a generalized macroscopic speed density relationship was derived from the generalized stimulus-response microscopic car-following model, which includes a speed exponent parameter m and distance headway exponent parameter l. With different combination of m and l values, almost all of the well-known macroscopic speed-density models can be derived from this generalized car-following model.

It was found that the relationship between headway and density has important implications on model derivation. The research showed that the traditional headway-density assumption does not hold for non-homogeneous traffic and slightly changing the headway-density relationship will result in different macroscopic models. Using a mathematical definition of density and a new headway-density approximation, a macroscopic model that includes relaxation, convection, anticipation and diffusion (or viscosity) components was derived from a microscopic model corresponding to the delayed response of drivers.

Chapter 4 investigated the compatibility between microscopic and macroscopic simulation models. Several important factors, such as simulation time step, traffic

demand that have essential impact on the model performance were analyzed. The predicted flow, density and speed from a macroscopic simulation model were compared with those from a microscopic simulation model, using METANET and VISSIM respectively, on a section of urban freeway. Three levels of traffic demands and seven different time step lengths in macroscopic simulation were applied to evaluate the compatibility of the two models. Based on the performance of the two models and comparison analysis, the following main conclusions were found:

- The prediction of traffic states from METANET model is generally consistent with that from VISSIM simulation. The simulated speed, density and flow from VISSIM model fluctuate with time frequently, while those from the METANET model are approximately the average value of that from VISSIM.
- In macroscopic simulation model, there exist optimum time step lengths corresponding to a particular roadway configuration and free-flow speed. The optimum time step lengths do not change significantly with traffic demand. For the studied freeway, the recommended time step length for VSL control is approximately 20s.
- When traffic demand is at moderate to heavy level, the predicted traffic states from the macroscopic simulation are consistent with those from the microscopic simulation. Under excessive traffic demand (stop-and-go traffic conditions), significant differences exist between the simulated speed and density from the two models evaluated. There are some limitations for

macroscopic model used in this study to accurately predict traffic states under stop-and-go traffic conditions.

- In VISSIM simulation, the change of speed limits can be captured immediately at the location of the speed limit. In METANET model, the model could not catch the sudden and significant change of traffic speed.

Chapter 5 systematically investigated the impact of merging and weaving terms in speed dynamics on the performance of macroscopic simulation models. Several merging and weaving formulas were evaluated and compared with the base model (without merging and/or weaving terms) with respect to the predicted speed, density and flow. Data from both microscopic simulation and field loop detectors were used in the model performance evaluation. Based on these data, all relevant model parameters were estimated in model calibration, using an optimization technique. Each macroscopic simulation model was independently calibrated and then used to simulate traffic operations on the studied freeway. The values of merging and/or weaving terms was calculated and compared with the total predicted speed from the model.

ANOVA was performed to evaluate the variation of prediction errors of different models. Based on which, the statistical significance of merging and weaving impacts on the performance of macroscopic models was evaluated. It was concluded that:

- The predicted traffic states from the models without merging and/or weaving terms is very similar to the models with merging and/or weaving terms. Merging and weaving terms have no significant impact on the performance of macroscopic simulation models.

- Based on the formulation of the merge and/or weave terms that appeared in the literature and were evaluated in this research, the value of the merge or weave term varied from -6% to 0% of the predicted speed, with the average being approximately -2%.
- Adding merging and/or weaving terms does not necessarily mean better accuracy in traffic prediction with macroscopic simulation models. There is no obvious improvement of traffic state prediction. However, the models with merging and/or weaving terms are not inferior to the original model either.
- Macroscopic simulation model performance is sensitive to traffic demand. The higher the traffic demand, the higher the prediction errors.
- Based on this study, merging and/or weaving terms can be omitted in macroscopic simulation. This can reduce model parameters that need to be calibrated in the multi-parameter optimization process.

In Chapter 6, the value of each component of the density dynamics and speed dynamics of macroscopic simulation models were quantitatively analyzed for both average values during the full simulation time period and at a specific time step. Various options to improve model prediction accuracy had been discussed. For density dynamics, boundary conditions on each segment were incorporated into the models. For speed dynamics, several improvements on the speed dynamics of the original macroscopic simulation model were proposed and implemented in the macroscopic simulation models. These include: (a) considering the convection effect at both upstream and downstream of the current segment; (b) adding a constant

factor to the convection term; (c) adding a dynamic factor to the anticipation term and (d) various combinations of different factors and formulations. The modified simulation models were applied to two freeways and compared with outputs from the original model, using both VISSIM simulation data and field measured data, respectively. Based on the modelling results, it shows that the models with the suggested improvements have obviously better prediction accuracy than the original model, especially for the congested traffic conditions. The improved models can catch most of the significant sudden speed drop resulted from traffic congestions. Based on the study, it was concluded that:

- In macroscopic simulation, the predicted density on a segment at a time step is mainly composed of the density on the segment in previous time step (on average over 99% of the total predicted density). The impact of inflow and outflow on the density dynamics of a segment in one time step is very small. Their values vary from -2.5% to 3.5% of the predicted density;
- The predicted speed on a segment at a time step is dictated by the speed on the segment in previous time step (on average over 99% of the total predicted speed). The value of relaxation, convection and anticipation terms are small (on average less than ±4% of the total predicted density) and they can partially offset each other. Their combined contribution to the speed dynamics (on average less than ±0.1% of the total predicted density) is smaller than the value of each individual term;

- Boundary conditions should be incorporated in the density dynamics of the macroscopic simulation models to represent the constraints in actual traffic flow on road segments as well as at on-ramps;
- Using the geometric mean speed of the current and upstream segment, or using the geometric mean speed of the current segment, upstream and downstream segment to replace the upstream speed in the convection term can obviously improve the model performance. It can help the model to catch the significant speed drop under congested traffic conditions;
- Adding a factor to the convection term can also improve the overall prediction accuracy. The effect is comparable to that of using the geometric mean speed of the current and upstream segment to replace the upstream speed in the convection term;
- Adding a factor to the convection term and simultaneously adding a dynamic factor to the anticipation term has similar improvement to that using the geometric mean speed of the current and upstream segment to replace the upstream speed in the convection term.
- By using the geometric mean speed of the current segment, upstream and downstream segment to replace the upstream speed in the convection term, it can achieve over 10% improvements on speed prediction, over 5% improvements on density prediction as well as obvious improvements on flow prediction.

7.2 Recommendations for Future Research

Traffic flow models have been studied for more than half a century. Due to the complexity of traffic and wide variations of driver population, vehicle components and environment, there is not a single traffic model that applies to all traffic situations. Further research to explore other forms of the traffic flow models for better representation of traffic state evolution and traffic control is desirable in both theoretical analysis and field applications. In this section we provide some recommendations for future research following the studies carried out in this dissertation. These recommendations are categorized into several topics, including traffic flow modelling, comparison with other traffic models, model improvements, fundamental diagram, model extension / application as well as model calibration and validation.

7.2.1 Traffic Flow Modelling

In the area of traffic flow theory, theoretical improvements are possible and desirable, especially in building models with increased insight into congestion formation, propagation, dissipation as well as on different congestion patterns.

As presented in Chapter 2 and Chapter 3, a class of macroscopic models can be derived from microscopic models. This research showed that the representation of headway-density relationship has a dominant role in model derivation. There may be other forms of formulation for the headway-density relationship, such as a traditional headway-density relationship plus a fluctuation term, as described in disturbance model for congesting modelling. These stochastic models may be more close to actual traffic because in traffic flow there are many random elements in both driver

behaviour and traffic conditions. Future studies can be carried out to further explore new modelling approaches, from which we may be able to find more appropriate models, especially for traffic congestion modelling.

7.2.2 Comparison with Other Models

This research is focused on the application of the second-order macroscopic simulation models to predict traffic states. Other macroscopic models based on the first-order model principles, such as CTM, has also been used in many studies. Based on the theoretical representation, the second-order models have more flexibility to describe complicated traffic states due to their explicit and adjustable speed dynamics. There are also debates as to which type of models is more accurate in field application. Therefore, a systematically comparative study between the first-order and second-order macroscopic simulation models under various traffic conditions is recommended to identify which model is more appropriate for certain traffic conditions. In addition, further cross-comparisons of the improved models with other forms of models (such as microscopic models, hybrid models and other macroscopic models) can be carried out in terms of accuracy and computational efforts.

7.2.3 Model Improvements

Chapter 5 of this dissertation showed that adding merging and weaving terms in the speed dynamics as formulated in the existing literatures does not have significant impact on the model performance. It was also showed that based on existing formulation, the value of weaving term is smaller than that of the merging term. This is not consistent with field observations. Other forms of weaving term may be

investigated to confirm whether this phenomenon is due to the configuration of weaving term or the nature of macroscopic simulation, or due to the parameters in model calibration. In future studies, special considerations should be given to the cross weaving (two-sided weaving) because it may have more impact on freeway operations than that of one-sided weaving.

It was showed in Chapter 6 that several improved models have obviously better performance than the original model. However, even the improved models did not catch the stop-and-go traffic conditions under all traffic condition and on all segments. It is suggested that other type of improvements be explored and compared with the approaches used in this study.

7.2.4 Fundamental Diagram

As discussed in Chapter 6, the speed dynamics of macroscopic simulation models rely on the speed-density relationship, or fundamental diagram (FD), to provide the desired speed in relaxation term. Calibration of FD may lead to errors. In addition, one speed-density relationship may not apply to various traffic states. It is recommended in future research and field applications that other forms of fundamental diagram be investigated. Alternatively, multi-region fundamental diagrams can also be applied for different ranges of traffic density.

7.2.5 Model Extension and Application

This study is focused on the fundamental aspects of macroscopic simulation under non-controlled situation. Although the approach and methodologies are applicable to the controlled case as well, the model improvement suggestions and conclusions should be tested for controlled cases by incorporating the improvement measures

into controlled modelling, such as RM and VSL, so that they can be implemented for field traffic control.

In addition, this study used data from two freeway corridors. In future research, more diverse field data are desirable to test the robustness and reliability of the macroscopic simulation models under different traffic and environment conditions.

Another relevant topic for future research is the study of large networks, such as regional freeways network system where different section of freeways may have different characteristics.

7.2.6 Model Calibration and Validation

The existing calibration process use optimization of a performance function. The parameters obtained represent a compromise among a group of parameters. In future studies it is recommended that the following directions be investigated to find whether better parameters or more efficient calibration methods exist:

- Using different objective functions to investigate if the result is robust.
- Using multiple objective functions to obtain better parameters.
- Using other optimization algorithms to investigate how the optimal set of parameters depends on the choice of the algorithm.
- The sensitivity of parameters on the model performance should also be studied.
- If field traffic states change dramatically over a very short time period, online calibration may be applied to adjust the models for such traffic conditions.

References

Abdel-Aty, M., Dilmore, J., and Dhindsa, A. (2006a). Evaluation of variable speed limits for real-time freeway safety improvement. *Accident Analysis and Prevention*, 38(2), pp.335-345.

Abdel-Aty, M., Dilmore, J., and Hsia, L. (2006b). Applying variable speed limits and the potential for crash migration. *Transportation Research Record*, No.1953, pp. 21-30.

Adams, W.F. (1936), Road traffic considered as a random series. *Journal of the Institution of Civil Engineers*, 4, UK. pp. 121-130.

Ahn, S. and Cassidy, M., (2007). Freeway traffic oscillations and vehicle lane-change maneuvers. *International Symposium of Traffic and Transportation Theory* (R. Alsop, M. Bell and B. Heydecker, Eds.) Elsevier, Amsterdam, pp. 691-710.

Al-Deek, H., Kanafani, A. (1993). Modelling the benefits of advanced traveler information systems in corridors with incidents. *Transportation Research C* 1 (4), 303–324.

Aw, A., Klar, A., Materne, T. and Rascle, M. (2002). Derivation of continuum traffic flow models from microscopic follow-the-leader models. *SIAM Journal on Applied Mathematics*, vol. 63, No.1, pp. 259-278.

Aw, A. and Rascle, M. (2000). Resurrection of second-order models of traffic flow. *SIAM Journal of Applied Mathematics*, 60, pp.916-938.

Bando, M., Hasebe, K., Nakayama, A., Shibata, A., and Sugiyama, Y. (1995). Dynamical model of traffic congestion and numerical simulation. *Physical Review E*, 51, pp. 1035–1042.

Banks, J. H. (2002). Review of empirical research on congested freeway flow. *Transportation Research Record*, vol. 1802, pp. 225–232.

Barcelo, J. (2010). Fundamentals of traffic simulation. *International Series in Operations Research & Management Science*, Vol 145. Springer-Verlag.

Beegala, A., Hourdakis, J. and Michalopoulos. P.G. (2005). Methodology for performance optimization of ramp control strategies through micro-simulation. *Transportation Research Record: Journal of the Transportation Research Board*, No.1925, TRB, National Academies, Washington, D.C., pp. 87–98.

Bellemans, Tom. (2003). Traffic control on motorways. PhD dissertation. Katholieke Universiteit Leuven, Belgium.

Berg, P., Mason, A. and Woods, A. W. (2000). Continuum approach to car-following models. *Physical Review E*, 61, pp 1056-1066.

Berthelin, F., Degond, P. Delitala, M. and Rascle, M. (2008). Model for the formation and evolution of traffic jams. *Archive for Rational Mechanics and Analysis*. Vol. 187, Issue 2, pp.185-220.

Bertini, R. L., Boice, S., and Bogenberger, K. (2006). Dynamics of variable speed limit system surrounding bottleneck on German autobahn. *Transportation Research Record*, No.1978, pp. 149-159.

Bose, A. and Ioannou, P. (2000). Shock waves in mixed traffic flow. 9th IFAC Symposium on Control in Transportation Systems. June 13-15, Braunschweig, Germany.

Bourrel, E. and Lesort, J.-B. (2003). Mixing micro and macro representations of traffic flow: a hybrid model based on the LWR theory. Transportation Research Board, CD-ROM. Washington DC.

Brackstone, M., McDonald, M. (1999). Car-following: A historical review. *Transportation Research, Part F* 2, pp. 181-196.

Bryne, B.F. (1980). Some errors in macroscopic traffic models based on car-following models, *Transportation Research, Part B*, Vol. 14B, pp.241-242.

Burghout, W., Koutsopoulos, H. and Andreasson, I. (2005). Hybrid mesoscopic-microscopic traffic simulation. *Transportation Research Record*, Vol. 1934, pp. 218–225, 2005.

Camacho, E.F. and Bordons, C. (1995). Model predictive control in the process industry. Berlin, Germany, Springer-Verlag.

Carlson, R.C., Papamichail, I., Papageorgiou, M. and Messmer, A. (2010). Optimal mainstream traffic flow control of large-scale motorway networks. *Transportation Research, Part C* 18, pp. 193–212.

Cassidy, M.J. and Mauch, M. (2001). An observed traffic pattern in long freeway queues. *Transportation Research A*, vol. 35, pp. 143-156.

Chandler, R. E., Herman, R., & Montroll, E. W. (1958). Traffic dynamics: studies in car following. *Operations Research*, 6, pp.165-184.

Chu, L., Liu, H.X. and Recker, W. (2004). Using microscopic simulation to evaluate potential intelligent transportation system strategies under nonrecurrent congestion. *Transportation Research Record: Journal of the Transportation Research Board*, No.1886, TRB, National Research Council, Washington, D.C., pp. 76–84.

Chung, K., Rudjanakanoknad, J., and Cassidy, M. J. (2007). Relation between traffic density and capacity drop at three freeway bottlenecks. *Transportation Research Part B*: Methodological, 41(1), pp. 82-95.

Cluitmans, M., Griez, T., Jacobs, K., Krieger, T. and Mehlkop, B. (2006). Comparison of a microscopic and a macroscopic model for the simulation of traffic flow phenomena. Maastricht University, The Netherlands. http://matthijs.cluitmans.net/simulation.pdf, Accessed on March 6, 2011.

Colombo, R. M. (2002a). Hyperbolic phase transitions in traffic flow. Society for industrial and applied mathematics. *SIAM Journal of Applied Mathematics*, 63(2), pp.708–721.

Colombo, R. M. (2002b). A 2x2 hyperbolic traffic flow model. *Mathematical and Computer Modelling*, vol. 35(5–6), pp. 683–688

Cremer, M. and Papageorgiou, M. (1981). Parameter identification for a traffic flow model. *Automatica*, 17(6), pp.837–843.

Cremer, M. and Ludwig, J. (1986). A fast simulation model for traffic flow on basic of boolean operations. *Mathematics and Computers in Simulation*. Vol. 28, Issue 4, pp. 297-303.

Daganzo, C. F. (1994). The cell transmission model: A dynamic representation of highway traffic consistent with the hydrodynamic theory. *Transportation Research, Part B*, Vol. 28B, No. 4, pp. 269-287.

Daganzo C.F. (1995a). Requiem for second-order fluid approximation of traffic flow. *Transportation Research, Part B*, Vol. 29. pp. 277-286.

Daganzo, C.F. (1995b). The cell transmission model, part II: Network traffic. *Transportation Research Part B*: Methodological, vol. 29, no. 2, pp. 79–93.

Daganzo, C.F (1995c). A finite difference approximation of the kinematic wave model of traffic flow. *Transportation Research Part B*: Methodological, vol. 29, No. 4, pp. 261–276.

Daganzo, C. F. (1999). Remarks on traffic flow modelling and its applications in traffic and mobility. Proceedings of the Traffic and Mobility Simulation, Economics and Environment Conference, pp. 105-115.

Daganzo, C. F. (2002a). A behavioural theory of multi-lane traffic flow. I: Long homogeneous freeway sections, *Transportation Research B*, 36, pp. 131-158.

Daganzo, C. F. (2002b). A behavioural theory of multi-lane traffic flow. II: Merges and the onset of congestion. *Transportation Research B*, 36, pp.159-169.

Del Castillo, J.M. (1996). A car-following model based on the Lighthill-Whitham theory. In J. B. Lesort editor, *Transportation and Traffic Theory*, proceedings of the 13th ISTTT, Oxford: Pergamon, pp. 517-538.

Drake, J.S., Schofer, J.L. and May, A.D. (1967). A statistical analysis of speed density hypotheses. *Highway Research Record*, No. 154, pp.53-87.

Drew, D.R. (1965). Deterministic aspects of freeway operations and control. *Highway Research Record*, No. 99, pp.48-58.

Edie, L.C. and Foote, R.S. (1958). Traffic flow in tunnels. Proceedings of Highway Research Board, 37. USA. p334-344.

Emmerink, R., Axhausen, K.W., Nijkamp, P., Rietveld, P. (1995). The potential of information provision in a simulated road transport network with non-recurrent congestion. *Transportation Research C* 3 (5), pp. 293-309.

Flynn, M.R., Kasimov, A.R., Nave, J.-C., Rosales, R. R. and Seibold, B. (2009). Self-sustained nonlinear waves in traffic flow. *Physical Review E*, Vol. 79, Issue 5, 056113.

Forbes, T.W. and Simpson, M.E. (1968). Driver and vehicle response in freeway deceleration waves. Transportation Science, Vol. 2(1), pp.77-104.

Gartner, N.H. (1984). Development of demand-responsive strategies for urban traffic control. in Proceedings of the 11th IFIP Conference on System Modelling and Optimization. (Edited by P. Thoft-Christensen, P.), Springer-Verlag New York. pp. 166-174.

Gartner, N.H., Messer, C.J. and Rathi, A. (2001). Traffic flow theory. The state-of-the art report, Technical report, Transportation Research Board, USA.

Gazis, D. C., Herman, R., and Potts, R.B. (1959). Car-follow theory of steady-state traffic flow. *Operations Research*, Vol. 7, pp. 499–505.

Gazis, D. C., Herman, R., and Rothery, R.W. (1961). Nonlinear follow-the-leader models of traffic flow. *Operations Research*, Vol. 9, pp. 545–567.

Gazis, D. C. (1967). Mathematical theory of automobile traffic. *Science*, New series, Vol. 157, No. 3786, pp. 273–281.

Ghods, A.H., Fu, L. and Rahimi-Kian, A. (2010). An efficient optimization approach to real-time coordinated and integrated freeway traffic control. *IEEE Transactions on Intelligent Transportation Systems*, Vol. 11, No. 4, pp.873-884.

Gomes, G., May, A. and Horowitz, R. (2004). Congested freeway micro simulation model using VISSIM. *Transportation Research Record: Journal of the Transportation Research Board,* No.1876, TRB, National Research Council, Washington, D.C., pp. 71–81.

Greenberg, H. (1959). An analysis of traffic flow. *Operations Research*, 7, No.l, pp. 79-85.

Greenshields, B.D. (1935). A study in highway capacity. *Highway Research Board*, Proceedings, Vol. 14, p. 458.

Hadiuzzaman, M., Qiu, T.Z. and Bhowmick, A. (2010). Simulation study for active traffic management implementation in Edmonton. University of Alberta (unpublished).

Hadiuzzaman, M., Qiu, T. Z., and Lu, X. Y. (2013). Variable speed limit control design for relieving congestion caused by active bottleneck. *Journal of Transportation Engineering*, 139(4), pp. 358-370.

Halkias, B., Kopelias, P., Papandreou, K., Politou, A., Prevedouros, P. and Skabardonis, A. (2007). Freeway bottleneck simulation, implementation, and evaluation. *Transportation Research Record: Journal of the Transportation*

Research Board, No.2012, Transportation Research Board of the National Academies, Washington, D.C., pp. 84–93.

Hall, R.W. (1996). Route choice and advanced traveler information systems on a capacitated and dynamic network. *Transportation Research C* 4 (5), pp. 289–306.

Hasan, M., Jha, M. and Ben-Akiva, M. (2002). Evaluation of ramp control algorithms using microscopic traffic simulation. *Transportation Research Part C* 10, pp. 229–256.

Hegyi, A., De Schutter, B. and Hellendoorn, J. (2005a). Optimal coordination of variable speed limits to suppress shock waves. *IEEE Transactions on Intelligent Transportation Systems* 6 (1), pp. 102–112.

Hegyi, A., De Schutter, B. and Hellendoorn, H. (2005b). Model predictive control for optimal coordination of ramp metering and variable speed limits. *Transportation Research Part C* 13, pp. 185–209.

Helbing, D. (1996). Gas-kinetic derivation of Navier-Stokes-like traffic equations. Physical Review E Vol. 53(3), pp. 2266-2381.

Helbing, D. (2001). Traffic and related self-driven many-particle systems. *Reviews of Modern Physics*, Vol. 73, pp. 1067-1141.

Helbing, D., Hennecke, A., Shvetsov, V. and Treiber, M. (2002). Micro- and macro-simulation of freeway traffic. *Mathematical and Computer Modelling* 35, pp. 517-547.

Helbing, D., Hennecke, A. and Treiber, M. (1999). Phase diagram of traffic states in the presence of inhomogeneities. *Physical Review Letters,* 82, pp. 4360-4363.

Herman, R., Montroll, E.W., Potts, R.B. and Rothery, R.W. (1959). Traffic dynamics: Analysis of stability in car-following. *Operations Research*, 7. pp. 86-106.

Heutinck, B.H., van den Berg, M., Hellendoorn, J. and Immers, L.H. (2006). Dynamic route guidance during maintenance works, a case study. 11th IFAC Symposium on Control in Transportation Systems, Volume No.11 Part 1.

Hicks, C.R and Turner, K.V. (1999). Fundamental concepts in the design of experiments, Fifth Edition, New York. Oxford University Press.

Hidas, P. (2002). Modelling lane-changing and merging in microscopic traffic simulation. *Transportation Research Part C* 10, pp. 351–371.

Hoogen, V. E., and Smulders, S. (1994). Control by variable speed sign: results of the Dutch experiment. In Proceedings of 7th Internal Conference on Traffic Monitoring and Control, London, England, April 26-28, no. 391, pp.145-149.

Hoogendorn, S.P. and Bovy, P.H.L. (2001). State-of-the-art of vehicular traffic flow modelling. Proceedings of the Institution of Mechanical Engineers, Part I. *Journal of Systems and Control Engineering*. June 1, pp. 283-303,

Ishak, S., Alecsandru, C. and Seedah, D. (2006). Improvement and evaluation of cell-transmission model for operational analysis of traffic networks, freeway case study. *Transportation Research Record: Journal of the Transportation Research Board,* No. 1965, Transportation Research Board of the National Academies, Washington, D.C., pp. 171–182.

Jiang, R., Wu, Q. and Zhu, Z. (2001). Full velocity difference model for a car following theory. *Physical Review E*, 64, 017101.

Kerner, B. S. (2009). Introduction to modern traffic flow theory and control, the long road to three-phase traffic theory. Springer-Verlag Berlin Heidelberg.

Kerner, B. S., and Konhauser, P. (1993). Cluster effect in initially homogeneous traffic flow. *Physical Review E*, 48, R2335-R2338.

Kerner, B.S. and Rehborn, H. (1998). Messungen des Verkehrsflusses: Charakteristische Eigenschaften von Staus auf Autobahnen. Internationales Verkehrswesen 50, pp.196-203.

Kikuchi, C., and Chakroborty, P. (1992). Car-following model based on a fuzzy inference system. *Transportation Research Record*, No. 1365, pp. 82-91.

Kim, Youngho. (2002). Online traffic flow model applying dynamic flow-density. PhD dissertation, Technischen Universität München, Germany.

Kotsialos, A., Papageorgiou, M., Diakaki, C., Pavlis, Y. and Middelham, F. (2002). Traffic flow modelling of large-scale motorway networks using the macroscopic modelling tool METANET. IEEE Transactions on Intelligent Transportation Systems. 3 (4), pp. 282-292.

Kotsialos, A., Papageorgiou, M. and Messmer, A. (1999). Integrated optimal control of motorway traffic networks. In 18th American Control Conference, pp. 2183–2187.

Koutsopoulos, H.N., Lotan, T. (1989). Effectiveness of motorist information systems in reducing traffic congestion. In proceedings of the Conference on Vehicle Navigation and Information Systems (VNIS), Toronto, Canada, pp. 275–281.

Lamon, F. (2008). Freeway traffic modelling and calibration for the Eindhoven network. MSc. thesis, Delft University of Technology, The Netherlands.

Laval, J. A. and Leclercq, L. (2010). A mechanism to describe the formation and propagation of stop-and-go waves in congested freeway traffic. *Philosophical Transactions of the Royal Society*, A 368, pp. 4519-4541.

Lee, C., Hellinga, B., and Saccomanno, F. (2003). Proactive freeway crash prevention using real-time traffic control. *Canadian Journal of Civil Engineering*, 30(6), pp. 1034-1041.

Lee, C., Hellinga, B., and Saccomanno, F. (2004). Assessing safety benefits of variable speed limits. *Transportation Research Record*, Vol. 1897, 183-190.

Lee, C., Hellinga, B., and Saccomanno, F. (2006). Evaluation of variable speed limits to improve traffic safety. *Transportation Research Part C*: Emerging Technologies, 14(3), pp. 213-228.

Lee, H.Y., Lee, H.-W. and Kim, D. (1998). Origin of synchronized traffic flow on highways and its dynamic phase transitions. *Physical Review Letter* 81, pp.1130.

Leutzbach, Wilhelm. (1988). Introduction to the theory of traffic flow. Springer.

Lighthill, M. J., and Whitham, J. B. (1955). On kinematic waves. I. Flow movement in long rivers. II. A theory of traffic flow on long crowded roads. In Proceedings of the Royal Society, London: Ser. A, vol 229(1178), pp. 281-345.

Liu, G., Lyrintzis, A. S. and Michalopoulos, P. G. (1996). Modelling of freeway merging and diverging flow dynamics. *Applied Mathematic Modelling*, Vol. 20, Issue 6, pp. 459-469.

Liu, G., Lyrintzis, A.S. and Michalopoulos, P.G. (1998). Improved higher-order model for freeway traffic flow. *Transportation Research Record*, Vol.1644, pp.37-46.

LeVeque, R. J. (1992). Numerical methods for conservation laws. second edition, Birkhauser Verlag, Berlin.

Lu, X.Y., Qiu, T.Z., Horowitz, R., Chow, A., Shladover, S. (2011). METANET model improvement for traffic control. 14th International IEEE Conference on Intelligent Transportation Systems, Washington, DC, USA. October 5-7.

Lu, X.Y., Qiu, T.Z., Varaiya, P.P., Horowitz, R. and Shladover, S.E. (2010). Combining variable speed limits with ramp metering for freeway traffic control. American Control Conference (ACC), Baltimore, MD, June 30-July 2.

Maciejowski, J.M. (2002). Predictive control: with constraints. Harlow, England: Prentice Hall.

Mahmassani, H., Jayakrishnan, R. (1991). System performance and user response under real-time information in a congested traffic corridor. *Transportation Research A* 25 (5), pp. 293–307.

May, A.D. (1990). Traffic flow fundamentals. Prentice Hall, Englewood Cliffs, New Jersey.

May A. D. and Keller, H. M. (1967). Non integer Car-Following Models. *Highway Research Record, Vol.* 199, pp. 19-32.

Messmer, A. and Papageorgiou, M. (1990). METANET: A macroscopic simulation program for motorway networks. *Traffic Engineering and Control*, 31, pp.466–470.

Messer, C.J. (1998). Simulation studies of traffic operations at oversaturated, closely spaced signalized intersections. *Transportation Research Record: Journal of the Transportation Research Board,* Vol.1646, pp.115-123.

Michalopoulos, P. G., Yi, P., and Lynrintzis, A. S. (1993). Continuum modeling of traffic dynamics for congested freeways. *Transportation Research B*, Vol. 27, Issue 4, pp.315-332.

Michaels, R.M. (1963). Perceptual factors in car-following. In International Symposium on Theory of Road Traffic Flow, Paris, France, pp. 44–59.

Mika, H.S., Kreer, J.B. and Yuan, L.S. (1969). Dual mode behaviour of freeway traffic. *Highway Research Record*, Vol. 279, pp.1-13.

Minitab, Inc. (2010). Minitab 16.

Montgomery, Douglas C. (1997). Design and Analysis of Experiments. Forth Edition, Wiley.

Munjal, P., Hsu, Y. S. and Lawrence, R. L. (1971). Analysis and validation of lane-drop effects on multilane freeways. *Transportation Research*, Vol. 5, Issue 4, pp. 257-266.

Munjal, P. and Pipes, L. A. (1971). Propagation of on-ramp density perturbations on unidirectional two and three-lane freeways. *Transportation Research*, Vol. 5, Issue 4, pp. 241-255.

Nagel, K. (1996). Particle hopping models and traffic flow theory. *Physical Review E* 53, pp. 4655-4672.

Nagel, K. (1998). From particle hopping models to traffic flow theory. *Transportation Research Record*, Vol. 1644, pp. 1-9.

Nagel, K. and Nelson, P. (2005). A critical comparison of the kinematic wave model with observational data. Proceedings of the 16th International Symposium on Transportation and Traffic Theory, pp. 145-163.

Nagel, K., Wagner, P. and Woesler, R. (2003). Still Flowing: approaches to traffic flow and traffic jam modelling. *Operations Research*, Vol. 51, No. 5, pp. 681-710.

Newell, G.F. (1961). Nonlinear effects in the dynamics of car following. *Operations Research*, Vol. 9, pp. 209-229.

Newell, G. F. (1965). Instability in dense highway traffic, a review. In proceedings of the Second International Symposium on Transportation and Traffic Theory, London, pp.73-83.

Ni, Daiheng (2013). A unified perspective on traffic flow theory, Part II: The unified diagram. *Applied Mathematical Sciences*, Vol. 7, 2013, no. 40, 1947 – 1963.

Nökel, K. and Schmidt, M. (2002). Parallel DYNEMO: Meso-scopic traffic flow simulation on large networks. *Networks and Spatial Economics*, Vol. 2, pp. 387–403.

Olstam, J.J., Tapani, A. (2004). Comparison of car-following models. Swedish National Road and Transport Research Institute. Publication Number: VTI Meddelande 960A. http://ftp.vti.se/EPiBrowser/Publikationer/M960A.pdf, Accessed on June 3, 2011.

Orosz, G, Wilson, R.E. Stepan, G. (2010). Traffic jams: dynamics and control. *Philosophical Transactions of the Royal Society*. A 368, pp. 4455-4479.

Papageorgious, M. (1990). Modelling and real-time control of traffic flow on the south part of Boulevard Peripherique in Paris: Part I: Modelling. *Transportation Research Part A*, Vol 24A, pp.345-359.

Papageorgious, M., Blosseville, J.M. and Hadj-Salem, H. (1989). Macroscopic modelling of traffic flow on the Boulevard Peripherique in Paris. *Transportation Research Part B,* 23, pp.29-47.

Paveri-Fontana, S.L. (1975). On Boltzmann-like treatments for traffic flow: A critical review of the basic model and an alternative proposal for dilute traffic analysis. *Transportation Research 9*, pp.225–235.

Payne, H.J. (1971). Models of freeway traffic and control. *Mathematical Models of Public Systems* (Simulation Council Proceedings), 1, pp.51–61.

Payne, H.J. (1979). FREFLO: A macroscopic simulation model of freeway traffic. *Transportation Research Record,* Vol. 722, pp. 68-77.

Persaud, B., Yagar, S., and Brownlee, R. (1998). Exploration of the breakdown phenomenon in freeway traffic. *Transportation Research Record*, Vol.1634, pp. 64-69.

Phillips, W.F. (1979). A kinetic model for traffic flow with continuum implications, Transportation Planning and Technology, Vol. 5, pp 131–138.

Piao, J. and McDonald, M. (2008). Safety impacts of variable speed limits - A simulation research. IEEE Conference on Intelligent Transportation Systems, Proceedings, ITSC, pp. 833-837.

Piccoli, B., and A. Tosin, A. (2011). Vehicular Traffic: A Review of Continuum Mathematical Models. *Mathematics of Complexity and Dynamical Systems*. pp. 1748-1770.

Pipes, L. A. (1953). An operational analysis of traffic dynamics. *Journal of Applied Physics*, 24. pp.274-281.

Pipes. L.A. (1967). Car following models and fundamental diagram of road traffic. Transportation Research, Vol.1, Issue 1, pp. 21-29.

Prigogine, I. and Herman, R. (1971). Kinetic theory of vehicular traffic. Elsevier.

PTV Planung Transport Verkehr AG. (2010, 2012). VISSIM 5.3, 5.40 user manual. Karlsruhe, Germany.

Richards, P. I. (1956). Shockwaves on the highway. *Operation Research*, 4(1), pp. 42-51.

Rothery, R.W. (1999), Car-following models. In Traffic Flow Theory. Transportation Research Board, USA.

Şahin, I., and Altun, I. (2008). Empirical research of behavioural theory of traffic flow: Analysis of recurrent bottleneck. *Transportation Research Record*, Vol. 2088, pp. 109-116.

Samwal, K.K., Petty, K., Walrand, J. and Fawaz, Y. (1996). An extended macroscopic model for traffic flow. *Transportation Research Part B*, Vol 30, Issue1, pp.1-9.

Shladover, S.E., Lu, X.Y., Cody, D., Nowakowski, C., Qiu, Z.T., Chow, A., O'Connell, J., Nienhuis, J. and Su, D. (2010). Development and evaluation of

selected mobility applications for VII. University Of California, Berkeley Research Report. UCB-ITS-PRR-2010-25.

Stewart, J., Baker, M. and Van Aerde, M. (1996). Evaluating weaving section designs using INTEGRATION. *Transportation Research Record: Journal of the Transportation Research Board,* Vol.1555, pp.33-41.

Tampère, C.M.J., Van Arem, B., and Hoogendoorn, S.P. (2003). Gas kinetic traffic flow modelling including continuous driver behaviour models. In proceedings of the 82nd Annual Meeting of the Transportation Research Board, Washington, U.S.A..

The MathWorks, Inc. (2010). Optimization Tool Box User's Guide.

Tian, Z.Z., Urbanik II, T., Engelbrecht, R. and Balke, K. (2002). Variations in capacity and delay estimates from microscopic traffic simulation models. *Transportation Research Record*: *Journal of the Transportation Research Board*, Vol. 1802, pp. 23-31.

TRB. (2010). Highway capacity manual. Transportation Research Board, National Academy of. Sciences, Washington, D.C.

Treiber, M. and Helbing, D. (1999). Explanation of observed features of self-organization in traffic flow. arXiv:cond-mat/9901239v1. http://arxiv.org/abs/cond-mat/9901239, Accessed on April 12, 2013.

Treiber, M. and Helbing, D. (2003). Memory effects in microscopic traffic models and wide scattering in flow-density data. *Physical Review E*, 68, pp. 046119.

Treiber, M., Hennecke, A. and Helbing, D. (1999). Microscopic simulation of congested traffic. In *Traffic and Granular Flow*, pp. 365–376.

Treiber, M., Hennecke, A., and Helbing, D. (1999). Derivation, properties, and simulation of a gas-kinetic-based, non-local traffic model. *Physical Review E*, 59, pp. 239–253.

Treiber, M., Hennecke, A. and Helbing, D. (2000). Congested traffic states in empirical observations and microscopic simulations. *Physical Review E*, 62, pp. 1805–1824.

Treiterer, J. and Taylor, J. I. (1966). Traffic flow investigations by photogrammetric techniques. *Highway Research Record*, Vol.142, pp.1-12.

Underwood, R.T. (1961). Speed, volume, and density relationships: Quality and theory of traffic flow. Yale Bureau of Highway Traffic, pp. 141-188.

Van der Horst, A.D. (2011). Calibration of the IDM and METANET traffic flow models. MSc. thesis. Delft University of Technology, The Netherlands.

Wagner, C., Hoffmann, C., Sollacher, R., Wagenhuber, J., and Schurmann, B. (1996) Second-order continuum traffic model. *Physical Review E* 54, pp.5073–5085

Wang, X., Hadiuzzaman, M. and Qiu, T.Z. (2012). Analyzing sensitivity of freeway capacity at a complex weaving segment. Annual Conference of Canadian Society for Civil Engineering (CSCE), 9th International Transportation Specialty Conference, Edmonton, Canada, June 2012.

Wang, Y., Papageorgiou, M., Sarros, G. and Knibbe, W. J. (2006). Feedback route guidance applied to a large-scale express ring road. *Transportation Research Record*, Vol.1965, pp. 79-88.

Wiedemann, R. (1974). Simulation des Strassenverkehrsflusses. University Karlsruhe, Germany.

Wu, N. (2002). Application and verification of macroscopic and microscopic simulation models – case study for NETCELL and VISSIM on congested freeway. In Proceedings of the International Conference on Traffic and Transportation Studies, Beijing, China.

Yeo, H. and Skabardonis, A. (2009). Understanding stop-and-go traffic in view of asymmetric traffic theory. In Proceedings of 18th International Symposium on Transportation and Traffic Theory (ISTTT), Hong Kong.

Yin, D. and Qiu, Z.T. (2011). Comparison of macroscopic and microscopic simulation models in modern roundabout analysis. *Transportation Research Record: Journal of the Transportation Research Board,* USA. No.2265, pp. 244-252.

Yin, D. and Qiu, T.Z. (2012). Improvement of traffic speed dynamics in METANET model. In proceedings of the 9th International Transportation Specialty Conference, Edmonton, Alberta. June 6-9.

Yin, D. and Qiu, Z.T. (2013). Compatibility analysis of macroscopic and microscopic traffic simulation modeling. Canadian Journal of Civil Engineering. 40(7), pp.613-622.

Zhang, H.M. (1998). A theory of nonequilibrium traffic flow. *Transportation Research, Part B*, Vol. 32, No. 7, pp.485-498.

Zhang, H.M. (2001). New perspectives on continuum traffic flow models. *Networks and Spatial Economics*, Vol. 1, Issue 1-2, pp.9-33.

Zhang, H.M. (2002). A non-equilibrium traffic model devoid of gas-like behaviour. *Transportation Research, Part B*, Vol. 36, No. 3, pp.275-290.

Zhang, H.M. (2003). Driver memory, traffic viscosity and a viscous vehicular traffic flow model. *Transportation Research, Part B*, Vol. 37, pp.27-41.

Zhang, H.M. (2009). Comment on "On the controversy around Daganzo's requiem for and Aw-Rascle's resurrection of second-order traffic flow models" by D. Helbing and A.F. Johansson. *The European Physical Journal B*, Vol. 69, pp. 563-568.